

JSCSEN 89(4)443-597(2024)

ISSN 1820-7421(Online)

Journal of the Serbian Chemical Society

Electronic
version

VOLUME 89

NO 4

BELGRADE 2024

Available on line at



www.shd.org.rs/JSCS/

The full search of JSCS
is available through

DOAJ DIRECTORY OF
OPEN ACCESS
JOURNALS

www.doaj.org

The **Journal of the Serbian Chemical Society** (formerly Glasnik Hemijskog društva Beograd), one volume (12 issues) per year, publishes articles from the fields of chemistry. The **Journal** is financially supported by the **Ministry of Education, Science and Technological Development of the Republic of Serbia**.

Articles published in the **Journal** are indexed in **Clarivate Analytics products: Science Citation Index-Expanded™** – accessed via **Web of Science®** and **Journal Citation Reports®**.

Impact Factor announced on 28 June, 2023: **1.000**; **5-year Impact Factor: 1.100**.

Articles appearing in the **Journal** are also abstracted by: **Scopus**, **Chemical Abstracts Plus (CAplusSM)**, **Directory of Open Access Journals**, **Referativnii Zhurnal (VINITI)**, **RSC Analytical Abstracts**, **EuroPub**, **Pro Quest** and **Asian Digital Library**.

Publisher:

Serbian Chemical Society, Karnegijeva 4/III, P. O. Box 36, 1120 Belgrade 35, Serbia
tel./fax: +381-11-3370-467, E-mails: **Society** – shd@shd.org.rs; **Journal** – jscs@shd.org.rs
Home Pages: **Society** – <http://www.shd.org.rs/>; **Journal** – <http://www.shd.org.rs/JSCS/>
Contents, Abstracts and full papers (from Vol 64, No. 1, 1999) are available in the electronic form at the Web Site of the **Journal** (<http://www.shd.org.rs/JSCS/>).

Internet Service:

Former Editors:

Nikola A. Pušin (1930–1947), **Aleksandar M. Leko** (1948–1954),
Panta S. Tutundžić (1955–1961), **Miloš K. Mladenović** (1962–1964),
Đorđe M. Dimitrijević (1965–1969), **Aleksandar R. Despić** (1969–1975),
Slobodan V. Ribnikar (1975–1985), **Dragutin M. Dražić** (1986–2006).

Editor-in-Chief:

BRANISLAV Ž. NIKOLIĆ, Serbian Chemical Society (E-mail: jscs-ed@shd.org.rs)

Deputy Editor:

DUŠAN SLADIĆ, Faculty of Chemistry, University of Belgrade

Sub editors:

Organic Chemistry

DEJAN OPSENICA, Institute of Chemistry, Technology and Metallurgy, University of Belgrade

Biochemistry and Biotechnology

JÁNOS CSANÁDI, Faculty of Science, University of Novi Sad

Inorganic Chemistry

OLGICA NEDIĆ, INEP – Institute for the Application of Nuclear Energy, University of Belgrade

Theoretical Chemistry

BILJANA GLIŠIĆ, Faculty of Science, University of Kragujevac

Physical Chemistry

IVAN JURANIĆ, Serbian Chemical Society

Electrochemistry

LJILJANA DAMJANOVIĆ-VASILJIĆ, Faculty of Physical Chemistry, University of Belgrade

Analytical Chemistry

SNEŽANA GOJKOVIĆ, Faculty of Technology and Metallurgy, University of Belgrade

Polymers

RADA BAOŠIĆ, Faculty of Chemistry, University of Belgrade

Thermodynamics

BRANKO DUNJIĆ, Faculty of Technology and Metallurgy, University of Belgrade

Chemical Engineering

MIRJANA KIJEVCANIN, Faculty of Technology and Metallurgy, University of Belgrade

Materials

TATJANA KALUĐEROVIĆ RADOIČIĆ, Faculty of Technology and Metallurgy, University of Belgrade

Metallic Materials and Metallurgy

RADA PETROVIĆ, Faculty of Technology and Metallurgy, University of Belgrade

Environmental and Geochemistry

ANA KOSTOV, Mining and Metallurgy Institute Bor, University of Belgrade

History of and Education in Chemistry

VESNA ANTIĆ, Faculty of Agriculture, University of Belgrade

English Language Editors:

DRAGICA TRIVIĆ, Faculty of Chemistry, University of Belgrade

Technical Editors:

LYNNE KATSIKAS, Serbian Chemical Society

Journal Manager & Web Master:

VLATKA VAJS, Serbian Chemical Society

Office:

JASMINA NIKOLIĆ, Faculty of Technology and Metallurgy, University of Belgrade

Editorial Board

VLADIMIR PANIĆ, Institute of Chemistry, Technology and Metallurgy, University of Belgrade

From abroad:

MARIO ZLATOVIĆ, Faculty of Chemistry, University of Belgrade

From Serbia:

VERA ČUŠIĆ, Serbian Chemical Society

Subscription:

Godišnja pretplata:

Nota:

Odlokum Odbora za hemiju Republičkog fonda za nauku Srbije,

br. 66788/1 od 22.11.1990. godine,

koja je kasnije potvrđena odlukom Saveta Fonda,

časopis je uvršten u kategoriju međunarodnih časopisa (M-23).

Takođe, aktom Ministarstva za nauku i tehnologiju Republike Srbije,

413-00-247/2000-01 od 15.06.2000. godine,

ovaj časopis je proglašen za publikaciju od posebnog interesa za nauku.

Impact Factor časopisa objavljen 28. juna 2023. godine je 1,000,

a petogodišnji Impact Factor 1,100.

Impact Factor

časopisa objavljen 28. juna 2023. godine je 1,000,

a petogodišnji Impact Factor 1,100.

Impact Factor

časopisa objavljen 28. juna 2023. godine je 1,000,

a petogodišnji Impact Factor 1,100.

Impact Factor

časopisa objavljen 28. juna 2023. godine je 1,000,

a petogodišnji Impact Factor 1,100.

Impact Factor

časopisa objavljen 28. juna 2023. godine je 1,000,

a petogodišnji Impact Factor 1,100.

Impact Factor

časopisa objavljen 28. juna 2023. godine je 1,000,

a petogodišnji Impact Factor 1,100.

Impact Factor

časopisa objavljen 28. juna 2023. godine je 1,000,

a petogodišnji Impact Factor 1,100.

Impact Factor

časopisa objavljen 28. juna 2023. godine je 1,000,

a petogodišnji Impact Factor 1,100.

Impact Factor

časopisa objavljen 28. juna 2023. godine je 1,000,

a petogodišnji Impact Factor 1,100.

Impact Factor

časopisa objavljen 28. juna 2023. godine je 1,000,

a petogodišnji Impact Factor 1,100.

Impact Factor

časopisa objavljen 28. juna 2023. godine je 1,000,

a petogodišnji Impact Factor 1,100.



CONTENTS*

Organic Chemistry

- P. B. Stanić, D. P. Ašanin, T. V. Soldatović and M. D. Živković*: Kinetic investigation of reactions of a 3-arylidene-2-thiohydantoin derivative with palladium(II) salts 443

Biochemistry and Bioengineering

- S. Bendjelloul, C. K. Bendeddouche, S. Bendeddouche, M. Sarri, F. Bensafiddine, N. Kambouche, L. Paquin, M. Yousfi and M. Harrat*: Co-detection of eugenol and butylated hydroxytoluene by green and selective hydrodistillation of *Heliotropium europaeum* L. using ionic liquids as additives 457
- A. N. Hmedat, M. C. Morejón, D. G. Rivera, N. D. Pantelić, L. A. Wessjohann and G. N. Kaluderović*: *In vitro* anticancer studies of a small library of cyclic lipopeptides against the human cervix adenocarcinoma HeLa cells..... 471

Theoretical Chemistry

- K. F. da Costa Serra, A. Khan, R. M. Trindade Fernandes, P. A. Muniz Vazquez and A. Khan*: Multivariate statistical analysis approach to investigate the thermodynamic quantities of the benign alternative fuel 485
- M. Rashid, MD T. Athar, A. Hussain, N. M. Almadani and A. Hussain*: A recent tactic for searching CDK-7 kinase inhibitor by NCI database screening 505

Physical Chemistry

- M. M. Budiul, M. Mateescu, G. Vlase, T. Vlase, S. Bocănici and I. A. Bradu*: Thermo-analytical and spectroscopic studies on medicated jellies with perphenazine 521

Electrochemistry

- I. V. Goroncharovskaya, A. K. Evseev, A. K. Shabanov and S. S. Petrikov*: Electrochemical analysis of antioxidant status of biological media in different sampling and storage conditions..... 539

Analytical Chemistry

- A. Dinçel, E. D. Gök-Topak and F. Onur*: Simultaneous determination of emtricitabine and tenofovir disoproxil fumarate in pharmaceutical preparations using spectrophotometric, chemometric and chromatographic methods..... 551

Environmental

- P. C. Bhomick, A. Supong, A. I. Sema and D. Sinha*: Defluoridation using pinecone-based activated carbon: Adsorption isotherm, kinetics, regeneration and co-ions effect investigation..... 565
- J. Jokić Govedarica, D. Tomašević Pilipović, V. Gvoić, Đ. Kerkez, A. Leovac Maćerak, N. Slijepčević and M. Bečelić-Tomin*: Cost-effective method of simultaneous removal of copper and phosphate on environmentally friendly nanomaterial..... 581
- Errata (Printed version only)* 597

Published by the Serbian Chemical Society
Karnegijeva 4/III, P.O. Box 36, 11120 Belgrade, Serbia
Printed by the Faculty of Technology and Metallurgy
Karnegijeva 4, P.O. Box 35-03, 11120 Belgrade, Serbia

* For colored figures in this issue please see electronic version at the Journal Home Page:
<http://www.shd.org.rs/JSCS/>



J. Serb. Chem. Soc. 89 (4) 443–455 (2024)
JSCS–5732

Kinetic investigation of reactions of a 3-arylidene-2-thiohydantoin derivative with palladium(II) salts

PETAR B. STANIĆ^{1*}, DARKO P. AŠANIN^{1#}, TANJA V. SOLDATOVIĆ^{2#}
and MARIJA D. ŽIVKOVIĆ^{3,4***}

¹University of Kragujevac, Institute for Information Technologies, Department of Science, Jovana Cvijića bb, 34000 Kragujevac, Serbia, ²State University of Novi Pazar, Department of Natural-Mathematical Sciences, Vuka Karadžića 9, 36300 Novi Pazar, Serbia, ³University of Kragujevac, Faculty of Medical Sciences, Department of Pharmacy, Svetozara Markovića 69, 34000 Kragujevac, Serbia and ⁴Center for Harm Reduction of Biological and Chemical Hazards, Faculty of Medical Sciences, University of Kragujevac, Svetozara Markovića 69, 34000 Kragujevac, Serbia

(Received 26 June, revised 23 July, accepted 14 August 2023)

Abstract: ¹H-NMR spectroscopy was used to monitor the reactions of an arylidene 2-thiohydantoin derivative, 3-((phenylmethylene)amino)-2-thioxo-4-imidazolidinone (**3**), with PdCl₂, *cis*-[PdCl₂(dmsO-S)₂] and K₂[PdCl₄] in DMSO-*d*₆ in order to elucidate the reaction kinetics and mechanism. The 2-thiohydantoin derivative **3** formed *cis*-[Pd(**3**-*N,S*)(dmsO-S)₂]⁺ complex (**5**) in reactions with PdCl₂ and *cis*-[PdCl₂(dmsO-S)₂], while no reaction with K₂[PdCl₄] was observed. A two-step mechanism for the reactions of **3** with PdCl₂ and *cis*-[PdCl₂(dmsO-S)₂] is proposed, in which fast coordination to the side chain nitrogen occurs in the first step, while chelation and coordination to the sulfur atom in the 2-thiohydantoin ring is the second, slower, rate-determining step. The reaction rate constants were calculated and reactivities of the 2-thiohydantoin derivative **3** towards the palladium(II) salts were compared and discussed. Reaction of **3** with *cis*-[PdCl₂(dmsO-S)₂] was faster than with PdCl₂. The investigated palladium(II) salts also react with the solvent, DMSO-*d*₆, and the influence of these side reactions on the outcome and kinetics of the 2-thiohydantoin derivative complexation reaction is discussed in detail. The obtained results of this study can have an impact in explanation of the coordination behavior of antitumor active palladium(II) and platinum(II) complexes.

Keywords: ¹H-NMR spectroscopy; reaction mechanism; 2-thioxo-4-imidazolidinone; coordination; Pd(II) complexes.

*,** Corresponding authors. E-mail: (*)petar.stanic@uni.kg.ac.rs; (**)mzikvovic@kg.ac.rs
Serbian Chemical Society member.
<https://doi.org/10.2298/JSC230626052S>

INTRODUCTION

Thiohydantoins are sulphur derivatives of hydantoin, in which one or both of the carbonyl groups in the cyclic ureide structure are replaced with a thiocarbonyl group.¹ Out of this class of compounds, 2-thiohydantoins are certainly the most prominent and extensively researched. 2-Thiohydantoins represent a valuable molecular scaffold, exhibiting various biological and pharmacological activities and they have found applications in both medicine and industry.^{2,3} They display a wide range of biological activities, such as antibacterial and antifungal,⁴ anti-HIV,⁵ anticarcinogenic,^{6,7} anti-ulcer and anti-inflammatory,⁸ anticonvulsive,⁹ antimutagenic¹⁰ and antimelanogenic.¹¹ 2-Thiohydantoins found various applications in industry, such as C-terminal protein sequencing standards,¹² textile printing reagents¹³ and polymerization and complexation catalysts.¹⁴

Coordination of active compounds with biologically relevant transition metal ions can, at times, increase their activities, especially in regards to anticarcinogenic activity.¹⁵ A newer, hybrid approach, in discovering new potential antitumor agents is coordination of active compounds with metal ions in order to improve their activity and selectivity.^{16,17} 2-Thiohydantoins have a great affinity for coordination with transition metal ions.^{18,19} Even though it is a small molecule, 2-thiohydantoin has four derivatization points, making its derivatives very versatile ligands. In addition to the heteroatoms in the ring, 2-thiohydantoin derivatives most often contain heteroatoms in the side chains of its substituents. Many kinds of various 2-thiohydantoin complexes have been synthesized and reported so far.^{20–26} In particular, transition metal complexes of arylidene 2-thiohydantoin derivatives have been researched extensively, largely due to the biological activities they exhibit, primarily antimicrobial and anticancer.^{21,27,28}

The aim of this study was to investigate the kinetics and mechanism of the coordination reactions of 3-((phenylmethylene)amino)-2-thioxo-4-imidazolidinone, an arylidene 2-thiohydantoin derivative, with some palladium(II) salts. As arylidene 2-thiohydantoin metal complexes, palladium(II) in particular,²⁸ show some promise as prospective antitumor agents, a better understanding of the mechanisms of their formation, coordination modes and kinetics might prove beneficial for the design and conceptualization of novel, more potent compounds.

EXPERIMENTAL

Materials and methods

All chemicals and reagents used in this investigation were commercially obtained (from either Sigma–Aldrich or Acros) and were high in purity. They were used as received, without additional purification. NMR spectra were recorded on a Varian Gemini-2000 spectrometer at 50 and 200 MHz. DMSO-*d*₆ was used as the solvent and all chemical shifts were referenced accordingly. Downfield shifts were recorded as positive numbers. Tetramethylsilane was used as the internal reference and all chemical shifts were rounded to the nearest 0.01 ppm.

Synthesis and characterization of 3-((phenylmethylene)amino)-2-thioxo-4-imidazolidinone (3)

3-((Phenylmethylene)amino)-2-thioxo-4-imidazolidinone (**3**) was synthesized using a slight modification of the formerly published procedure.²⁸ Benzaldehyde (0.01 mol) and thiosemicarbazide (0.01 mol) in methanol (30 mL) were heated for 3 h under reflux and cooled thereafter. Ethyl chloroacetate (0.01 mol) and anhydrous sodium acetate (0.03 mol) were added *in situ* and the mixture was heated for another 6 h under reflux. Upon the completion of the reaction, the mixture was cooled at room temperature and then added to cold water, for the resulting product to precipitate. The product was filtered off, rinsed with hot water, dried and re-crystallized from hot methanol. Structure and purity of the compound was confirmed by NMR (¹H and ¹³C) and IR spectroscopy. The corresponding IR and NMR (¹H and ¹³C) spectra, as well as analytical and spectral data are provided in the Supplementary material to this paper.

¹H-NMR kinetic experiments

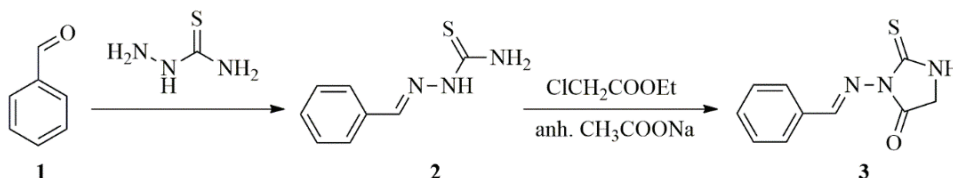
¹H-NMR kinetic measurements of the reactions of 3-((phenylmethylene)amino)-2-thioxo-4-imidazolidinone (**3**) (0.021 mmol) with PdCl₂, *cis*-[PdCl₂(dms_o-S)₂] and K₂[PdCl₄] (0.021 mmol) in DMSO-*d*₆ (0.6 mL) were performed in standard 5 mm NMR tubes at room temperature in an overnight experiment. DMSO-*d*₆ solutions of the reactants (0.3 mL each) were freshly prepared right before the start of the experiment. After the mixing of the reactants, 29 spectra in total were recorded overnight for each of the experiments. The first six spectra were recorded with no delay, then the next three with a 5 min delay, then sets of three every 10, 15 and 30 min, and finally the last 11 spectra were recorded with an hour delay between them. The concentrations of the products at given experiment intervals were determined by integrating suitable proton signals in the ¹H-NMR spectra. The first-order rate constants were determined according to:

$$\ln c = -kt + \ln c_0 \quad (1)$$

where *c* is concentration, *c*₀ is starting concentration, *k* is the first-order rate constant and *t* is experiment time.

RESULTS AND DISCUSSION

3-((Phenylmethylene)amino)-2-thioxo-4-imidazolidinone (**3**) was synthesized from benzaldehyde in a reaction with thiosemicarbazide (Scheme 1). Nucleophilic addition of thiosemicarbazide to benzaldehyde (**1**) yields thiosemicarbazone (**2**). Thiosemicarbazone (**2**) then undergoes a cyclocondensation reaction with ethyl chloroacetate in the presence of anhydrous sodium acetate, forming the arylidene 2-thiohydantoin derivative, 3-((phenylmethylene)amino)-2-thioxo-4-imidazolidinone (**3**).



Scheme 1. Synthesis of 3-((phenylmethylene)amino)-2-thioxo-4-imidazolidinone (**3**).

For the purpose of investigating the kinetics and mechanism of 3-arylidene-2-thiohydantoin coordination with Pd(II), a kinetic time-dependent experiment, monitoring the reactions of 3-((phenylmethylene)amino)-2-thioxo-4-imidazolidinone (**3**) with PdCl₂, *cis*-[PdCl₂(dms_o-S)₂] and K₂[PdCl₄] in DMSO-*d*₆, was performed. DMSO-*d*₆ was used because it is suitable for dissolving both the 2-thiohydantoin derivative and the metal salts. Coordination of **3** to Pd(II) was tracked through the changes in specific signals in the spectra.

¹H-NMR spectra of the reaction of 3-((phenylmethylene)amino)-2-thioxo-4-imidazolidinone (**3**) with *cis*-[PdCl₂(dms_o-S)₂] in DMSO-*d*₆ are shown in Fig. 1. Signals of the coordinated 3-((phenylmethylene)amino)-2-thioxo-4-imidazolidinone (**3**) can be observed, even from the first spectrum.

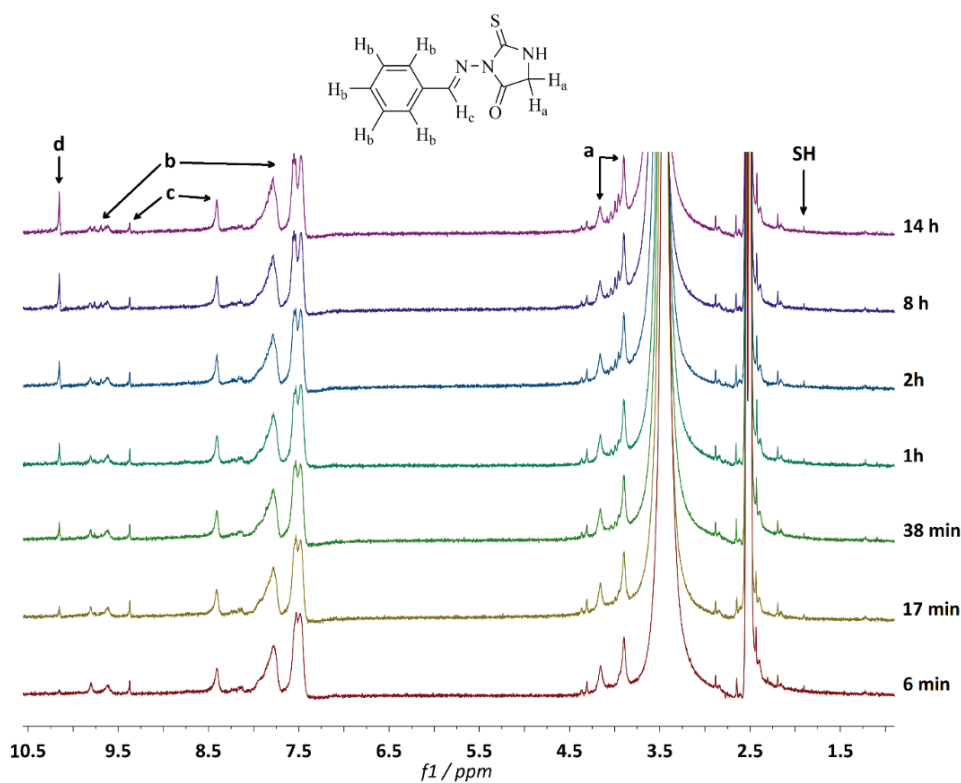
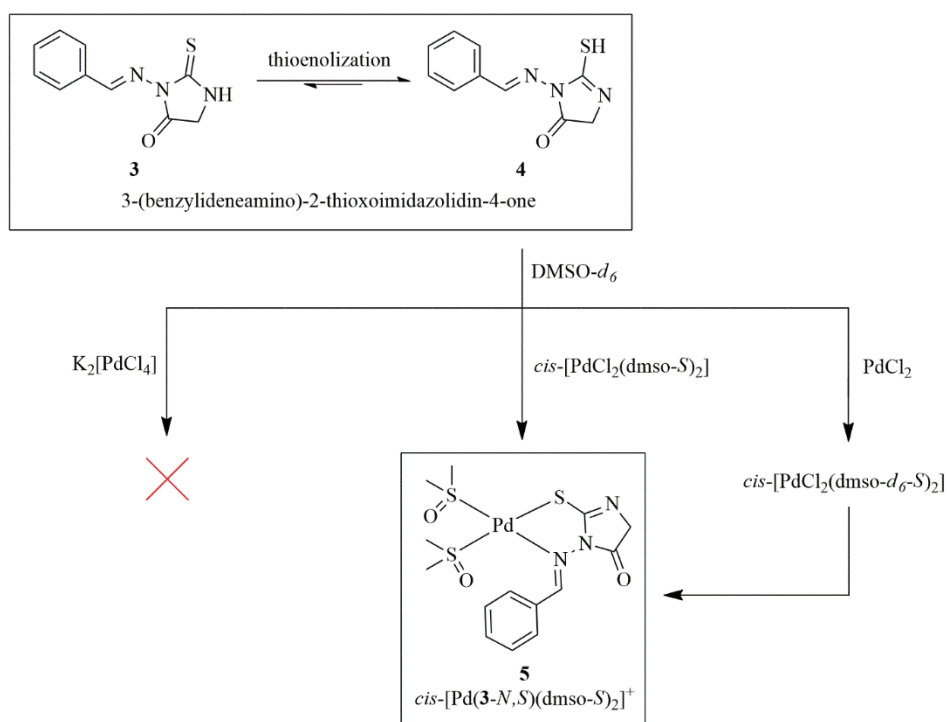


Fig. 1. Time-dependent ¹H-NMR spectra of the reaction of 3-((phenylmethylene)amino)-2-thioxo-4-imidazolidinone (**3**) and *cis*-[PdCl₂(dms_o-S)₂] in DMSO-*d*₆.

As can be seen from Fig. 1, the singlet of the 2-thiohydantoin ring CH₂ group (a) is shifted downfield from 3.90 to 4.15 ppm. Multiplets of the aromatic benzene ring protons (b) moved downfield from 7.25–7.95 to 9.57–9.84 ppm, while the singlet of the double bond CH proton (c) is shifted downfield from 8.41

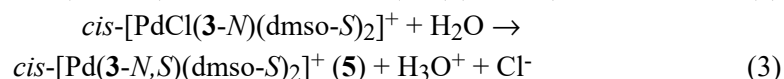
to 9.37 ppm. Signals of the coordinated 2-thiohydantoin derivative (a, b and c) can be observed from the first spectrum and their intensities do not change throughout the experiment. This, in fact, indicates fast initial coordination, too fast for the NMR time-scale.

One more thing that implies coordination is the absence of the broad singlet of the 2-thiohydantoin ring NH proton. 2-Thiohydantoin is known to exist in two tautomeric forms in equilibrium (Scheme 2).²⁹ It is proposed that the thio-enol tautomeric form (**4**) is responsible for coordination and furthermore, that this “keto-enol” equilibrium shifts to the thio-enol form during the reaction.²⁷ The SH protons of the thio-enol tautomer can be seen in the spectra as a singlet at 1.85 ppm (Fig. 1). Furthermore, a newly formed singlet at 10.15 ppm (d) can be observed increasing in intensity throughout the experiment. The new singlet at 10.15 ppm belongs to hydrochloric acid that forms from the deprotonation of the 2-thiohydantoin ring and the chloride anions that are substituted from *cis*-[PdCl₂(dms_o-S)₂].



Scheme 2. Reactions of 3-((phenylmethylene)amino)-2-thioxo-4-imidazolidinone (**3**) with PdCl₂, *cis*-[PdCl₂(dms_o-S)₂] and K₂[PdCl₄]. No reaction of **3** was observed with K₂[PdCl₄] during the course of the experiment (see Fig. S-4).

The reaction as a whole is proposed to proceed in two steps. In the first step (Eq.(2), initial coordination takes place through the nitrogen in the side chain. This is the faster reaction step, which is supported by the presence of the signals of the complex (a, b and c) in the first spectrum of the experiment, that then do not change in intensity during the experiment. The second, slower reaction step is diprotonation of the 2-thiohydantoin ring and coordination through the sulfur atom in the ring (Eq (3)). The resulting complex (**5**) is a five-membered chelate with palladium(II) coordinated to the 2-thiohydantoin ring sulfur and the double bond nitrogen in the side chain:



Even though the spectral data clearly shows a reaction between the 2-thiohydantoin derivative **3** and $cis-[PdCl_2(dms\text{-}S)_2]$, it does not necessarily give a clear insight in the chemistry of reaction beyond modes of coordination. Concentrations of the formed complex **5** were calculated by integration of the suitable proton signal at 10.15 ppm (Fig. 2). As hydrochloric acid forms equimolarly with the complex **5**, according to Eq. (3), concentrations determined from that signal can be regarded as concentrations of complex **5**. The singlet at 10.15 ppm was integrated against the singlet of the uncoordinated 2-thiohydantoin derivative **3** at 8.40 ppm. The relative changes of the intensity of the singlet at 10.15 ppm is directly proportional to the change in concentration of complex **5**, and the concentrations were calculated from the relative integral values.

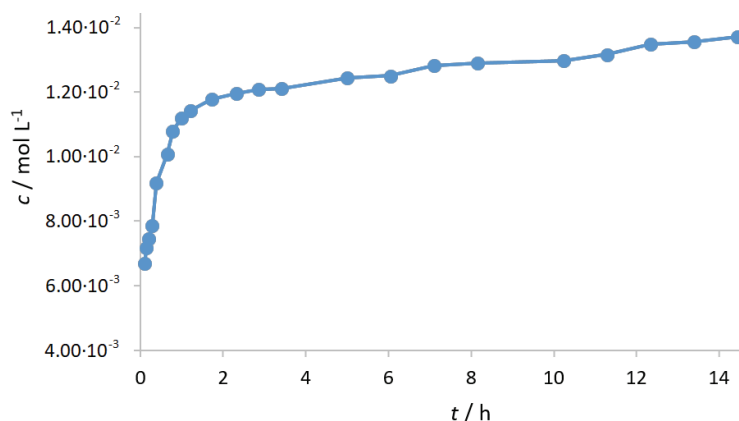


Fig. 2. Changes in product concentration, $cis-[Pd(\mathbf{3-N,S})(dms\text{-}S)_2]^+$, during the substitution reaction of $cis-[PdCl_2(dms\text{-}S)_2]$ with 2-thiohydantoin derivative **3** in $DMSO-d_6$.

It can be seen in the plot that after about an hour into the experiment, complex formation slows down drastically. If we take into consideration the stoichio-

metry of the system, at the end of the experiment, more than half of the initial amount of the 2-thiohydantoin derivative **3** has not undergone any sort of reaction, implying that the reaction system is a bit more complex and that *cis*-[PdCl₂(dmsO-S)₂] undergoes multiple competing reactions.

In order to gain a deeper insight into the details of the mechanism of the reaction, a plot of the logarithm of the product concentration vs experiment time was analyzed (Fig. 3). In the plot, it is clearly visible that this is not a linear first-order reaction, but instead, two linear slopes can be observed. This goes along with the conclusion that multiple processes are occurring, not just the reaction of *cis*-[PdCl₂(dmsO-S)₂] with 2-thiohydantoin derivative **3**. For the first hour, the reaction direction can be described with the equation $y = (1.63 \pm 0.17) \times 10^{-4}x - 5.01$. After about an hour, the reaction kinetics change course and the new direction can be described with the equation $y = (3.36 \pm 0.20) \times 10^{-6}x - 4.46$. The first phase of the reaction is significantly faster, with the slope coefficient $k_1 = 1.63 \times 10^{-4} \text{ s}^{-1}$, than the second phase with the coefficient $k_2 = 3.36 \times 10^{-6} \text{ s}^{-1}$. A change in the system occurred and a chemical species emerged, the concentration of which has only become significant after an hour into the experiment.

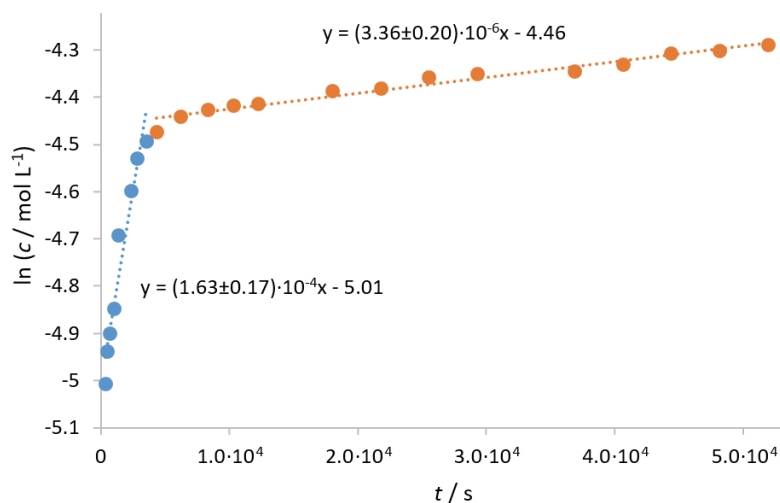
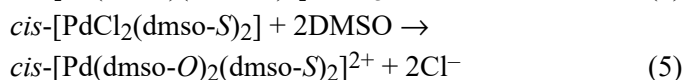
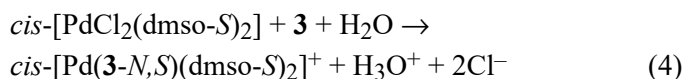


Fig. 3. First-order plot for the substitution reaction of *cis*-[PdCl₂(dmsO-S)₂] with 2-thiohydantoin derivative **3** in DMSO-*d*₆.

cis-[PdCl₂(dmsO-S)₂] most likely engages in a parallel reaction with the solvent, as it is known that *cis*-[PdCl₂(dmsO-S)₂] can react with DMSO, yielding *cis*-[Pd(dmsO-O)₂(dmsO-S)₂]²⁺.^{30,31} *cis*-[PdCl₂(dmsO-S)₂] has two molecules of DMSO in *cis*-configuration bonded through sulfur atoms. DMSO molecules coordinated through the sulfur atoms exhibit a very strong *trans* effect on the neighbouring chlorido ligands, which in turn weakens their bonds with palla-

dium(II). With this in mind, *cis*-[PdCl₂(dmsO-S)₂], apart from reaction with the 2-thiohydantoin derivative **3**, reacts with DMSO, forming tetrakis(dimethyl sulphoxide)palladium(II), *cis*-[Pd(dmsO-O)₂(dmsO-S)₂]²⁺, with the other two DMSO molecules bonded through the oxygen. There is a slight deviation from the ideal square-planar structure in *cis*-[Pd(dmsO-O)₂(dmsO-S)₂]²⁺, the biggest of which being the angle between the two sulfur bonded DMSO molecules, due to steric repulsions between the methyl groups of one DMSO and the sulfoxy group of the other. These steric repulsions prohibit the *S*-bonding of the other DMSO molecules, which is believed to be the main reason for coordination through oxygen.³⁰

Two parallel reactions of *cis*-[PdCl₂(dmsO-S)₂] take place during the experiment. The first is with the 2-thiohydantoin derivative **3** (Eq. (4)) and the other is with the solvent, DMSO, Eq. (5):



The reaction is faster in the first phase, during the first hour of the experiment ($k_1 = 1.63 \times 10^{-4} \text{ s}^{-1}$), up until a dynamic equilibrium is achieved and a significant amount of *cis*-[Pd(dmsO-O)₂(dmsO-S)₂]²⁺ is formed, then the complex formation reaction (Eq (4)) slows down in the second phase ($k_2 = 3.36 \times 10^{-6} \text{ s}^{-1}$), because there is a significantly smaller amount of the reactant, *cis*-[PdCl₂(dmsO-S)₂], in the system.

Coordination of 3-((phenylmethylene)amino)-2-thioxo-4-imidazolidinone (**3**) in the reaction with PdCl₂ takes place in the same manner as with *cis*-[PdCl₂(dmsO-S)₂]. All the same signals with identical chemical shifts can be observed in the spectra of the reaction (Fig. 4). Pairs of signals of the coordinated and uncoordinated **3**, among which are singlets of the 2-thiohydantoin ring CH₂ group protons (a), multiplets of the aromatic benzene ring protons (b) and singlets of the double bond CH proton (c), can be seen at the same chemical shift in the spectra. Thio-enol tautomer –SH proton is at 1.85 ppm, the broad singlet of the 2-thiohydantoin ring –NH proton is missing and the HCl singlet at 10.15 ppm increases throughout the experiment.

Upon calculating the concentrations of the formed *cis*-[Pd(**3**-*N,S*)(dmsO-S)₂]⁺ complex (**5**, Eq. (3)) from the spectral data, an obvious difference in reaction rates was observed and it was noticed that the reaction with PdCl₂ is slower than with *cis*-[PdCl₂(dmsO-S)₂]. Changes in complex **5** concentrations over the course of the experiment are shown in Fig. 5. The difference in the kinetics of the systems are somewhat perplexing, as spectral data confirms that the same reaction product is formed in both cases.

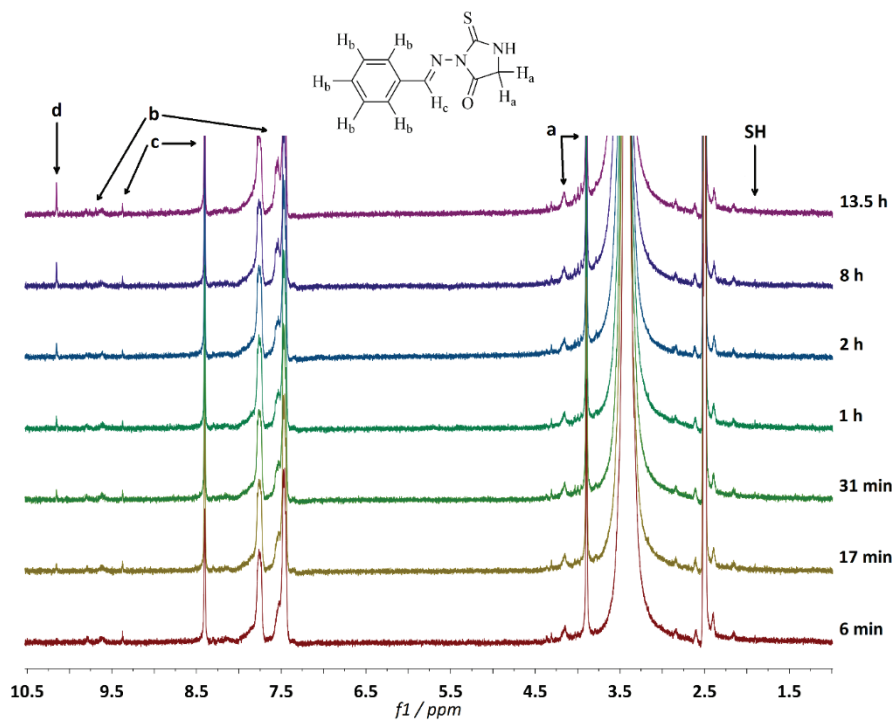


Fig. 4. Time-dependent $^1\text{H-NMR}$ spectra of the reaction of 3-((phenylmethylene)amino)-2-thioxo-4-imidazolidinone (**3**) and PdCl_2 in $\text{DMSO-}d_6$.

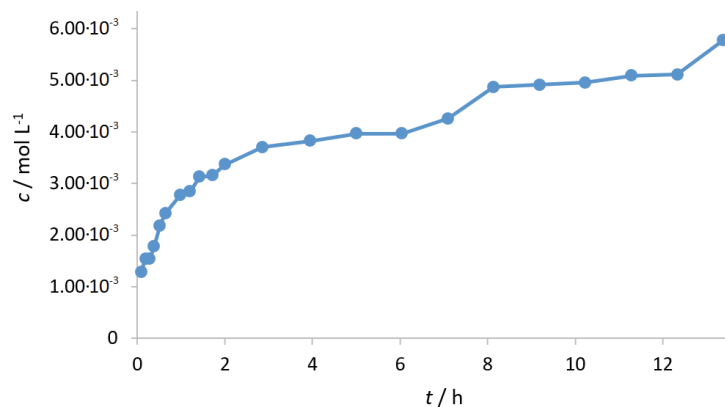
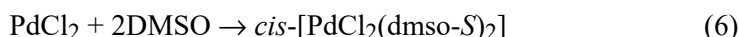


Fig. 5. Changes in $\text{cis-}[\text{Pd}(\mathbf{3-N,S})(\text{dmsO-S})_2]^+$ complex (**5**) concentration during the substitution reaction of PdCl_2 with 2-thiohydantoin derivative **3** in $\text{DMSO-}d_6$.

In order to get to the bottom of this, a plot of the logarithm of the product concentration vs. experiment time was analyzed (Fig. 6). As with $\text{cis-}[\text{PdCl}_2(\text{dmsO-S})_2]$, in this case there are also two phases, with two linear slopes

that intercept after little over an hour. The first phase can be described with the equation $y = (1.80 \pm 0.22) \times 10^{-4}x - 6.59$, while the second phase can be described with the equation $y = (1.25 \pm 0.09) \times 10^{-5}x - 5.77$. The first phase, where most of the complex is formed, has a coefficient $k_1 = 1.80 \times 10^{-4} \text{ s}^{-1}$, which is very close to the slope coefficient of the first phase of the reaction of $cis\text{-}[\text{PdCl}_2(\text{dms}\text{-}\text{S})_2]$ ($k_1 = 1.63 \times 10^{-4} \text{ s}^{-1}$). It is known that PdCl_2 has great affinity towards DMSO and reacts with it to form $cis\text{-}[\text{PdCl}_2(\text{dms}\text{-}\text{S})_2]$,³² according to:



It can be concluded that in both cases, basically the same reaction occurs (Eq. (4)), which is supported by the very close values of the reaction coefficients k_1 . The reaction is slower with PdCl_2 because the salt itself does not react with the 2-thiohydantoin derivative **3**. Only when a sufficient amount of $cis\text{-}[\text{PdCl}_2(\text{dms}\text{-}\text{S})_2]$ forms does the reaction take place. The lower rate of the reaction with PdCl_2 can be explained with the lower reactant concentration.

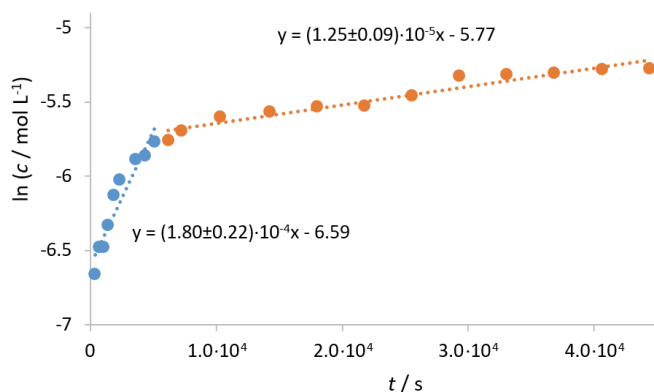


Fig. 6. First-order plot for the substitution reaction of PdCl_2 with 2-thiohydantoin derivative **3** in $\text{DMSO-}d_6$.

In the case of the third examined palladium(II) salt, $\text{K}_2[\text{PdCl}_4]$, there was no reaction with 3-((phenylmethylene)amino)-2-thioxo-4-imidazolidinone (**3**) during the course of the experiment. No signals of a newly formed 2-thiohydantoin complex species of any kind could be observed (Fig. S-4). The four chlorido ligands in $\text{K}_2[\text{PdCl}_4]$ are kinetically equivalent and a strong possibility is that all of them were substituted with DMSO, as tetrachloroplatinate(II) and also tetrachloropalladate(II) can react with DMSO in this manner.³³ This would prohibit the reaction with the 2-thiohydantoin derivative **3**.

CONCLUSION

Reactions of an arylidene 2-thiohydantoin derivative, 3-((phenylmethylene)amino)-2-thioxo-4-imidazolidinone (**3**) with PdCl_2 , $cis\text{-}[\text{PdCl}_2(\text{dms}\text{-}\text{S})_2]$ and

$K_2[PdCl_4]$ in $DMSO-d_6$ were monitored in a time-dependent kinetic 1H -NMR experiment. In the cases of $PdCl_2$ and $cis-[PdCl_2(dmsO-S)_2]$, the complex $cis-[Pd(3-N,S)(dmsO-S)_2]^+$ (**5**) was formed, with palladium(II) coordinated through the nitrogen in the side chain and the 2-thiohydantoin ring sulfur atom. The mechanism of complex **5** formation consists of two steps. The first step is fast monodentate coordination of **3** via its nitrogen atom in the side chain. This step is too fast for the NMR time-scale, but it is confirmed with the corresponding signals of the complex **5** that are unchanged during the course of the experiment. The second, rate determining step of the reaction is chelation of the intermediate $cis-[PdCl(3-N)(dmsO-S)_2]^+$ complex through deprotonation of the 2-thiohydantoin ring of **3** and its coordination with the sulfur atom, finally yielding to the formation of complex **5**. Most of the complex **5** is formed during the first hour of the experiment. It is concluded that simultaneously, a competing reaction with the solvent occurs during which $cis-[Pd(dmsO-O)_2(dmsO-S)_2]^{2+}$ is formed, which ultimately halts the reaction. No reaction with $K_2[PdCl_4]$ was observed during the course of the experiment.

Acknowledgements: The authors are grateful for financial support from the Ministry of Education, Science and Technological Development of the Republic of Serbia (Agreements Numbers 451-03-68/2022-14/200378, 451-03-68/2022-14/200252 and 451-03-47/2023-01/200111) and the Faculty of Medical Sciences, University of Kragujevac (JP02/20).

SUPPLEMENTARY MATERIAL

Additional data and information are available electronically at the pages of journal website: <https://www.shd-pub.org.rs/index.php/JSCS/article/view/12456>, or from the corresponding author on request. CCDC 2269543-2269546.

ИЗВОД

КИНЕТИЧКО ИСПИТИВАЊЕ РЕАКЦИЈА 3-АРИЛИДЕНСКОГ ДЕРИВАТА 2-ТИОХИДАНТОИНА СА СОЛИМА ПАЛАДИЈУМА(II)

ПЕТАР Б. СТАНИЋ¹, ДАРКО П. АШАНИН¹, ТАЊА В. СОЛДАТОВИЋ² и МАРИЈА Д. ЖИВКОВИЋ^{3,4}

¹Универзитет у Крагујевцу, Институт за информационе технологије, Сектор за природно-машињачке науке, Јована Цвијића бб, 34000 Крагујевац, ²Државни универзитет у Новом Пазару, Дејаршман за природно-машињачке науке, Вука Караџића 9, 36300 Нови Пазар, ³Универзитет у Крагујевцу, Факултет медицинских наука, Дејаршман за фармацију, Светозара Марковића 69, 34000 Крагујевац и ⁴Центар за смањење штетности биолошких и хемијских хазарда, Факултет медицинских наука, Универзитет у Крагујевцу, Светозара Марковића 69, 34000 Крагујевац

Протонска НМР спектроскопија је употребљена за праћење реакције арилиденског деривата 2-тиохидантоина, 3-((фенилметил)амино)-2-тиоксо-4-имидазолидинона (**3**), са $PdCl_2$, $cis-[PdCl_2(dmsO-S)_2]$ и $K_2[PdCl_4]$ у $DMSO-d_6$, да би се испитали кинетика и механизам реакције. Испитивани дериват 2-тиохидантоина **3** је награтио комплекс $cis-[Pd(3-N,S)(dmsO-S)_2]^+$ (**5**) у реакцији са $PdCl_2$ и $cis-[PdCl_2(dmsO-S)_2]$, док са $K_2[PdCl_4]$ није уочена реакција. Претпостављен је двостепени механизам за реакције **3** са $PdCl_2$ и $cis-[PdCl_2(dmsO-S)_2]$, у коме се у првом кораку одиграва брза координација за азот из бочног низа, а хелатизација и координовање за тиохидантоински сумпор је други, спорији корак, који одређује брзину реакције. Израчунате су константе брзине реакције и реак-

тивности деривата 2-тиохидаптоина **3** према солима паладијума(II) су упоређене и дискутоване. Реакција **3** са *cis*-[PdCl₂(dmsO-S)₂] је била бржа од реакције са PdCl₂. Испитиване соли паладијума(II) су такође реаговале са растварачем (DMSO-*d*₆) и утицај ових реакција на исход и кинетику реакције комплексирања деривата 2-тиохидаптоина је детаљно дискутован. Резултати добијени у оквиру овог истраживања могу имати утицај на појашњење координационог понашања антитуморски активних комплекса паладијума(II) и платине(II).

(Примљено 26. јуна, ревидирано 23. јула, прихваћено 14. августа 2023)

REFERENCES

1. M. A. Metwally, E. Abdel-Latif, *J. Sulfur Chem.* **33** (2012) 229 (<https://www.doi.org/10.1080/17415993.2011.643550>)
2. S. H. Cho, S. H. Kim, D. Shin, *Eur. J. Med. Chem.* **164** (2019) 517 (<https://doi.org/10.1016/j.ejmech.2018.12.066>)
3. P. P. Gawas, B. Ramakrishna, N. Veeraiah, V. Nutalapati, *J. Mater. Chem., C* **9** (2021) 16341 (<https://www.doi.org/10.1039/D1TC04090A>)
4. J. Marton, J. Enisz, S. Hosztafi, T. Timar, *J. Agr. Food Chem.* **41** (1993) 148 (<https://www.doi.org/10.1021/jf00025a031>)
5. A. I. Khodair, H. I. el-Subbagh, A. A. el-Emam, *Boll. Chim. Farm.* **136** (1997) 561 (<https://pubmed.ncbi.nlm.nih.gov/9440349>)
6. A. M. Al-Obaid, H. I. El-Subbagh, A. Khodair, M. M. A. Elmazar, *Anti-cancer Drug* **7** (1996) 873 (<https://www.doi.org/10.1097/00001813-199611000-00009>)
7. S. Suzen, E. Buyukbingol, *Farmaco* **55** (2000) 246 ([https://www.doi.org/10.1016/S0014-827X\(00\)00028-8](https://www.doi.org/10.1016/S0014-827X(00)00028-8))
8. A. C. W. Curran, *U.S. Patent 3,984,430* (1976)
9. M. M. W. Habib, M. A. O. Abdelfattah, A. H. Abadi, *Arch. Pharm.* **348** (2015) 868 (<https://www.doi.org/10.1002/ardp.201500272>)
10. A. Takahashi, H. Matsuoka, Y. Uda, *Environ. Mutagen Res.* **26** (2004) 1 (<https://www.doi.org/10.3123/jems.26.1>)
11. H. R. Kim, H. J. Lee, Y. J. Choi, Y. J. Park, Y. Woo, S. J. Kim, M. H. Park, H. W. Lee, P. Chun, H. Y. Chung, H. R. Moon, *Med. Chem. Commun.* **5** (2014) 1410 (<https://www.doi.org/10.1039/C4MD00171K>)
12. B. Mo, J. Li, S. Liang, *Anal. Biochem.* **252** (1997) 169 (<https://www.doi.org/10.1006/abio.1997.2278>)
13. J. Nelson, M. Helber, M. Brick, *U.S. Patent 5,695,917* (1997)
14. S. S. Kandil, G. B. El-Hefnawy, E. A. Baker, *Thermochim. Acta* **414** (2004) 105 (<https://www.doi.org/10.1016/j.tca.2003.11.021>)
15. J. A. Crim, H. G. Petering, *Cancer Res.* **27** (1967) 1278 (<https://pubmed.ncbi.nlm.nih.gov/4952520>)
16. V. R. Martínez, M. V. Aguirre, J. S. Todaro, E. G. Ferrer, P. A. M. Williams, *Biol. Trace Elem. Res.* **197** (2020) 454 (<https://www.doi.org/10.1007/s12011-019-02013-w>)
17. M. Pitucha, A. Korga-Plewko, A. Czynkowska, B. Rogalewicz, M. Drozd, M. Iwan, J. Kubik, E. Humeniuk, G. Adamczuk, Z. Karczmarzyk, E. Fornal, W. Wysocki, P. Bartnik, *Int. J. Mol. Sci.* **22** (2021) 3104 (<https://www.doi.org/10.3390/ijms22063104>)
18. R. M. El-Bahnasawy, M. M. Shoukry, M. M. Hussein, *J. Chem. Sci.* **96** (1986) 309 (<https://www.doi.org/10.1007/BF02895726>)
19. D. C. Dash, F. M. Meher, P. C. Mohanty, J. Nanda, *Indian J. Chem., A* **26** (1987) 698 (<http://nopr.niscpr.res.in/handle/123456789/47907>)

20. S. Abdullah, R. Al Hassani, A. J. Atia, A. Hussein, *Acta Chim. Pharm. Indica* **6** (2016) 80 (<https://www.tsijournals.com/abstract/synthesis-characterization-and-enzyme-activity-of-coii-niii-cuii-pdii-ptiv-and-cdii-complexes-with-2thioxoimidazolidin4o-11471.html>)
21. K. Tishchenko, E. Beloglazkina, M. Proskurnin, V. Malinnikov, D. Guk, M. Muratova, O. Krasnovskaya, A. Udina, D. Skvortsov, R. R. Shafikov, Y. Ivanenkov, V. Aladinskiy, I. Sorokin, O. Gromov, A. Majouga, N. Zyk, *J. Inorg. Biochem.* **175** (2017) 190 (<https://www.doi.org/10.1016/j.jinorgbio.2017.07.015>)
22. A. Fedorchuk, E. Goreshnik, Y. Slyvka, M. Mys'kiv, *Acta Chim. Slov.* **67** (2020) 1148 (<https://www.doi.org/10.17344/acsi.2020.6045>)
23. P. Arrizabalage, P. Castan, J.-P. Laurent, *Transit. Met. Chem.* **5** (1980) 324 (<https://www.doi.org/10.17344/acsi.2020.6045>)
24. J. S. Casas, E. E. Castellano, M. D. Couce, N. Playá, A. Sánchez, J. Sordo, J. M. Varela, J. Zukerman-Schpector, *J. Coord. Chem.* **47** (1999) 299 (<https://www.doi.org/10.1080/00958979908023062>)
25. R. M. Mahfouz, A. S. El Shahawy, A. A. Hassan, *Transit. Met. Chem.* **19** (1994) 385 (<https://www.doi.org/10.1007/BF00139309>)
26. D. C. Dash, P. Naik, S. K. Naik, R. K. Mohapatra, S. Ghosh, *J. Indian Chem. Soc.* **86** (2009) 969 (<https://doi.org/10.5281/zenodo.5816598>)
27. L. A. Ismail, R. Zakaria, E. M. Hassan, M. Y. Alfaiqi, A. A. Shati, S. E. I. Elbehairi, A. A. El-Bindary, R. F. M. Elshaarawy, *RSC Adv.* **12** (2022) 28364 (<https://www.doi.org/10.1039/D2RA05233D>)
28. B. Šmit, R. Z. Pavlović, A. Radosavljević-Mihailović, A. Došen, M. G. Čurčić, D. S. Šeklić, M. N. Živanović, *J. Serb. Chem. Soc.* **78** (2013) 217 (<https://www.doi.org/10.2298/JSC120725154S>)
29. P. E. Allegretti, M. de las Mercedes Schiavoni, C. Guzmán, A. Ponzinibbio, J. J. P. Furlong, *Eur. J. Mass Spectrom.* **13** (2007) 291 (<https://www.doi.org/10.1255/ejms.885>)
30. B. F. G. Johnson, J. Puga, P. R. Raithby, *Acta Crystallogr., B* **37** (1981) 953 (<https://www.doi.org/10.1107/S0567740881004743>)
31. B. B. Wayland, R. F. Schramm, *Inorg. Chem.* **8** (1969) 971 (<https://www.doi.org/10.1021/ic50074a050>)
32. J. Selbin, W. E. Bull, L. H. Holmes, *J. Inorg. Nucl. Chem.* **16** (1961) 219 ([https://www.doi.org/10.1016/0022-1902\(61\)80493-4](https://www.doi.org/10.1016/0022-1902(61)80493-4))
33. L. I. Elding, A. B. Gröning, *Inorg. Chim. Acta* **31** (1978) 243 ([https://www.doi.org/10.1016/s0020-1693\(00\)95010-2](https://www.doi.org/10.1016/s0020-1693(00)95010-2)).



J. Serb. Chem. Soc. 89 (4) S148–S154 (2024)

SUPPLEMENTARY MATERIAL TO
**Kinetic investigation of reactions of a 3-arylidene-2-thio-
hydantoin derivative with palladium(II) salts**

PETAR B. STANIĆ^{1*}, DARKO P. AŠANIN^{1#}, TANJA V. SOLDATOVIĆ^{2#}
and MARIJA D. ŽIVKOVIĆ^{3,4***}

¹University of Kragujevac, Institute for Information Technologies, Department of Science, Jovana Cvijića bb, 34000 Kragujevac, Serbia, ²State University of Novi Pazar, Department of Natural-Mathematical Sciences, Vuka Karadžića 9, 36300 Novi Pazar, Serbia, ³University of Kragujevac, Faculty of Medical Sciences, Department of Pharmacy, Svetozara Markovića 69, 34000 Kragujevac, Serbia and ⁴Center for Harm Reduction of Biological and Chemical Hazards, Faculty of Medical Sciences, University of Kragujevac, Svetozara Markovića 69, 34000 Kragujevac, Serbia

J. Serb. Chem. Soc. 89 (4) (2024) 443–455

3-((Phenylmethylene)amino)-2-thioxo-4-imidazolidinone (**3**). Yield 1.158 g (72 %). IR (KBr): 3419m, 3055m, 3032w, 2967m, 2768m, 1711s, 1645s, 1591s, 1490w, 1445w, 1409w, 1345m, 1327m, 1310m, 1249s, 1225m, 1213m, 1074w, 1039w, 969m, 877m, 854m, 835m, 788m, 756m, 734m, 713m 695m, 629w cm⁻¹. ¹H NMR (200 MHz, DMSO-*d*₆, δ): 8.40 (s, 1H), 7.75 (m, 2H), 7.45 (m, 3H), 3.89 (s, 2H). ¹³C NMR (50 MHz, DMSO-*d*₆, δ): 174.33, 165.51, 156.31, 134.31, 130.76, 128.96, 127.76, 33.26.

*,** Corresponding authors. E-mail: (*)petar.stanic@uni.kg.ac.rs; (**)mzikvovic@kg.ac.rs

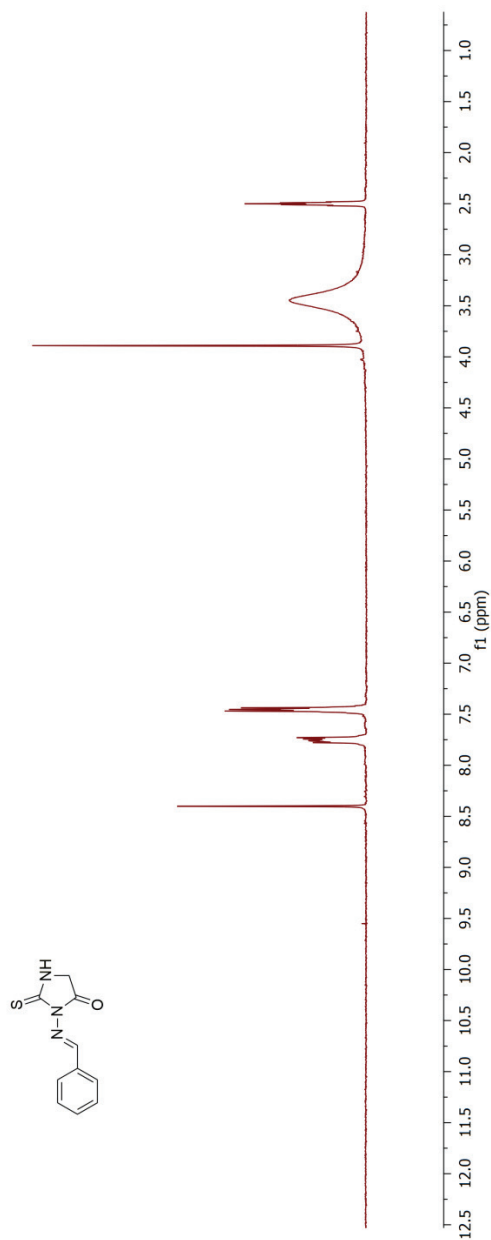


Fig. S-1. ¹H NMR spectra of 3-((phenylmethylene)amino)-2-thioxo-4-imidazolidinone (3).

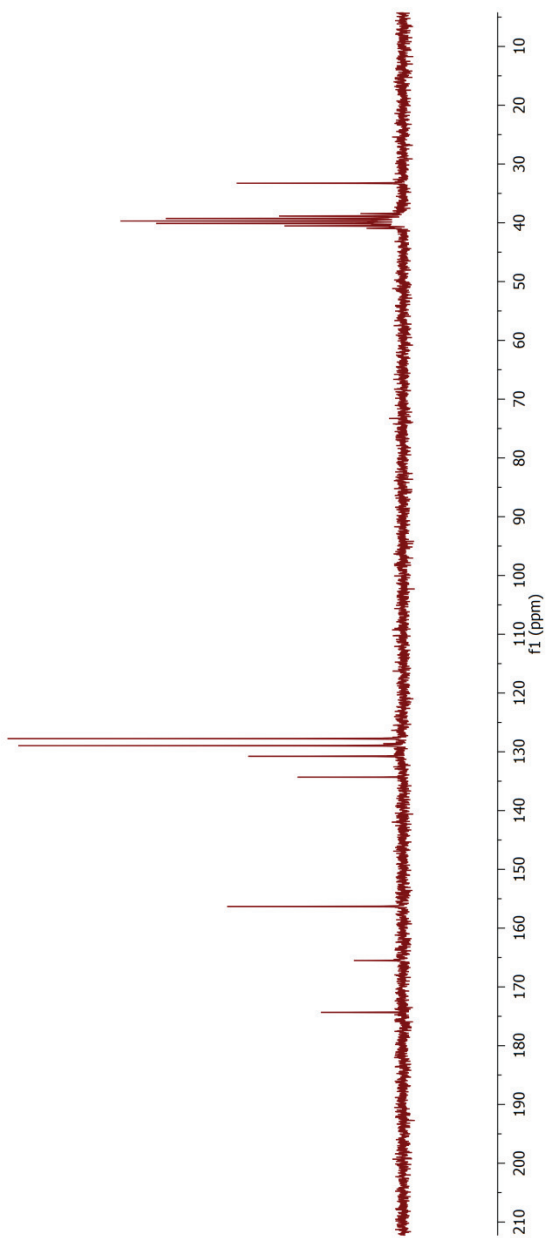


Fig. S-2. ^{13}C NMR spectra of 3-((phenylmethylene)amino)-2-thioxo-4-imidazolidinone (3).

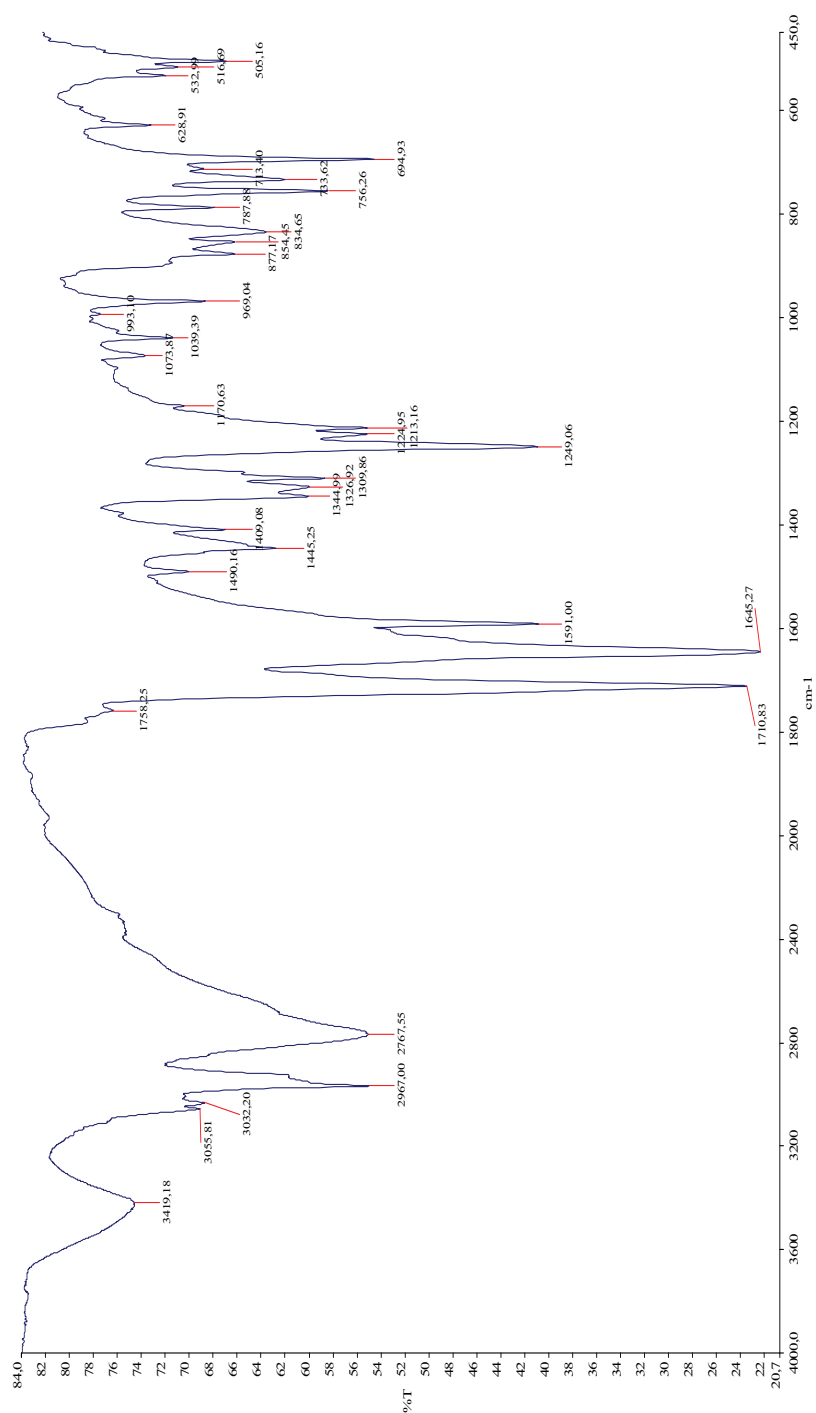


Fig. S-3. IR spectra of 3-((phenylmethylene)amino)-2-thioxo-4-imidazolidinone (3).

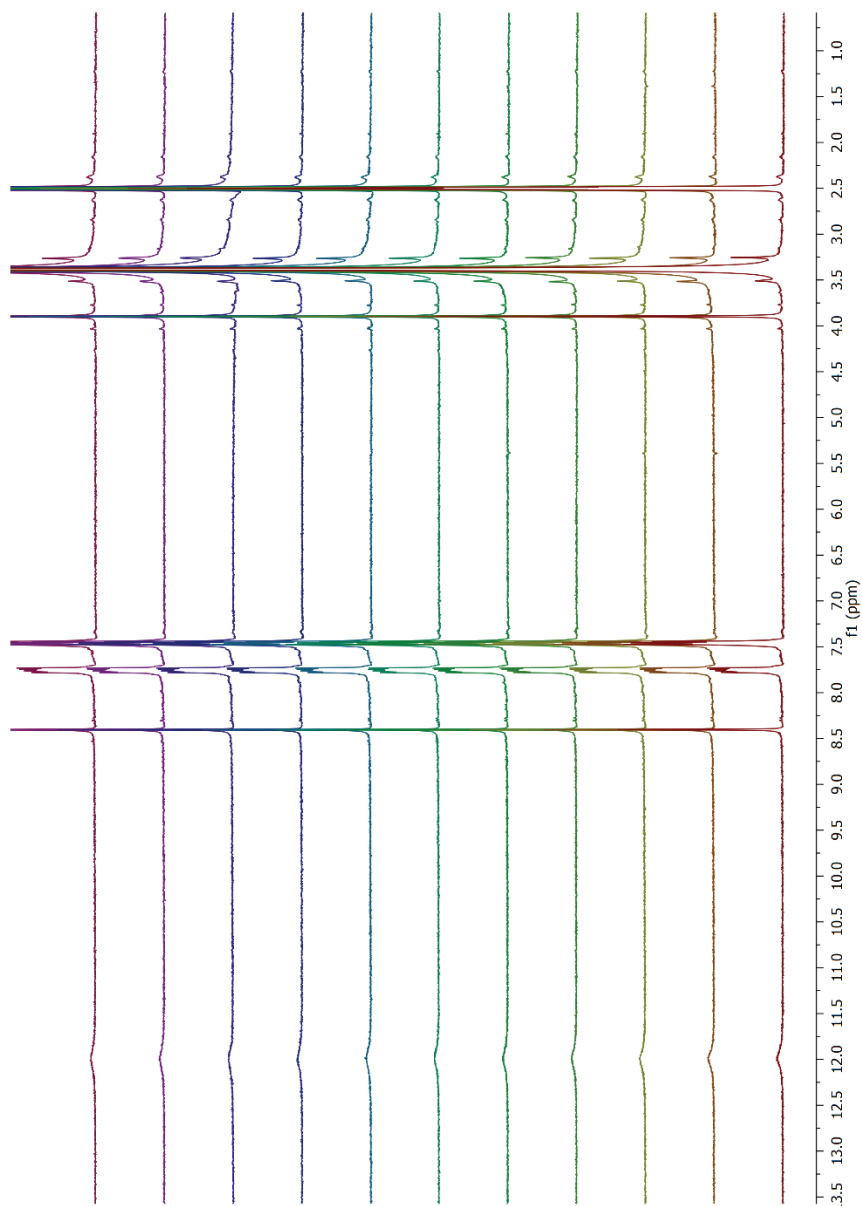


Fig. S-4. ^1H NMR kinetic experiment of 3-((phenylmethylene)amino)-2-thioxo-4-imidazolidinone (**3**) and $\text{K}_2[\text{PdCl}_4]$ in $\text{DMSO-}d_6$. No reaction takes place.

Table S-I. Time and concentration parameters for the reaction of 3-((phenylmethyl-ene)amino)-2-thioxo-4-imidazolidinone (**3**) and *cis*-[PdCl₂(dms-*S*)₂]

<i>t</i> / s	<i>c</i> / mol L ⁻¹	ln (<i>c</i> / mol L ⁻¹)
340	0.006693	-5.00669
512	0.007168	-4.93813
684	0.007443	-4.90048
1028	0.00785	-4.84722
1372	0.009175	-4.69125
2316	0.010082	-4.59697
2788	0.0108	-4.52819
3560	0.011186	-4.4931
4332	0.011415	-4.47287
6176	0.011786	-4.44085
8320	0.011965	-4.42581
10292	0.012082	-4.41601
12264	0.012107	-4.41394
18008	0.01244	-4.38688
21780	0.012507	-4.38144
25552	0.012825	-4.35634
29324	0.012904	-4.35023
36868	0.012972	-4.34499
40640	0.013172	-4.32969
44412	0.013482	-4.30637
48184	0.013561	-4.30056
51956	0.013732	-4.288

Table S-II. Time and concentration parameters for the reaction of 3-((phenylmethyl-ene)amino)-2-thioxo-4-imidazolidinone (**3**) and PdCl₂

<i>t</i> / s	<i>c</i> / mol L ⁻¹	ln (<i>c</i> / mol L ⁻¹)
333	0.001286	-6.65642
677	0.001536	-6.47874
1021	0.001539	-6.47642
1365	0.001782	-6.32992
1837	0.002182	-6.12743
2309	0.002421	-6.02338
3553	0.002779	-5.8858
4325	0.002843	-5.86293
5097	0.003129	-5.76716
6169	0.003157	-5.75807
7241	0.003371	-5.6924
10285	0.003704	-5.59844
14229	0.003829	-5.56524
18001	0.003964	-5.53041
21773	0.003972	-5.52861
25545	0.004261	-5.4583
29317	0.004868	-5.32508
33089	0.004911	-5.31632
36861	0.004957	-5.30691
40633	0.005093	-5.2799
44405	0.005111	-5.2764
48177	0.005779	-5.15358



J. Serb. Chem. Soc. 89 (4) 457–469 (2024)
JSCS–5733

Co-detection of eugenol and butylated hydroxytoluene by green and selective hydrodistillation of *Heliotropium europaeum* L. using ionic liquids as additives

SARA BENDJELLOUL¹, CHOUKRY KAMEL BENEDEDOUCHE^{1*}, SOUHILA BENEDEDOUCHE¹, MADANI SARRI^{2**}, FERIHA BENSAFIDDINE³, NADIA KAMBOUCHE¹, LUDOVIC PAQUIN⁴, MOHAMED YOUSFI⁵ and MOHAMED HARRAT⁵

¹Laboratory of Applied Organic Synthesis, Faculty of Exact and Applied Sciences, University Oran1 Ahmed Ben Bella, BP 1524 El M'Naouer, 31000, Oran, Algeria, ²Faculty of Sciences, University of M'sila, PO Box 166 Ichebilia, 28000 M'sila, Algeria, ³Platform of Physico-Chemical Analysis, PTAPC-Laghout-CRAPC, Laghouat, Algeria, ⁴Université de Rennes 1, Sciences Chimiques de Rennes, UMR CNRS 6226, Groupe Ingénierie Chimique et Molécules pour le Vivant (ICMV), Bât. 10A, Campus de Beaulieu, Avenue du Général Leclerc, CS 74205, 35042 Rennes Cedex, France and ⁵Laboratory of Fundamental Sciences, University Amar Telidji of Laghouat, Laghouat, Algeria

(Received 13 July, revised 26 July, accepted 6 October 2023)

Abstract: This study is the beginning of the research that focuses on unconventional ionic liquids (ILs) hydrodistillation (HD) extraction of the essential oil of *Heliotropium europaeum* L. using ILs as additives. Two ILs based on 1-butyl-3-methylimidazolium were used by switching the anions (Cl⁻ and PF₆⁻). The effect of mass percent of the added ILs on its yield and composition was evaluated. Compared to the conventional HD, ILs-HD gives a higher yield of essential oils (0.10–0.36 %). Particularly, with [C₄mim][PF₆], the observation of morphological changes using scanning electron microscopy (SEM) confirmed the effectiveness of the ionic liquid in this distillation process. The GC–MS analysis of essential oils (EOs) revealed the presence of sixty-six compounds in HD, ILs-HD methods. Gas chromatography–mass spectrometry analysis of the EOs revealed the predominance of eugenol (1.70–72.35 %), butylated hydroxytoluene (8.95–65.39 %) and phytol (18.20 %). The new distillation methods of *H. europaeum* with ILs identifies more compounds (50 compounds in ILs-HD [C₄mim][PF₆]; 22 compounds in ILs-HD ([C₄mim][Cl]) than conventional hydrodistillation (25 compounds in HD). Therefore, the ILs-based hydrodistillation approach is superior in improving the production of EOs. It is important to emphasize that the data presented in this study are not yet available for any of this Algerian *Heliotropium* species of genus and pre-

* Corresponding authors. E-mail: (*kchoukry@yahoo.fr; (**)madani.sarri@univ-msila.dz
<https://doi.org/10.2298/JSC230713075B>

sent the great potential of this medicinal plant as a source of novel bioactive extracts with possible therapeutic uses.

Keywords: Boraginaceae; medicinal plant; essential oils; GC–MS; Algeria.

INTRODUCTION

In recent years, the world has been increasingly interested in using medicinal plants to prevent or treat many diseases, especially during these recent years when plants and essential oils are increased. In fact, essential oils (EOs) are characterized to have several medicinal and biological activities, particularly anticancer, antidiabetic, antimicrobial, anti-inflammatory and antioxidant, which are also used in food preservation.¹ The EOs are a mixture of volatile molecules that include classes of compounds with concentration variability and characterized by the preponderance of terpenes especially, mono and sesquiterpenes.^{2,3}

Among the most used methods in the extraction of essential oils, hydrodistillation (HD) is the most widely used method. For the purposes of enhancing recovery and decreasing extraction time, the traditional hydrodistillation can be facilitated with chemicals,⁴ physical⁵ or biological techniques.⁶ Mainly, ionic liquids (ILs) have recently received great attention and they were considered as green solvents due to their excellent properties such as low vapour tension, non-flammable, thermal stability, selective extraction ability, comprehensive dissolving capacity and excellent structural designability. ILs can be used to pretreat plant material before hydrodistillation⁷ or as an additive during distillation.⁸ As an ideal substitute for volatile organic solvents, the widespread use of ILs can bring even more significant price cuts for EOs extraction. In fact, ILs have been successfully recovered and reused in the hydrodistillation of Eos,⁹ thereby reducing costs.

The genus *Heliotropium* belong to Boraginaceae family includes 250–300 species; the native range of *Heliotropium europaeum* is Macaronesia, Europe to Mediterranean region, Arabian Peninsula and India.¹⁰ The heliotrope name derives from the fact that these plants turn their leaves to the sun.¹¹ Additionally, in Algeria, seven species belong this genus are *H. luteum* Poiret, *H. supinum* L., *H. europaeum* L., *H. strigosum* Willd., *H. curassavicum* L., *H. anchusifolium* Poiret and *H. bacciferum* Forsk.¹² Also, this plant is an herbaceous annual, grows primarily in the subtropical biome and in the crop fields; it is known in Algeria under the name “Daharet ech chems and Aquerbana”.¹² *Heliotropium* genus have been used in traditional medicine for the treatment of acne and cattle wounds,¹³ rheumatism, putrefaction, pyoderma and ringworm infection,¹⁴ snake bites and scorpion stings,¹⁵ ulcers, venereal diseases, sore throat,¹⁶ cough and fever.¹⁷ Also, it has been used externally for healing wounds, and treatment of warts.¹⁸ The genus *Heliotropium* revealed the presence of many biological activities such as antimicrobial, antiviral and antitumor,¹⁹ anti-plasmodial and antitrypano-

somal,²⁰ anti-inflammatory,^{21–23} anti-tuberculosis²⁴ and wound healing.²⁵ Some species of *Heliotropium* have been investigated for their phenolic compounds: kaempferol, silybin, caffeic acid, genistein and apigenin,²⁶ quinones, sterols, flavonoids and triterpenoids.^{27,28} Phytochemical reports on *H. europaeum* are very limited and majority of these studies are focused on the presence of toxins in pyrrolizidine alkaloids.²⁹

In this study, two ILs, 1-butyl-3-methylimidazolium chloride [C₄mim][Cl] and 1-butyl-3-methylimidazolium hexafluorophosphate [C₄mim][PF₆], were used as additives in hydrodistillation which was applied for the extraction of EOs from *H. europaeum*. In addition, the proposed ILs- hydrodistillation (HD) method was compared to the HD method on the yields and chemical composition of essential oils of *H. europaeum*. Besides, ILs have been efficiently recycled and reused in the experiments. As far as we know, the distillation methods using ILs as additives of *H. europaeum* essential oil has not been reported previously in Algeria.

EXPERIMENTAL

Plant material

The aerial parts of *H. europaeum* were collected from Blida district, Algeria in the August 2020. The plant was identified by Dr. W. Khitri and confirmed through the Flora of Algeria¹². The voucher specimen [He/2248QS] was deposited at the herbarium of Pharmacy Department, Faculty of Medicine, Ahmed Ben Bella Oran1 University. The aerial parts were washed to remove soil particles and then dried at room temperature in the shade. In addition, the aerial parts were cut into small pieces and then stored in glassware until use.

Synthesis of ILs

Synthesis of 1-butyl-3-methylimidazolium chloride [C₄mim][Cl]. [C₄mim][Cl] was obtained by reacting 1-methylimidazole with 1-chlorobutane.³⁰ Typically, under an inert atmosphere, a mixture of 1-methylimidazole (9.9997 g, 0.1218 mol, 1 eq.) and 1-chlorobutane (16.9110 g, 0.1872 mol, 1.5 eq.) was introduced in a 100 mL round bottom flask and heated under reflux at 85 °C for 72 h. A viscous pale-yellow liquid was obtained and after cooling to ambient temperature the residue was washed once with ethyl acetate and three times with diethyl ether. Afterwards, the solvent was removed by evaporation under vacuum at 70 °C for 2 h to get [C₄mim][Cl] as a white solid (19.1098 g) obtained in 89.82 % yield, and stored in closed desiccators before use. The purity of the IL was checked by proton and carbon nuclear magnetic resonance (¹H- and ¹³C-NMR) spectrometry and the NMR spectrum characteristic showed no organic impurities in the IL.

Synthesis of 1-butyl-3-methylimidazolium hexafluorophosphate [C₄mim][PF₆]. [C₄mim][PF₆] was obtained by metathesis of the chloride ion of [C₄mim][Cl] using potassium hexafluorophosphate.³¹ 20.0000 g (0.1 mol) of [C₄mim][Cl] salt and 18.4060 g (0.1 mol) of potassium hexafluorophosphate are solubilized in acetonitrile using a 100 mL round bottom flask at room temperature. The mixture was maintained under vigorous agitation for 24 h. Two phases formed and were separated, and then the solvent was removed by evaporation under vacuum, the organic IL phase was washed with water (3×25 mL) until the negative silver nitrate test. The [C₄mim][PF₆] IL was then dried for 6 h under vacuum at 75 °C to afford 12.7717 g of

C₄mim][PF₆] as a light-yellow viscous liquid, and then stored in closed desiccators before use. The purity of the IL was checked by proton and carbon nuclear magnetic resonance (¹H- and ¹³C-NMR) spectrometry and the NMR spectrum characteristic showed no organic impurities in the IL.

Spectral data of the synthesized compounds are given in Supplementary material to this paper.

Sample preparation

Hydrodistillation was carried out for three hours using water recycling Dean-stark type apparatus, according to the European Pharmacopoeia. The plant material (20 g) was chopped into small pieces and mixed with different ionic liquids solutions (200 mL) of [C₄mim][Cl] with respective concentrations of 0, 2.5, 5 and 10 %. In the case of [C₄mim][PF₆], only a concentration of 5 % was used. The mixture was put in a 500 mL round bottom flask, and then a Dean-stark type apparatus was connected. After that, the round bottom flask was placed onto a heating mantle for 3 h. Then, the essential oil was collected, dehydrated with anhydrous Na₂SO₄, and filtered. It was then weighed and stored in amber glass vials at 4 °C in the dark until chromatographic analysis. The hydrodistillation of the aerial part of *H. europaeum* gave yellowish oil.

The weight of the volatile oils of the *H. europaeum* was calculated by weight according to the following equation:

$$\text{Essential oil (\%)} = \text{Weight volatile essential oil extracted} \times 100 / \text{Wight of sample} \quad (1)$$

Essential oil analysis

The chemical composition of *H. europaeum* essential oil was analysed by gas chromatography coupled to mass spectrometry (GC-MS, Shimadzu QP2020 Instruments) equipped with a capillary column (phase: Crossbond[®] 5 % diphenyl/95 % dimethyl polysiloxane) dimensions of which are 30 m×0.25 mm and 0.25 μm film thickness, and with the following conditions: a volume of 0.5 μL solution, prepared by 10 vol. % of the sample dilution in *n*-hexane, was injected in split mode (80:1). Injector and detector temperatures were maintained at 250 and 310 °C, respectively, the column temperature was programmed at 60 °C fixed for 3 min then increased to 310 °C with the increment of 2 °C/min, and then maintained at 310 °C for 10 min. Helium (99.995 % purity) was used as a carrier gas, with a flow rate of 1 ml/min. The conditions of the mass spectrometer are as follows: ionization voltage 70 eV, ion source temperature 200 °C, and electron ionization mass spectra were acquired over the mass range of 45–600 *m/z*.

Identification of essential oil components

Identification established was based on the molecular structure, molecular mass and calculated fragments. Linear retention indices (*LRI*) were calculated for separate compounds relative to a homologous *n*-alkanes serial (*n*-C₈–C₄₀). The name, retention time, area and base *m/z* of the components of the test materials were ascertained. Components were identified by comparison of their calculated with those of literature,³² as well as their mass spectra with those recorded by the NIST17³³ (National Institute of Standards and Technology) and ADAMS³⁴ libraries. In this study, all chemicals were obtained from Sigma–Aldrich Chemical Co.

Scanning electronic microscopy (SEM)

To study the impact of the ILs used as an additive by the hydrodistillation of *H. europaeum* essential oil a scanning electron microscope (SEM) was used to examine the morphological changes of plant cells. The dry samples of *H. europaeum* were scanned before and after treatment by IL using the Quattro SEM system (Thermoscientific Company, USA). The tested samples were fixed on a specimen holder with aluminium tape. Then the tested samples were pattered with gold and examined under high vacuum conditions at an accelerating voltage of 12.5 kV (20 μm , 1000 magnification).

Recovery and recycling of ILs

To exhibit the ability to recover the ILs used in this work and reused it subsequently in another extraction of *H. europaeum* essential oil, the biomass obtained from the hydrodistillation was removed by filtration, and the resulting aqueous solution was extracted three times by 10 ml of dichloromethane. Furthermore, the anhydrous CaCl_2 was added and filtered. However, a dark ionic liquid was obtained after evaporation under reduced pressure. Though, the analysis of the HNMR of the two ionic liquids after and before use presents no substantial difference. So, the reused ionic liquid was stored in desiccators for further extraction.

RESULTS AND DISCUSSION

During the distillation process, the efficiency depends on the EOs yields and chemical composition. In addition, this work was carried out to inspect the extraction of EO from the *H. europaeum* plant using ionic liquids as additives during the hydrodistillation methods. In this study, two ILs, hydrophilic and hydrophobic, were used, respectively, $[\text{C}_4\text{mim}][\text{Cl}]$ and $[\text{C}_4\text{mim}][\text{PF}_6]$, and two effects were examined.

Effect of $[\text{C}_4\text{mim}][\text{Cl}]$ concentration on extraction efficiency of essential oil

The IL concentration is crucial in extracting analytics from drugs.³⁵ To study the effect of ILs concentration, the various concentrations of aqueous ILs (2.5, 5, 10 %) were used for the essential oil extraction. The results are summarized in Fig. 1, which presents distillation methods.

The yield of essential oil using the different concentrations of ILs (0, 2.5, 5 and 10 %) are 0.052, 0.1, 0.22 and 0.36 %, respectively. The result demonstrates that the yield of EO obtained without using $[\text{C}_4\text{mim}][\text{Cl}]$ was the lowest and that EO yields increased gradually from 2.5 to 10 %. A high EOs yield (0.36 %) was obtained when the concentration was 10 % with IL-HD. This result is explained by the fact that the use of IL as an additive during hydrodistillation improved the cell disruption.³⁶ When the concentration is further increased the viscosity is also augmented, which diminishes the penetration of ILs solution into the interior of the sample matrix, preventing more constituent extractions.³⁷ Furthermore, the butylated hydroxytoluene (BHT) extraction is higher with the use of 5 % of IL (Table S-I of the Supplementary material). Also, the reduction of the amounts of ILs in order to save costs seems more sensible to us. So, 5 % of the IL is chosen as the relevant concentration.

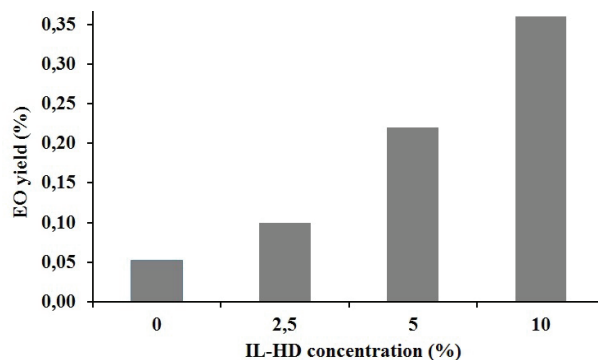


Fig. 1. Effect of ionic liquids concentration on yields of essential oils.

Effect of anion on extraction efficiency of essential oil

The choice of the IL is a crucial step for effective extraction. In fact, 1-butyl-3-methylimidazolium with PF_6^- was studied and compared to Cl^- . As an outcome, yield enhancement was observed with PF_6^- . It grows up to *ca.* 0.67 % with the same concentration. It seems that the ionic liquid $[\text{C}_4\text{mim}][\text{PF}_6]$ can strongly interact with cellulose, which is the main component of the cell walls of the plant, causing the dissolution of cellulose, which leads to the release of more compounds.³⁸ The essential oil composition analysis obtained using PF_6^- leads to eugenol as the main product. It is acquired at *ca.* 72.35 %. In contrast, the use of Cl^- shows the butylated hydroxytoluene as the main component when all concentrations are used (Table S-I).

SEM observation

SEM was used to examine the morphological changes before and after extraction with different distillation methods.

As a result, when the ILs were used, the material morphology was significantly changed. In fact, the changes in morphological structure observed for the ILs-HD samples (c and d in Fig. 2) were markedly different from those examined by HD samples.

In the case of the ILs-HD sample, the external cells were severely damaged, there was a considerable destruction of cells, showing that most cell walls were crimped and broken, which explains the improvement in EOs yield and detection of more volatile compounds. However, it can be seen that the morphological structure of the HD (b in Fig. 2) sample became wrinkled, but there was no rupture of cell walls as observed in the ILs-HD methods.

Comparative analysis of different distillation procedures

The chemical composition of *H. europaeum* EOs extracted with or without using ILs showed significant differences and these results are contrary to those

observed by Chiappe.⁸ In fact, not only the EO yield was affected by these different distillation methods and different concentrations, but also the relative peak area of each volatile compound, as shown in the typical gas chromatographic profile given in Figs. 3–6.

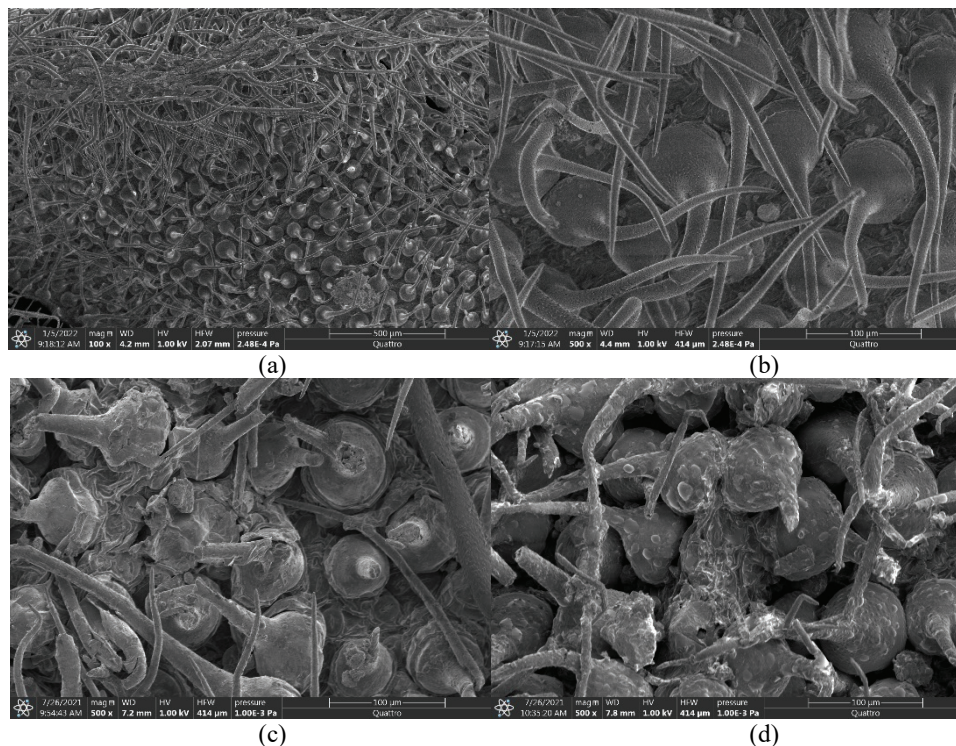


Fig. 2. Images of SEM of *H. europaeum* L.: a) before extraction, b) treated by HD, c) treated by IL HD [C₄mim][Cl] and d) treated by IL HD [C₄mim][PF₆].

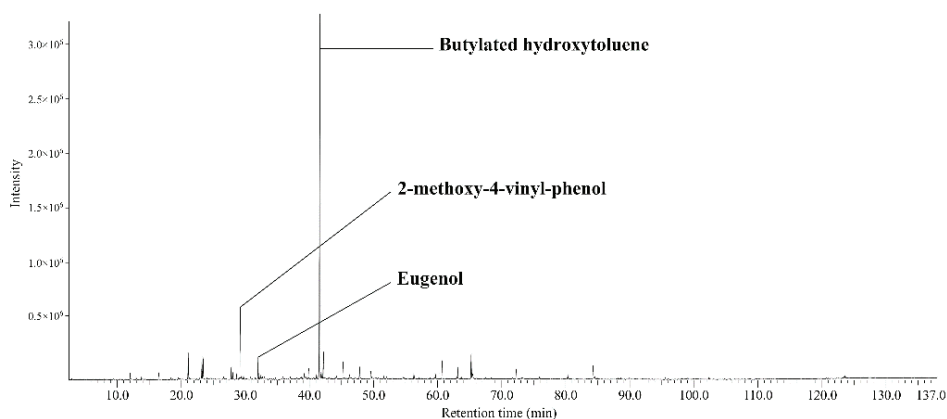
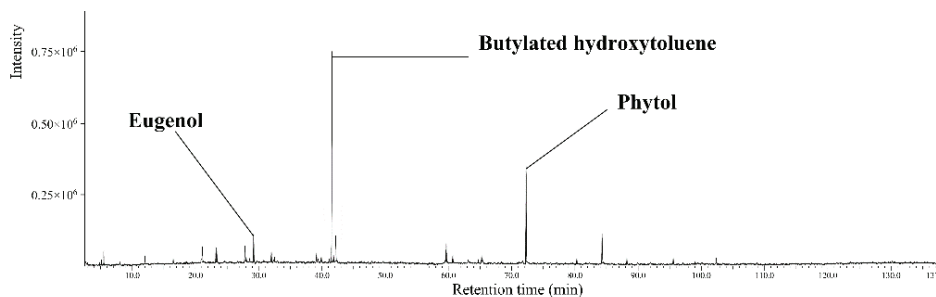
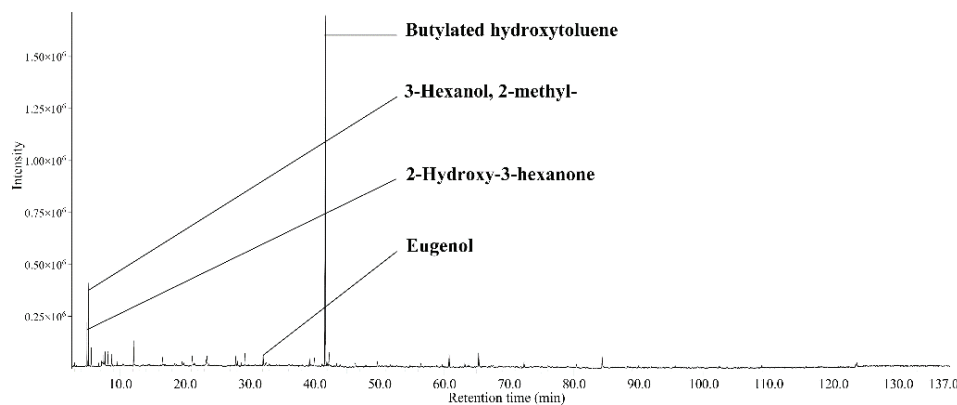
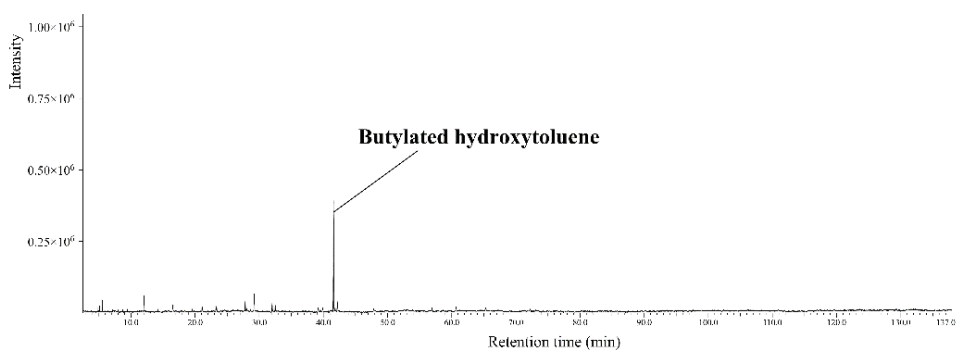


Fig. 3. TIC chromatogram of essential oils, HD method.

Fig. 4. TIC chromatogram of essential oils IL-HD [C₄mim][Cl] 2.5 % method.Fig. 5. TIC chromatogram of essential oils IL-HD [C₄mim][Cl] 5 % method.Fig. 6. TIC chromatogram of essential oils IL-HD [C₄mim][Cl] 10 % method.

The total number of volatile components detected was sixty-six compounds and they were identified in the present study of the EO of *H. europaeum* which includes both major and minor constituents. The main constituents in EOs obtained by different methods ILs-HD with [C₄mim][Cl] with different concen-

trations 2.5, 5 and 10 %, and HD method were: butylated hydroxytoluene with area percentages of 39.96, 65.39, 59.07 and 57.08 %, respectively. However, this compound was observed at only 8.95 % using $[C_4mim][PF_6]$.

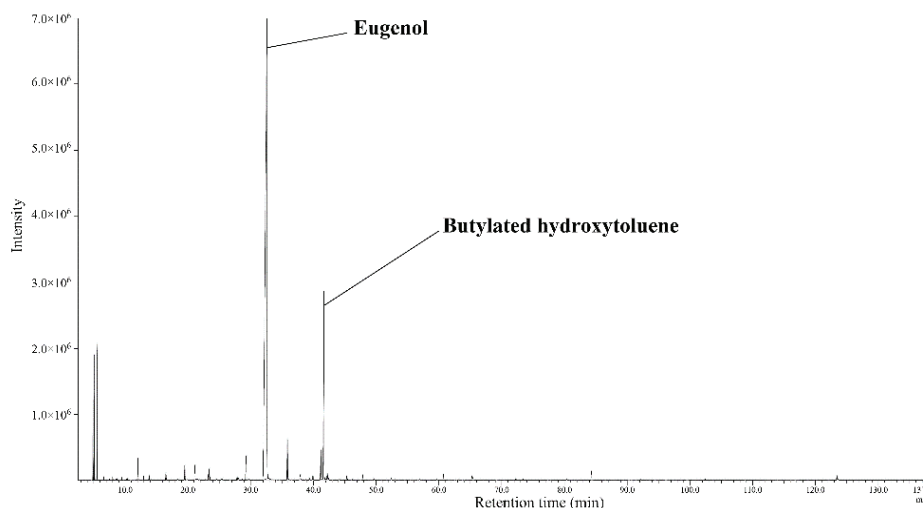


Fig. 7. TIC chromatogram of essential oils IL-HD $[C_4mim][PF_6]$ method.

On the other hand, the use of $[C_4mim][PF_6]$ gave eugenol as the main constituent with the area percentage of 72.35 %. On the contrary, this product was obtained with area percentages of 4.94, 1.65, 9.46 and 9.08 %, respectively, using $[C_4mim][Cl]$ with different concentrations of 2.5, 5 and 10 %, and the HD methods. This selective extraction can be explained by the probability of dissolution of the eugenol in $[C_4mim][PF_6]$ because eugenol is polar. It was observed in another study that the $[C_4mim][PF_6]$ tended to interact more strongly with polar solutes.³⁹ Thus, $[C_4mim][PF_6]$ can be able to aid fibre expansion and liberate the content in plant tissues so that more eugenol can be released.

There is no report in the literature on the composition of the EOs of *H. europaeum* with ILs. Only one publication was found, which showed the obtained EO through simple hydrodistillation without ILs.¹⁸ Except for eugenol, phytol, β -ionone and hexacosane, the EO obtained by IL differed profoundly from the literature report.¹⁸ Notably, compounds such as silphiperfol-6-en-5-one, geranyl acetone and *cis*-linoleic acid methyl ester were conspicuously absent in our oil samples.

Phytol was seen as the second most abundant constituent component in the essential oil obtained by IL-HD with $[C_4mim][Cl]$ in 2.5 % with the area percentage of 18.20 %. Also, this component is present in the essential oil obtained by IL-HD with $[C_4mim][PF_6]$, but with a small area ratio of 0.06 %, this compound is considered a good antimicrobial and anti-inflammatory agent.³⁹

Additionally, higher concentrations of compounds have been observed in the EOs derived from IL-HD using [C₄mim][PF₆]. This outcome could be attributed to the physical and chemical characteristics of [C₄mim][PF₆], which are significantly influenced by water saturation and the presence of dissolved substances or ions, which naturally occur during liquid–liquid extraction involving ILs.³⁹ Moreover, these findings also highlight the significant role of the organic anion present in ILs, which might be attributed to the hydrogen bond interaction between ILs ions and the constituents of the cell wall (mainly composed of cellulose). This interaction serves as a key factor in inducing changes in plant tissue and facilitating the release of more volatile compounds.⁴⁰ Based on these results, it can be concluded that the composition of the major components in the EO of *H. europaeum* is dependant on the specific distillation process employed.

CONCLUSION

In this work, two ionic liquids were successfully used as additives to efficiently extract essential oils from *H. europaeum* L. by hydrodistillation. The unique properties of non-volatility enable these ionic liquids to be used as extractants in hydrodistillation. The anion's nature can significantly affect both the solubilization capacity and the selectivity of the ionic liquid. Among the studied ionic liquids, [C₄mim][PF₆] has a higher selectivity and extraction efficiency, indicating that ionic liquids can be used to recover volatile analytes. The observation of morphological changes using scanning electron microscopy confirmed the effectiveness of the ionic liquid in this distillation process. The new method brings about more identified compounds than the conventional hydrodistillation with the satisfactory essential oils yield and composition and the application of gas chromatography–mass spectrometry was effective in identifying sixty-six compounds from *H. europaeum*. The essential oil composition of *H. europaeum* growing naturally in Algeria revealed that these species are richer in volatile composition than genotypes from Iran.¹¹ This variation may be related to different environmental and climatic conditions. In addition, it is necessary to investigate in detail the reasons for the loss of some volatile components with ionic liquids in the future. These results shed light into the phytochemistry of this unexplored species of the Flora of Algeria. The second step will be to evaluate and valorise the biological activities of the essential oil of this plant.

SUPPLEMENTARY MATERIAL

Additional data and information are available electronically at the pages of journal website: <https://www.shd-pub.org.rs/index.php/JSCS/article/view/12488>, or from the corresponding author on request.

ИЗВОД

КОДЕСТИЛАЦИЈА ЕУГЕНОЛА И БУТИЛОВАНОГ ХИДРОКСИТОЛУЕНА ПРИМЕНОМ
ЗЕЛЕНЕ СЕЛЕКТИВНЕ ДЕСТИЛАЦИЈЕ ЕТАРСКОГ УЉА ИЗ *Heliotropium europaeum* L.
ВОДЕНОМ ПАРОМ УЗ ЈОНСКЕ ТЕЧНОСТИ КАО АДТИВЕ

SARA BENDJELLOUL¹, CHOUKRY KAMEL BENEDEDDOUCHE¹, SOUHILA BENEDEDDOUCHE¹, MADANI SARRI²,
FERIHA BENSFIDDINE³, NADIA KAMBOUCHE¹, LUDOVIC PAQUIN⁴, MOHAMED YOUSFI⁵
и MOHAMED HARRAT⁵

¹Laboratory of Applied Organic Synthesis, Faculty of Exact and Applied Sciences, University Oran1 Ahmed Ben Bella, BP 1524 El M'Naouer, 31000, Oran, Algeria, ²Faculty of Sciences, University of M'sila, PO Box 166 Ichebilia, 28000 M'sila, Algeria, ³Platform of Physico-Chemical Analysis, PTAPC-Laghouat-CRAPC, Laghouat, Algeria, ⁴Université de Rennes 1, Sciences Chimiques de Rennes, UMR CNRS 6226, Groupe Ingénierie Chimique et Molécules pour le Vivant (ICMV), Bât. 10A, Campus de Beaulieu, Avenue du Général Leclerc, CS 74205, 35042 Rennes Cedex, France и ⁵Laboratory of Fundamental Sciences, University Amar Telidji of Laghouat, Laghouat, Algeria

У раду је описана дестилација воденом паром уз примену јонских течности као адитива (IL-HD) у циљу изоловања етарског уља *Heliotropium europaeum* L. Две јонске течности на бази 1-бутил-3-метилимидазола су коришћене уз измену аниона (Cl⁻ и PF₆⁻). Испитан је утицај количине јонске течности на принос и састав уља. У поређењу са стандардном дестилацијом воденом паром (HD), IL-HD повећава принос етарског уља (0,10–0,36 %). Применом [C₄mim][PF₆], примећена је морфолошка промена, што је утврђено скенирајућом електронском микроскопијом (SEM). Тиме је потврђена ефективност јонских течности током дестилације. Анализа етарских уља гасном хроматографијом–масеном спектрометријом потврдила је присуство 66 једињења након HD и IL-HD. Доминантни су еугенол (1,70–72,35 %), бутиловани хидрокситолуен (8,95–65,39 %) и фитол (18,20 %). Новом методом дестилације са јонским течностима, у етарском уљу *H. europaeum* идентификовано је више једињења (50 након IL-HD [C₄mim][PF₆], 22 након IL-HD [C₄mim][Cl]) него стандардном дестилацијом воденом паром (25 једињења). Закључено је да се дестилацијом уз промену јонских течности повећавају приноси етарског уља. Резултати приказани у овом раду нису публиковани ни за једну врсту *Heliotropium* пореклом из Алжира, а литература указује на велики потенцијал ове медицинске биљке као извора нових биоактивних супстанци за терапеутске сврхе.

(Примљено 13. јула, ревидирано 26. јула, прихваћено 6. октобра 2023)

REFERENCES

1. J. Sharifi-Rad, A. Sureda, G. C. Tenore, M. Daglia, M. Sharifi-Rad, M. Valussi, R. Tundis, M. Sharifi-Rad, M. R. Loizzo, A. O. Ademiluyi, *Molecules* **22** (2017) 70 (<https://doi.org/10.3390/molecules22010070>)
2. A. M. Abd El-Gawad, A. G. El Gendy, A. I. Elshamy, E. A. Omer, *J. Essent. Oil Bear. Plants* **19** (2016) 1684 (<https://doi.org/10.1080/0972060X.2016.1205523>)
3. A. I. Elshamy, A. M. Abd-ElGawad, Y. A. El-Amier, A. E. N. G. El Gendy, S. L. Al-Rowaily, *Flavour Fragr. J.* **34** (2019) 316 (<https://doi.org/10.1002/ffj.3512>)
4. G. Lei, P. Mao, M. He, L. Wang, X. Liu, A. Zhang, *J. Chem. Technol. Biotechnol.* **91** (2016) 1896 (<https://doi.org/10.1002/jctb.4785>)
5. G. Lei, L. Wang, X. Liu, A. Zhang, *J. Chem. Eng. Data* **61** (2016) 2499 (<https://doi.org/10.1021/acs.jced.6b00205>)
6. K. B. Śmigielski, M. Majewska, A. Kunicka-Styczyńska, M. Szczęśna-Antczak, R. Gruska, Ł. Stańczyk, *J. Food Qual.* **34** (2014) 219 (<https://doi.org/10.1111/jfq.12092>)

7. J. Jiao, Q. Y. Gai, Y. J. Fu, Y. G. Zu, M. Luo, C. J. Zhao, C. Y. Li., *Separ. Purific. Technol.* **107** (2013) 228 (<https://doi.org/10.1016/j.seppur.2013.01.009>)
8. C. Chiappe, B. Melai, G. Flamini, L. Pistelli, , *RSC Adv.* **5** (2015) 69894 (<https://doi.org/10.1039/C5RA12649E>)
9. L. Wang, M. Bai, Y. Qin, B. Liu, Y. Wang, Y. Zhou, *Molecules* **23** (2018) 2309 (<https://doi.org/10.3390/molecules23092309>)
10. Kew, *Plants of the World 2023* (accessed on 22/06/2023), [https://powo.science.kew.org/results?q=Heliotropium europaeum](https://powo.science.kew.org/results?q=Heliotropium+europaeum)
11. F. Selvi, M. Bigazzi, *Flora* **196** (2001) 269 ([https://doi.org/10.1016/S0367-2530\(17\)30056-7](https://doi.org/10.1016/S0367-2530(17)30056-7))
12. P. Quézel, S. Santa, *Nouvelle flore de l'Algérie et des Régions Désertiques Méridionales*, Vol. 2, Centre National de la Recherche Scientifique, Paris, 1963 (<https://www.ipni.org/p/20008139-1>)
13. R. Qureshi, G.R. Bhatti, *Fitoterapia* **79** (2008) 468 (<https://doi.org/10.1016/j.fitote.2008.03.010>)
14. C. Wiart *Medicinal plants of Asia and the Pacific*, CRC Press, Boca Raton, FL, 2006 (<https://doi.org/10.1201/9781420006803>)
15. M. Thulin, *Flora of Somalia*. Pteridophyta; Gymnospermae; Angiospermae (Annonaceae-Fabaceae), Vol. 1, CBC Publishing press, Harare, 1993 (ISBN: 9780947643553)
16. G. Asprey, P. Thornton, *The West Ind. Med. J.* **4** (1955) 69 (https://caymannature.files.wordpress.com/2019/08/medicinal-plants-jamaica-1953_asprey-thornton.pdf)
17. G. H. Schmelzer, A. Gurib-Fakim, *Plant Resources of Tropical Africa. Medicinal Plants I*, PROTA Foundation, Wageningen, 2008 (ISBN: 9789057822049).
18. M. Saeedi, K. Morteza-Semnani, *Chem. Nat. Comp.* **45** (2009) 98 (<https://doi.org/10.1007/s10600-009-9239-8>)
19. M. Reina, A. Gonzalez-Coloma, C. Gutierrez, R. Cabrera, J. Henriquez, L. Villarreal, *Phytochemistry* **46** (1997) 845 ([https://doi.org/10.1016/S0031-9422\(97\)00354-3](https://doi.org/10.1016/S0031-9422(97)00354-3))
20. E. Abdel-Sattar, F. M. Harraz, S. M. Al-Ansari, S. El-Mekkawy, C. Ichino, H. Kiyohara. *J. Nat. Med.* **63** (2009) 232 (<https://doi.org/10.1007/s11418-008-0305-5>)
21. H. Khan, M.A. Khan, F. Gul, S. Hussain, N. Ashraf, *Toxicol. Ind. Health* **31** (2013) 1281 (<https://doi.org/10.1177/0748233713491813>)
22. K. Srinivas, M.E. Rao, S.S. Rao, *Ind. J Pharmacol.* **32** (2000) 37 (https://ijp-online.com/temp/IndianJPharmacol32137-4643626_125356.pdf)
23. A. Kulkarni-Almeida, A. Suthar, A. Goswami, R. Vishwakarma, V.S. Chauhan, A. Balakrishnan, *Phytomedicine* **15** (2008) 1079 (<https://doi.org/10.1016/j.phymed.2008.04.013>)
24. T. Machan, J. Korth, B. Liawruangrath, S. Liawruangrath, S. G., Thailand. *Flavour Fragr. J.* **21** (2006) 265 (<https://doi.org/10.1002/ffj.1577>)
25. J. S. Reddy, P. R. Rao, M. S. Reddy, *J Ethnopharmacol.* **79** (2002) 249 ([https://doi.org/10.1016/S0378-8741\(01\)00388-9](https://doi.org/10.1016/S0378-8741(01)00388-9))
26. H. J. Walaa, M. N. Hamad, *Plant Iraq. J. Pharm. Sci.* **30** (2021) 158 (<https://doi.org/10.31351/vol30iss2pp158-166>)
27. P. R. Cheeke, *J. Animal Sci.* **66** (1988) 2343 (<https://doi.org/10.2527/jas1988.6692343x>)
28. N. Yassa, H. Farsam, A. Shafiee, A. Rustaiyan, *Planta Med.* **62** (1997) 583 (<https://doi.org/10.1055/s-2006-957984>)
29. M. A. Fayed, *Phytomedicine Plus* **1** (2021) 100036 (<https://doi.org/10.1016/j.phyplu.2021.100036>)

30. S. Bendeddouche, C. K. Bendeddouche, H. Benhaoua, *Lett. Org. Chem.* **18** (2021) 929 (<https://doi.org/10.2174/1570178618666210901142356>)
31. S. Park, R. J. Kazlauskas, *J. Org. Chem.* **66** (2001) 8395 (<https://doi.org/10.1021/jo015761e>)
32. V. Babushok, P. Linstrom, I. Zenkevich, *J. Phys. Chem. Ref. Data* **40** (2011) 043101 (<https://doi.org/10.1063/1.3653552>)
33. NIST17, *Mass spectral library (NIST/EPA/NIH)*, National Institute of Standards and Technology, Gaithersburg, 2017 (DVD-ROM ISBN: 978-1-119-41223-6)
34. R. Adams, *Identification of essential oil components by gas chromatography/mass spectrometry*, 4th ed., Allured Publishing Corp., Carol Stream, IL, 2007 (ISBN-10: 1932633219)
35. Y. Zhou, D. Wu, P. Cai, G. Cheng, C. Huang, Y. Pan, *Molecules* **20** (2015) 7684 (<https://doi.org/10.3390/molecules20057683>)
36. M. H. Duan, M. Luo, C. J. Zhao, W. Wang, Y. G. Zu, D. Y. Zhang, X. H. Yao, Y. J. Fu, *Separ. Purific. Technol.* **107** (2013) 26 (<https://doi.org/10.1016/j.seppur.2013.01.003>)
37. W. Wang, Q. Li, Y. Liu, B. Chen, *Ultrasonics Sonochem.* **24** (2014) 13 (<https://doi.org/10.1016/j.ultsonch.2014.10.009>)
38. D.A. Fort, R.C. Remsing, R.P. Swatloski, P. Moyna, G. Moyna, R.D. Rogers, *Green Chem.* **9** (2007) 63 (<https://doi.org/10.1039/B607614A>)
39. D.W. Armstrong, L. He, Y.S. Liu, *Anal. Chem.* **71** (1999) 3873 (<https://doi.org/10.1021/ac990443p>)
40. I. Kilpeläinen, H. Xie, A. King, M. Granstrom, S. Heikkinen, D. S. Argyropoulos, *J. Agric. Food Chem.* **55** (2007) 9142 (<https://doi.org/10.1021/jf071692e>).



SUPPLEMENTARY MATERIAL TO
**Co-detection of eugenol and butylated hydroxytoluene by green
and selective hydrodistillation of *Heliotropium europaeum* L.
using ionic liquids as additives**

SARA BENDJELLOUL¹, CHOUKRY KAMEL BENDEDDOUCHE^{1*}, SOUHILA
BENDEDDOUCHE¹, MADANI SARRI^{2**}, FERIHA BENSAFIDDINE³,
NADIA KAMBOUCHE¹, LUDOVIC PAQUIN⁴, MOHAMED YOUSFI⁵
and MOHAMED HARRAT⁵

¹Laboratory of Applied Organic Synthesis, Faculty of Exact and Applied Sciences, University Oran1 Ahmed Ben Bella, BP 1524 El M'Naouer, 31000, Oran, Algeria, ²Faculty of Sciences, University of M'sila, PO Box 166 Ichebilia, 28000 M'sila, Algeria, ³Platform of Physico-Chemical Analysis, PTAPC-Laghout-CRAPC, Laghouat, Algeria, ⁴Université de Rennes 1, Sciences Chimiques de Rennes, UMR CNRS 6226, Groupe Ingénierie Chimique et Molécules pour le Vivant (ICMV), Bât. 10A, Campus de Beaulieu, Avenue du Général Leclerc, CS 74205, 35042 Rennes Cedex, France and ⁵Laboratory of Fundamental Sciences, University Amar Telidji of Laghouat, Laghouat, Algeria

J. Serb. Chem. Soc. 89 (4) (2024) 457–469

1-Butyl-3-methylimidazolium chloride [*C₄mim*][Cl]. ¹H-NMR (300 MHz, DMSO) δ ppm: 0.75 (t, J = 7.2 Hz, 3H), 1.09-1.16 (m, 2H), 2.02-1.45 (m, 2H), 3.91 (s, 3H), 4.23 (t, J = 6.7 Hz, 2H), 7.98 (s, 1H), 8.09 (s, 1H), 9.84 (s, 1H). ¹³C NMR (75 MHz, DMSO) δ ppm: 13.6 (CH₃-CH₂), 19.1 (CH₂-CH₃), 31.9 (CH₂-CH₂-CH₃), 36.1 (CH₃-N), 48.7 (CH₂-N), 122.7 (CHNCH₃), 123.9 (CH-N-CH₂), 137.2 (NCHN).

1-Butyl-3-methylimidazolium hexafluorophosphate [*C₄mim*][PF₆]. ¹H-NMR (300 MHz, DMSO) δ ppm: 0.90 (t, J = 7.4 Hz, 3H), 1.22-1.34 (m, 2H), 1.68-1.87 (m, 2H), 3.85 (s, 3H), 4.16 (t, J = 7.2 Hz, 2H), 7.61 (t, J = 1.7 Hz, 1H), 7.67 (t, J = 1.7 Hz, 1H), 9.00 (s, 1H). ¹³C NMR (75 MHz, DMSO) δ ppm: 13.4 (CH₃-CH₂), 19.2 (CH₂-CH₃), 31.7 (CH₂-CH₂-CH₃), 35.9 (CH₃-N), 49.0 (CH₂-N), 122.5 (CHNCH₃), 123.9 (CH-N-CH₂), 136.8 (NCHN).

* Corresponding authors. E-mail: (*)kchoukry@yahoo.fr; (**)madani.sarri@univ-msila.dz

Table S-I. Chemical composition of the essential oil of aerial parts of *H. europaeum* by HD and ILs-HD methods

N°	Component ^a	RI ^b	Relative area percentages (%)				
			HD	IL-HD [C ₄ mim] [Cl]			IL-HD [C ₄ mim] [PF ₆]
				A	B	C	
1	2-Hydroxy-3-hexanone	843	-	-	3.32	0.64	1.71
2	Hex-3(Z)-enol	848	-	-	-	-	0.07
3	3-Hexanol, 2-methyl-	853	-	0.45	6.37	1.60	2.75
4	Guanidine carbonate	868	-	1.31	1.52	3.34	2.82
5	2,5-Dimethyl pyrazine	908	-	-	-	-	0.08
6	Cyclohexanemethanamine, n-propyl-	930	-	-	0.91	-	-
7	3-Pentanol, 2,4-dimethyl-	930	-	-	-	-	0.02
8	butanamine, N-cyclohexylmethyl-1-propyl-	932	-	-	1.23	-	-
9	RS-2,3-hexanediol	942	-	-	-	-	0.07
10	1,3-Cyclohexanediol	942	-	-	1.72	-	-
11	Benzaldehyde	955	-	-	-	-	0.03
12	Borane, diethyl-propylamino	956	-	-	0.96	-	-
13	5-Methyl furfural	958	-	-	-	-	0.04
14	Phenol	977	-	-	-	-	0.08
15	Pyrazine, 2-ethyl-6-methyl-	996	-	-	-	-	0.03
16	Pyrazine, 2-ethyl-5-methyl-	999	-	-	-	-	0.04
17	Pyrazine, trimethyl-	1001	-	-	-	-	0.04
18	1-Hexanol, 2-ethyl-	1026	-	-	-	-	0.03
19	Benzyl alcohol	1030	0.60	1.08	3.08	6.53	0.71
20	Cyclopentyl isothiocyanate	1047	-	-	-	-	0.13
21	2-Buten-1-ol, 3-methyl-, benzoate	1062	-	-	-	-	0.22
22	Phenylethyl Alcohol	1110	0.68	0.61	0.98	-	0.28
23	2-Hexanol, 2,3-dimethyl-	1158	-	-	-	-	0.52
24	L-Valine, N-cyclopropylcarbonyl-, methyl ester	1183	3.15	2.72	1.10	-	-
25	Pyrrolo[1,2-a]pyrazine, octahydro-2-methyl-	1184	-	-	-	-	0.66
26	Benzofuran, 2,3-dihydro (coumaran)	1218	2.13	2.85	-	1.61	0.22
27	4-tert-Butyl-2-methylthiazole	1220	3.31	1.87	1.04	-	0.67
28	Indole	1289	1.35	2.79	1.40	4.01	0.15
29	Thymol	1292	0.78	-	-	-	-
30	Carvacrol	1301	0.56	-	-	-	0.03
31	2-methoxy-4-vinyl-phenol	1310	9.08	4.94	1.65	9.46	1.30
32	Lupinine	1318	0.27	-	-	-	-
33	Eugenol	1354	2.82	1.76	1.70	3.98	72.35
34	2-Heptyl-5-(5-hexenyl)pyrrolidine	1360	0.37	-	-	-	-
35	Isobutyl (1-propoxypropan-2-yl) carbonate	1362	-	0.64	-	2.49	-
36	Caryophyllene	1416	-	-	-	-	1.75

Table S-I. Continued

N°	Component ^a	RI ^b	Relative area percentages (%)				
			HD	IL-HD [C ₄ mim] [Cl]			IL-HD [C ₄ mim] [PF ₆]
				A	B	C	
37	α-Humulene	1450	-	-	-	-	0.20
38	2,5-Cyclohexadien-1-one, 2,6-bis(1,1-dimethylethyl)-4-methylene-	1471	-	-	-	-	0.04
39	2,6-Di(t-butyl)-4-hydroxy-4-methyl-2,5-cyclohexadien-1-one	1470	0.57	-	0.93	-	-
40	1-Dodecanol	1471	-	-	-	-	0.07
41	β-Ionone	1483	1.28	-	-	-	0.15
42	1-Dodecanamine, N, N-dimethyl	1504	-	-	-	-	1.34
43	Butylated hydroxytoluene	1512	57.08	39.96	65.39	59.07	8.95
44	Methanone, dicyclohexyl-	1515	1.03	1.09	-	-	0.09
45	2(4H)-Benzofuranone, 5,6,7,7a-tetrahydro-4,4,7a-trimethyl-, (R)-	1521	4.15	5.74	2.49	5.66	0.35
46	Phenol, 2-methoxy-4-(2-propenyl)-, acetate	1526	-	-	-	-	0.04
47	Megastigmatrienone	1574	2.06	-	-	-	0.18
48	Caryophyllene oxide	1578	-	-	-	-	0.07
49	Phthalic acid, ethyl pentadecyl ester	1592	0.33	-	-	-	-
50	Diethyl Phthalat	1592	-	-	-	-	0.04
51	Spiro[3.6]deca-5,7-dien-1-one,5,9,9-trimethyl	1620	-	-	-	-	0.24
52	Methyl dihydrojasmonate	1652	0.64	-	-	-	0.06
53	1-Tetradecanamine, N,N-dimethyl-	1704	-	-	-	-	0.06
54	Octanoic acid, octyl ester	1778	0.53	-	-	-	-
55	2-Pentadecanone, 6,10,14-trimethyl-	1844	0.46	3.28	-	-	-
56	1,2-Benzenedicarboxylic acid, bis(2-methylpropyl) ester	1865	2.29	0.88	2.00	1.62	0.27
57	7,9-Di-tert-butyl-1-oxaspiro(4,5)deca-6,9-diene-2,8-dione	1914	1.25	-	-	-	-
58	Dibutyl phthalate	1958	3.22	0.95	2.22	-	0.19
59	n-Hexadecanoic acid	1963	-	-	-	-	0.13
60	Phytol	2105	-	18.20	-	-	0.06
61	Oleic Acid	2129	-	-	-	-	0.06
62	Pentatriacontane	2274	-	1.05	-	-	-
63	Diisooctyl adipate	2357	-	6.18	-	-	0.39
64	Hexacosane	2440	-	0.91	-	-	-
65	Octacosane	2737	-	0.74	-	-	0.04
66	Benzenepropanoic acid, 3,5-bis(1,1-dimethylethyl)-4-hydroxy-, octadecyl ester	3177	-	-	-	-	0.19

^a Components are listed according to their elution from a HP-5MS column; RI^b: retention index relative to standard mixture of n-alkanes ; HD: Hydrodistillation; .A: ILs-HD [C₄mim] [Cl] 2.5%; B: ILs-HD [C₄mim] [Cl] 5%, C: ILs-HD [C₄mim] [Cl] 10%.



J. Serb. Chem. Soc. 89 (4) 471–484 (2024)
JSCS–5734

***In vitro* anticancer studies of a small library of cyclic lipopeptides against the human cervix adenocarcinoma HeLa cells**

ALI N. HMEDAT^{1,2}, MICJEL C. MOREJÓN^{1,3}, DANIEL G. RIVERA^{1,4}, NEBOJŠA Đ. PANTELIĆ^{5,6#}, LUDGER A. WESSJOHANN¹ and GORAN N. KALUĐEROVIĆ^{1,5*}

¹Department of Bioorganic Chemistry, Leibniz Institute of Plant Biochemistry, Weinberg 3, 06120 Halle (Saale), Germany, ²Department of Pharmaceutics and Pharmaceutical Technology, Faculty of Pharmacy, Yarmouk University, Irbid 21163, Jordan, ³Department of Environmental Microbiology Electrobiotechnology, Helmholtz Centre for Environmental Research – UFZ, Permoserstr. 15, 04318 Leipzig, Germany, ⁴Center for Natural Products Research, Faculty of Chemistry, University of Havana, Zapata y G, 10400, Havana, Cuba, ⁵Department of Engineering and Natural Sciences, University of Applied Sciences Merseburg, Eberhard-Leibnitz-Strasse 2, 06217 Merseburg, Germany and ⁶Department of Chemistry and Biochemistry, Faculty of Agriculture, University of Belgrade, Nemanjina 6, 11080 Belgrade, Serbia

(Received 9 January, revised 12 January, accepted 20 February 2024)

Abstract. Various cyclic lipopeptides (CLPs, 23 compounds) were tested for their antitumor potential against human cervix adenocarcinoma HeLa cells. From the fast screening (tested concentrations: 0.01 and 10 μM) compound **10** ((12*S*,6*S*,10*S*,13*S*)-6-((*R*)-sec-butyl)-7-(2-(dodecylamino)-2-oxoethyl)-13-isopropyl-82-nitro-2,5,12,15-tetraoxo-4,7,11,14-tetraaza-1(1,2)-pyrrolidina-8(1,4)-benzenacyclopentadecaphane-10-carboxamide) was identified as active against HeLa cell line. The MTT 3-(4,5-dimethylthiazol-2-yl)-2,5-diphenyltetrazolium bromide and CV (crystal violet) assays revealed at least five times higher cytotoxic potential of **10** ($IC_{50} = 12.3 \pm 1.8 \mu\text{M}$, MTT; $9.4 \pm 1.5 \mu\text{M}$; CV) in comparison to control drug natural occurring CLP surfactin ($IC_{50} = 64.9 \pm 0.8 \mu\text{M}$, MTT; $76.2 \pm 1.6 \mu\text{M}$; CV). The cell cycle analysis performed by DAPI (4',6-diamidino-2-phenylindole) assay indicated the involvement of apoptosis in HeLa cell death upon treatment with **10**, which was confirmed by apoptosis assay (annexin V/PI). Furthermore, during this process caspase activation could be detected (ApoStat assay, immunocytochemistry caspase-3 analysis). The flow cytometry analysis did not display induction of autophagy as a possible death mechanism in HeLa cells upon **10** treatment. The current findings could be used

* Corresponding author. E-mail: goran.kaluderovic@hs-merseburg.de

Serbian Chemical Society member.

<https://doi.org/10.2298/JSC240109018H>

to design more effective CLPs based on **10** structure as potential anticancer agents.

Keywords: cancer; surfactin; proliferation; apoptosis; cell cycle; autophagy.

INTRODUCTION

Cancer is the second-most common cause of death worldwide, exceeded only by heart disease, and accounts for nearly 1 of every 4 deaths.^{1–3} Due to the toxicity, and the high price of currently used therapeutics for the treatment of various types of tumours, new alternatives are extremely desired.^{4–6} The development of synthetic organic chemistry over the last years had a great impact on the anticancer drug's development, in addition to antimicrobial and other medicinal drugs.^{7–9} One important strategy in developing effective anticancer agents is to synthesize compounds similar to bioactive natural occurring products like lipopeptides.^{10,11}

A number of bacterial and fungal species produce cyclic lipopeptides (CLPs), most of which have important biological functions.^{12–14} The plentiful structural diversity of CLPs suggests that these metabolites have different natural roles, some of which may be unique to the biology of the producing organism.¹⁵ CLPs are exhibiting a wide diversity of biological applications, ranging from antibacterial, antifungal and anticancer activities to their employment as biosurfactants, ionophores and sequestering agents.^{16,17}

Surfactin (Fig. 1), a bacterial CLP, is produced by various strains of *Bacillus*.^{18,19} The surfactant properties and biological activities of surfactin analogues appear very interesting in the perspective of their utilization both in cosmetic and in pharmaceutical fields. How this molecule can be effective in various biological events is still mostly unknown; however, it is theorized that the structural and lipophilic properties of surfactin may affect the stability of biological membrane.²⁰ On the other hand, growth inhibition in a tumor cell by surfactin could be related to induction of apoptosis and cell cycle arrest *via* the suppression of cell survival-regulating signals such as ERK and PI3K/Akt.^{21,22}

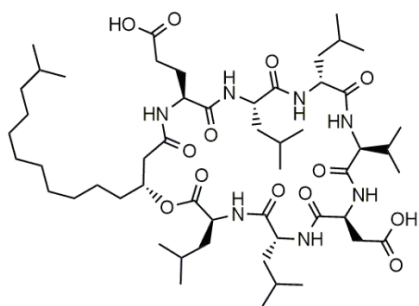


Fig. 1. Surfactin; a heptapeptide bearing a β -hydroxy fatty acid.

Recently, a multicomponent macrocyclization strategy was employed to synthesize natural product-like cyclic lipopeptides.¹⁰ This specific multicomponent reaction might be used for rapid production of natural product analogues, having amide instead of ester bond(s), for biological screening. Substituting the ester bond found in natural depsipeptide CLPs with an amide bond could potentially enhance stability, alongside the benefits of macrocyclization and *N*-alkylation. In the current study, the evaluation of the anticancer activity of a selected lipopeptide library on the HeLa cancer cells were conducted. For the most active compound mechanism of action was determined.

EXPERIMENTAL

Chemicals

CLPs were collected from the compounds library of the Leibniz Institute of Plant Biochemistry Halle, Germany. The structures of the selected CLPs were confirmed by ¹H- and ¹³C-NMR spectroscopy as well as with mass spectrometry and are in accordance with the compounds previously reported by Wessjohann and coworkers.²³ Digitonin (Riedel De Haen Seelze, Germany), surfactin, crystal violet (CV – histochemical stain, bind to duplex DNA), paraformaldehyde, 3-(4,5-dimethylthiazol-2-yl)-2,5-diphenyltetrazolium bromide (MTT – reduced to formazan by metabolically active cells), acridine orange (AO – monitor and quantify autophagy by assessing changes in the acidity of cellular compartments), 4',6-diamidino-2-phenylindole (DAPI – nuclear staining in cells, Sigma–Aldrich, Germany), RPMI (Roswell Park Memorial Institute) medium 1640, trypan blue stain 0.4 %, caspase-3 rabbit Ab, secondary anti-rabbit Alexa Fluor 488 antibody (Life Technologies, Germany), Dulbecco's phosphate-buffered saline (DPBS), trypsin EDTA (PAN Biotech, Germany), 4-amino-5-methylamino-2,7'-difluorofluorescein diacetate (DAF-FM – detection and quantification of low concentrations of nitric oxide, Cayman chemical company, Germany), fetal calf serum, penicillin/streptomycin, HEPES (PAA laboratories, Germany), DMSO (Duchefa Biochemie, Germany), acetic acid 33 % (Roth company, Germany), dihydrorhodamine (DHR – detection of ROS and RNS), carboxyfluorescein succinimidyl ester (CFSE – utilized to track different generations of actively dividing cells through the process of dye dilution), ApoStat (identify and measure caspase activity in apoptotic cells), Annexin V (protein, labeled with a fluorochrome FITC, that has a high affinity for phosphatidylserine, a phospholipid that is exposed on the outer surface of the cell membrane during early stages of apoptosis) and PI (a DNA-intercalating dye, impermeable to live cells) were obtained commercially (DB Biosciences, USA). Stock solutions of CLPs, including surfactin, were prepared in DMSO at concentration of 20 mM. Human cervix adenocarcinoma (HeLa) and NIH3T3 mouse fibroblast cells were obtained from Ontochem (Halle, Germany). HeLa and NIH3T3 cells were grown in RPMI 1640 nutrition medium supplemented with 10 % fetal calf serum (FCS) and 1 % penicillin/streptomycin at 37 °C in a humidified atmosphere containing 5 % CO₂. For MTT and CV assays, HeLa and NIH3T3 cells were seeded at density 2.000 and 10.000 cells/well, respectively, in 96 well plates, while for flow cytometry experiments at 1×10⁵ HeLa cells/well in the 6 well plates. Working concentrations were prepared from stock solutions in nutrition medium.

Fast screening and determination of IC₅₀ concentrations (MTT and CV assays)

After the HeLa cells were seeded and incubated for 24 h, 100 µL of various concentrations of CLPs, in quadruplicate, were added into the wells. For the fast screening, two con-

centrations (0.01 and 10 μM) of CLPs were used, while in experiments for IC_{50} values determination using different concentrations (0.625, 1.25, 2.5, 5, 10, 20, 40 and 80 μM). NIH3T3 cells were seeded and incubated for 24 h, afterwards treated with the IC_{50} concentrations of **10** and surfactin. The MTT (3-(4,5-dimethylthiazol-2-yl)-2,5-diphenyltetrazolium bromide) and CV (crystal violet) assays, upon 72 h of treatment, were performed as described in the literature.²⁴ All experiments were performed in biological triplicates. The absorbance was measured with an automated microplate reader (Spectramax from Molecular Devices) at 540 nm (reference 670 nm). IC_{50} values, defined as the concentrations of the compound at which 50 % of cell inhibition occur were calculated using four-parameter logistic function and presented as mean from three independent experiments.

Cell cycle analysis

HeLa cells (1×10^5 cells/well) were cultivated with the IC_{50} or $2 \times IC_{50}$ doses of active compounds for 72 and 48 h, respectively. Then the supernatant (which contains the floating dead cells) from each well and the attached cells belong to the same well were collected in 5 mL test tubes. Cells were washed with phosphate buffered saline (PBS) and fixed in ethanol 70 % at 4 °C overnight. Afterwards, cells were washed in PBS and the cell pellet was taken and resuspended in 1 mL of DAPI (4',6-diamidino-2-phenylindole) solution (1 vol. % Triton X-100 and 1 $\mu\text{g mL}^{-1}$ DAPI in PBS) for staining. Prepared samples were stored in the dark for 10 min then the distribution of cells in different cell cycle phases was determined with FACS Aria III (DB Biosciences).²⁵

Annexin V/PI assay

HeLa cells were incubated with IC_{50} or $2 \times IC_{50}$ doses of active compounds for 72 h. Cells were washed and trypsinated, then collected and washed with PBS. Cells had been stained with 100 μL of working Ann V/PI solution (93 μL of $1 \times$ Annexin binding buffer (ABB) + 5 μL Ann V + 2 μL PI per sample) for 15 min at 37 °C in dark. Afterwards, staining was stopped by adding 900 μL of $1 \times$ ABB per sample. Treated and untreated cells were examined by flow cytometry analysis with FACS Aria III (DB Biosciences).²⁶

ApoStat staining

Investigated cancer cells were incubated with IC_{50} or $2 \times IC_{50}$ doses of active CLPs for 72 h. Cells were washed and trypsinated, then collected and washed with PBS. Cells were incubated with 100 μL of working ApoStat solution (99 μL of PBS 5 % FCS + 1 μL ApoStat per sample) for 30 min at 37 °C. Later, 1 mL of PBS per sample was used to stop staining and washing out unbound ApoStat. Examine cells were suspended in 1 mL PBS for flow cytometry analysis with FACS Aria III (DB Biosciences).²⁵

Immunocytochemistry

Cells (1×10^5 cells/well) were cultivated with the $2 \times IC_{50}$ dose of active compounds for 48 h. The medium was removed and cells were fixed with paraformaldehyde 4 % for 15 min at room temperature. Permeability was improved by incubating the treated cells with 0.25 % Triton X-100 in PBS for 10 min then cells had been washed with PBS 3 times for 5 min. In order to avoid unspecific antibody binding, 10 % FCS in PBS-T (PBS with 0.1 % Triton X-100) was added for 30 min at room temperature. Afterwards, cells were incubated with Rabbit anti-caspase 3 (1:400 dilution in 1 % bovine serum albumin PBS-T) over the night at 5–10 °C. Anti-rabbit Alexa Flour 488 secondary antibody was used in dilution 1:200 in 1 % BSA PBS-T for 30 min at RT in dark place. Nucleus staining was performed with DAPI 1 $\mu\text{g mL}^{-1}$ in PBS

by incubating the cells with DAPI for 1 min in dark place. Finally, the preparations were used to take the images by fluorescence microscope.

Analysis of autophagy

For this purpose, cells were incubated with IC_{50} or $2 \times IC_{50}$ doses of active compounds for 72 and 48 h, respectively. Cells were washed and trypsinated, consequently collected and washed with PBS before staining in 10 μ M acridine orange solution for 15 min at 37 °C in dark. Afterwards, cells were washed with PBS and the cell pellet was resuspended in 500 μ L PBS for flow cytometry analysis with FACS Aria III (DB Biosciences).²⁵

CFSE staining

The assay was performed as described by supplier.²⁷ Cells were stained with 1 μ M of carboxyfluorescein succinimidyl ester (CFSE) for 15 min at 37 °C and then exposed to the IC_{50} dose of active compounds for 72 h. At the end of cultivation, cells were washed with PBS and trypsinated, washed in PBS and resuspended in 500 μ L of PBS for measurement. Proliferation activity of the treated cells was analysed by FACS Aria III (DB Biosciences).

Investigation of ROS/RNS

For detection of reactive oxygen species/reactive nitrogen species (ROS/RNS), dihydro-rhodamine (DHR) which is redox-sensitive dye was used.²⁸ The cells were stained with 1 μ M DHR for 20 min at 37 °C. Afterward, the cells were treated with the IC_{50} dose of investigated compounds for 72 h. Subsequently, the cells were collected by trypsinization and washed with PBS before flow cytometry analysis.

DAF-FM assay

For NO production evaluation, cells were treated with IC_{50} and $2 \times IC_{50}$ for 72 h. The medium was discarded from all wells which had been washed with PBS 2 times. Then, 1 mL per well of working DAF-FM (4-amino-5-methylamino-2,7'-difluoro fluorescein diacetate) solution (5 μ M DAF-FM in white medium with 10 % FCS) was added and incubated with cells at 37 °C for 1 h for staining. The staining solution was dropped and wells washed with PBS 2 times before incubated with the white medium for 15 min at 37 °C. Afterwards, cells had been trypsinated and collected from all wells in tubes for FACS analysis.²⁵

RESULTS AND DISCUSSION

Cytotoxicity and toxicity studies

Various CLPs (23 synthetic compounds) and surfactin (natural occurring compound, herein control) were at first fast screened against HeLa cell lines, using MTT (3-(4,5-dimethylthiazol-2-yl)-2,5-diphenyltetrazolium bromide) and CV (crystal violet) assays in order to select the most active compounds (72 h treatment, Figs. 2 and S-1 of the Supplementary material to this paper). From all tested synthetic CLPs only compound **10** (Fig. 3a) exhibited antitumor activity against HeLa cell line at the higher investigated concentration (10 μ M).

Furthermore, the MTT and CV assays were carried out in order to determine cytotoxic potential of selected synthetic and naturally occurring compounds (Fig. 3b). Based on the recommendation of National Cancer Institute, active compounds have IC_{50} value $< 30 \mu\text{g mL}^{-1}$.²⁹ The activity of **10** is in the range of active compounds ($IC_{50} = 12.3/9.4 \mu\text{M}$, MTT/CV, corresponds to 9.8/

/7.5 $\mu\text{g mL}^{-1}$, MTT/CV). Surprisingly, surfactin expressed much lower activity than **10** against HeLa cells. The lower activity of surfactin, a cyclic ester, in comparison to **10**, instead of lactone an *N*-substituted amide moiety is present, may be due to the fact that surfactin is more susceptible to hydrolysis/proteolysis reactions in which ring-opened compounds are produced. Such products are more exposed to degradative process in the physiological medium, thus in that way bioavailability is decreased. However, amide-containing compounds are also susceptible to hydrolysis, but it occurs at an extremely slower rate than the hydrolysis of lactone.³⁰ The cyclic moiety of CLPs is important for their high surfactant activity and destruction of the cyclic structure in surfactin may lead to decrease its cytotoxic activity.³¹

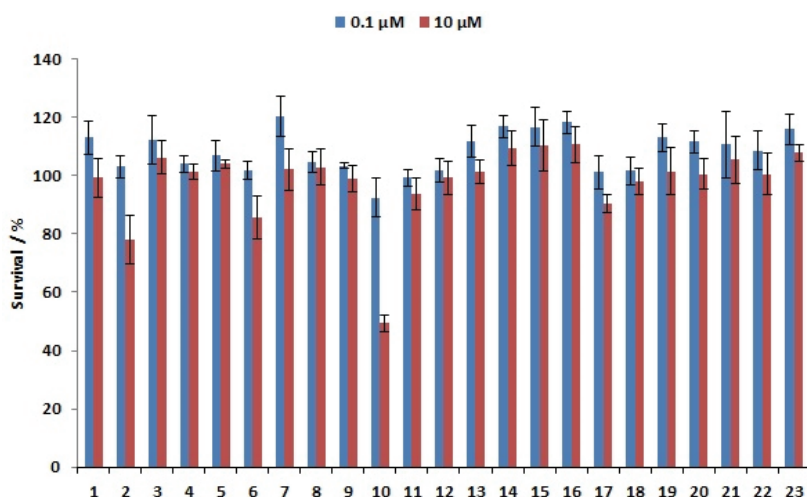


Fig. 2. The viability of HeLa cells treated with CLPs (CV assay). Cells were treated with 2 concentrations (0.1 and 10 μM) of CLPs for 72 h. Data represent absorbance measurements normalized to control-untreated cells. Values are expressed as means and standard deviations obtained from independent experiments. For MTT results please see supplementary material (Fig. S-1).

In order to explore does **10** or surfactin have an effect on normal cells, mouse embryonic NIH3T3 fibroblast cells were incubated with IC_{50} concentrations of selected compounds (Fig. 3c). Both MTT and CV assays demonstrated that surfactin was more toxic to NIH3T3 cells than compound **10**. The survival rate of the cells treated with **10** (91 %) showed that this synthetic CLP selectively acts on tumor cells (at the same concentration 50 % of HeLa cells are death). On the other hand, the IC_{50} concentration of surfactin, determined on HeLa cells, decreased the cell viability of normal cells to 15 %, thus is more active against normal than tumor cells.

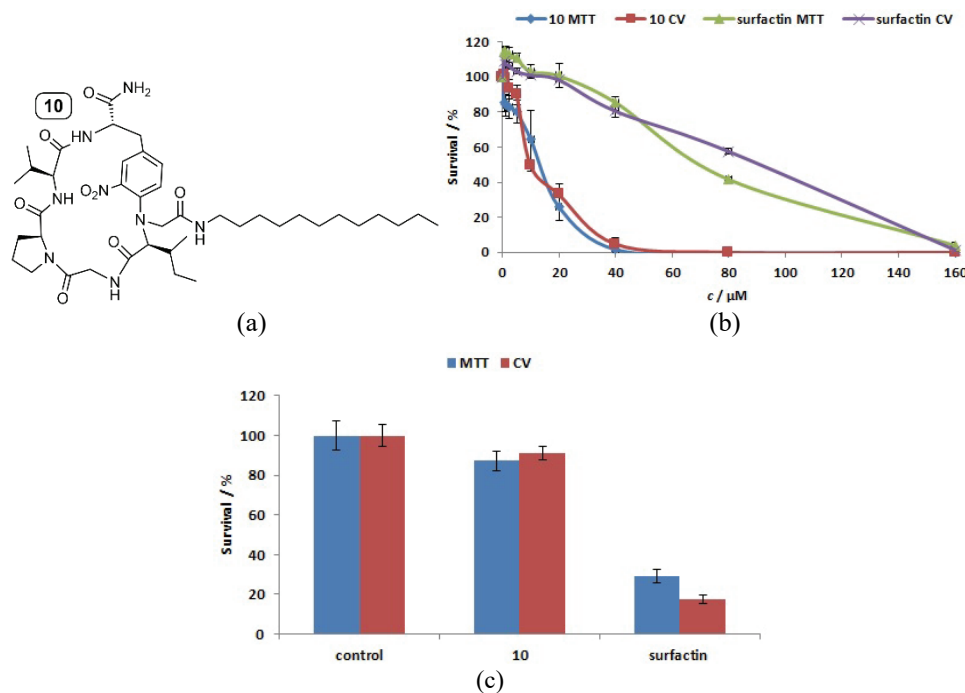


Fig. 3. a) The structure of **10**; b) dose-dependent response of the HeLa cells upon treatment with CLPs (MTT and CV assays). HeLa cells were treated with serial dilutions of **10** and surfactin for 72 h. IC_{50} : **10**, $12.3 \pm 1.8 \mu\text{M}$ (MTT) and $9.4 \pm 1.5 \mu\text{M}$ (CV); surfactin, $64.9 \pm 0.8 \mu\text{M}$ (MTT) and $76.2 \pm 1.6 \mu\text{M}$ (CV). The data represent absorbance measurements normalized to control-untreated cells. The dose-response curves and IC_{50} values show mean values \pm SD of three independent experiments with six parallel measurements in each case; c) the effect of **10** and surfactin on the viability of normal mouse NIH3T3 fibroblasts. NIH3T3 cells were untreated or treated with the IC_{50} concentrations of **10** and surfactin for 72 h then cell viability was determined by MTT and CV assays. Values are expressed as means and standard deviations obtained from three independent experiments.

Mechanism of action

To investigate the mode of action HeLa cells were treated with both synthetic and naturally occurring compounds, **10** and surfactin, and at first distribution of the cells in the cell cycle was analysed using flow cytometry (DAPI assay, Fig. 4a).²⁵ Based on the obtained results, cells treated with **10** as well as surfactin, showed enhanced cell number in sub-G1 phase which might indicate an involvement of apoptosis in cell death induced by these compounds.³² Both compounds do not express cytostatic potential, thus their action is mainly due to the cytotoxic action (Fig. 4b). The apoptotic mode of cell death was confirmed with Annexin V/PI assay (Fig. 4c). There was a recognized increase in early and late apoptotic cell populations (Ann^+/PI^- and Ann^+/PI^+ , respectively) in the HeLa

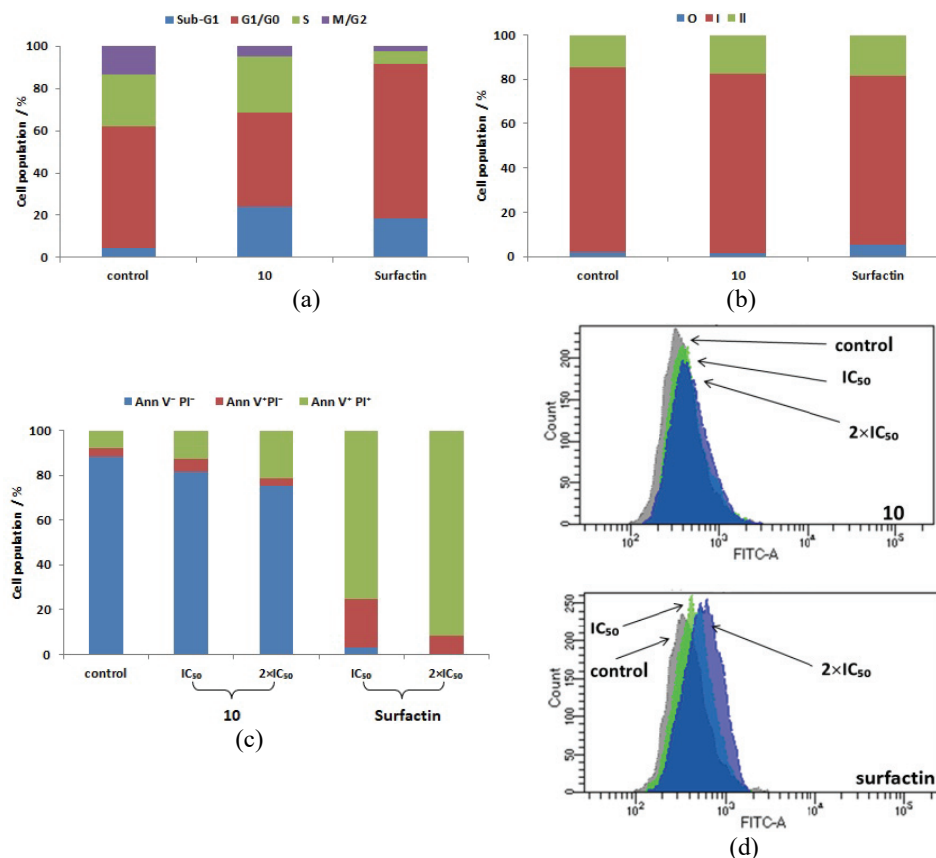


Fig. 4. a) Flow cytometry analysis of cell cycle distribution of HeLa cells. Cells were treated with DMSO as vehicle control or IC_{50} concentrations of **10** and surfactin for 72 h then stained with DAPI. The DNA content was then determined by flow cytometry. The cell population was analyzed as cell numbers at each cell cycle phase relative to the total population; b) flow cytometer analysis for cell proliferation assay of CFSE-labelled HeLa upon treatment with DMSO as vehicle control, IC_{50} concentrations of **10** or surfactin for 72 h.; c) detection of apoptosis with Annexin-V-FITC and propidium iodide staining. HeLa cells were treated with DMSO as vehicle control, the IC_{50} or $2 \times IC_{50}$ concentrations of **10** and surfactin for 72 h then stained with Annexin V and PI for FACS analysis. Annexin V positive cells represent percentages of late and early apoptotic HeLa cells; d) representative images for caspase activation in HeLa cells upon treatment with CLPs (ApoStat assay). HeLa cells were treated with DMSO as vehicle control, the IC_{50} concentrations of **10** or surfactin for 72 h, stained with ApoStat and measured by flow cytometry to determine the percentage of cells expressing active caspases. Results are expressed as means obtained from three independent experiments (a, b and c).

cells treated with **10**. On the other hand, massive late apoptosis was detected for the HeLa cells treated with surfactin. Apoptosis initiation and execution are accompanied by complex cascades of intra-cellular events that may include

members of the caspase family.³³ Flow cytometry was used to evaluate activation of caspases in HeLa cells upon treatment (ApoStat assay). An obvious upregulation of caspases could be noted upon treatment with both compounds (Fig. 4d). Moreover, activation of caspase-3 executor could be confirmed using immunocytochemistry analysis (Fig. 5). Fluorescent examination of treated HeLa cells gives definite proof of involvement of caspase in the apoptotic mode of cell death using selected CLPs.

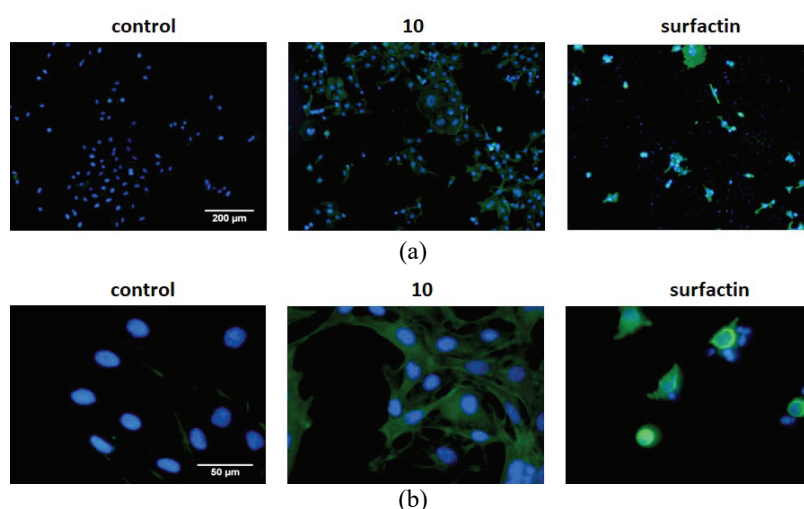


Fig. 5. Representative fluorescence images, a) 10 \times and b) 40 \times , of caspase-3 activation HeLa cells upon treatment with **10** and surfactin ($2\times IC_{50}$, 48 h, nuclei – DAPI stained, caspase-3 – primary rabbit antibody, secondary anti-rabbit Alexa Fluor 488 antibody).

Autophagy might be involved in various cellular processes such as cell differentiation as well as in a cell death mechanism involving autophagosomal/lysosomal degradation of cellular components.^{34,35} In the current study, it was sought to determine whether treatment of cells with active CLPs results in an induction of autophagy of cancer cells. For this purpose, cells previously treated with active CLPs were collected and analysed using flow cytometry (acridine orange assay, Fig. S-2 of the Supplementary material).²⁵ Upon treatment with **10** or surfactin, HeLa cells did not show any elevated presence or acidic vesicles, autophagosomes, meaning that autophagy is not involved in the death process.

To investigate whether ROS/RNS, as well as NO species, are generated by CLPs, DHR (dihydrorhodamine) or DAF-FM (4-amino-5-methylamino-2,7'-difluorofluorescein diacetate), respectively, prestained HeLa cells were incubated with selected CLPs (Fig. 6a and b). Flow cytometry analysis showed no increase in the ROS/RNS formation, moreover, **10** suppressed the formation of the men-

tioned species. Surfactin enhanced the production of NO, while **10** had no impact on its production.

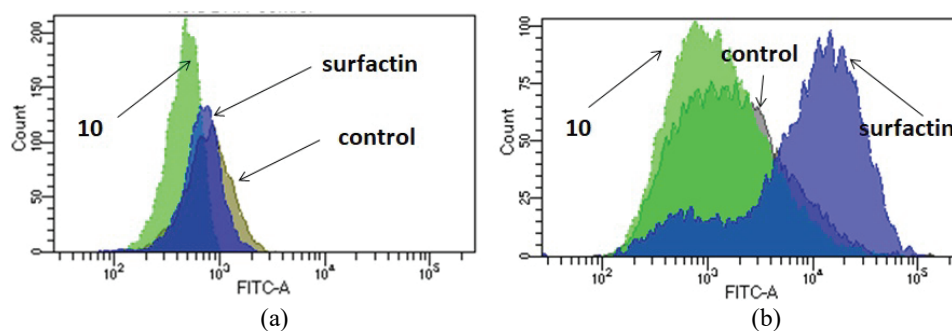


Fig. 6. a) Flow cytometry analysis for ROS/RNS production in HeLa cells upon treatments with DMSO as vehicle control, IC_{50} concentrations of **10** or surfactin for 72 h (DHR assay); b) NO generation in treated and untreated HeLa cells. HeLa cells were treated with DMSO as vehicle control, IC_{50} concentrations of **10** or surfactin for 72 h then stained with DAF-FM solution for FACS analysis. Representative images are shown.

Compound **10** shows an activity surpassing that of the natural compounds surfactin or even emodin (four-fold).²⁵ On the other hand, **10** exhibits lower activity than cisplatin against HeLa cells,³⁶ however with notable advantages. In contrast to cisplatin, **10** displays selectivity by being inactive against normal fibroblast cells. While cisplatin has severe side effects, optimizing the chemical structure of compound **10** could enhance its cytotoxicity. In modern anticancer therapy, it is also important to prioritise selectivity over potency in drug development. Compound **10** may act by reducing its nitro group, producing free-radical intermediates and reactive metabolites that interact with DNA, leading to the inhibition of nucleic acid and protein synthesis.^{37,38} The deadly effects on HeLa cancer cells and the cytotoxic action of **10** may be related to the covalent binding of the reduced metabolites to cellular macromolecules or interactions with cytoplasmic and membrane enzymes. Analysis of cells treated with **10** revealed an increase in late and early apoptotic HeLa cells. Among the nitro group-containing compounds investigated herein, only compound **10** demonstrated relevant activity. The incorporation of the nitro-phenyl group into a peptide cycle makes the possibility of intercalation of **10** into DNA highly improbable, as there is no conformation that permits flat aromatic intercalation.

CONCLUSION

Lipopeptides represent a class of microbial surfactants, that has achieved increasing scientific, therapeutic and biotechnological interest. The main aim of the current work was *in vitro* anticancer investigation for a library of synthetic CLPs. For this purpose, the HeLa cell line was used and cytotoxicity was assessed

with MTT and CV assays. As a result, 23 compounds were examined and many of them exhibited a high cytotoxic response during the primary screening.

The IC_{50} value was established for active CLPs in order to attain the most important structural features that may contribute to their cytotoxic activity. Synthetic CLP (**10**) revealed a better cytotoxic profile ($12.3 \pm 1.8 \mu\text{M}$ (MTT) and $9.4 \pm 1.5 \mu\text{M}$ (CV)) in comparison to natural CLP surfactin ($64.9 \pm 0.8 \mu\text{M}$ (MTT) and $76.2 \pm 1.6 \mu\text{M}$ (CV)) due to structural modifications, such as lactone group replacement, the introduction of nitro functional group and lipophilicity improvement. Additionally, active CLP showed a higher safety profile against NIH3T3 than surfactin.

Accumulation of treated cells in the sub-G phase might indicate apoptosis as a possible mechanism of action. This assumption was confirmed by annexin V/PI assay. In addition, active CLP had been displayed to provoke late apoptosis and cell death in HeLa cells. Results reported in this research contribute to understanding CLPs cytotoxicity, the structural features that might be involved in their activity and their possible mechanisms of action. Finally, these findings may be used to design more effective and less harmful CLPs as potential anticancer agents.

SUPPLEMENTARY MATERIAL

Additional data and information are available electronically at the pages of journal website: <https://www.shd-pub.org.rs/index.php/JSCS/article/view/12766>, or from the corresponding author on request.

Acknowledgement. This work was done within the agreement between the Faculty of Agriculture University of Belgrade and the Ministry of Education, Science, and Technological Development of the Republic of Serbia (Grant No. 451-03-47/2023-01/200116).

ИЗВОД

IN VITRO АНТИКАНЦЕРОГЕНО ИСПИТИВАЊЕ МАЛЕ БИБЛИОТЕКЕ ЦИКЛИЧНИХ ЛИПОПЕПТИДА НА НЕЛА ХУМАНИМ ЋЕЛИЈАМА АДЕНОКАРЦИНОМА ГРЛИЋА МАТЕРИЦЕ

ALI N. HMEDAT^{1,2}, MICHEL C. MOREJÓN^{1,3}, DANIEL G. RIVERA^{1,4}, НЕБОЈША Ђ. ПАНТЕЛИЋ^{5,6},
LUDGER A. WESSJOHANN¹ и ГОРАН Н. КАЛУЂЕРОВИЋ^{1,5}

¹Department of Bioorganic Chemistry, Leibniz Institute of Plant Biochemistry, Weinberg 3, 06120 Halle (Saale), Germany, ²Department of Pharmaceutics and Pharmaceutical Technology, Faculty of Pharmacy, Yarmouk University, Irbid 21163, Jordan, ³Department of Environmental Microbiology Electrobiotechnology, Helmholtz Centre for Environmental Research – UFZ, Permoserstr. 15, 04318 Leipzig, Germany, ⁴Laboratory of Synthetic and Biomolecular Chemistry, Faculty of Chemistry, University of Havana, Zapata y G, 10400 Havana, Cuba, ⁵Department of Engineering and Natural Sciences, University of Applied Sciences Merseburg, Eberhard-Leibnitz-Strasse 2, 06217 Merseburg, Germany и ⁶Департаман за хемију и биохемију, Пољопривредни факултет, Универзитет у Београду, Немањина 6, Београд-Земун

Антитуморски потенцијал разних цикличних липопептида (CLP, 23 једињења) је испитиван на HeLa хуманим ћелијама аденокарцинома грлића материце. Из брзог скрининга (испитане концентрације: 0,01 и 10 μM) једињење **10** ((12S,6S,10S,13S)-6-((R)-секбутил)-7-(2-(додециламино)-2-оксоетил)-13-изопропил-82-нитро-2,5,12,15-тетраоксо-4,7,11,14-тетрааза-1(1,2)-пирролидина-8(1,4)-бензенциклопентадекафан-10-карбоксамид)

је идентификовано као активно на HeLa ћелијама. МТТ (3-(4,5-диметилтиазол-2-ил)-2,5-дифенилтетразолиум-бромид) и CV (кристал виолет) тестови показали су да једињење **10** има најмање 5 пута већи цитотоксични потенцијал ($IC_{50} = 12,3 \pm 1,8 \mu\text{M}$, МТТ; $9,4 \pm 1,5 \mu\text{M}$; CV) у поређењу са природним CLP контролним леком, сурфацин ($IC_{50} = 64,9 \pm 0,8 \mu\text{M}$, МТТ; $76,2 \pm 1,6 \mu\text{M}$; CV). Анализа ћелијског циклуса, извршена помоћу DAPI (4'6-диамидино-2-фенилиндол) теста, указује на учешће апоптозе у смрт HeLa ћелија након третирања са **10**, што је потврђено тестом за апоптозу (Annexin V/PI). Поред тога, током овог процеса може се детектовати активација каспазе (ApoStat тест и имуноцитохемијска каспаза-3 анализа). Анализа проточне цитометрије није показала индукцију аутофагије као могући механизам смрти HeLa ћелија након третирања са **10**. Ови налази могу да се користе у дизајнирању побољшаних CLP, заснованих на структури једињења **10**, као потенцијалних агенаса против рака.

(Примљено 9. јануара, ревидирано 12. јануара, прихваћено 20. фебруара 2024)

REFERENCES

1. R. L. Siegel, K. D. Miller, N. S. Wagle, A. Jemal, *Ca Cancer J. Clin.* **73** (2023) 17 (<https://doi.org/10.3322/caac.21763>)
2. M. Malvezzi, C. Santucci, P. Boffetta, G. Collatuzzo, F. Levi, C. La Vecchia, E. Negri, *Ann. Oncol.* **34** (2023) 410 (<https://doi.org/10.1016/j.annonc.2023.01.010>)
3. M. Muscaritoli, J. Arends, P. Bachmann, V. Baracos, N. Barthelemy, H. Bertz, F. Bozzetti, E. Hütterer, E. Isenring, S. Kaasa, *Clin. Nutr.* **40** (2021) 2898 (<https://doi.org/10.1016/j.clnu.2021.02.005>)
4. S. Liu, Q. Sun, X. Ren, *J. Hematol. Oncol.* **16** (2023) 38 (<https://doi.org/10.1186/s13045-023-01430-8>)
5. S. L. Gupta, S. Basu, V. Soni, R. K. Jaiswal, *Mol. Biol. Rep.* **49** (2022) 9903 (<https://doi.org/10.1007/s11033-022-07525-8>)
6. K. O'Brien, K. Ried, T. Binjemain, A. Sali, *Cancers* **14** (2022) 5933 (<https://doi.org/10.3390/cancers14235933>)
7. Y. F. Mustafa, *Appl. Nanosci.* **13** (2023) 1907 (<https://doi.org/10.1007/s13204-021-01872-x>)
8. S. Motyka, K. Jaferník, H. Ekiert, J. Sharifi-Rad, D. Calina, B. Al-Omari, A. Szopa, W. C. Cho, *Biomed. Pharmacother.* **158** (2023) 114145 (<https://doi.org/10.1016/j.biopha.2022.114145>)
9. Z. Breijyeh, R. Karaman, *Antibiotics* **12** (2023) 628 (<https://doi.org/10.3390/antibiotics12030628>)
10. M. C. Morejón, A. Laub, G. N. Kaluđerović, A. R. Puentes, A. N. Hmedat, A. J. Otero-González, D. G. Rivera, L. A. Wessjohann, *Org. Biomol. Chem.* **15** (2017) 3628 (<https://doi.org/10.1039/c7ob00459a>)
11. S. Lai, Q. Zhang, L. Jin, *Antibiotics* **12** (2022) 42 (<https://doi.org/10.3390/antibiotics12010042>)
12. S. Singh, R. A. Sequeira, P. Kumar, V. A. Ghadge, P. Vaghela, A. K. Mohanty, A. Ghosh, K. Prasad, P. B. Shinde, *ACS Omega* **7** (2022) 46646 (<https://doi.org/10.1021/acsomega.2c05587>)
13. D. P. Fewer, J. Jokela, L. Heinilä, R. Aesoy, K. Sivonen, T. Galica, P. Hrouzek, L. Herfindal, *Physiol. Plant.* **173** (2021) 639 (<https://doi.org/10.1111/ppl.13484>)
14. J. Steigenberger, Y. Verleysen, N. Geudens, A. Madder, J. C. Martins, H. Heerklotz, *Biophys. J.* **122** (2023) 950 (<https://doi.org/10.1016/j.bpj.2022.07.033>)

15. C. Wan, X. Fan, Z. Lou, H. Wang, A. Olatunde, K. R. Rengasamy, *Crit. Rev. Food Sci. Nutr.* **62** (2022) 7976 (<https://doi.org/10.1080/10408398.2021.1922355>)
16. A. Evidente, *Int. J. Mol. Sci.* **23** (2022) 12342 (<https://doi.org/10.3390/ijms232012342>)
17. J. G. Tank, R. V. Pandya, *Peptides* **155** (2022) 170836 (<https://doi.org/10.1016/j.peptides.2022.170836>)
18. A. Théâtre, C. Cano-Prieto, M. Bartolini, Y. Laurin, M. Deleu, J. Niehren, T. Fida, S. Gerbinet, M. Alanjary, M. H. Medema, *Front. Bioeng. Biotechnol.* **9** (2021) 623701 (<https://doi.org/10.3389/fbioe.2021.623701>)
19. A. Rosier, M. Pomerleau, P. B. Beauregard, D. A. Samac, H. P. Bais, *Plants* **12** (2023) 1007 (<https://doi.org/10.3390/plants12051007>)
20. J.-F. Liu, S. M. Mbadinga, S.-Z. Yang, J.-D. Gu, B.-Z. Mu, *Int. J. Mol. Sci.* **16** (2015) 4814 (<https://doi.org/10.3390/ijms16034814>)
21. Y.-S. Wu, S.-C. Ngai, B.-H. Goh, K.-G. Chan, L.-H. Lee, L.-H. Chuah, *Front. Pharmacol.* **8** (2017) 761 (<https://doi.org/10.3389/fphar.2017.00761>)
22. T. T. T. Vo, Y. Wee, H. C. Cheng, C. Z. Wu, Y. L. Chen, V. P. Tuan, J. F. Liu, W. N. Lin, I. T. Lee, *Oral Dis.* **29** (2023) 528 (<https://doi.org/10.1111/odi.13950>)
23. M. C. Morejón, *New Multicomponent Strategies to Cyclic Lipopeptides*, Universitäts-und Landesbibliothek Sachsen-Anhalt, Halle (Saale), 2018 (<https://doi.org/10.1515/bd.2003.37.1.41>)
24. T. Krajnović, N. Đ. Pantelić, K. Wolf, T. Eichhorn, D. Maksimović-Ivanić, S. Mijatović, L. A. Wessjohann, G. N. Kaluđerović, *Materials* **15** (2022) 5028 (<https://doi.org/10.3390/ma15145028>)
25. I. Morgan, L. A. Wessjohann, G. N. Kaluđerović, *Cells* **11** (2022) 168 (<https://doi.org/10.3390/cells11010168>)
26. S. B. Kntayya, M. D. Ibrahim, N. Mohd Ain, R. Iori, C. Ioannides, A. F. Abdull Razis, *Nutrients* **10** (2018) 718 (<https://doi.org/10.3390/nu10060718>)
27. N. Ganesan, S. Ronsmans, P. Hoet, *Heliyon* **9** (2023) e19242 (<https://doi.org/10.1016/j.heliyon.2023.e19242>)
28. N. Yusof, N. M. Yasin, R. Yousuf, A. A. Wahab, S. A. Aziz, *Bangladesh J. Med. Sci.* **21** (2022) 626 (<https://doi.org/10.3329/bjms.v21i3.59577>)
29. I. Canga, P. Vita, A.I. Oliveira, M. Á. Castro, C. Pinho, *Molecules* **27** (2022) 4989 (<https://doi.org/10.3390/molecules27154989>)
30. R. Gómez-Bombarelli, E. Calle, J. Casado, *J. Org. Chem.* **78** (2013) 6868 (<https://doi.org/10.1021/jo400258w>)
31. K. Liu, Y. Sun, M. Cao, J. Wang, J. R. Lu, H. Xu, *Curr. Opin. Colloid Interface Sci.* **45** (2020) 57 (<https://doi.org/10.1016/j.cocis.2019.12.005>)
32. M. Delgado, R. R. Rainwater, B. Heflin, A. Urbaniak, K. Butler, M. Davidson, R. M. Protacio, G. Baldini, A. Edwards, M. R. Reed, *J. Biol. Chem.* **298** (2022) 101939 (<https://doi.org/10.1016/j.jbc.2022.101939>)
33. M. Maruoka, P. Zhang, H. Mori, E. Imanishi, D. M. Packwood, H. Harada, H. Kosako, J. Suzuki, *Mol. Cell* **81** (2021) 1397 (<https://doi.org/10.1016/j.molcel.2021.02.025>)
34. J. Debnath, N. Gammoh, K. M. Ryan, *Nat. Rev. Mol. Cell Biol.* **24** (2023) 560 (<https://doi.org/10.1038/s41580-023-00585-z>)
35. Y. Zhou, H. Manghwar, W. Hu, F. Liu, *Int. J. Mol. Sci.* **23** (2022) 7301 (<https://doi.org/10.3390/ijms23137301>)
36. G. N. Kaluđerović, V. M. Đinović, Z. D. Juranić, T. P. Stanojković, T. J. Sabo, *J. Inorg. Biochem.* **99** (2005) 488 (<https://doi.org/10.1016/j.jinorgbio.2004.10.025>)

38. Z. T. A. Ribeiro, E. Machado-Ferreira, L. F. Guimarães, J. Cavaleiro, A. M. A. Britto, N. Redua, L. M. P. de Souza, A. S. Pimentel, P. H. S. Picciani, O. N. Oliveira, C. B. Barreto, C. A. G. Soares, *Colloids Surfaces, A* **626** (2021) 126984 (<https://doi.org/10.1016/j.colsurfa.2021.126984>)
39. R. Csuk, L. Heller, B. Siewert, A. Gutnov, O. Seidelmann, V. Wendisch, *Bioorg. Med. Chem. Lett.* **24** (2014) 4011 (<https://doi.org/10.1016/j.bmcl.2014.06.021>).

SUPPLEMENTARY MATERIAL TO
***In vitro* anticancer studies of a small library of cyclic lipopeptides against the human cervix adenocarcinoma HeLa cells**

ALI N. HMEDAT^{1,2}, MICJEL C. MOREJÓN^{1,3}, DANIEL G. RIVERA^{1,4}, NEBOJŠA Đ. PANTELIĆ^{5,6}, LUDGER A. WESSJOHANN¹ and GORAN N. KALUĐEROVIĆ^{1,5*}

¹Department of Bioorganic Chemistry, Leibniz Institute of Plant Biochemistry, Weinberg 3, 06120 Halle (Saale), Germany, ²Department of Pharmaceutics and Pharmaceutical Technology, Faculty of Pharmacy, Yarmouk University, Irbid 21163, Jordan, ³Department of Environmental Microbiology Electrobiotechnology, Helmholtz Centre for Environmental Research – UFZ, Permoserstr. 15, 04318 Leipzig, Germany, ⁴Center for Natural Products Research, Faculty of Chemistry, University of Havana, Zapata y G, 10400, Havana, Cuba, ⁵Department of Engineering and Natural Sciences, University of Applied Sciences Merseburg, Eberhard-Leibnitz-Strasse 2, 06217 Merseburg, Germany and ⁶Department of Chemistry and Biochemistry, Faculty of Agriculture, University of Belgrade, Nemanjina 6, 11080 Belgrade, Serbia

J. Serb. Chem. Soc. 89 (4) (2024) 471–484

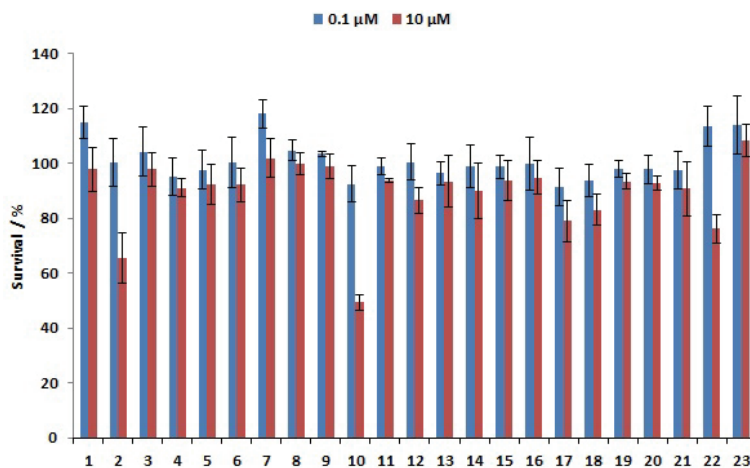


Fig. S-1. Cytotoxicity effects of CLPs against HeLa cell line (MTT assay). Cells were treated with 2 concentrations (0.1 and 10 μM) of CLPs for 72 h. Data represent absorbance measurements normalized to control-untreated cells. Values are expressed as means and standard deviations obtained from independent experiments.

* Corresponding author. E-mail: goran.kaluderovic@hs-merseburg.de

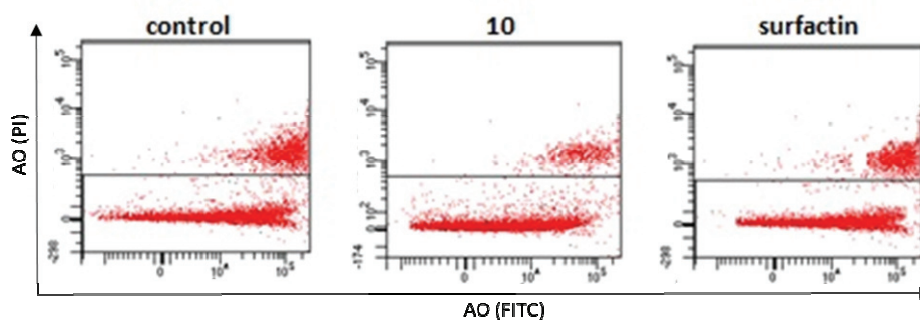


Fig. S-2. Detection of autophagy induction in AO-stained cells using FACS analysis. HeLa cells were treated with DMSO as vehicle control, $2\times IC_{50}$ concentrations of **10** or surfactin for 48 h, stained with AO and then analyzed by flow cytometry. FITC (x-axis) indicates green color intensity, while PI (y-axis) shows red color intensity. Representative images from three independent experiments are shown.

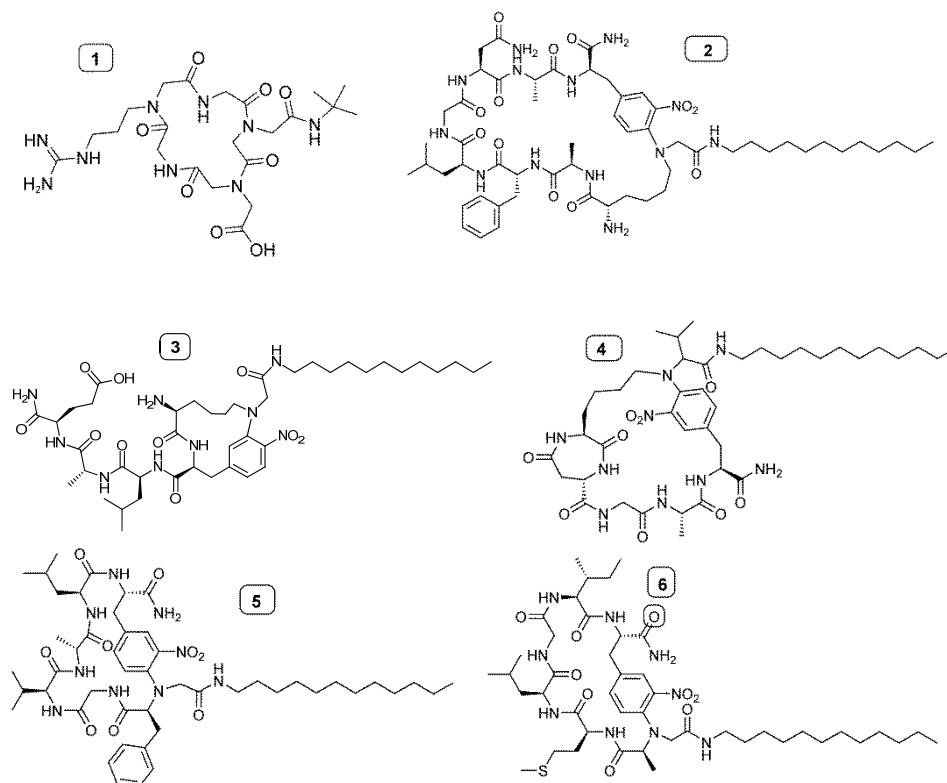


Fig. S-3. Chemical structures of investigated cyclic lipopeptides.

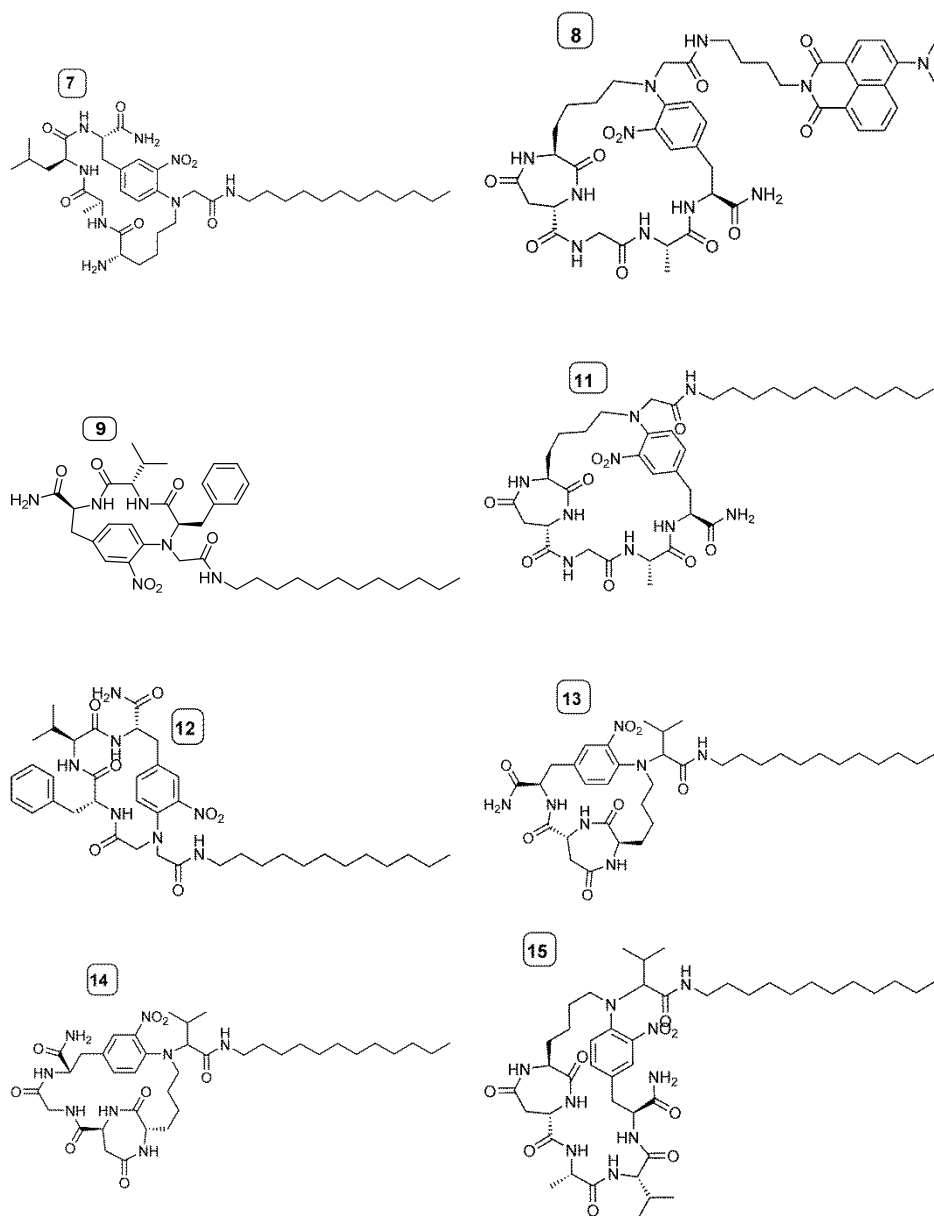


Fig. S-3. Continued.

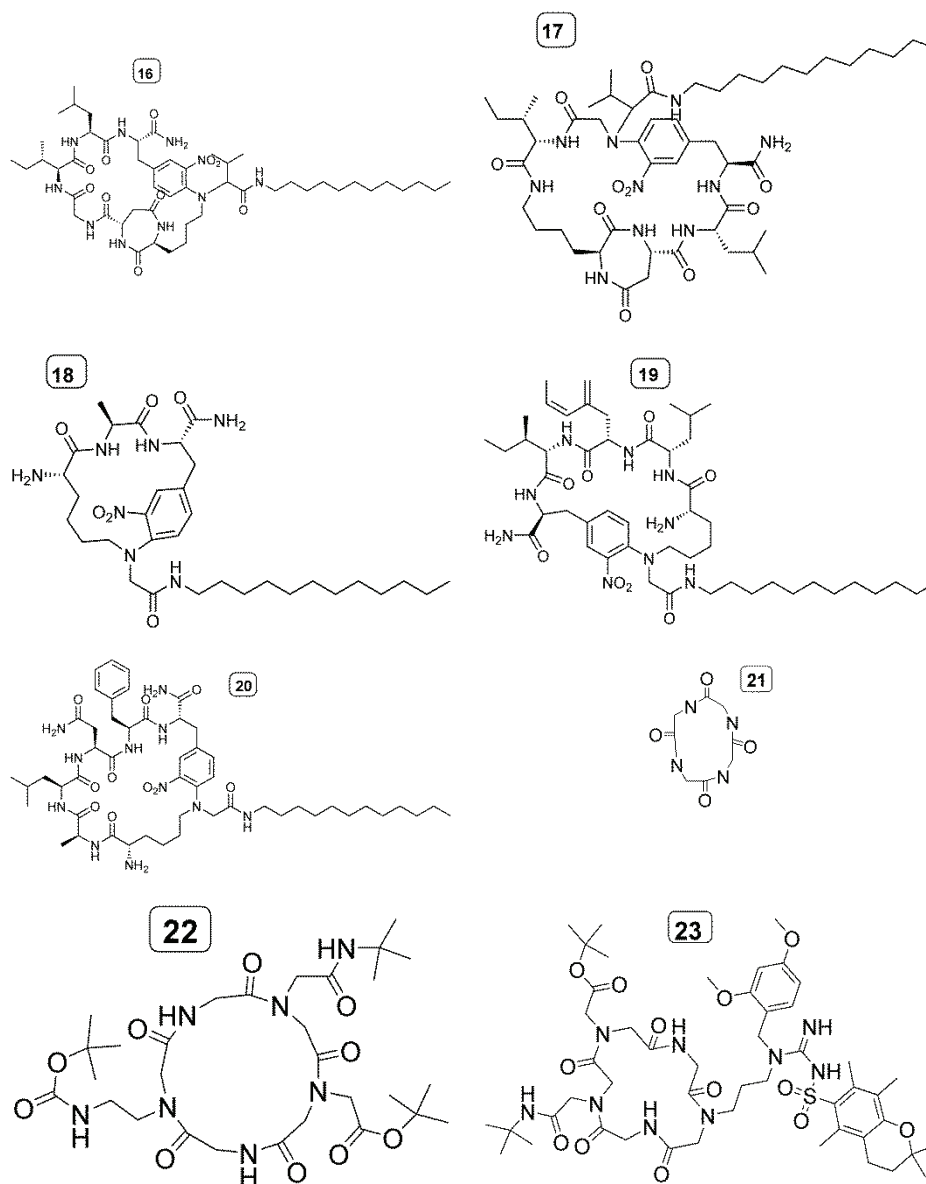
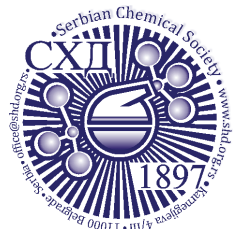


Fig. S-3. Continued.



J. Serb. Chem. Soc. 89 (4) 485–503 (2024)
JSCS–5735

Multivariate statistical analysis approach to investigate the thermodynamic quantities of the benign alternative fuel

KASSIO FELIPE DA COSTA SERRA¹, ALAMZEB KHAN², RAQUEL MARIA TRINDADE FERNANDES³, PEDRO ANTONIO MUNIZ VAZQUEZ⁴ and ALAMGIR KHAN^{3*}

¹Programa de Pós-Graduação Engenharia Aeroespacial, Universidade Estadual do Maranhão – UEMA, Cidade Universitária Paulo VI, Campus São Luís/MA, CEP 65000-00, Brasil, ²Laboratório de Ressonância Paramagnética Eletrônica (LARPE), Departamento de Física, Universidade Estadual de Londrina (UEL), Londrina, PR, Brasil, ³Departamento de Química, Centro de Educação, Ciências Exatas e Naturais – CECEN, Universidade Estadual do Maranhão – UEMA, Cidade Universitária Paulo VI, Campus São Luís/MA, CEP

65000-00, Brasil and ⁴Departamento de Físico-Química, Instituto de Química, Universidade Estadual de Campinas – UNICAMP, Caixa Postal 6154, Campinas, SP, 13083-970, Brasil

(Received 30 May, revised 29 August, accepted 20 November 2023)

Abstract: In order to extract meaningful interpretation from the large data and provide their value to the application areas, chemical data analysis has become a serious challenge in the development and applications of new protocols, technique and methodologies for the mathematical modelling communities and other data science societies. Therefore, in the present work a rapid and robust box-and-whisker plot and multivariate principal component statistical techniques (PCA) are being proposed for the evaluations of the thermodynamic molecular properties data of the benign fuel structures. We observed that, the box-and-whisker plot technique successfully explored all of the thermochemical molecular properties precisely, and described symmetrical distribution of the data along the median values with respect to the rise in temperature. Moreover, applying the PCA technique, the score-plots of PCs diagnosed the peculiar molecular properties variations after a certain peak of temperature with descendant variation in the statistical parameters. Furthermore, PCA parameters not only segregated the thermodynamic properties of propanol and butanol but also, their variations with the temperature. Thus, we concluded that, Box-whisker and PCA statistical techniques are robust and rapid method for the assessment and evaluation of the large molecular thermodynamic quantities data.

Keywords: computational study; benign fuels; statistical analysis; DFT; thermodynamic quantities.

* Corresponding author. E-mail: alamgir@cecen.uema.br
<https://doi.org/10.2298/JSC230530090S>

INTRODUCTION

Over the last few decades, Researchers have been testing some novel fuels by integrating biofuels and conventional fuels, taking into consideration the greenhouse gas emissions as well as calorific capacity (improved octane number and cetane number).¹ In this regard, efforts are being taken to develop alternative and renewable fuels that can produce useful energy while reducing global warming and, as a corollary, environmental pollution.² The blending of ethanol–gasoline, butanol–gasoline, butanol–diesel, butanol–biodiesel, diesel–biodiesel, kerosene–biokerosene have been tested.^{3–5} Butanol is considered to be one of the most promising biofuels with several advantages over bioethanol and has been utilized in large-scale processes in recent decades.⁶ In addition, studies demonstrate that butanol is far more useful than ethanol, with a higher calorific value (29.2 MJ/dm³), lower heat of vaporization (0.43 MJ/kg), and less corrosive properties. Furthermore, it has been discovered that the energy content per volume unit of butanol is comparable to that of gasoline and higher than that of ethanol.⁷ Because of butanol's specific mass and viscosity similarity to those of diesel, it has good solubility in heavier hydrocarbons as well, so it can be added to diesel in higher proportions.⁸

Since conventional investigations involved expensive and time-consuming experimental trial and error technique to determine the energy storage or transformation of innovative materials.⁹ As a result, the scientific community is increasingly supporting the development of atomistic modelling methodologies for use in energetic materials (EM) research and development programs. Where, the change of heat of formation ($\Delta_f H^\circ$) is regarded to be a significant property in predicting the performance during designing and manufacturing of the new energetic materials in technological applications.¹⁰ Moreover, an energetic molecule's $\Delta_f H^\circ$ value should be as high as possible, as this ensures that the chemical material will be unstable when disintegrated into its constituent parts in their standard forms.

Therefore, it appears that a high-density material with such a high heat of formation would be a suitable candidate to be used as a fuel. In this regard, a range of computational approaches based on semi-empirical, *ab initio*, and Density functional theory (DFT methodologies) have become powerful tools for predicting the structures and thermochemical molecular characteristics of materials in recent decades.^{10,11} Aside from measuring molecular characteristics, a trustworthy and efficient analysis of chemical data is also believed essential. Whenever a massive quantity of data is involved in a short period of time, evaluation is becoming a challenge for the researcher. To address this problem, certain systematic approaches for big data analysis projects are being developed. Furthermore, several analysis features such as data analysis, data preprocessing strategy development, visualization of data, and validation of the model are all taken into

account. To extract useful analytical information from spectral data, several multivariate statistical analysis (MVA) techniques are proposed.^{12,13} Typically, these methods use two- or three-dimensional graphs to facilitate multivariate understanding of complex data sets. Pattern recognition, classification and multivariate calibration may all be done with a simple MVA of PCA approach. This statistical method is frequently used to reduce the size of a data set, detect sample similarity, display data structure and find outliers (abnormal samples).¹² Another MVA calibration method is partial least square (PLS), which uses the principal component analysis technique to reduce the dimensionality of the data set in preparation for subsequent spatial correlations.¹²

Therefore, in the present work a robust statistical multivariate PCA technique is presented to explore and diagnose the thermochemical properties differences with respect to temperature (5 to 1500 K), in between the isomers of butanol and propanol fuels additives, based on the small structural effects. The thermodynamic data (*i.e.*, enthalpy change of formation, specific isobaric heat capacity, entropy change of formation, and Gibbs energy change of formation) were computationally predicted for the gaseous state of different chemical structures (isomers of propanol and butanol) used as benign fuel (oxygenated and environmental friendly), using DFT and semi-empirical method. The quality of the thermodynamic quantities is being verified by comparing with literature values using root-mean square error (*RMSE*) and Box-and-whisker technique.

EXPERIMENTAL

In this study, Becke 3-parameter hybrid functional combined with the gradient-correlation functional of Lee–Yang–Parr (B3LYP)¹⁴ and pure functional of Perdew, Burke and Ernzerhof as made into a hybrid by Adamo (PBE0)¹⁵ were tested in the computations using DFTs. All electron Dunning's correlation-consistent (triple zeta) polarized basis set (cc-pVTZ)¹⁶ was employed. A semi-empirical method at the PM6 Hamiltonian was also employed, as implemented in Gaussian.¹⁷ Ground state equilibrium geometry, hessian matrix and normal modes of the vibrations were computed for the gas state 1-propanol, 2-propanol, 1-butanol, 2-butanol and *tert*-butanol molecules, using the afore mentioned methods. The thermodynamic properties like enthalpy, entropy, Gibbs energies and specific isobaric heat values were extracted at different temperatures from the normal-modes computational Gaussian-output-files. All the computations were made at different temperatures of 5, 100, 200, 300, 400, 500, 600, 700, 800, 900, 1000, 1100, 1200, 1300, 1400 and 1500 K. All the computations were performed using the electronic structure program Gaussian09¹⁸ and Statsoft Statistica.¹⁸

Statistical analysis of data

The acquired data have undergone a thorough descriptive statistical analysis,^{19,20} including the Shapiro–Wilk normality test, mean, standard deviation, variance and coefficient of variation. Root mean-square error (*RMSE*) of the data has also been calculated between the thermochemical properties (*i.e.*, enthalpy change of formation, specific heat at constant pressure, entropy change of formation and Gibbs energy change of formation) for the target molecules in order to investigate a comparison in between the expected results obtained with our

proposed computational methods compared to those of the literature.²¹⁻²⁴ The *RMSE* were calculated for the data set as:²⁵

$$RMSE = \sqrt{\frac{\sum_{i=1}^n e_i^2}{n}} \quad (1)$$

Where, e_i represents the error in between the computed obtained values and the literature values,²¹⁻²⁴ and n represents the observation of each parameter at the given temperature.

Before doing the Principal PCA on the data, the data distribution of the computational values were also examined using a Box-plot²⁶ (skewness) of the entire data set and as well as for the individual property. The Box-whisker-plot also helped to understand the symmetry distribution in the thermodynamic quantities data-set. Multivariate PCA was performed to reduce the dimensionality problem and possible exploratory analysis of the molecular structures, temperature dependence and proposed theoretical methods used in the computation of thermodynamic properties. PCA was performed for the whole data set, including the enthalpies, entropies, Gibbs energies and specific heat values at constant pressure, considering the proposed theoretical protocols by using cc-pVTZ basis functions at DFT level of theory (*i.e.*, B3LYP & PBE0 functionals) and PM6 semi-empirical method. The “Statistica” a Data Analysis Software System¹⁸, version 8, was used for performing PCA and other basic statistical analysis.

RESULT AND DISCUSSION

In this section, the results of the computations for the thermodynamic properties (*i.e.*, specific isobaric heat capacity (C_p), enthalpy (H), entropy (S) and Gibbs energy), using cc-pVTZ basis set at DFT functionals (*i.e.*, PBE0 and B3LYP functional) level along with semi-empirical method, for a set of 1-propanol, 2-propanol, 1-butanol, 2-butanol and *tert*-butanol molecules is presented. The computed thermodynamic molecular properties were validated by comparing theoretically predicted values against experimental values collected from the literature.²¹⁻²⁴

Descriptive statistical analysis

The dispersion or variability of a data set inside a statistical function provides an explanation for the numerical values. Researchers utilize variability to calculate the separation between data points and the distribution's center.^{19,20,27} This type of study allows the researcher to investigate the heterogeneity or homogeneity of each data set, while understanding the variability of the different data-sets.^{19,20,27} In order to understand the similarities and differences between the results obtained, a thorough descriptive statistical analysis for each parameter has been calculated. Firstly, we tested the statistical dispersion techniques to study the theoretical models. In this regard, to evaluate how well our proposed computationally modeled data fit to a normal distribution, the Shapiro–Wilk normality test²⁷ approach for the standardized data-set was being performed. The results are presented in Table I and Fig. 1. On the basis of our data distribution results applying the Shapiro–Wilk normality test null hypothesis for the data is to be

normally distributed, we can say that our data is not normally distributed because the p value at the 5 % level of significance compared to 0.05 is smaller than the obtained value, as can be seen in the Table I.

TABLE I. Shapiro–Wilk normality variable test utilizing standardized full thermodynamic data set, mean and standard deviation (St. Dev.) calculated for each thermodynamic quantity absolute error in between the obtained the literature values.²¹⁻²⁴ In the acronym Pxy and Bxy, P and B stand for propanol and butanol, respectively. Subscripts such as “ $x = 1, 2$ or 3” are used to number the isomers 1-propanol, 2-propanol, 1-butanol, 2-butanol and *tert*-butanol, while “ $y = 1, 2$ or 3” stand for the PBE0, B3LYP and PM6 methods, respectively

Sample	Statistics	P value	Enthalpy		Entropy		Specific heat		Gibbs energy	
			Mean	St. Dev.	Mean	St. Dev.	Mean	St. Dev.	Mean	St. Dev.
P11	0.943	0.007	2.60	2.10	2.43	1.19	5.03	3.28	25.70	2.64
P12	0.941	0.006	1.84	1.72	1.50	0.83	2.98	1.62	18.90	1.25
P13	0.941	0.006	2.60	2.10	2.43	1.19	5.03	3.28	25.70	2.64
P21	0.942	0.007	3.12	1.89	3.41	1.90	5.12	2.64	7.42	1.27
P22	0.943	0.007	2.14	1.42	1.96	1.22	5.18	2.49	9.33	0.99
P23	0.940	0.006	3.12	1.89	3.41	1.90	5.12	2.64	7.42	1.27
B11	0.941	0.006	2.49	1.47	2.72	1.50	3.98	1.84	23.49	1.21
B12	0.941	0.006	1.27	0.88	1.08	0.77	3.92	1.96	26.02	0.85
B13	0.941	0.006	2.49	1.47	2.72	1.50	3.98	1.84	23.49	1.21
B21	0.943	0.007	2.95	1.69	3.08	1.84	5.00	2.82	23.21	2.58
B22	0.946	0.010	1.70	1.17	1.87	1.15	4.67	2.39	30.17	8.58
B23	0.940	0.006	2.95	1.69	3.08	1.84	5.00	2.82	23.21	2.58
B31	0.945	0.009	2.94	1.76	3.60	2.09	3.45	1.99	4.22	6.43
B32	0.944	0.009	1.66	1.06	1.61	0.94	3.60	1.84	2.78	6.98
B33	0.942	0.007	2.94	1.76	3.60	2.09	3.45	1.99	4.22	6.43

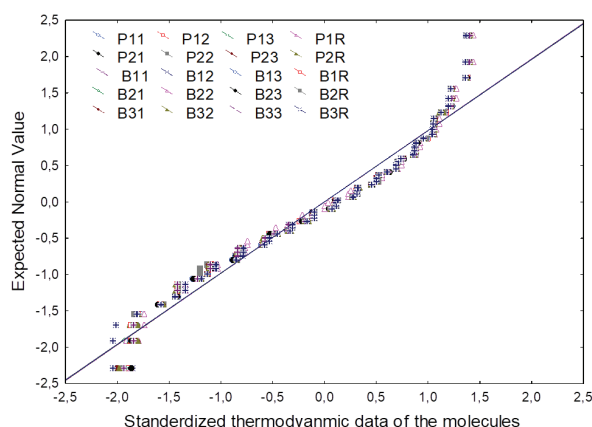


Fig. 1. Shapiro–Wilk normality variable test for the standardized full thermodynamic data set. Where, in the acronyms Pxy and Bxy, P and B stand for propanol and butanol, respectively. Subscripts such as “ $x = 1, 2$ or 3” are used to number the isomers 1-propanol, 2-propanol, 1-butanol, 2-butanol and *tert*-butanol, while “ $y = 1, 2$ or 3” stand for the PBE0, B3LYP and PM6 methods, respectively.

Since we are using the temperature dependence thermodynamic molecular properties data for the different isomers of propanol and butanol molecules, the thermodynamic properties have been steadily increasing and decreasing with the change in temperature. This made our data-set redundant toward normality, as can be seen in Fig. 1. When the Shapiro–Wilk normality test diagram was analyzed, a significant positive skew in the data was shown to be caused by the increase in thermodynamic properties brought on by raising the temperature. Consequently, it appears towards the end of the curve as a tail.

The standard deviation, variance and coefficient variance values were also used to test for statistical dispersion, however we found that the measurement of these statistical distribution techniques, due to the lack of normal distribution, are not appropriate for the current thermodynamic features. Thus, the precision of the results is being estimated, using the absolute error data in between the literature^{21–24} and the obtained values, by calculating the mean, standard deviation, variance and coefficient of variation. The results are illustrated in Tables I and II.

TABLE II. Root-mean square error (*RMSE*), Variance (Var.) and percent coefficient of the variance (*%CV*) calculated in between the thermodynamic quantities calculated by using the theoretical data set at computational level to the reference data of NIST web book for the molecules of interests. In the acronym Pxy and Bxy, P and B stand for propanol and butanol, respectively. Subscripts such as “x = 1, 2 or 3” are used to number the isomers 1-propanol, 2-propanol, 1-butanol, 2-butanol and *tert*-butanol, while “y = 1, 2 or 3” stand for the PBE0, B3LYP and PM6 methods, respectively

Sample	Enthalpy			Specific heat			Entropy			Gibbs energy		
	<i>RMSE</i>	Var.	<i>%CV</i>	<i>RMSE</i>	Var.	<i>%CV</i>	<i>RMSE</i>	Var.	<i>%CV</i>	<i>RMSE</i>	Var.	<i>%CV</i>
P11	0.84	4.43	80.94	1.81	1.43	49.16	6.34	10.77	65.30	6.17	6.99	10.29
P12	0.66	2.97	93.54	1.17	0.68	55.22	4.53	2.61	54.13	4.53	1.56	6.62
P13	2.15	4.43	80.94	2.98	1.43	49.16	1.84	10.77	65.30	1.17	6.99	10.29
P21	1.18	3.59	60.70	2.35	3.59	55.67	1.45	6.94	51.46	1.80	1.61	17.07
P22	0.70	2.01	66.23	1.90	1.49	62.16	2.18	6.20	48.03	2.24	0.98	10.61
P23	2.07	3.59	60.70	3.60	3.59	55.67	2.12	6.94	51.46	0.74	1.61	17.07
B11	0.97	2.17	59.09	1.83	2.26	55.15	5.05	3.38	46.16	5.62	1.47	5.15
B12	0.38	0.78	69.66	1.29	0.59	71.32	6.27	3.84	49.96	6.22	0.73	3.27
B13	2.10	2.17	59.09	3.34	2.26	55.15	1.56	3.38	46.16	2.06	1.47	5.15
B21	1.01	2.86	57.22	2.11	3.38	59.67	5.37	7.95	56.33	5.58	6.67	11.13
B22	0.49	1.38	69.16	1.55	1.32	61.62	6.58	5.69	51.09	7.48	73.54	28.42
B23	2.13	2.86	57.22	2.15	3.38	59.67	1.94	7.95	56.33	2.52	6.67	11.13
B31	1.22	3.10	59.88	2.01	4.38	58.15	1.74	3.98	57.77	1.79	41.36	152.39
B32	0.55	1.13	63.79	1.37	0.88	58.09	0.45	3.40	51.20	1.74	48.68	251.14
B33	2.42	3.10	59.88	3.62	4.38	58.15	6.01	3.98	57.77	4.31	41.36	152.39

To understand the deviations and spreading in the molecular properties data-set, root mean square error (*RMSE*) a regression analysis bi-variate technique, variance and coefficient of variations of the absolute errors were calculated.

Table II provides an illustration of the calculated values for the *RMSE*, variance (Var.) and percent coefficient of variations (*%CV*).

The *RMSE* identifies the degree to which the data deviates from actual or published values.^{21–24} Root mean-square error (*RMSE* or *RMS* deviation) between each computed thermodynamic quantity at DFT levels of theory and semi-empirical technique to that of the reference values for the tested benign energy fuels has been calculated for the sake of comparison and evaluation. The results show that, in comparison to other computational approaches, the semi-empirical method PM6 exhibits some higher variations in accuracy for the Enthalpy change of formation and the specific heat at constant pressure. While, an uncommon case for the *tert*-butanol molecule has also been noted, with some greater deviations for entropy and Gibbs energy. Additionally, after analysis, the largest deviations were found for the enthalpy, specific heat at constant pressure, entropy and Gibbs energy to be 2.42, 3.62, 6.01, and 4.31 kJ/mol, respectively. While the global *RMS* deviation was also being calculated, the thermodynamic characteristics of 2-butanol at the B3LYP level and 1-butanol using PBE0, B3LYP and PM6 approaches exhibit larger deviations when compared to the other molecular systems. The global *RMSE* for the theoretical approaches shows an overall variance for the PBE0, B3LYP and PM6 of 9.65, 9.80 and 9.65 kJ/mol, respectively. Therefore, it can be inferred that all theoretical methods, precisely and in good accordance with each other, determined thermodynamic properties.

Additionally, Var. and *%CV* of the absolute error between the obtained data and that of the reference data were calculated; the results of these calculations can be seen in Table II. The statistical concept of *%CV* is a statistical technique to measure the dispersion of data points, by displaying the size of standard deviation to its mean values in a data series around the mean.²⁸

Due to the consistent increase or decrease of the thermodynamic properties, our standardized data set confirms a rejection of the null hypothesis, which led to certain greater variability and the standard deviation numbers. Therefore, the variance and percent coefficient of variance of the data set to that of the reference data set (*i.e.*, absolute error) were determined in order to evaluate the efficiency of the theoretical approaches and the nature of the acquired data set (as shown in Table II). On analyzing the calculated values, the lowest percent dispersion of the absolute error data observed for the 1-butanol using the B3LYP, PBE0 and PM6 techniques, respectively, was 3.27, 5.15 and 5.15 %. While, using the PBE0, PM6 and B3LYP techniques, the highest *%CV* observed for the *tert*-butanol was 152.39, 152.39 and 251.14 %, respectively. As therefore, the descriptive statistical evaluation of the current investigation has demonstrated that our theoretical methodologies were efficient at acquiring and estimating the molecular characteristics with experimental precision.

Box-Whisker-plot

The distribution of the computational thermodynamic characteristics results acquired, at the DFT levels (*i.e.*, PB3LYP and PBE0) using cc-pVTZ, as well as the reference data was examined by the box-and-whisker plot.²⁶ The plots of all the distribution data is depicted in the Fig. 2. The analysis of the box-and-whisker diagram not only assisted in detecting the outliers in the data-set, but also provide an overall picture of the data's typical distribution.

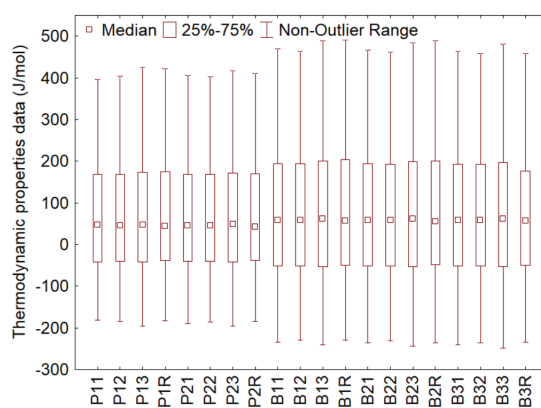


Fig. 2. Box-plot for the different molecular structures used for the computation of complete thermodynamic properties data using DFT and semi-empirical methods. Where, P_{xy} and B_{xy} stands for P = propanol, B = butanol; $x = 1$ or 2 propanol and 1, 2 or *tert*-butanol; $y = 1, 2, 3$ for PBE0, B3LYP and PM6 DFT methods, respectively, while P2R and B3R means literature values²¹⁻²⁴ for 2-propanol and *tert*-butanol.

Since, the thermodynamic data set is constituted of specific heat, Gibbs energy, enthalpy and entropy data set, which described the characteristics of energetic materials and, are highly reliant on the temperature conditions. Thus, a very similar behaviour in variation with respect to temperature has been observed for each thermodynamic property. Therefore, these small increments values influence the overall computational thermochemical data distribution for the chemical substance of interest. The box plots are made up of two parts; 1) a box which depicts the data spread at 25 to 75 %, and 2) whiskers which depict the data spread from underneath the 25 % to the minimum point and over 75 % to the maximum point.¹² While examining the graph (as shown in Fig. 2), it has been observed that, the lower quartile (lower end of the box, Q_1) for the propanol and butanol isomers spanned from -195.11 to -35.31 J/mol and -248.77 to -45.50 J/mol, respectively.

Furthermore, the highest quartile (upper end of the box, Q_3) that constitute almost 25 % of the data set, have values in the range from 153.37 to 425.51 and 175.49 to 490.36 J/mol for the propanol and butanol isomers, respectively. Sur-

prisingly, all of the molecules' interquartile ranges or mid-spreads are quite comparable, suggesting that our theoretical approaches computed the thermochemical molecular properties in accordance with each other and with the reference data. Using the B3LYP DFT approach, a box-plot demonstrated a small interquartile range for propanol isomers and a higher interquartile range for butanol isomers. Moreover, the propanol and butanol isomers' median value (Q_2) appears to be pushed more towards the lower quartile. Additionally, the thermochemical data was spread more than 30 % towards the upper quartile, demonstrating that the range between $(Q_1-Q_2) < (Q_2-Q_3)$ in the computed data seems to have a positive symmetry or positive skew.

The individual thermodynamic property (*i.e.*, specific isobaric heat capacity (Cp), enthalpy change of formation ($\Delta_f H^\circ$), entropy change of formation ($\Delta_f S^0$) and Gibbs energy change of formation ($\Delta_f G^0$)) was also analysed by the Box-Whisker plot, in order to determine the discrepancies and departures in the computed data-set, respectively. The Box-plot statistical data distribution analysis is depicted in Fig. 3. After the statistical analysis of computed enthalpy molecular property of the aforementioned isomers of propanol and butanol molecules, it was observed that, Q_1 varied from -126.44 to -62.83 J/mol and Q_3 varied from 55.34 to 179.07 J/mol, respectively. Moreover, the Fig 3b showed that the molecular property data was spread more than 59 % towards the upper quartile, which means that there exist a positive skew in the obtained computed characteristic.

Analysing the data-set for the specific heat, entropy and Gibbs energy (as depicted in Fig. 3b-d), a variation has been observed from -248.77 to -71.72 J/mol, -156.60 to -34.64 J/mol, 174.89 to 324.68 J/mol for the lower quartile, and 80.64 to 189.02 J/mol, 44.59 to 92.73 J/mol and 357.90 to 490.36 J/mol for the upper quartile, respectively. Unexpectedly, the data set for all three parameters were spread at least 43.04 % towards the lower quartile, suggesting that the thermochemical data set for each property exhibit some negative symmetry.

Principal component analysis

The multivariate PCA was performed to reduce the dimensionality problem and possible exploratory analysis of the proposed computed thermodynamic physicochemical properties of the molecules. The summarized eigenvalues and the variance variabilities on each principal component for each data set constituting of 15 cases (*i.e.*, temperature variations) for each thermodynamic property using the 22 variables (*i.e.*, molecular structures at the given model) are being summarized and illustrated in Table III.

Normally, PCA data processing comprises of two distinct steps,²⁹ the first step is the PCA "data compression" step, which removes the redundancy in the original data, where the first few main components (PC) generally describe most of the information contained in the original data. The second stage is the "cluster

visualization” formed in the datasets, making a two-dimensional graph of the principal components. Information regarding data analysis is being obtained by interpreting PCA parameters such as loadings, scores, eigenvectors, eigenvalues, etc., of the principal components (PCs).

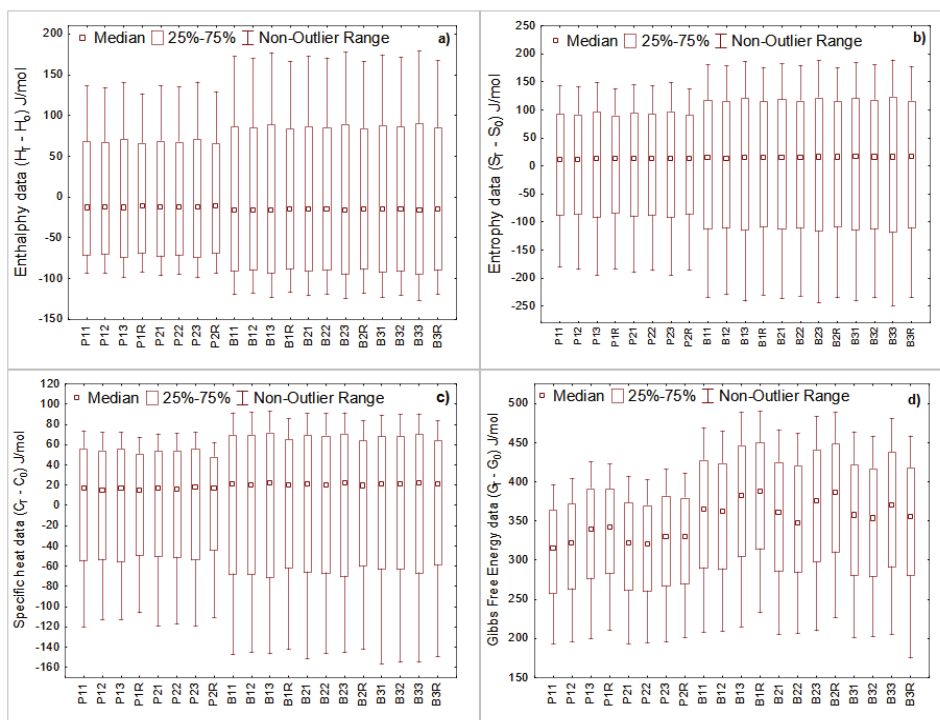


Fig. 3. Box-plot for the different molecular structures used for the computation of thermodynamic properties using DFT and semi-empirical methods, where, the individual data is depicted in sub-figure; a) enthalpy data, b) entropy data, c) specific isobaric heat coefficient data and d) Gibbs energy data. P_{xy} and B_{xy} stands for P = propanol, B = butanol; x = 1 or 2 propanol and 1, 2 or *tert*-butanol; y = 1, 2, 3 for PBE0, B3LYP and PM6 DFT methods, respectively, while P2R and B3R means literature values²¹⁻²⁴ for 2-propanol and *tert*-butanol.

The molecules of interests were similar in chemical nature and almost of the same size having same number of basis functions, which make a difficulty in the understanding the small variance in the molecular properties. Thus, the principal components (PCs) and their eigenvalues is used to identify the most important molecular changes and inclinations in the data sets.³⁰ PCA for the molecules of interest was performed in two steps: for the entire data set, including the specific isobaric heat capacity, Gibbs energy, enthalpy and entropy data set, and individually for each thermochemical property, taking into account computational methodologies, temperature variation and molecular structure effect.

TABLE III. Eigenvalues and proportion of total variability of thermodynamic properties computed at DFT/cc-pVTZ methodologies and PM6 semi-empirical method for the molecules of interests

Property	PCA parameter	PC1	PC 2	PC3
Complete data	Eigenvalues	21.9498	0.0473	0.0013
	% variability	99.7718	0.2151	0.0058
Specific heat	Eigenvalues	21.9989	0.0009	0.0002
	% variability	99.9950	0.0041	0.0008
Enthalpy	Eigenvalues	21.9993	0.0006	0.0001
	% variability	99.9969	0.0026	0.0005
Gibbs energy	Eigenvalues	21.9853	0.0104	0.0034
	% variability	99.9334	0.0474	0.0155
Entropy	Eigenvalues	21.9989	0.0009	0.0002
	% variability	99.9950	0.0041	0.0008

The first three principal components (PCs) were the most important, accounting for 99.992 % of the total variance in molecular properties. PCs are fitted to a data set in PCA so that the first PC may explain as much of the original variation between the cases as possible. The second PC, on the other hand, is adjusted orthogonally to the first PC and is intended to characterize the majority of the remaining variances and so on.²⁹ According to the Table III, the 1st and 2nd principal components in this analysis demonstrate an overall variance of at least 99.980 % for characteristics of interest.

Temperature dependence on the thermodynamic quantities (Score-plots)

The scores are the projections of molecular property at each temperature using the computational methods along the principal component line, and plotting them in the form of a bi-plot can explore the similarities and differences in between them, resulting in the development of groups.³⁰ The bi-plots in between the T -distributions for the complete thermodynamic data set is depicted in Fig. 4.

It can be observed that, the dataset's score-plot PC1–PC2 (as can be seen Fig. 4b) efficiently showed the distribution and categorization of thermochemical property variation with temperature. Based on the orientation of PC2 over PC1, it was possible to detect temperature variation in two agglomerating groups, indicating a variance of 99.998 % for the entire thermochemical properties data set. Aside from grouping the distinct factors, the bi-plot of scores can also disclose and identify data outliers in the data. While, on PC1 and PC2, for the molecule of interest, we discovered an interesting ascending and descending order in each molecular feature with an increase in temperature, correspondingly. The Gibbs energy and entropy molecular properties were found to follow a similar pattern as temperature rises, with the only difference being such a rapid downward order in the variation of the Gibbs energy as compared to the entropy variation, due to the small intermission of increment of molecular property.

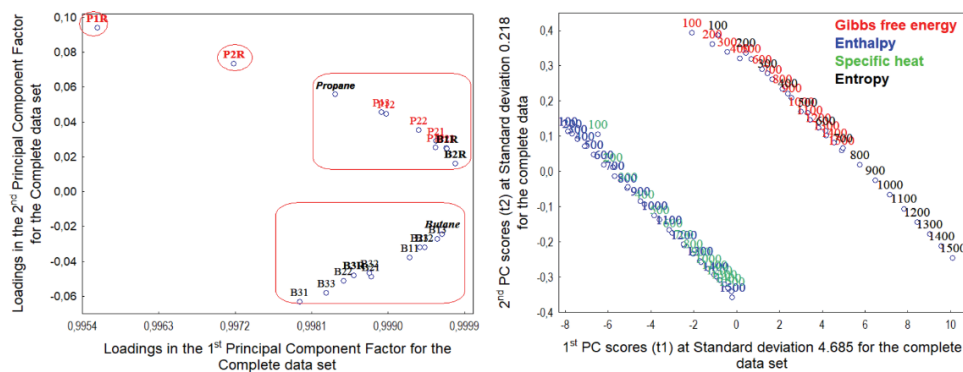


Fig. 4. Plots graphs representing the combination of loadings coefficient (a) and scores (b) for the 1st and 2nd principal components obtained from the thermodynamic quantities data analysis of interest at all the applied computational methods. Pxy and Bxy stands for P = propanol, B = butanol; x = 1 or 2 propanol and 1, 2 or *tert*-butanol; y = 1, 2, 3 for PBE0, B3LYP and PM6 DFT methods, respectively, while P2R and B3R means literature values²¹⁻²⁴ for 2-propanol and *tert*-butanol.

Since, the entropy and Gibbs energy of a chemical structure is thought to be strongly affected by the physical state of the molecules, particularly intermolecular forces affecting the entropy of the substances and the dependence of the Gibbs energy on the entropy value. Which gives the similar results in the computation process for the present studies gas-phase geometries of interest. The response of the specific isobaric heat capacity and enthalpy variation with temperature, on the other hand was found to be equivalent, where both thermodynamic variables represent the heat content of a chemical substance. To understand in detail the behaviour of each molecular property with respect to the temperature variation, the thermochemical properties were studied separately.

The molecular structures showed an upward and subsequently a declining order on the 2nd PC for the specific isobaric heat capacity values and entropy molecular properties, according to the score-plot (explored in Fig. 5). It's possible that the declining order after 700 K is due to a modest increase in molecular characteristics as temperature rises. Furthermore, the enthalpy of molecular structures first display an ascending order on PC2 from negative to positive scores values, culminating at 700 K, followed by a decline in molecular characteristics.

This suggests that the temperature of 700 K is assumed to be a critical temperature for the specific heat, enthalpy, and entropy of the molecular structures of interest, with a consequent decrease in computed values. In contrast, after examining Fig. 5b, it was observed that the Gibbs energy property appears different from the other three molecular thermochemical properties. In comparison to the other computed values, PCA separated the molecular feature for all the molecules at 100 K. In addition, the score-plots separated the data into three groups, each

varying from 200 to 400 K, 500 to 900 K and 1000 to 1500 K. This unexpectedly fluctuating molecular property behaviour may be due to the propanol isomers, that have a smaller number of carbon and hydrogen atoms than the butanol isomers, leading to a lower molecular property increment. Thus, resulted in the segregation of the Gibbs energy in to three different increment order with the variation of temperature.

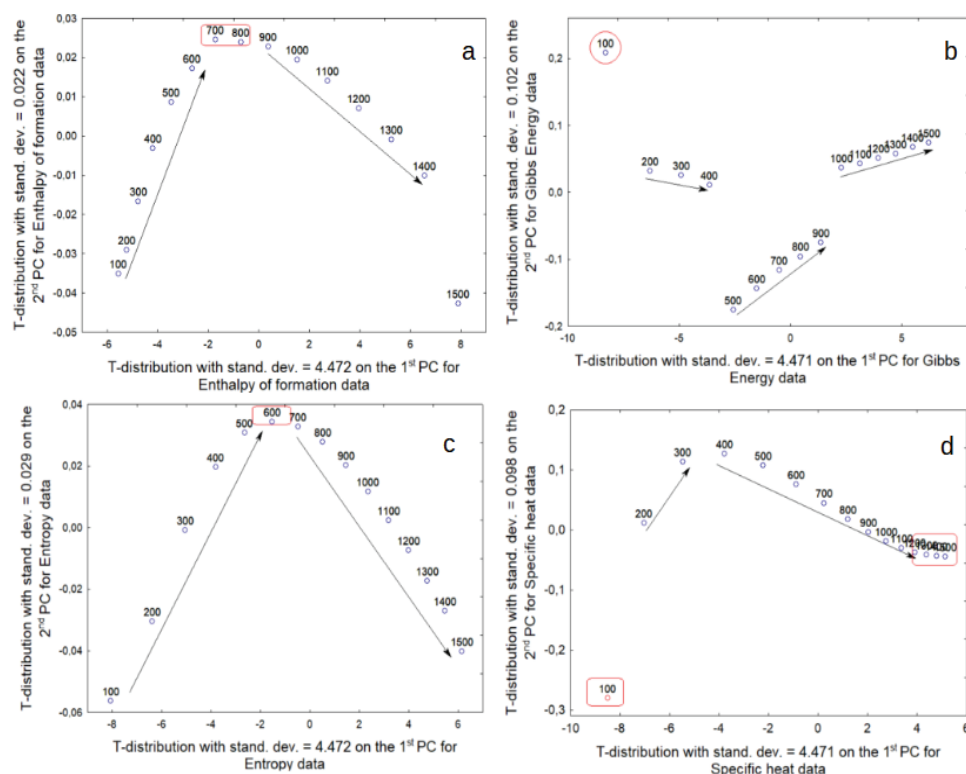


Fig. 5. Score (t) plots in between the 1st and 2nd principal components obtained for the thermodynamic characteristics data analysis of interest for all the applied computational methods; a) enthalpy, b) Gibbs energy, c) entropy, d) specific heat at constant pressure data.

Exploration of thermochemical properties (loading-coefficients plots)

The analysis of loading factors is suggested as a very useful tool to explore the importance of the variables based on the correlations in between them,³¹ which in the present case is applied to the thermochemical properties of the molecular structures using the theoretical methods. In the current research, the association between thermodynamic quantities for each molecular structure at the given theory level was evaluated for the entire data set, taking into consideration commonalities and contrasts with reference data, and subsequently, the indi-

vidual molecular property analysis were also performed for each computed thermochemical characteristic. Since the thermochemical property represents the energy content of a chemical substance, it varies and depends on the number and nature of chemical bonds. In this situation, we were studying the propanol and butanol isomers, which have almost the same amount of chemical linkages and are very much similar in nature. As a result, the variance in thermochemical characteristics with temperature is remarkably similar.

During the principal component analysis of the data set, a strong correlation on the first principal component resulted in the aggregation of all the loading factors values on it. Such agglomeration problems can be solved, while examining the latent minuscule information caused by the high associations between the strong correlated variables, by making a possible projection bi-plot in between the loading-coefficients of two principal components.¹⁴ For each variable, which is the molecular property computed at the computational method for the molecular structures, the loading factor values on each component represent how much of the characteristic is common in between the molecular structure on that PC. Khan *et al.*¹¹ had used arrows projected strategy to assess the vanishingly small differences in between the theoretical methodologies used to compute Raman intensities, where a smaller angle than 45° was considered positive and stronger correlation, 90° was considered insignificant correlation, and above 135° up to 180° was considered negative strong correlation in between the variables of interest. The authors of the present study utilized a bi-plot between the PC2 and PC3 where the ascending shift on 3rd PC from -0.01354 to 0.01808 values to classify and grouping in between the variables of interest. Upon analysing, it was observed that the 1st PC×2nd PC factor loadings bi-plots values successfully separated the structural isomers of propanol and butanol. It means that, the smaller variance on 1st by 2nd component can explore the hidden minuscule variation in between the chemical compounds of similar nature containing almost similar number of atoms. On the other hand, while studying the loadings on the principal components, it also helped us to diagnose the strong similarities in the results in between the utilized different computational methodologies.

Where, we have observed that the semi-empirical methodology successfully computed the thermodynamic quantities of the benign biofuel as precisely to that of DFT methodologies. Furthermore, the loading-coefficients for the specific isobaric heat capacity, enthalpy, entropy and Gibbs energy for the isomeric structures of the propanol and butanol molecules were analysed in detail for the quanti-quali similarities and differences in between molecular properties for the structural isomers to the reference data, as illustrated in the Fig. 5. PCA computed the loading values considerably differently since each molecular thermochemical property of interest varies with temperature differently.

This allows us to investigate the materials' molecular energetic characteristics. In the analyses of the enthalpy data, the loading coefficient bi-plots (as seen in the Fig. 6a) classified the molecular property computed for each molecule of propanol and butanol isomers at the theoretical level in well-distributed correlated way. Where, plotting the loadings coefficients for the 2nd PC upon 1st PC segregated the correlated molecular property for the isomers of propanol and butanol molecular properties much closer to the traditional fuels, *i.e.*, propane and butane molecular property along with their reference data. It is suggested that variation of enthalpy of formation for the molecules varied with same fraction. Interestingly, the *tert*-butanol molecule represents a small dissimilarities in the molecular property compared to the other molecules, which can be visualized in the score-plot analysis. Furthermore, the loading-coefficients values on the 3rd component spread the molecular property against 2nd PC, while examining the PCA loading-coefficient for the specific isobaric heat capacity data set (as shows in the Fig. 6d). The bi-plot distributed the molecular properties equally in all sides, where the *tert*-butanol was being segregated from the rest of the molecules

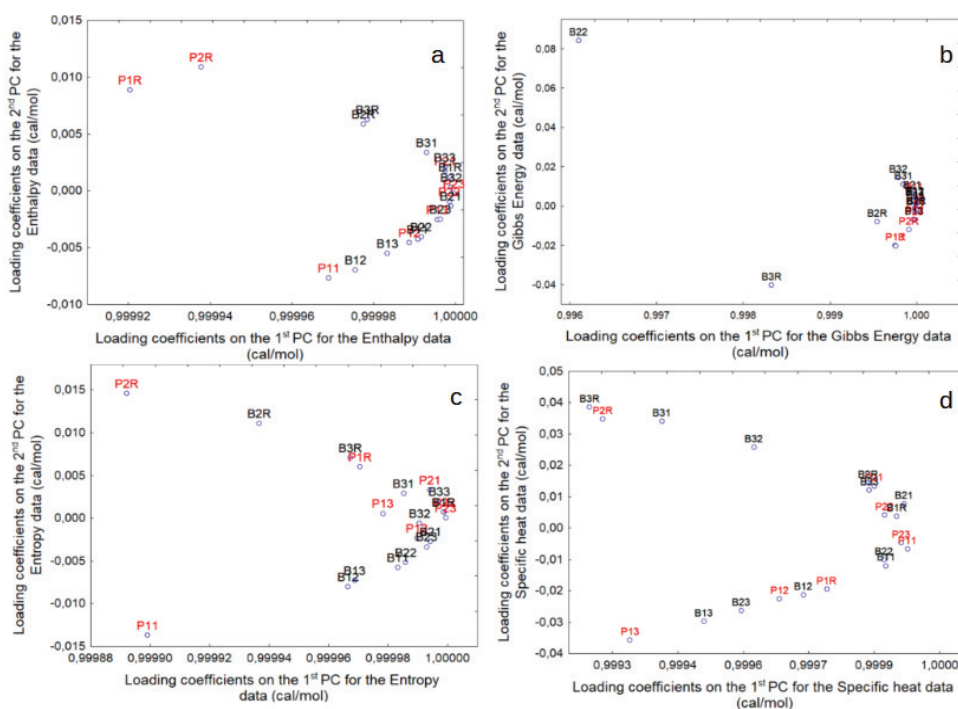


Fig. 6. Plots graphs representing the combination of loadings for the 1st and 2nd principal components obtained of the thermodynamic quantities data analysis of interest at all the applied computational methods: a) enthalpy, b) Gibbs energy, c) entropy and d) specific heat at constant pressure data.

due to high specific heat content by these structures. PCA interestingly separated the molecular property of butane and propane from the rest of structures due to absence of the “O–H” group in them. On investigating the loading bi-plots for the entropy property (illustrated in the Fig. 6c), the loading points for data-set was all agglomerated in between the -0.0199 to 0.0081 on the PC2. A strong correlation has been observed for all the other structures. In addition, the molecular property for the 1-propanol using the DFT methods were found separated from the rest of the molecules.

While analysing the values of the loading coefficients of the Gibbs energies, we discovered that the molecular property behaved very similarly to the entropy of a system, except for the case of 2-butanol using DFT method, which shows a dissimilarity in molecular property compared to the other structures. Since, Gibbs energy change is a derived quantity that blends the enthalpy and entropy change in the computational equations for a chemical substance.³² Thus, it resulted in very competitive similarities to the entropy behaviour.

CONCLUSIONS

The present investigation concludes that high-level electronic structure calculations combined with multivariate statistical analysis was very much successful investigating the different thermodynamic properties of the various chemical structures of interests. The *RMS* deviations of the molecular properties for the given structures represent a lot of similarities in the computed values and the literature values. The box-and-whisker plot statistical technique demonstrated that all the thermochemical quantities are precise and symmetrically distributed along the median values according to the rise in temperature. The principal component analysis explored the minuscule changes in the thermochemical properties for the molecular structures of interests containing the same number of bonds and types of atoms rapidly. Furthermore, the score-plots diagnosed the molecular properties variations after a certain peak of temperature with descendant variation in the statistical parameters. In addition, the loading-coefficient parameters explored and categorized the propanol from the butanol molecular properties, where a modest difference in the molecular properties is being found.

Finally, we suggest that PCA is a robust statistical method which can be applied not only to evaluate the molecular thermodynamic quantities, but in future it can also be applied to the other computational molecular properties data set.

Acknowledgment. The authors thank the *Instituto de Química* (IQM/UNICAMP) for the use of the availability of Computational facilities in Campinas. Mr. Serra thanks the UEMA postgraduate program for the monthly stipend and the use of universities resources.

ИЗВОД

ПРИСТУП МУЛТИВАРИЈАНТНОМ СТАТИСТИЧКОМ АНАЛИЗОМ ПРИ
ИСТРАЖИВАЊУ ТЕРМОДИНАМИЧКИХ ВРЕДНОСТИ БЕЗОПАСНОГ
АЛТЕРНАТИВНОГ ГОРИВАKASSIO FELIPE DA COSTA SERRA,¹ ALAMZEB KHAN,² RAQUEL MARIA TRINDADE FERNANDES,³
PEDRO ANTONIO MUNIZ VAZQUEZ⁴ и ALAMGIR KHAN³

¹Programa de Pós-Graduação Engenharia Aeroespacial, Universidade Estadual do Maranhão – UEMA, Cidade Universitária Paulo VI, Campus São Luís/MA, CEP 65000-00, Brasil, ²Laboratório de Ressonância Paramagnética Eletrônica (LARPE), Departamento de Física, Universidade Estadual de Londrina (UEL), Londrina, PR, Brasil, ³Departamento de Química, Centro de Educação, Ciências Exatas e Naturais – CECEN, Universidade Estadual do Maranhão – UEMA, Cidade Universitária Paulo VI, Campus São Luís/MA, CEP 65000-00, Brasil, ⁴Departamento de Físico-Química, Instituto de Química, Universidade Estadual de Campinas – UNICAMP, Caixa Postal 6154, Campinas, SP, 13083-970, Brasil

За добијање смисленог тумачења, из мноштва података и обезбеђивања њихове ваљаности у подручју примене, анализа хемијских података је постала озбиљан изазов у развоју и примени нових протокола, техника и методологија за заједнице математичког моделовања и друга друштва за науку о подацима. Зато се у овом раду предлажу брзе и робустне технике „box-and-whisker plot” и статистичке технике мултиваријантне анализе главних компоненти (PCA) за оцену података термодинамичких молекулских особина структура молекула безопасних горива. Опазили смо да „box-and whisker plot” техника успешно истражује све термохемијске молекулске особине прецизно, и описује симетричну расподелу података дуж медианских вредности у односу на пораст температуре. Поред тога, применом PCA технике, графици оцена (score-plots) главних компоненти су дијагностиковали необичне варијације у молекулским особинама након одређеног врхунца температуре са опадајућом варијацијом статистичких параметара. Даље, PCA параметри не само да раздвајају термодинамичке особине пропанола и бутанола, већ такође, њихове варијације са температуром. Тако, закључујемо да су „Box-and-whisker” и PCA статистичке технике робустан и брз метод за процењивање и вредновање мноштва података о молекулским термодинамичким величинама.

(Примљено 30. маја, ревидирано 29. августа, прихваћено 20. новембра 2023)

REFERENCES

1. J. G. Yu, Q. J. Xiang, M. H. Zhou, *Appl. Catal., B* **90** (2009) 595 (<https://doi.org/10.1016/j.apcatb.2009.04.021>)
2. A. A. Khan, M. Tahir, *J. CO2 Util.* **29** (2019) 205 (<https://doi.org/10.1016/j.jcou.2018.12.008>)
3. O. Doğan, *Fuel* **90** (2011) 2467 (<https://doi.org/10.1016/j.fuel.2011.02.033>)
4. H. F. Mustafa, S. Abdullah, M.Z. Abdullah, K. Sopian, A. K. Ismail, *Renew. Energy* **74** (2015) 505 (<https://doi.org/10.1016/j.renene.2014.08.061>)
5. N. Yilmaz, A. Atmanli, *Energy* **140** (2017) 1378 (<https://doi.org/10.1016/j.energy.2017.07.077>)
6. P. Durre, *Curr. Opin. Biotechnol.* **22** (2011) 331 (<https://doi.org/10.1016/j.copbio.2011.04.010>)
7. Y. Dahman, C. Dignan, A. Fiayaz, A. Chaudhry, in *Biomass, Biopolymer-Based Materials, and Bioenergy*, D. Verma, E. Forunati, S. Jain, X. Zhang, Eds., Woodhead

- Publishing Series in Composites Science and Engineering, Woodhead Publishing, Elsevier, New York, 2019, p. 241 (<https://doi.org/10.1016/B978-0-08-102426-3.00013-8>)
8. A. T. Balaban, *HYLE* **19** (2013) 107 (<https://www.hyle.org/journal/issues/19-1/balaban.htm>)
 9. X. Wu, F. Kang, W. Duan, J. Li, *Prog. Nat. Sci.: Mater. Int.* **29** (2019) 247 (<https://doi.org/10.1016/j.pnsc.2019.04.003>)
 10. K. E. Gutowski, R. D. Rogers, D. A. Dixon, *J. Phys. Chem., B* **111** (2007) 4788 (<https://doi.org/10.1021/jp066420d>)
 11. A. Khan, P. A. M. Vazquez, R. M. T. Fernandes, *Spectrochim. Acta, A* **245** (2021) 118891 (<https://doi.org/10.1016/j.saa.2020.118891>)
 12. E. Szymanska, *Anal. Chim. Acta* **1028** (2018) 1 (<https://doi.org/10.1016/j.aca.2018.05.038>)
 13. A. M. Souza, R. Poppi, *J. Quim. Nova* **35** (2012) 223 (<http://dx.doi.org/10.21577/0100-4042.20170480>)
 14. A. D. Becke, *J. Chem. Phys.* **98** (1993) 5648 (<https://doi.org/10.1063/1.464913>)
 15. C. Adamo, B. V. Toward, *J. Chem. Phys.* **110** (1999) 6158 (<https://doi.org/10.1063/1.478522>)
 16. T. H. Dunning, K. A. Peterson, D. W. Woon, P. V. R. Schleyer, “*Encyclopedia of Computational Chemistry*”, Wiley, New York. 1998, pp. 88–115
 17. *Gaussian 09, Revision B.01*, Gaussian, Inc., Wallingford CT, 2009
 18. StatSoft Inc. (2004). Statistica (data analysis software system), version 7. Available from www.statsoft.com
 19. W. J. Dixon, F. J. Massey, Jr., *Introduction to statistical analysis*, McGraw-Hill, New York, 1951
 20. R. McGill, J. W. Tukey, W. A. Larsen, *Am. Statistician* **32** (1978) 12 (<https://doi.org/10.2307/2683468>)
 21. E. Stromsoe, H. G. Ronne, A. L. Lydersen, *J. Chem. Eng. Data* **15** (1970) 286 (<https://doi.org/10.1021/je60045a040>)
 22. J. Chao, K. R. Hall, K. N. Marsh, R. C. Wilhoit *J. Phys. Chem. Ref. Data* **15** (1986) 1369 (<https://doi.org/10.1063/1.555769>)
 23. J. Chao, F. D. Rossini, *J. Chem. Eng. Data* **10** (1965) 374 (<https://doi.org/10.1021/je60027a022>)
 24. Daniel Siderius, NIST Standard Reference Simulation Website - SRD 173 (2017) National Institute of Standards and Technology, (<https://doi.org/10.18434/mds2-232>) (Accessed 2023-10-04)
 25. T. Chai1, R. R. Draxler, *Geosci. Model Dev. Discuss.* **7** (2014) 1525 (<http://doi.org/10.5194/gmdd-7-1525-2014>)
 26. E. Nikolic-Doric, K. Cobanovic, Z. Lozanov-Crvenkovic, in *Proceedings of International Conference on Teaching Statistics* (2006) Slavador, Brasil, ICOT 7 Published By IASE, Belgium, 2006, C137 (ISBN: 978-90-73592-24-7)
 27. A. R. Henderson, *Clin. Chim. Acta* **366** (2006) 112 (<https://doi.org/10.1016/j.cca.2005.11.007>)
 28. C. E. Brown, in *Applied Multivariate Statistics in Geohydrology and Related Sciences*, C. E. Brown, Ed., Springer, Berlin, 1998, p. 155 (http://doi.org/10.1007/978-3-642-80328-4_13)

29. T. Jolliffe, in *Principal Component Analysis*, T. Jolliffe, Ed., Springer Series in Statistics, Springer, New York, 1986, p. 115 (https://doi.org/10.1007/978-1-4757-1904-8_7)
30. F. Mabood, G. Abbas, F. Jabeen, Z. Naureen, A. Al-Harrasi, A. M. Hamaed, J. Hussain, M. Al-Nabhani, M. S. Al-Shukaili, A. Khan, S. Manzoor, *Food Addit. Contam., A* **35** (2018) 404 (<https://doi.org/10.1080/19440049.2017.1418090>)
31. F. Mabood, S. A. Gilani, M. Albroumi, S. Alameri, M. M. O. Al-Nabhani, F. Jabeen, A. Alharrasi, R. Boqué, S. Farooq, A. Hamaed, A. Naureen, A. Khan, Z. Hussain, *Fuel* **197** (2017) 388 (<https://doi.org/10.1016/j.fuel.2017.02.041>)
32. A. D. McQuarrie, J. D. Simon, *Physical Chemistry: A Molecular Approach*, University Science Books, Melville, NY, 1997, p. 1396 (ISBN 978-0935702996).



J. Serb. Chem. Soc. 89 (4) 505–519 (2024)
JSCS–5736

A recent tactic for searching CDK-7 kinase inhibitor by NCI database screening

MOHAMMAD RASHID^{1*}, MD TANWIR ATHAR¹, AFZAL HUSSAIN², NORAH M. ALMADANI³ and ASHFAQ HUSSAIN⁴

¹Department of Pharmacognosy and Pharmaceutical Chemistry, College of Dentistry and Pharmacy, Buraydah Private Colleges, Buraydah-51418, Saudi Arabia, ²Department of Bioinformatics, Maulana Azad National Institute of Technology Bhopal, Madhya Pradesh-462003, India, ³Biochemistry Department, Faculty of Science, University of Tabuk, Tabuk-47914, Saudi Arabia and ⁴Department of Electronics Engineering, Rajasthan Technical University, Kota-324010, India

(Received 26 June, revised 9 August, accepted 21 October 2023)

Abstract: The present study was based on an exploration of NCI database for searching specific CDK-7 kinase inhibitor by HTVS, SP, XP, molecular docking, molecular dynamic simulation, and ADMET evaluation. The best CDK-7 kinase inhibitors (NCI613391, NCI169676, NCI281246, NCI339580) were identified *via* NCI database screening. The stability of binding interaction between receptor protein and protein-ligand complex of potent finding compounds (NCI613391) was further confirmed by dynamics simulations and MM-GBSA. The *RMSD* value of receptor and receptor–ligand complexes was analysed, and it revealed the stability of binding interactions and remained stable throughout the simulation. The *RMSF* values and gyration radius of the unbound receptor and backbone atoms of the complex were found to be equal, which indicates that the drug molecule inside the CDK7 receptor is also stable. The study of MM-GBSA data also revealed stronger binding interactions of ligands to CDK7 receptors. With the exception of NCI169676, all compounds were shown to be substrates for CYP450 2D6, CYP450 3A4, inhibitors of CYP450 2C9, and non-inhibitors of p-glycoprotein. All compounds were qualified and found suitable to be as drug-likeness according to the Lipinski rule, Ghose filter, MDDR like rule and CMC-like rule. The compound (NCI613391) exhibited human intestinal absorption (76.08%), displayed negative AMES and T.E.S.T (US-EPA) toxicity with OSIRIS property and found to be a promising CDK-7 kinase inhibitor and its efficacy may be further explored in clinical trials.

Keywords: NCI database; CDK-7 kinase inhibitor; dynamic simulation; molecular docking; T.E.S.T (US-EPA); Lipinski's rule; OSIRIS property.

* Corresponding author. E-mail: Rashid.Mohd@bpc.edu.sa; rashidpharm2008@gmail.com
<https://doi.org/10.2298/JSC230624083R>

INTRODUCTION

Cancer is a word for a condition in which cells divide *via* mitosis without regulation of the cell cycle (uncontrolled cell growth), hence cell cycle is a well-known feature of cancer's foundation.¹ Cyclin-dependent kinase-7 (CDK7) protein levels are raised in many forms of cancer cells, and cell development is also dependent on CDK7 activity in comparison to normal tissues, and thus it's a source of clinical conditions. Many types of cancer cells have elevated amounts of the protein cyclin-dependent kinase-7 (CDK7), and in contrast to normal tissues, CDK7 activity is required for cell development, which is a source of clinical consequences.² These results suggest that cyclin-dependent kinase-7 inhibitors (CDK7i) may represent a promising therapeutic target for cancer, and recent papers have emphasized the critical role of CDK7i in the development of many cancer types.^{3,4}

A cyclin-dependent protein kinase called cyclin-dependent kinase-7 (CDK7) regulates cell cycle progression by phosphorylating to other CDKs and altering their activity. The ability of cyclin-dependent kinase-7 inhibitors (CDK7i) to overcome the resistance to cancer treatments and to stop the cell cycle, induce apoptosis, and suppress transcription, particularly of super enhancer-associated genes in cancer, has also been demonstrated in preclinical research. For these reasons, the authors selected CDK7i as a potent therapeutic target. Due to its simultaneous involvement in regulating the cell cycle and modulating transcription, cyclin-dependent kinase-7 (CDK7) has been investigated as an anticancer therapeutic target and numerous CDK7 selective inhibitors have been developed and tried as cancer therapies.^{5,6} For the treatment of advanced solid tumours, four selective CDK7 inhibitors (ICEC0942, SY-1365, SY-5609 and LY340515) have recently advanced to Phase I/II clinical trials. These studies also showed that CDK7i has the ability to overcome cancer therapy resistance (for details see Supplementary material to this paper).

The National Cancer Institute (NCI) of the National Institutes of Health, United States of America, is the world-oriented organization for searching and developing novel potent therapeutic agents for fighting with multiple types of cancer cells.^{7,8} That's why authors choose NCI databases as repurposing for searching for new molecules as potent and specific CDK7 inhibitors by SBVS followed by molecular dynamics (MD) simulations and MM/GBSA evaluation to know the ligand-receptor binding interaction and to establish the stability in the binding pocket of receptor.^{9,10} Lack of knowledge on ADMET, drug similarity, drug score, and bioactivity profile are the main causes of drug failure during the development stages. Thus, the authors also predicted the physiochemical characteristic, ADMET, drug score and bioactivity profile by Molinspiration, Pre-ADMET prediction, Osiris property explorer and T.E.S.T. (US-EPA).

EXPERIMENTAL

Protein structure preparation and selection

The cyclin-dependent kinase 7 (CDK-7) protein was retrieved and obtained from the Protein Data Bank (PDB ID: 1UA2), in addition to being generated using the protein production tool in the Maestro Schrodinger software (<https://www.rcsb.org/structure/1ua2>). The constructed protein was given bonding instructions, the hydrogen atoms were integrated, and the structure was subjected to energy minimization using an OPLS-2005 force field with an energy cutoff value of 0.30 Å for root mean square deviation (RMSD).¹¹

National Cancer Institute (NCI) Database Compounds and reference ligand preparation

The NIH-NCI (National Institutes of Health-National Cancer Institute, USA) release database was used to collect the molecular series (database). (<https://cactus.nci.nih.gov/ncicadd/about.html>, 2022). The ligand was then prepared using Schrödinger software's LigPrep module.¹²

Preparation of the grid

The receptor grid generation panel and glide framework were used to generate the grid of the prepared target protein (CDK7). For CDK7, the adenosine triphosphate (ATP) molecule was selected eccentrically. With the partial charge cutoff set to 0.25, the scaling factor was set to 1.0.¹³

Molecular docking and screening

Structure-based virtual screening (SBVS) uses a computer approach known as molecular docking to anticipate how ligands (drug-like small molecules) would interact with a target receptor's binding site, which is often a protein structure.¹⁴ To get best result, high-throughput virtual screening (HTVS), standard precision (SP), extra precision (XP) docking was employed, and XP descriptors information was also picked for pose viewing.

Analysis of drug-like characteristics

Screened National Cancer Institute (NCI) compounds were chosen for the drug-like property assessment. These properties were subject to Lipinski's rule of five. Molecular weight (MW), hydrogen bond acceptor (HBA), total solvent accessible surface area (SASA), human oral absorption (HIA), hydrogen bond donor (HBD) and predicted aqueous solubility (QPlogS) were among the parameters collected. The Pfizer rule implicitly states that a medicine must have a balanced hydrophilic-lipophilic nature.¹⁵

MM/GBSA evaluation method for drug-target binding energy analysis

The drug-target binding energy was calculated by using the MM/GBSA method of Schrodinger software. The stability of target protein and ligand complexes is determined using this binding energy calculation.¹⁶

Simulation of molecular dynamics (MD)

A computer simulation technique for analysing the physical motions of atoms and molecules is called molecular dynamics (MD). For a predetermined period of time, the atoms and molecules are permitted to come into contact, giving insight into the dynamic evolution of the system. In addition to the protein structure of CDK7 Kinase (PDB code 1UA2), the top three docked complexes, NCI613391 (-13.063 kJ/mol) was subjected to 200 ns MD simulations utilizing the CHARMM27 all-atom force field using Gromacs 2021.3 software (<http://www.gromacs.org>).¹⁷ The protonation state was checked by using GROMACS pdb2gmx program and missing hydrogens were added. The parameters for the ligand coordinates and

topology were obtained using the Swiss param. Na⁺ and Cl⁻ were used to do the neutralization process, and the TIP3P water cube model was used to perform the solvation (<https://en.wikipedia.org/wiki/Moleculardynamics>, 2022).¹⁸⁻¹⁹

Lipinski's rule and drug similitude

When a ligand molecule violates the Lipinski rule of 5, which is when it has more than five hydrogen bond donors, a molecular weight greater than 500, a log *P* value greater than 5, and a total of N and O greater than 10, poor absorption or penetration is much more likely to happen.²⁰ To assess whether a particular molecule is similar to well-known drugs, numerous chemical features and attributes must be carefully balanced.²¹

Prediction of drug-likeness characteristics

The Pre ADMET program's tool forecasts drug-like features based on Lipinski's rule in addition to other well-known rules such the Ghose filter,²² CMC,²³ WDI²⁴ and MDDR.^{25,26} These laws acted as filters, separating chemicals with drug-like properties from those without. The Ghose filter uses the following factors to predict the drug-likeness: molecular weight between 160 and 480, molar refractivity between 40 and 130, predicted log *P* in between -0.4 and 5.6, and the total number of atoms between 20 and 70 (for details see Supplementary material).^{26,27}

A Molinspiration algorithm for predicting drug similarity

Molinspiration (2018.02 version) was used to add a SMILES representation of the NCI-screened compounds in order to predict drug-like characteristics and bioactivity scores against drug targets like enzymes, nuclear receptors, GPCR ligands and ion channel modulators (<https://www.molinspiration.com/cgi/properties>). The SMILES representation was created using the Chem. Bio draw Ultra software (11.0 versions). To determine the percentage of absorption, the formula %Ab = 109 - (0.345TPSA) was employed (for details see Supplementary material).^{26,27}

Examining Osiris's potential as a drug and its relevant properties

It was developed by T. Sander and used for the first time at Actelion Pharmaceuticals Ltd. as a part of the compound registration system in the drug development division. It is used to determine pharmacokinetic parameters such as toxicity potential, solubility, overall drug-likeness and drug score of compounds (www.organicchemistry.org/prog/peo/, for details see Supplementary material).^{26,28}

Acute toxicity prediction by Pre ADMET program and T.E.S.T. tool

The acute toxicity was anticipated using the mutagenicity of Ames test (<https://preadmet.bmdrc.kr/toxicity/>) and the T.E.S.T. tool (version 4.2.1), a US Environmental Protection Agency program (<https://www.epa.gov/chemical-research/toxicity-estimation-software-tool-test>).^{27,29,30} Dr. Ames developed the straightforward Ames test to determine whether a material is mutagenic or not. It uses several strains of the bacterium *Salmonella typhimurium*, which needs histidine to develop due to the gene changes in histidine production (for details see Supplementary material).³¹⁻³⁴

RESULTS AND DISCUSSION

Target protein docking score and analysis

In order to examine the potential for NCI selected top drug-like compounds to be involved in the CDK7 kinase binding pocket, the molecular docking simul-

ations were carried out. The results of energies and various interactions with the residues of the amino acids in the CDK7 binding pocket are listed in Tables I and S-II of the Supplementary material. Four hydrogen bonds were found to exist between NCI613391 and GLU20, THR170, MET94, and GLU95 (2.15, 1.43, 2.30 and 1.68 Å, respectively). Four hydrogen bonds were found in NCI613391, including one with MET94 (2.30 Å), thought to be crucial for the action and others with GLU20 (2.15 Å), THR170 (1.43 Å), and GLU95 (1.68 Å). Table S-I show the docking rating and binding interaction of NCI-screened compounds with the target protein's active site residues (see Supplementary material). The NCI-screened molecular docking and their Lig plot chart interaction diagram demonstrates the interaction discovered with the target protein of top scored score and is displayed in Figs. 1 and S-2 (Supplementary material).

TABLE I. The molecular docking analysis of NCI ten best finding compounds against the residue protein of CDK7 kinase; E_b – free binding energy; H-bond – number of H-bonds; residues – interacting residues

Compd. ID	H-Bonding interactions				Hydrophobic interaction and salt bridge	
	E_b kJ/mol	H-bonds	Residue	distance Å	Tot. Numb.	Residue
NCI613391	-73.25	4	GLU20 THR170 MET94 GLU95	2.15, 1.43, 2.30, 1.68	7	LEU18, ALA39, PHE91, PHE93, MET94, VAL100, LEU144
NCI169676	-64.36	2	GLU20 THR170	1.85, 1.72	7	VAL100, LEU18, MET94, PHE93, PHE91, ALA39, LEU144
NCI281246	-53.57	2	GLU95 MET94	1.86, 2.08	7	LEU18, VAL26, MET94, PHE93, PHE91, ALA39, LEU144
NCI339580	-59.83	4	LEU18 GLU99 MET94 THR170	2.41, 2.13, 2.11, 1.74	7	LEU18, MET94, PHE93, PHE91, ALA39, LEU144, VAL26

Drug-likeness properties and ADME/T analysis of best NCI screened compounds

All of the NCI-screened compounds were found to have oral absorption within the range of the human oral absorption limit, which is between 36.306 and 73.745 (25 % less and >80 % high). Compound NCI169676 was found to have high oral absorption (73.745) and molecular weights also to be under the limit of 500 Da. The aqueous solubility ($QPlogS$) of all investigated compounds was found to be within the acceptable range (-6.5 to 0.5) with values ranging from -1.162 to -3.246 and hydrogen bond donor (HBD) count in between 2 and 4,

which is below the permitted limit (≤ 5). The number of hydrogen bond acceptor (*HBA*) of all compounds was also observed under permissible limit (≤ 10) that is in between 6 and 9 (Table S-III of the Supplementary material).

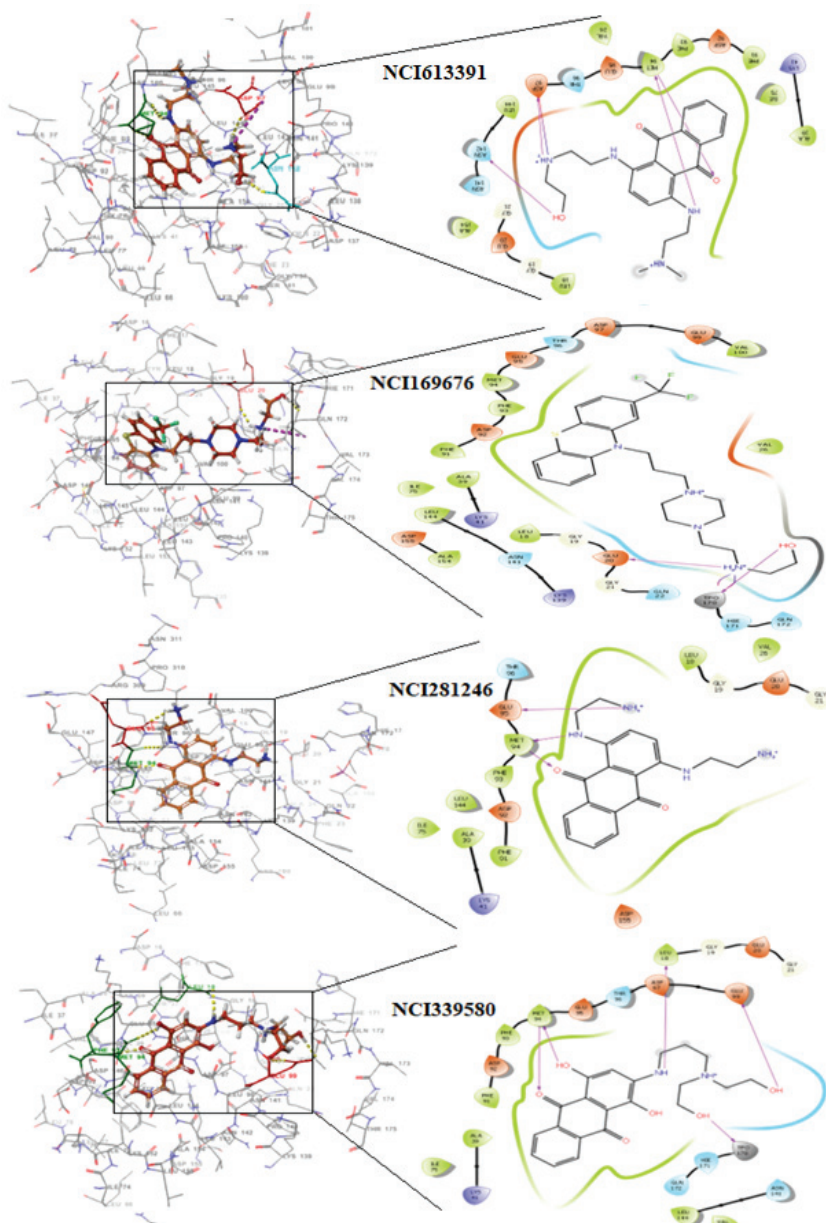


Fig. 1. NCI docking scores molecule binding interaction diagram and corresponding lig-plot interaction diagram by docking analysis in the active site residues of CDK7 kinase protein.

The *SASA* of NCI-screened compounds was found to be between 604 and 832 under the limit (300–1000) in the current investigation, indicating good oral bioavailability (Table S-III and Fig. S-3 of the Supplementary material). Additionally, the skin permeability (*QPlogP_w*) of compounds subjected to NCI screening was found to be in between 12 and 17, within the permissible range (4.0–45.0). *QPplorz* was in the range of 32.904–47.868 (permissible scale: 13.0–70.0), *QPlogPoct* in the range of 19.887–26.284 (permitted scale: 8.0–35.0), *QplogPo/w* in the range of 0.8–3.729 (permitted scales: –2.0–6.5) and *QPlogPC16* within the range of 11.341–16.161 (permitted scales: 4.0–18.0). Skin permeability in form of *QPlogP_w* (permitted scale: 4.0–45.0) and binding to human serum albumin in form of *QPlogK_p* (permitted scale: –8.0 to 1.0) were observed in the acceptable ranges of 12.183–17.178 and –5.387 to –7.577, respectively. In the range of –0.064 to 0.576 independent aqueous solubility in the form of *QPlogK_{hsa}* was also observed within the permissible limit (–1.5 to 1.5) (Table S-IV of the Supplementary material).

Prime MM/GBSA module for drug-target binding energy assessment

The NCI compounds that were screened, specifically NCI613391 (complex with PDB ID: 1UA2), exhibit a high amount of binding free energy ($G_{bind} = -73.25$ kJ/mol). Among all the molecules, the ligand (NCI613391) complex had the largest negative binding free energy (–73.25 kJ/mol), while NCI281246 had the lowest (–53.57 kJ/mol). Despite having a higher hydrogen occupancy than other compounds, compound NCI613391 complex shows a more stable engagement in the active free binding site of receptor. Since the NCI281246 complex has the lowest free binding energy, its interaction with the CDK7 active site during binding is the weakest. Surprisingly, the compound NCI613391 was found to have superior binding affinity to the CDK7 receptor binding site when compared to other substances. The compounds ΔG values were further broken down into their component parts, which are shown in Table S-V and Fig. S-4 (Supplementary material).

Structural analysis of NCI screened ligands by molecular dynamic simulation (MD)

In the ATP binding pocket, the ligand NCI NCI613391 interacts with GLU20, THR170, MET94 and GLU95 *via* stable hydrogen bonds with distances of 2.15, 1.43, 2.30 and 1.68 Å, respectively. NCI613391 had the highest docking score (–13.06 kJ/mol), and 63 % of its bonds were H-bonds. The ligand NCI613391's amide moiety (N-terminal) joins MET94 through its C-terminal in a strong H-bond. Because of the binding linker (residue) that is primarily conserved on the protein's alpha helix (GLU20 & THR170) and coil (MET94 & GLU95), the secondary structure of CDK7's alpha helix and coil was made to

stabilize hydrogen bonding more. LEU18, ALA39, PHE91, PHE93, MET94, VAL100 and LEU144 all showed interactions with the hydrophobic benzene pie (π). The NCI NCI613391 molecule has the largest percentage of H-bonds among the compounds, and its H-bonding network appears to be fairly stable in the *RMSD*, *RMSF* and radius of gyration (*Rg*, Fig. 2A).

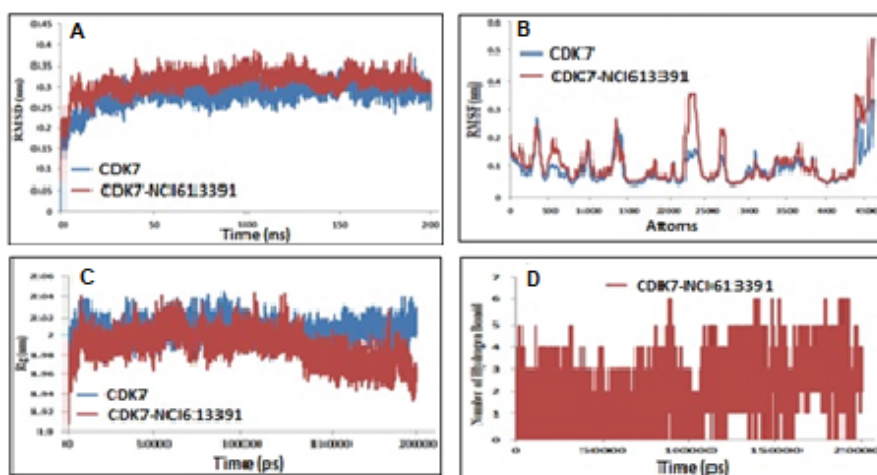


Fig. 2. MD simulation trajectory plot of CDK7 receptor protein backbone over a time period of 200 ns with NCI screened HIT molecules. A: the *RMSD* of NCI613391. B: the *RMSF* of the NCI613391. C: the *Rg* of the NCI613391. D: the hydrogen bond analyses of the NCI613391.

How much a protein changes when its primary coordinates are altered is determined by the *RMSD* score. Following a start time of 15 ns in the given MD simulation, the investigated ligand-receptor targets showed effective conversion. In terms of their backbone, the obtained complex *RMSD* trajectories rise throughout the first frames until the *RMSDs* level off at about 20 ns, at which point the subsequent trajectories continued around the corresponding average values until 200 ns in the case of the ligand (NCI613391). Through the course of the MD simulation, the latter differential dynamic behaviour grants NCI613391 a more stable and confinement-friendly environment inside the CDK7 kinase binding site. The ligand (NCI613391) extends to the ATP binding site to gain additional strength thanks to the four hydrogen bonds and the highest hydrogen bond occurrence percentage. In addition, the ligand has extensive VdW interactions with the seven nearby residues (LEU18, ALA39, PHE91, PHE93, MET94, VAL100 and LEU144). Throughout the simulation, the stability profile of NCI-screened drug in association with the CDK7 kinase was monitored using the GROMACS command line `gmx_rmsd` to calculate the *RMSD* values.

Additionally, the ligands showing significant *RMSD* values for their specific ligand–protein complexes would indicate insufficient ligand accommodation within the examined pocket across the chosen MD simulation time-frames. Using the initial structure as a frame of reference (0 to 200 ns), the *RMSD* values for the protein backbone and possible inhibitors were evaluated. The *RMSDs* of the free CDK7 kinase receptor and CDK7+NCI613391 complexes are shown in Fig. 2A. While the *RMSD* values of the analysed parameters for the complexes CDK7+NCI613391 gradually increased from 0 to 50 ns and remained stable after equilibration during simulation duration, the complex CDK7+NCI613391 was discovered to be equal to the receptor CDK7 Kinase protein.

The NCI screened for ligand-bound protein relative to the CDK7 kinase to calculate the residue root-mean-square fluctuation (*RMSF*) in order to get further understanding of the stability of the ligand binding complex. Using the GROMACS “*gmx rmsf*” command line, the individual backbone *RMSF* of each protein was calculated. This flexibility validation criterion was developed to offer information on the contribution of specific protein residues to structural fluctuations in the ligand–protein complex. In the reduced beginning structures, *RMSF* calculates the average deviation over time for each residue from its reference position. The backbone atoms’ *RMSF* value was calculated, and the *RMSF* figure shows (Fig. 2B) that the fluctuations are on an atom-scale. The CDK7 kinase protein complexes (CDK7+NCI613391) were discovered to have low *RMSF* values and the atoms’ fluctuations data was found to be essentially equal to that of the free receptor. As a result, the *RMSF* plot showed that the binding interactions of all the tested medications were shown to be stable within the receptors and that the simulation analysis study had no appreciable impact on the receptor’s flexibility.

Rg was applied throughout the entire MD trajectories by GROMACS “*gmx gyrate*” command script in order to learn more about the stability of the ligand complex. The *Rg*, which is calculated during molecular simulation, is also used to determine how compact a protein is; if the protein is particularly compact, it will not fold readily and the complex will be stable in both folded and unfolded states. The distance between all scattering components and the molecular centre of mass is measured as the radius of gyration, which is widely used to reflect structural changes in a substance. The CDK7 kinase receptor and CDK7+NCI613391 complexes was all identified by the *Rg* plot as having similar properties. As shown in Fig. 2C, the *Rg* values of protein and protein–drug candidate complexes showed a striking similarity and a stable folded structure to the protein complex. The *Rg* values from the current investigation support NCI613391–CDK7 complex’s improved stability. The ligand (NCI613391) complex was discovered to have low and average *Rg* values, which point to the ligand’s compactness and stability in CDK7 kinase binding site.

In NCI613391, four hydrogen bonds were observed, one with MET94 (2.30 Å) which is assumed to be essential for the activity and another with GLU20 (2.15 Å), THR170 (1.43 Å) and GLU95 (1.68 Å). Two hydrogen bonds were observed for NCI122039, one of them with GLU95 (1.85 Å) and another with MET94 (1.81 Å) which is assumed to be essential for the activity. For compound NCI196464, one hydrogen bond was observed with MET94 which is assumed to be essential for the activity. The more H-bonding and its occupancy at the active binding site of receptor, directs the more stability of complex. More stable complex of compounds NCI613391 contains four H-bond with GLU20, THR170, MET94 and GLU95 (60 % H-bond occupancy, Fig. 2D). In the entire simulation, the ligand (NCI613391) showed the highest hydrogen bond occupancy with CDK7 residues protein.

The physicochemical properties prediction

Interestingly, the molecular weight of NCI-screened compounds was found in the range of 297.17–426.79 (under the Lipinski limit), which is less than 500 and easily transported, diffused and absorbed in comparison to heavy molecules. The number of hydrogen bond acceptors (*n*-ON, O and N atoms) was found within the Lipinski limit range, which is less than 10. The number of hydrogen bond donors (*n*-OHNH, NH and OH) of compounds were also found to be within the Lipinski limit range, that is, less than 5, except for compounds NCI613391 and NCI281246 (six donors were found). The lipophilicity of compounds was also found to be within a range limit that is less than 5, which is an indication for good lipid solubility that will help the drug interact with membranes. As the number of rotatable bonds increases, the molecule becomes more flexible and adaptable for efficient interaction with a particular binding pocket. Remarkably, all compounds were found to have rotatable bonds within range limits 2–10, except the compound NCI613391, which was flexible within the Lipinski limit (Table S-VI of the Supplementary material). The *TPSA* was calculated from the surface areas that are occupied by oxygen and nitrogen atoms and hydrogen atoms attached to them, thus it is closely related to the hydrogen bonding potential of compounds (Table S-VII of the Supplementary material).

The score of bioactivity

The compound NCI613391 was found to have better ligands for protease inhibitors, nuclear receptor ligands, GPCR ligands, kinase inhibitors, enzyme inhibitors, ion channel modulators and nuclear receptor ligands (Table S-VIII of the Supplementary material).

The Osiris property explorer

The obtained results clearly showed that the compound NCI613391, which showed green colour with the tumorigenic effect and the reproductive effect

would be safe. All the tested compounds showed green colour indication with the tumorigenic effect except NCI339580 and the reproductive effect except NCI169676. Most of the compounds were observed to have an irritant effect, except NCI169676 (Table S-IX of the Supplementary material).

The prediction of ADME/T properties by pre-ADMET server

All compounds displayed negative carcinogenicity in rats as well as mice, except compounds NCI294726 (Table S-X of the Supplementary material). The obtained result from the pre-ADMET server revealed that the compounds NCI169676 showed high human intestinal absorption (HIA) scores of more than 90 % in comparison to other compounds. The compounds NCI613391, NCI281246 and NCI339580 were observed to have a better human intestinal absorption (HIA) score. All of the compounds were found to have a low value of blood–brain barrier (BBB) penetration (<1). The skin permeability value in cm/h ($\log Kp$) was also found within the limit range of NCI screened compounds (Table S-XI of the Supplementary material).

The acute toxicity prediction by T.E.S.T. (US-EPA) web-based server

The hierarchical clustering method predicted an oral rat LD50 in the range of 1.94–2.36 (–Log 10, mol/kg). The consensus approach, hierarchical clustering, FDA and nearest neighbour determined that the drugs' mutagenic values fell within the ranges of 0.53–0.95, 0.66–0.81, 0.53–0.97 and 0.33–0.67 mol/kg, whereas the FDA method and the nearest neighbour technique and other toxicity outcomes are shown in Table S-XII (Supplementary material).

The Prediction of metabolism by pre-ADMET web server

All the compounds showed inhibition of CYP450-2C9 except NCI169676. Regarding the substrate of CYP450-3A4, all the compounds exhibited as substrates except the compound NCI169676 (non-substrate). All of the NCI screened compounds were found to be non-inhibitors of p-glycoprotein, except the compound NCI169676 (Table S-XIII of the Supplementary material).

Drug likeness and rule violation prediction of NCI screened compounds

Drug-like characteristics of NCI-screened compounds were estimated by various drug-like rules, like Lipinski's rule, the Ghose filter, the lead-like rule, CMC, WDI and MDDR, on a single platform that is a pre-ADMET web tool. The NCI screened compounds were found to have drug likeness as per the MDDR like rule, and zero violations were observed (Table S-XIV of the Supplementary material).

CONCLUSION

The compounds (NCI613391, NCI169676, NCI281246 and NCI339580) were identified from NCI database screening based on their close binding interaction with CDK-7 kinase active site residues and then processed for ADMET evaluation. The best compound (NCI613391) was further examined for their capacity to maintain the stability of receptors and receptor-ligand complexes across a 200 ns molecular dynamics simulation. The *RMSD* value of receptor and receptor-ligand complexes was calculated, and it showed that the compounds were found to be stable and remained stable throughout the simulation study. The parallel *RMSF* and gyration radius values of the unbound receptor and backbone atoms of the receptor-ligand complex suggest that the drug molecules inside the CDK7 kinase receptor are also stable. All the compounds were qualified and observed suitable as drug likeness according to the Lipinski rule, Ghose filter, MDDR-like rule and CMC-like rule. Except for NCI169676 and NCI196464, all the compounds were discovered to be CYP450 2D6 substrates, weak substrates for CYP450 3A4 and non-inhibitors of p-glycoprotein. The MM-GBSA and ADMET values of compounds were also displayed in the favourable range, but compound (NCI169676) observed to possess excellent drug likeness (3.54), drug score (0.24), human intestinal absorption (95.36 %) and also displayed a negative AMES and T.E.S.T. toxicity test compared to other compounds with green colour indication. The compound (NCI613391) was found to be a powerful and effective inhibitor of CDK7 kinase and may be further investigated in clinical trials to study its efficacy.

SUPPLEMENTARY MATERIAL

Additional data and information are available electronically at the pages of journal website: <https://www.shd-pub.org.rs/index.php/JSCS/article/view/12455>, or from the corresponding author on request.

Acknowledgment. This project was supported by the Scientific Research Centre at Buraydah Private Colleges under the research project (BPC-SRC/2022-001).

ИЗВОД

СКОРАШЊА ТАКТИКА ПРЕТРАЖИВАЊА ИНХИБИТОРА CDK-7 КИНАЗЕ
СКРИНИНГОМ NCI БАЗЕ ПОДАТАКА

MOHAMMAD RASHID¹, MD TANWIR ATHAR¹, AFZAL HUSSAIN², NORAH M. ALMADANI³ и ASHFAQ HUSSAIN⁴

¹Department of Pharmacognosy and Pharmaceutical Chemistry, College of Dentistry and Pharmacy, Buraydah Private Colleges, Buraydah-51418, Saudi Arabia, ²Department of Bioinformatics, Maulana Azad National Institute of Technology Bhopal, Madhya Pradesh-462003, India, ³Biochemistry Department, Faculty of Science, University of Tabuk, Tabuk-47914, Saudi Arabia и ⁴Department of Electronics Engineering, Rajasthan Technical University, Kota-324010, India

Ова студија се заснива на претраживању NCI базе података за налажење специфичног инхибитора CDK-7 киназе помоћу HTVS, SP, XP, молекулског докинга, симулације молекулске динамике и процењивањем ADMET. Најбољи инхибитори CDK-7 кин-

азе (NCI613391, NCI169676, NCI281246, NCI339580) су идентификовани скринингом NCI базе података. Стабилност везивне интеракције између рецепторског протеина и протеин-лиганд комплекса нађеног потентног једињења (NCI613391) даље је потврђена симулацијом динамике и MM-GBSA. Вредност RMSD рецептора и рецептор–лиганд комплекса је анализирана, и показала је стабилност везивних интеракција која остаје постојана током симулације. Нађено је да су вредности RMSF и радијус гирације неvezаног рецептора и атома основног ланца комплекса једнаки, што указује да је молекул лека унутар CDK7 рецептора такође стабилан. Проучавање MM-GBSA података такође открива јаче везивне интеракције лиганата са CDK7 рецепторима. Са изузетком NCI169676, за сва једињења се показало да су супстрати за CYP 450 2D6, CYP 450 3A4, да су инхибитори за CYP 450 2C9, и нон-инхибитори р-гликопротеина. Сва једињења су била квалификована и погодна као лековима слична, на бази правила Липинског, Ghose филтера, правила MDDR сличности, и правила СМС сличности. Једињење (NCI613391) је испојило апсорпцију у човечјој утроби (76,08 %), и показује негативне AMES и T.E.S.T (US-EPA) токсичности са OSIRIS Property, а нађено је да је обећавајући инхибитор CDK-7 киназе, док његова ефикасност може даље да се испита у клиничким трајалима.

(Примљено 26. јуна, ревидирано 9. августа, прихваћено 21. октобра 2023)

REFERENCES

1. L. Kolloch, T. Kreinest, M. Meisterernst, A. Oeckinghaus, *Int. J. Mol. Sci.* **23** (2022) 812 (<http://dx.doi.org/10.3390/ijms23020812>)
2. P. Hazel, S. H. Kroll, A. Bondke, M. Barbazanges, H. Patel, M. J. Fuchter, R. C. Coombes, S. Ali, A. G. Barrett, P. S. Freemont, *Chem. Med. Chem.* **13** (2018) 207 (<http://dx.doi.org/10.1002/cmdc.201700826>)
3. M. E. Noble, J. A. Endicott, L. N. Johnson, *Science* **303** (2004) 1800 (<http://dx.doi.org/10.1126/science.1095920>)
4. S. Larochele, J. Chen, R. Knights, J. Pandur, P. Morcillo, H. Erdjument-Bromage, P. Tempst, B. Suter, R. P. Fisher, *The EMBO J.* **20** (2001) 3749 (<http://dx.doi.org/10.1093/emboj/20.14.3749>)
5. X. Li, D. C. Dean, J. Yuan, T. H. Temple, J. C. Trent, A. E. Rosenberg, S. Yu, F. J. Hornicek, Z. Duan, *Biomed. Pharmacother.* **149** (2022) 112888 (<http://dx.doi.org/10.1016/j.biopha.2022.112888>)
6. G. Lolli, L.N. Johnson, *Cell Cycle* **4** (2005) 565 (<https://pubmed.ncbi.nlm.nih.gov/15876871/>)
7. E. Chipumuro, E. Marco, C. L. Christensen, N. Kwiatkowski, T. Zhang, C. M. Hatheway, B. J. Abraham, B. Sharma, C. Yeung, A. Altabef, *Cell* **159** (2014) 1126 (<http://dx.doi.org/10.1016/j.cell.2014.10.024>)
8. Q. Li, S. Pan, T. Xie, H. Liu, *Blood Sci.* **3** (2021) 65 (<http://dx.doi.org/10.1097/BS9.0000000000000073>)
9. X. Barril, F. Javier Luque, *J. Comput. Aided Mol. Des.* **26** (2012) 81 (<http://dx.doi.org/10.1007/s10822-011-9506-1>)
10. F. Godschalk, S. Genheden, P. Söderhjelm, U. Ryde, *Phys. Chem. Chem. Phys.* **15** (2013) 7731 (<http://dx.doi.org/10.1039/c3cp00116d>)
11. G. Madhavi Sastry, M. Adzhigirey, T. Day, R. Annabhimoju, W. Sherman, *J. Comput. Aided Mol. Des.* **27** (2013) 221 (<http://dx.doi.org/10.1007/s10822-013-9644-8>)

12. *Schrödinger Preparation Wizard*, Lig prep. version 2.6, Glide version 5.8 (2012) (http://gohom.win/ManualHom/Schrodinger/Schrodinger_2012_docs/gleide/gleide_quick_start.pdf)
13. A. Hussain, C. K. Verma, *Biomed. Res.* **28** (2017) 5805 (<https://www.alliedacademies.org/articles/molecular-docking-and-in-silico-admet-study-reveals-354aminomethyl-piperidin1yl-methyl1hindol2yl1hindazole6carbonitrile-as-a-poten.pdf>)
14. A. Hussain, C. K. Verma, *J. Cancer. Res. Ther.* **15** (2019) 1131 (http://dx.doi.org/10.4103/jcrt.JCRT_47_18)
15. QikProp version 4.4 (2010), Schrödinger, LLC, New York, NY, 2015 (http://gohom.win/ManualHom/Schrodinger/Schrodinger_2015-2_docs/qikprop/qikprop_user_manual.pdf)
16. S. V. Pattar, S. A. Adhoni, C. M. Kamanavalli, S. S. Kumbar, *Beni-Suef Univ. J. Basic Appl. Sci.* **9** (2020) 36 (<https://doi.org/10.1186/s43088-020-00059-7>)
17. A. Hussain, C.K. Verma, U. Chouhan, *Saudi J. Biol. Sci.* **24** (2017) 1229 (<http://dx.doi.org/10.1016/j.sjbs.2015.10.003>)
18. V. Kumar, S. Parate, G. Thakur, G. Lee, H.-S. Ro, Y. Kim, H.J. Kim, M. O. Kim, K. W. Lee, *Biomedicines* **9** (2021) 1197 (<http://dx.doi.org/10.3390/biomedicines9091197>)
19. P. V. Rusina, I. Y. Titov, M. V. Panova, V. S. Stroylov, Y. R. Abdyusheva, E. Y. Murlatova, I. V. Svitanko, F. N. Novikov, *Mendeleev Commun.* **30** (2020) 430 (<http://dx.doi.org/10.1016/j.mencom.2020.07.008>)
20. C. A. Lipinski, F. Lombardo, B. W. Dominy, P. J. Feeney, *Adv. Drug Deliv. Rev.* **23** (1997) 3 ([http://dx.doi.org/10.1016/s0169-409x\(00\)00129-0](http://dx.doi.org/10.1016/s0169-409x(00)00129-0))
21. P. Ertl, B. Rohde, P. Selzer, *J. Med. Chem.* **43** (2000) 3714 (<http://dx.doi.org/10.1021/jm000942e>)
22. A. K. Ghose, V. N. Viswanadhan, J. J. Wendoloski, *J. Comb. Chem.* **1** (1999) 55 (<http://dx.doi.org/10.1021/cc9800071>)
23. T. I. Oprea, *J. Comput. Aided Mol. Des.* **14** (2000) 251 (<http://dx.doi.org/10.1023/a:1008130001697>)
24. A. Kulkarni, Y. Han, A. J. Hopfinger, *J. Chem. Inf. Comput. Sci.* **42** (2002) 331 (<http://dx.doi.org/10.1021/ci010108d>)
25. M. Rashid, *Bioorg. Chem.* **96** (2020) 103576 (<http://dx.doi.org/10.1016/j.bioorg.2020.103576>)
26. S. Kumar, F. Abbas, I. Ali, M. K. Gupta, S. Kumar, M. Garg, D. Kumar, *Phytomed Plus* **3** (2023) 100419 (<https://doi.org/10.1016/j.phyplu.2023.100419>)
27. M. Rashid, O. Afzal, A. S. A. Altamimi, *J. Chil. Chem. Soc.* **66** (2021) 5164 (<http://dx.doi.org/10.4067/S0717-97072021000205164>)
28. S. Thomas, *Explorer, OSIRIS Property*, Actelion Pharmaceuticals Ltd., Allschwil, 2001 (<https://www.organic-chemistry.org/prog/peo/>)
29. T. Martin, *Toxicity estimation software tool (TEST)*, US Environmental Protection Agency, Washington DC, 2016 (<https://www.epa.gov/sites/default/files/2016-05/documents/600r16058.pdf>)
30. N. Sripriya, M. R. Kumar, N. A. Karthick, S. Bhuvaneswari, N. K. U. Prakash, *Drug Chem. Toxicol.* **44** (2019) 480 (<http://dx.doi.org/10.1080/01480545.2019.1614023>)
31. F. S. Prasetya, W. Destiarani, I. R. C. Prihastaningtyas, M. U. K. Agung, M. Yusuf, *J. Appl. Pharm. Sci.* **13** (2023) 068 (<http://dx.doi.org/10.7324/JAPS.2023.10012>)
32. B. N. Ames, E. Gurney, J. A. Miller, H. Bartsch, *Proc. Natl. Acad. Sci. USA* **69** (1972) 3128 (<http://dx.doi.org/10.1073/pnas.69.11.3128>)

33. P. J. Eddershaw, M. Dickins, *Pharm. Sci. Technol. Today* **2** (1999) 13
([http://dx.doi.org/10.1016/s1461-5347\(98\)00108-4](http://dx.doi.org/10.1016/s1461-5347(98)00108-4))
34. J. H. Lin, M. Yamazaki, *Clin. Pharmacokinet.* **42** (2003) 59
(<http://dx.doi.org/10.2165/00003088-200342010-00003>)
35. G. Lolli, E. D. Lowe, N. R. Brown, L. N. Johnson, *Structure* **12** (2004) 2067
(<http://dx.doi.org/10.1016/j.str.2004.08.013>).



SUPPLEMENTARY MATERIAL TO
**A recent tactic for searching CDK-7 kinase inhibitor by NCI
database screening**

MOHAMMAD RASHID^{1*}, MD TANWIR ATHAR¹, AFZAL HUSSAIN², NORAH M.
ALMADANI³ and ASHFAQ HUSSAIN⁴

¹Department of Pharmacognosy and Pharmaceutical Chemistry, College of Dentistry and
Pharmacy, Buraydah Private Colleges, Buraydah-51418, Saudi Arabia, ²Department of
Bioinformatics, Maulana Azad National Institute of Technology Bhopal, Madhya
Pradesh-462003, India, ³Biochemistry Department, Faculty of Science, University of Tabuk,
Tabuk-47914, Saudi Arabia and ⁴Department of Electronics Engineering, Rajasthan
Technical University, Kota-324010, India

J. Serb. Chem. Soc. 89 (4) (2024) 505–519

INTRODUCTORY DETAILS

A cyclin-dependent protein kinase called cyclin-dependent kinase-7 (CDK7) regulates cell cycle progression by phosphorylating to other CDKs and altering their activity. Together with cyclin H and a third protein (a RING finger protein termed MAT1), the phosphorylation of CDK7 is necessary for both its stability and function. Cell cycle progression and transcription in the form of transcription factor TFIIH are regulated by the CDK7 catalytic subunit of CDK-activating kinase (CAK). Cell cycle progression is influenced by the threonine phosphorylation of cyclin-connected kinases CDK1, CDK2, CDK4, and CDK6 by CDK-activating kinase (CAK). RNA polymerase II (Pol II) is stimulated by CAK through serine phosphorylation (Ser5) of the repetitive C-terminal domain (CTD) of its large subunit (POLR2A), allowing escape from the promoter and transcript elongation. Transcription elongation is promoted by CDK7 phosphorylating CDK9, and CDK9 phosphorylating Pol II CTD Ser2.

Furthermore, in model systems, combinations of CDK7i with other targeted cancer medicines, including as BET inhibitors, BCL2 inhibitors, and hormone therapy, have demonstrated success. A promising clinical candidate, ICEC0942 potently reduced the growth of a variety of cancer cell lines and ER+ breast cancer xenografts. This was due to ICEC0942's good ADME and pharmacokinetic (absorption, distribution, metabolism, and excretion) characteristics. The medication is currently being tested in a Phase I/II clinical trial for patients with

* Corresponding author. E-mail: Rashid.Mohd@bpc.edu.sa; rashidpharm2008@gmail.com

advanced solid tumours, including a concentrated cohort of those with breast and prostate cancer. The medicine was licensed to Carrick Therapeutics.

EXPERIMENTAL DETAILS

National Cancer Institute (NCI) Database Compounds and Reference Ligand Preparation

A research division of the National Cancer Institute's chemical biology lab is known as CADD (computer-aided drug design) (<https://cactus.nci.nih.gov>, 2022). The NCI's (National Institutes of Health) Chemical Biology Laboratory (CBL), located at the Frederick National Laboratory for Cancer Research (FNLCR), formerly NCI-Frederick, houses the computer-aided drug design (CADD) group.

Preparation of the Grid

The receptor grid generation panel is used to specify a receptor structure as well as configure the grid generation task. This operation generates the grid files that depict the receptor's active site for glide ligand docking jobs. A prepared structure is required for receptor grid generation: an all-atom structure with acceptable bond ordering and formal charges.

Molecular Docking & Screening

All the generated NCI compounds were subjected to Lipinski filtration and reactive functionality analyses. To get the best result, HTVS (High-throughput virtual screening), SP (standard precision), XP (extra precision) screening, and docking were employed, and the XP descriptor information was also picked for pose viewing.

Simulation of Molecular Dynamics (MD)

In order to restrict the covalent bonds, the LINCS (linear constraint solver) methodology was used, and in order to deal with the long-range coulombic interactions, the particle mesh Ewald (PME) method was applied. Production MD runs lasted 200 ns at a constant temperature of 300 K, and MD trajectories were captured every 2.0 ps. Gromacs' built-in utilities, including gmx rms, hbond, rmsf, gyrate, and others, as well as the H-bonds plugin found in the VMD (Visual molecular dynamics) tool, were used to post-molecularly dynamically evaluate the trajectories. With a donor-acceptor distance cutoff of 3.5Å and a bond angle cutoff of 20Å the H-bonds plugin of VMD was employed to evaluate the involvement of intermolecular hydrogen bonds established by the ligand throughout the MD run during each of the two complexes, in addition to specific contacts with the key binding site residues of the CDK7 Kinase.

A Molinspiration Algorithm for Predicting Drug Similarity

Based on the five Lipinski criteria, the Molinspiration web software examined the physical characteristics of molecules. The smiles' representation was created using the ChemBioDraw Ultra software (11.0 version). A range of molecular characteristics, including topological polar surface area (TPSA), partition coefficient (LogP), molecular weight, hydrogen bond donors and acceptors, rotatable bonds, atom count, and departures from Lipinski's rule of five, were used to assess the compound's drug-likeness. To determine the percentage of absorption, the formula %Ab = 109 - [0.345 x TPSA] was employed. A substance meets Lipinski's criteria for a drug if it has a partition coefficient below 5, a polar surface area below 140 Å², a H bond acceptor and donor below 10, and a molecular weight below 500 daltons. The Rule of 5 is another name for the rule because the border values are 5,

2*5, 500, and 5. A problem with a molecule's bioavailability may arise if it violates more than one of these rules.

The sum of the contributions based on fragments and the correction factors is known as the LogP (Octanol/water partition coefficient). Topological Polar Surface Area (TPSA), which describes drug absorption, is the sum of the contributions produced by O- and N-centred polar fragments and includes intestinal absorption, bioavailability, Caco-2 permeability, and blood-brain barrier penetration. The entire quantity of a training set's fragment contributions to the actual 3D volume is the molecule's volume. The n-rotb (number of rotatable bonds), which is distinct from any individual non-ring bond and attached to a non-terminal heavy (non-hydrogen) atom, is a gauge of molecular flexibility.

Toxicity Assessment

The results of virtual screening are valued and colour coded as green/red/ yellow for properties such as effect on mutagenic, reproductive system, irritant effect, and tumorigenicity. Properties shown in red indicate high risks of undesired effects, while properties shown in green indicate drug conformity, compatibility, and safety. For the results prediction, the compound charges must be balanced and atom valences must not be exceeded for a proper chemical structure. A single bond connecting a positive charge on the nitrogen with a negative charge on one of the oxygens is required for drawing nitro-groups. Mutagenic or poor intestinal absorption are depicted in red, indicating a significant chance of unwanted consequences, whereas a green colour indicates drug-like action.

Higher-molecular-weight compounds are less likely to be absorbed and so never reach the site of action. Because low hydrophilicities and consequently large logP values induce poor absorption or penetration, the logP value must be less than 5.0. With more than 80% of drugs on the market having an estimated logS value greater than -4, a compound's water solubility has a significant impact on its absorption and distribution qualities. The capacity of the molecule to traverse membranes is improved if the inputs of all polar atoms exposed to the surface of the molecule amount to more than 80 or 100. To assess a compound's pharmacological similarity, many methods use topological descriptors, fingerprints of MDL structure keys, or other features like cLogP and molecular weights. The drug score, which can be used to determine if a molecule would be suitable for use as medication, is a condensed combination of rug similarity, cLogP, logS, molecular weight, and toxicity concerns.

Examining Osiris's Potential as a Drug and Its Relevant Properties

To prevent destructive compounds from further processing in the drug discovery and development unit, toxicity risk assessment is essential. The toxicity evaluation risk alarms indicate that the depicted structure may be hazardous for the stated risk category, and toxicity hazards are calculated using a colour code. The red hue signifies a greater danger of side effects or negative qualities like mutagenic or poor intestine absorption, whereas the green colour suggests drug-like pharmacological behaviour. Although the green hue reflects the desirable benefits of the chemical, the hazardous hazards (unwanted) consequences of the molecule are displayed in red. The mutagenic, tumorigenic, irritating, and reproductive toxicity hazards were assessed using a pre-computed set of structural fragments based on compound categorization from the Registry of Toxic Effects of Chemical Substances (RTECS) database.

Acute toxicity prediction by Pre ADMET program and T.E.S.T. tool

To avoid the 50% failure rate of drug candidates due to insufficient ADME/Toxicity inadequacies during the development stage, it is necessary to conduct ADME/Toxicity

screening at an early stage in the discovery phase. The Pre ADMET program is divided into four sections, as follows: This section comprises the determination of physicochemical characteristics such as lipophilicity (logP), molecular weight, polar surface area, and water solubility, all of which are directly connected to ADME/Toxicity qualities. Drug similarity prediction; The drug-similarity prediction module is based on Lipinski's and Lead-like. ADME prediction; Caco2 cell model and the MDCK (Madin Darby canine kidney) cell model are indicated as accurate in-vitro models for oral medication absorption prediction. Pre-ADMET also includes an in-silico human intestinal absorption (HIA) and skin permeability model for identifying possible medication candidates for oral and transdermal drug administration. Infiltration of the blood-brain barrier (BBB) provides information on therapeutic drugs in the central nervous system (CNS), plasma protein binding models in drug disposition, and drug effectiveness in the distribution stage.

The quantitative structure-activity relationship (QSAR) and Quantitative Structure-Property Relation (QSPR) of dangerous compounds were predicted using molecular properties of compounds as a descriptor using T.E.S.T software (version 4.2.1). These molecular features are crucial for predicting QSAR of harmful compounds. By using a type of approach such as consensus, hierarchical clustering, The United States food and drug administration (US-FDA), and closest neighbour method, the T.E.S.T. software program evaluated the acute toxicity of compounds, such as oral lethal dose for 50% of test rats (LD50), and mutagenic of compounds. The descriptors of synthetic and natural compounds in the T.E.S.T tool are based on the molecular structures of the substances.

Dr. Ames developed the straightforward Ames' test to determine whether a material is mutagenic or not. It uses several strains of the bacterium *Salmonella typhimurium*, which needs histidine to develop due to gene changes in histidine production. Ames TA100 (+S9) findings from the in-vitro test on the TA100 strain (metabolic activation by rat liver homogeneity). Results of the in-vitro test on the TA100 strain by Ames TA100 (-S9) (No metabolic activation). Results of the in-vitro test on the TA1535 strain by Ames, strain TA1535 (+S9) (Metabolic activation by rat liver homogeneity). Ames TA1535 (-S9); the TA1535 strain's in-vitro test results (No metabolic activation). By leaving the strictness of fingerprint matching at default and choosing all models, the pre-ADMET web-based application was able to forecast the first phase of metabolism for the chemical. Cytochrome P450 (CYP450), also known as the isozymes group and engaged in the metabolism of medicines, fatty acids, steroids, bile acids, and other carcinogens, is the most significant parameter. A family of heme proteins called cytochrome P450 enzymes are involved in the metabolism of numerous pharmacologically active substances. They can interact with other medications when taken together and result in undesirable side effects.

ADDITIONAL RESULT AND DISCUSSION

Target Protein Docking Score and Analysis

The NCI database (<https://cactus.nci.nih.gov/ncicadd/about.html>, 2022) was used to ascertain the binding affinity and interactions of several molecules with the selected target protein, CDK7 kinase. Ten compounds were found after reviewing the NCI database; their names are NCI613391 (-13.06 kJ/mol), NCI169676 (-11.91 kJ/mol), NCI281246 (-11.74 kJ/mol) and NCI339580 (-11.58 kJ/mol). Among these top NCI compounds, the NCI613391 molecule has the highest docking score (-13.06 kJ/mol) in comparison to the other molecules. The

same residues that the ATP molecule binds to are found in the active site of the target protein (CDK7 kinase), where all drugs bind. This indicates that the molecules have potent inhibitory properties and is firmly docked in the target protein's active region. The docking score and binding interaction of NCI-screened compounds with the target protein's active site residues are displayed in Tables S-I and S-II, respectively. This interaction with the target protein is shown in Fig S-1. by the NCI-screened top molecular docking score and their Lig plot interaction diagram and for other best finding molecules shown in Fig. S-1. Fig. S-2 displays the plot chart of compounds that the NCI screened using a docking score comparison.

Table S-I: Docking scores, smiles, formula and 2D structure of NCI-screened compounds.

NCI Compd.	Docking score (kJ/mol)	2D Chemical structure
613391	-13.06	
169676	-11.91	
281246	-11.74	

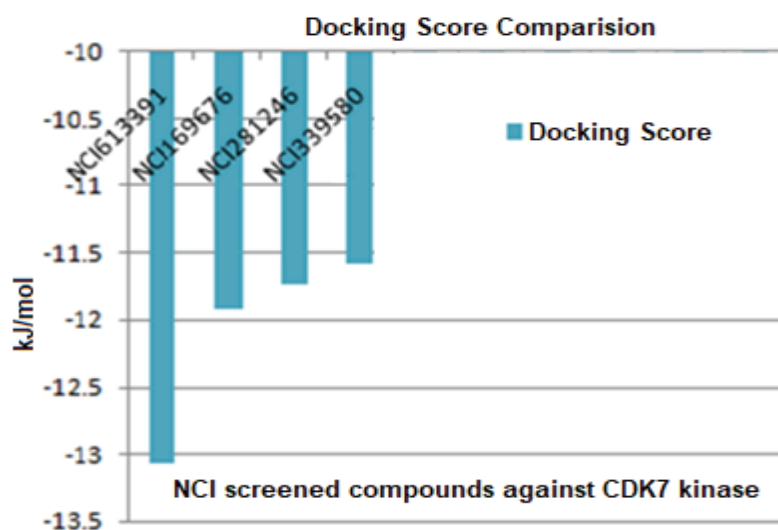
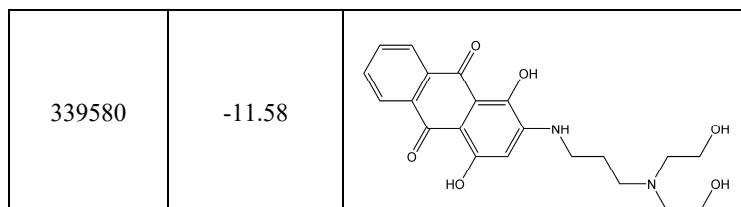


Fig. S-1. The docking score comparison of NCI screened ten best finding compounds in the active binding site residues of CDK7 kinase protein.

Drug-Likeliness properties and ADME/T analysis of best NCI screened compounds

The physiochemical characteristics of the compounds that passed the NCI screening, as determined by the QikProp module of Schrödinger, are listed in Tables S-III and S-IV. All of the substances that passed the NCI screening were found to have oral absorption that was between 25% less and >80% higher than the human oral absorption limit, or 36.306 to 73.742. Compound NCI281246 had the lowest oral absorption (36.306 and 25% less) while compound NCI613391 had the highest oral absorption (73.74%). The hydrogen bond donor (HBD) count of every component was determined to be between 2 and 4, which is less than the allowed limit of 5. The total number of hydrogen bond acceptors (HBA) was also reported to be below the permitted limit (10), which is in the range of 6 to 9 (Table S-III). All NCI-screened compounds have solvent accessible surfaces in total below the permissible range (300-1000), which may be found in 636.839 and 832.142. All compounds under investigation had aqueous solubility (QPlogS) values between -1.162 and 4.213, which was within the permitted range (-6.5 to 0.5).

Table S-II: Drug-like properties analysis by Lipinski's Rule of Five of NCI screened compounds.

Comp. Id ^a	MW ^b	QPlogS ^c	SASA ^d (Å)	HB Acceptor ^e	HB Donor ^f	HOA ^g (%)
NCI613391	477.0021	-2.856	832.142	9.9	4	39.882
NCI169676	480.5903	-3.246	798.355	7.7	2	73.745
NCI281246	324.3816	-1.162	604.145	6	4	36.306
NCI339580	400.4304	-2.212	700.349	9.9	3	49.074

Comp. Id^a; Compound Id, Mol. Wt.^b; Molecular weight in daltons (permissible scale is: ≤500), QPlog S^c; Prediction of aqueous solubility (permissible scale is: -6.5 to 0.5), SASA^d; Total solvent accessible surface area in Å (permissible scale is: 300-1000), HB Acceptor^e; Hydrogen bond acceptor (permissible scale is: ≤10), HB donor^f; Hydrogen bond donor (permissible scale is: ≤5), Human oral absorption^g (permissible scale is: <25% less and >80% high)

The NCI-screened compounds were discovered to have molecular weights between 308 and 480 Dalton, which is less than 500 Dalton (within the Lipinski limit) and indicates that they are more easily transported, dispersed, and absorbed than heavier molecules. Comparatively, NCI169676 had a larger molecular weight (480), and NCI281246 had the lowest (324). All molecules scored well in this investigation, however NCI169676 shown the exceptional human oral absorption (73.74%), with the human oral absorption percentage for the NCI tested compounds ranging from 36 to 73%. On the other hand, the number of hydrogen bond donors (n-OHNH, NH, and OH) of the molecules was found to be below 5 (1 to 4), which is compatible, and the number of hydrogen bond acceptors (n-ON, O, and N atoms) was less than 10 (under the Lipinski limit), which indicated good binding strength of molecules with CKD7 receptor binding pocket (Table S-III).

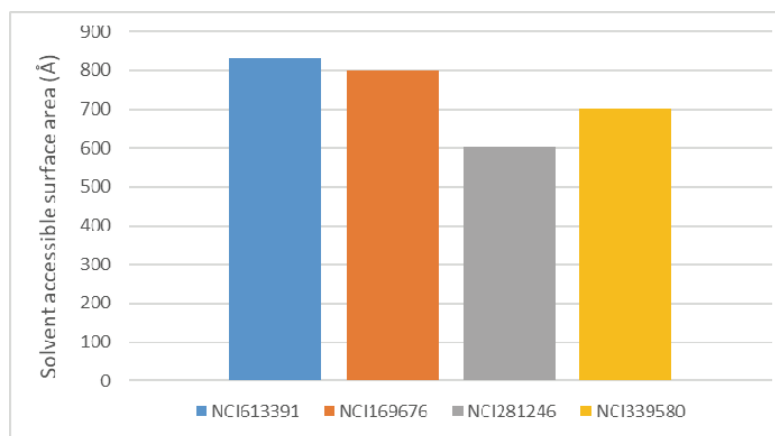


Fig. S-3. The solvent accessible surface area of NCI screened ten best finding compounds.

The partition coefficient (QPlogPo/w) and water solubility (QPlogS) of NCI-screened compounds were also found to be within the range limits of 0.8 to 3.729 and -2.005 to -3.647, respectively. This is a sign of a drug's interaction with cell membranes, as well as its absorption and distribution in the body. It was also discovered that all molecules' projected water-octanol coefficient fell within the permitted range (16 to 26), indicating excellent permeability through cell membranes. The SASA of NCI-screened compounds was found to be between 604 and 832 under the limit (300-1000) in the current investigation, indicating good oral bioavailability (Table S3 and Fig. S3). Additionally, between 9 and 17, within the permissible range (4.0 - 45.0), the skin permeability (QPlogPw) of compounds subjected to NCI screening was discovered. Due to the fact that all NCI tested compounds satisfied the pharmacokinetic characteristics within the permissible range of Lipinski's guidelines set for human usage, this suggests that they have the potential to be drug-like molecules.

Table S-IV. Drug-like properties analysis of the NCI-screened compounds.

Compd. Id	QP polrz	QPlogP oct	QPlogP o/w	QPlog PC16	QPlogP w	QPlog Kp	CIQ PlogS	QPlog Khsa
NCI1613391	45.882	26.284	1.74	16.161	17.178	-7.207	-2.858	-0.064
NCI169676	47.868	23.372	3.729	14.099	12.183	-5.387	-3.647	0.576
NCI281246	32.904	19.887	0.8	11.796	14.027	-7.577	-2.005	-0.157
NCI339580	37.417	22.427	0.762	13.763	15.798	-6.289	-3.208	-0.45

The polarizability value is predicted in cubic angstroms (Å), QPplorz; Predicted in octanol/gas partition coefficient (the permissible scale is in between 13.0 – 70.0), QPlogPoct; Predicted in octanol/water partition coefficient (permissible scale is in between 8.0 – 35.0), QPlogPo/w; Predicted in hexadecane/gas partition coefficient (permissible scale is: -2.0 – 6.5), QPlogPC16; Predicted in water/gas partition coefficient (permissible scale is: 4.0 – 18.0), QPlogPw; Predicted in skin permeability (permissible scale is: 4.0 – 45.0), QPlogKp;

Prediction of binding to human serum albumin (log K_p ; permissible scale is: -8.0 to 1.0), CIQPlogS; permissible scale is: -6.5 to 0.5), QPlogKhsa; Conformation-independent predicted aqueous solubility (permissible scale is: -1.5 to 1.5).

Prime MM/GBSA module for Drug-Target Binding Energy Assessment

Prime MM/GBSA module for Drug-Target Binding Energy Assessment of NCI Screened Molecules

The NCI-screened medication with the target CDK7 kinase protein was scored using the MM/GBSA-based rescoring method. The NCI compounds that were screened, notably NCI613391 (complex with PDB ID: 1UA2), exhibit a significant amount of binding free energy ($G_{\text{bind}} = -73.25$ kJ/mol). The interaction between the ligand and receptor molecule was shown by the complex's binding free energy using a simulation-based methodology. Table S5 lists the specifics and remaining substances that bind free energy as complexes. Finding the protein-ligand binding affinity can be made much easier with the use of the main MM/GBSA module. The protein-ligand complexes that were chosen had this module added to them. A surface generalized born solvation model for polar solvation (GSGB), OPLS molecular mechanics energies (EMM), and a nonpolar solvation term (GNP) are all included in it. Total binding free energy is calculated using the equation: $\Delta G_{\text{bind}} = G_{\text{complex}} - (G_{\text{protein}} + G_{\text{ligand}})$, where ΔG_{bind} is the total binding free energy of the complex, G_{complex} is the total energy of the complex, G_{protein} is the energy of the receptor without ligand, and G_{ligand} is the energy of the unbound ligand, and $G = \text{EMM} + \text{GSGB} + \text{GNP}$. In Fig. S3, the projected binding energy of the best-finding compounds from the NCI-screened data base is shown.

Table S-V. Prime MM/GBSA calculated binding energy in kcal/mol of NCI screened compounds.

Compd Id ^a	Gevdw ^b (kJ/mol)	GsolLipo ^c (kJ/mol)	Gcoul ^d (kJ/mol)	Gcovalent ^e (kJ/mol)	GsolGB ^f (kJ/mol)	ΔG_{bind}^g (kJ/mol)
NCI613391	-53.19	-23.18	-101.45	4.674	103.23	-73.25
NCI169676	-42.96	-28.13	-95.97	5.51	101.15	-64.36
NCI281246	-38.22	-21.39	-73.34	1.89	79.28	-53.57
NCI339580	-47.92	-18.42	-72.26	8.92	73.29	-59.84

Compd Id^a; Compound Id, Gevdw^b; Van der Waal energy, GsolLipo^c; lipophilic energy, Gcoul^d; Coulomb energy, Gcovalent^e; Covalent energy, GsolGB^f; Generalized born electrostatic solvation energy, ΔG_{bind}^g ; Free binding energy.

Molecular mechanics generalized born surface area (MM-GBSA) algorithm was used to calculate the free binding energy (ΔG) of the receptor-ligand system. The best finding compounds from the NCI screening were found to have free binding energies ranging from -73.25 to -53.57 kJ/mol. Among all the molecules, the ligand (NCI613391) complex had the largest negative binding free energy (-73.25 kJ/mol), while NCI281246 had the lowest (-53.57 kJ/mol). Despite having

a higher hydrogen occupancy than other compounds, compound NCI613391 complex showed a more stable engagement in the active free binding site of receptor. The top-scoring NCI screened compounds, such as NCI613391, had average ΔG values of -73.25 kJ/mol, respectively. Surprisingly, compound NCI613391 was found to have superior binding affinity to the CDK7 receptor binding site when compared to other substances. Compounds' ΔG values were further broken down into their component parts, which are shown in Table S5 and Fig. S4. Van der Waals interactions have a significant role in the binding of substances to the CDK7 receptor in the disintegration component of ΔG , followed by electrostatic interactions and SASA energy. Furthermore, the polar solvation energy of the compounds found in the NCI screening process favourably influenced the binding site and resisted the formation of the complex.

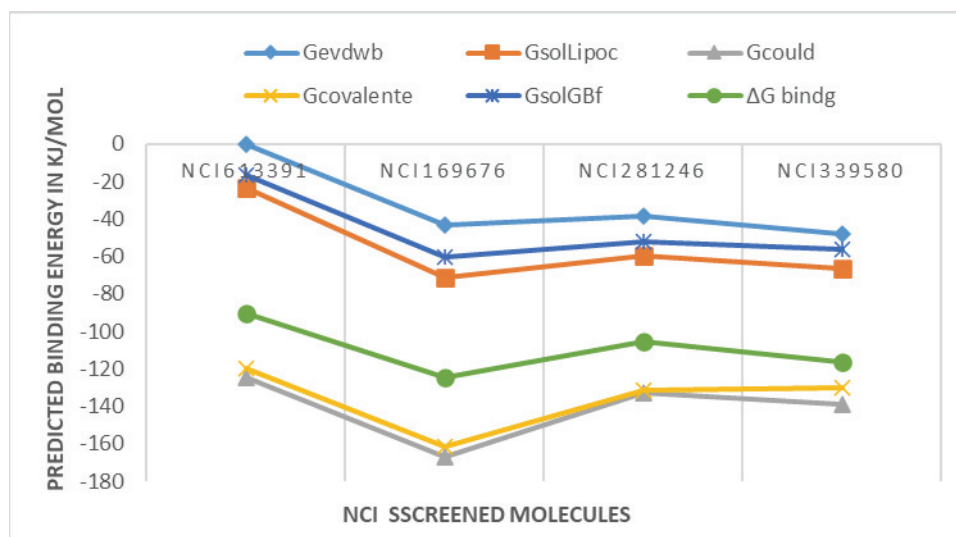


Fig. S-4. The predicted binding energy MM/GBSA calculation of best finding NCI screened molecules.

Structural analysis of NCI Screened Ligands by Molecular Dynamic Simulation (MD)

The importance of molecular dynamics simulation in computer-assisted drug design is for the assessment of dynamic and thermodynamic parameters of biological systems under specific circumstances involving physiological factors. The NCI compound NCI613391 (-13.06 kJ/mol) that was evaluated for molecular docking analysis was found to have the greatest docking scores and affinities with the target CDK7 kinase protein, therefore it was selected for the additional analysis using MD simulation. In order to evaluate the stability of the ligand-protein complex as well as the primary intermolecular interactions over the simulation period, an MD simulation study was conducted on the best docked

pose of a chosen NCI chemical in complex with the target CDK7 kinase protein. The radius of gyration (rGyr) during MD simulation was used to determine the target protein's structurally compact residues. As can be seen, there was no discernible variation in the rGyr readings, and the compactness persisted for the entire 200 ns. Observing the variations in the examined complex's molecular surface area (MolSA), polar surface area (PSA), and solvent accessible surface area (SASA) further suggested the presence of stable ligand-protein complexes.

The importance of Molecular Dynamic simulation in computer-aided drug design is in the estimation of dynamic and thermodynamic parameters of living systems under specific situations involving physiological parameters. In MM/GBSA computation, the screened NCI compounds NCI613391 (-13.06 kJ/mol) was found to have the highest docking score and affinity with the target CDK7 kinase protein, so these were chosen for further analysis by MD simulation. An MD simulation study was performed on the best docked pose of a selected NCI compound in complex with the target CDK7 kinase protein in order to investigate the stability of the ligand-protein complex as well as the main intermolecular interactions during the simulation period. The simulated complex was inspected for different standard simulation parameters such as backbone root-mean-square deviations (RMSDs) for all Ca carbon atoms of protein, the root means square fluctuations (RMSFs) of individual amino acid residues, intermolecular interactions involved, radius of gyration (rGyr) and hydrogen bond analysis. However, minor fluctuation was visible in both proteins during the initial period, which then stabilized for the remainder of the simulation period. A system showing steady fluctuations is usually considered stable and deemed to be properly equilibrated. Stable RMSF plots were obtained during the entire simulation period.

The residues of structural compactness of the target protein were ascertained by the radius of gyration (rGyr) during MD simulation. As can be seen, no significant deviation was noticed in the values of rGyr and the compactness was maintained throughout the 200 ns. In addition, the existence of stable ligand-protein complexes was also implied by observing the changes in various surface areas, such as molecular surface area (MolSA), polar surface area (PSA), and solvent accessible surface area (SASA) of the studied complex. The structural disturbances and real movement of a receptor and ligand complex under possible biological settings are simulated via MD simulation. During the MD simulation analysis, we confirmed the docking orientations using the RMSD, a well-established indicator for protein stability as well as equilibrating, and the averaged behavioural pattern for the complete protein structure could be seen.

The RMSD (Root-Mean-Square Deviation)

Fig. 5-A displays the RMSDs of the free CDK7 kinase receptor and the CDK7+NCI613391 complexes. For the complexes CDK7+NCI613391, the

RMSD values of the analyzed parameters gradually increased from 0 to 50 ns and remained stable after reaching equilibration during simulation duration. The complex CDK7+NCI613391 was shown lower RMSD value and found equal to the receptor CDK7 Kinase protein. These drug candidates complex naming CDK7+NCI613391 was found stable in active residue of CDK7 Kinase receptor and provide a solid foundation for research work and illustrated in Fig. 5-A.

The RMSF (Root-Mean-Square fluctuations)

The RMSF value of backbone atoms was determined, and the RMSF plot indicates that the variations are at the atom scale. The atoms' fluctuations data was found to be substantially equal to the free receptor (CDK7 kinase protein), and the complexes (CDK7+NCI613391, was found to have low RMSF values. Thus, the RMSF plot revealed that the binding interactions of all the tested drugs were observed to be stable within the receptors, and that there was no significant effect on the receptor's flexibility during the simulation analysis study. The RMSF values of CDK7 kinase alone and in combination with NCI613391, was displayed in Fig. 5-B.

The Radius of Gyration (Rg)

During the molecular simulation, the radius of gyration (Rg) is used to estimate the compactness of a protein; if the protein is very compact, it will not fold easily and the complex will be stable in folded or unfolded forms. The Rg plot revealed that the CDK7 kinase receptor, CDK7+NCI613391 complex have similar characteristics. In comparison to the protein complex, the Rg values of protein and protein-drug candidate complexes demonstrated a significant resemblance and a stable folded structure, as illustrated in Fig. 5-C.

The Hydrogen Bond Analysis

MD simulations of all complicated trajectories were examined for the number of hydrogen bonds generated. During MD simulations, it has been shown that the CDK7+NCI613391, complexes formed more hydrogen bonds, as illustrated in Fig. 5-D. Thus, throughout the simulation time, NCI613391 was able to sustain a robust contact with the binding pocket of CDK7 kinase. The ligand (NCI613391) was shown maximum hydrogen bond occupancy with CDK7 residues protein in overall simulation.

The Physicochemical Properties Prediction

All the compounds did not violate Lipinski's rule of five or Ghose filter, except NCI613391 and NCI281246 (only one violation detected), which showed 0-1 violations and are expected to be orally active. Molecular hydrophobicity or lipophilicity is indicated by the logP or partition coefficient. The logP values of all compounds were found to be less than 5 and were not in violation of Lipinski's rule of five or the Ghose filter, suggesting good permeability across the cell membrane. The molecular weight of compounds was found to be less

than 500, and thus these molecules are anticipated to be easily transported, diffused, and absorbed in comparison to large molecules. The numbers of hydrogen bond donors (NH and OH) in the compounds were found in accordance with Lipinski's rule of five, which is less than 5. TPSA of the compound was observed in the range of 43.66–130.32Å, which is below the limit of 160Å. The percentages of absorption for the compounds calculated from TPSA were in the range of 64.04–93.94 and indicated good oral bioavailability (Table S6). The molar refractivity of compounds was found in the range 100.27–136.82 except for compounds NCI613391 and NCI169676 (131.46 and 136.82, respectively), and polar surface area was found in the range 34.14–37.38 that is obeyed by the Ghose filter.

Table S-VI: Physicochemical characteristics of NCI-screened compounds by Lipinski's rule of five.

Compd. ID	Abs %	miLogP (o/w)	TPSA (Å ²)	n atoms	n-ON	n-OH/NH	n-violation	n-rotb	MV (cm ³ /m)
RO5		<5			<10	<5	≤1		
NCI613391	66.66	2.05	122.71	32	8	6	1	12	415.46
NCI169676	93.94	3.94	43.66	33	5	2	0	10	426.79
NCI281246	70.97	0.90	110.24	24	6	6	1	6	297.17
NCI339580	64.04	1.96	130.32	29	8	5	0	9	357.45

%Abs, TPSA, n atoms, n-rotb, and MV are the abbreviations for percentage of absorption, Topological polar surface area, number of atoms, number of rotatable bonds, and molecular volume (cm³/mol) respectively. n-OH/NH is the number of hydrogen bond donors, n-ON is the number of hydrogen bond acceptors, and miLogP is the logarithm of the partition coefficient between n-octanol and water. n violations are number of violations of Rule of Five and RO5 is Rule of five.

Table S-VII: Ghose filter foresaw drug-like characteristics of NCI-screened compounds.

Compd.	Log-P (log10)	MR (m ³ /mol)	The number of atoms	PSA (Å ² molecule ⁻¹)	C-Indication
The Ghose filter	-0.4-5.6	40-130	20-70	<140	Green
NCI613391	-0.581	131.46	32	34.14	Pink
NCI169676	1.877	136.82	33	35.02	Pink
NCI281246	-0.82	100.27	24	34.14	Pink
NCI339580	-0.179	112.77	29	37.38	Green

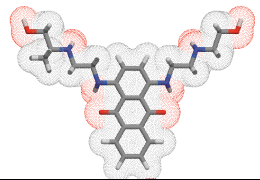
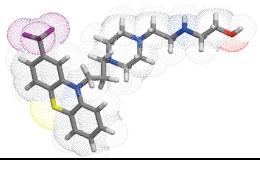
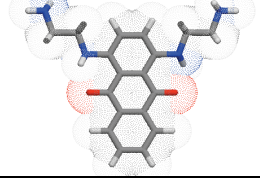
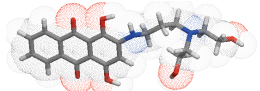
Log-P: Partition coefficient; MR: Molar Refractivity; PSA: Polar Surface Area; C- Indication: Color Indication.

The score of Bioactivity

Compound NCI613391 also demonstrated excellent binding with all targets other than nuclear receptor ligand (moderate activity). All compounds were found to have outstanding activity scores against GPCR ligand affinity, ion channel modulator, kinase inhibitor, and enzyme inhibitor (moderate activity).

Entire compounds demonstrated outstanding activity scores against protease inhibitor activity. Compound NCI613391 was found to have better ligands for protease inhibitors, nuclear receptor ligands, GPCR ligands, kinase inhibitors, enzyme inhibitors, ion channel modulators, and nuclear receptor ligands (Table S8) than the other examined compounds. The most promising compounds, including NCI169676, NCI281246 and NCI339580 which are projected to function across more than three pathways, were identified using the bioactivity ratings (Table S8). If a chemical's bioactivity score is greater than 0.00, it is thought to have significant biological activity; values between -0.50 and 0.00 are seen to be moderately active; and values less than -0.50 are thought to be inert.

Table S-VIII: Bioactivity score rating of NCI screened compounds against the various targets.

Compd. ID	Structure 3D	GPCR ligand	Ion channel modulator	Kinase inhibitor	Nuclear receptor ligand	Protease inhibitor	Enzyme inhibitor
NCI613391		0.15	0.05	0.15	-0.27	0.21	0.09
NCI169676		0.24	0.15	0.05	0.06	0.03	0.13
NCI281246		0.10	0.02	0.29	-0.31	0.15	0.19
NCI339580		0.06	0.00	0.20	-0.02	0.04	0.21

GPCR stands for "G-protein coupled receptor," which is active >0, moderately active -5.0-0.0, and inactive -5.0.

The Osiris Property Explorer

This program predicts the properties of investigated compounds on the basis of functional group similarity with the extensively in-vitro and in-vivo studied compounds present in its database. The obtained results clearly showed that the compound NCI613391, which showed green colour with Tumorigenic effect and Reproductive effect would be safe. All the tested compounds showed green colour indication with tumorigenic effect except NCI339580, and reproductive effect except NCI169676. Most of the compounds were observed to have an irritant effect, except NCI169676 (Table S9).

Table S-IX: Osiris property explorer toxicity and drug-relevant properties of NCI screened compounds.

Compd. ID	The Prediction of Toxicities				The Drug-relevant properties			
	Tumorigenic effect	Reproductive effect	Irritant effect	Mutagenicity	cLog P	Solubility	Drug-likeness	Drug Score
NCI613391	L	L	H	H	0.89	-4.49	-1.77	0.17
NCI169676	L	H	L	H	3.84	-3.99	3.54	0.24
NCI281246	L	L	H	H	0.49	-4.59	-5.12	0.17
NCI339580	H	L	H	H	1.10	-3.48	-1.71	0.11

L - low or no risk, H - high toxicity risk.

The Prediction of ADME/T Properties by pre-ADMET server

The NCI-screened compounds showed negative AMES toxicity results, indicating that the majority of compounds had little mutagenic potential. All compounds displayed negative carcinogenicity in rats as well as mice. Pharmacokinetic parameters like absorption, bioavailability, and distribution of NCI screened compounds were predicted by pre-ADMET tool through a type of test (Table S10). The obtained result from the pre-ADMET server revealed that the compounds NCI169676 showed excellent human intestinal absorption (HIA) scores of more than 90% in comparison to other compounds. The compounds NCI613391, NCI281246, NCI339580, were observed to have a better human intestinal absorption (HIA) score (Table S11) than the rest. The highest HIA score suggests that when these compounds are given orally, the substance may be better absorbed from the intestinal system. Entire compounds were found to have a low value of blood-brain barrier (BBB) penetration (<1). The skin permeability value in cm/hour (logKp) was also found within the limit range of NCI screened compounds. The compound (NCI613391) was found to have excellent HIA (76.08%), cell permeability by Caco-2 (20.65) and MDCK (0.06), solubility in

water (31.38) and buffer (0.27) in mg/mL, and a blood-brain barrier (BBB) penetration value of 0.05 (Table S11).

Table S-X: Pre ADMET toxicity prediction by Ames's test of NCI-screened compounds.

Compd. ID	The prediction of toxicity	Test Name	Test Values
NCI1613391	Ames's test	+S9 (Ames TA100)	-
		-S9 (Ames TA100)	-
		+S9 (Ames TA1535)	-
		-S9 (Ames TA1535)	+
	Carcinogenicity	Mouse	-
		Rat	-
NCI169676	Ames's test	+S9 (Ames TA100)	+
		-S9 (Ames TA100)	-
		+S9 (Ames TA1535)	-
		-S9 (Ames TA1535)	-
	Carcinogenicity	Mouse	-
		Rat	-
NCI281246	Ames's test	+S9 (Ames TA100)	-
		-S9 (Ames TA100)	-
		+S9 (Ames TA1535)	-
		-S9 (Ames TA1535)	+
	Carcinogenicity	Mouse	-
		Rat	-
NCI339580	Ames's test	+S9 (Ames TA100)	-
		-S9 (Ames TA100)	-
		+S9 (Ames TA1535)	-
		-S9 (Ames TA1535)	-
	Carcinogenicity	Mouse	-
		Rat	-

-: Negative; +: Positive

Table S-XI: Pharmacokinetic parameters value of NCI screened compounds by pre-ADMET tool.

Compd. ID	Parameters	Test name for the prediction of ADME	Test values
NCI613391	Absorption	The % of Human intestinal abs. (HIA)	76.083419
		<i>In-vitro</i> cell perm. by Caco-2 in nm/sec	20.6528
		<i>In-vitro</i> cell perm. by MDCK in nm/sec	0.0642523
		<i>In-vitro</i> skin perm. in cm/h (logK _p)	-4.31999
	Bioavailability	The solubility in buffer in mg/mL	0.271736
		The solubility in pure water in mg/mL	31.3839
	Distribution	<i>In-vitro</i> the % of plasma protein binding	28.655152
NCI169676	Absorption	The % of Human intestinal abs. (HIA)	95.854664
		<i>In-vitro</i> cell perm. by Caco-2 in nm/sec	24.2669
		<i>In-vitro</i> cell perm. by MDCK in nm/sec	0.130145
		<i>In-vitro</i> skin perm. in cm/h (logK _p)	-2.42092
	Bioavailability	The solubility in buffer in mg/mL	166.508
		The solubility in pure water in mg/mL	18.1855
	Distribution	<i>In-vitro</i> the % of plasma protein binding	51.308648
NCI281246	Absorption	The % of Human intestinal abs. (HIA)	88.329084
		<i>In-vitro</i> cell perm. by Caco-2 in nm/sec	21.0049
		<i>In-vitro</i> cell perm. by MDCK in nm/sec	2.95133
		<i>In-vitro</i> skin perm. in cm/h (logK _p)	-4.59474
	Bioavailability	The solubility in buffer in mg/mL	0.768911
		The solubility in pure water in mg/mL	1.64088
	Distribution	<i>In-vitro</i> the % of plasma protein binding	52.762220
NCI339580	Absorption	The % of Human intestinal abs. (HIA)	75.723043
		<i>In-vitro</i> cell perm. by Caco-2 in nm/sec	19.3925
		<i>In-vitro</i> cell perm. by MDCK in nm/sec	0.318305
		<i>In-vitro</i> skin perm. in cm/h (logK _p)	-4.53595
	Bioavailability	The solubility in buffer in mg/mL	134.576
		The solubility in pure water in mg/mL	494.614
	Distribution	<i>In-vitro</i> the % of plasma protein binding	47.437082
	<i>In-vivo</i> blood brain barrier (BBB) penetration (C. brain/C. blood)	0.0633325	

The Acute Toxicity Prediction by T.E.S.T. (US-EPA) web-based server

The acute toxicity of NCI screened compounds was predicted by the T.E.S.T. (US-EPA) web-based server by different approaches such as consensus, hierarchical clustering, United States food and drug administration (US-FDA),

and closest neighbour method. The obtained results were found within in the limit under the different approaches like the consensus method predicted an oral rat LD50 in the range of 2.10-4.33 (-Log10 (mol/kg), the hierarchical clustering method predicted an oral rat LD50 in the range of 1.94-2.36 (-Log10 (mol/kg), the FDA method predicted an oral rat LD50 in the range of 1.75-4.81 (-Log10 (mol/kg), and the nearest neighbour method predicted an oral rat LD50 in the range of 2.04-4.34. The consensus approach, Hierarchical clustering, FDA and Nearest neighbour determined that the drugs' mutagenic values fell within the ranges of 0.53-0.95, 0.66-.81, 0.53-0.97, and 0.33-0.67, whereas the FDA method and the nearest neighbour technique and other toxicity outcomes are shown in Table S12.

Table S-XII: Results of projected toxicities of NCI screened compounds from the T.E.S.T. (US-EPA).

Methods	Toxicity parameters	Toxicity results of NCI screened compounds			
		1	2	3	4
Consensus	LD50 value (Oral rat) in -log10 (mol/kg)	2.42	4.33	2.10	2.28
	The value of Mutagenicity	0.77	0.53	0.95	0.86
	Bioaccumulation factor Log10	0.37	N/A	0.75	0.22
	The value of developmental toxicity	0.80	1.07	0.64	0.79
Hierarchical clustering	LD50 value (Oral rat) in -log10 (mol/kg)	2.36	3.83	1.94	2.35
	The value of Mutagenicity	0.66	0.72	0.90	0.81
	Bioaccumulation factor Log10	0.71	N/A	0.64	0.65
	The value of developmental toxicity	0.67	1.07	0.83	0.77
FDA	LD50 value (Oral rat) in -log10 (mol/kg)	2.79	4.81	2.31	1.98
	The value of Mutagenicity	0.97	0.53	0.96	0.77
	Bioaccumulation factor Log10	1.18	N/A	N/A	0.52
	The value of developmental toxicity	1.01	0.96	0.23	0.68
Nearest neighbor	LD50 value (Oral rat) in -log10 (mol/kg)	2.12	4.35	2.04	2.50
	The value of Mutagenicity	0.67	0.33	1.00	1.00
	Bioaccumulation factor Log10	1.23	1.58	2.22	0.78
	The value of developmental toxicity	0.67	1.00	N/A	1.00

NCI screened compounds, 1 (NCI613391), 2 (NCI169676), 3 (NCI281246) and 4 (NCI339580)

*The Prediction of Metabolism by pre-ADMET web server***Table S-XIII:** Inhibition and substrate of NCI-screened compounds to cytochrome P450 enzymes and p-glycoprotein.

Compd. ID	Inh. of CYP450 2C19	Inh. of CYP450 2C9	Inh. of CYP450 2D6	Subst. of CYP450 2D6	Inh. Of CYP450 3A4	Subst. of CYP450 3A4	Inhibitor P-gp
NCI613391	NI	I	NI	S	NI	WS	NI
NCI169676	I	NI	I	S	NI	NS	I
NCI281246	NI	I	NI	S	NI	WS	NI
NCI339580	NI	I	NI	S	I	WS	NI

Cytochrome P450 enzyme (CYP450) & P-glycoprotein (P-gp), NI - Non-inhibitor, I - inhibitor, S – substrate, WS – weakly substrate, NS – non-substrate

Drug likeness and Rule Violation Prediction of NCI Screened Compounds

Drug-like characteristics of NCI-screened compounds were estimated by various drug-like rules, like Lipinski's rule, the Ghose filter, the lead-like rule, CMC, WDI, and MDDR, on a single platform that is a pre-ADMET web tool. The NCI screened compounds were found to have drug likeness as per the MDDR like rule, and zero violations were observed. The NCI screened compounds according to Lipinski's rule of five and found them suitable without crossing the violation. All compounds qualified for the CMC rule except compound NCI169676 (just one violation). The compound (NCI613391) was qualified for the CMC rule, suitable as Lipinski's rule, and to have drug-like properties by the MDDR rule with zero violation (Table S14). The well-known rule for the prediction of drug likeness of newly designed molecules is Lipinski's rule, usually called the rule of five, but another well-known rule, the lead-like rule, was developed from a quantitative survey based upon 18 lead and drug pairs of chemical structure.

Table S-XIV: Drug likeness and violation prediction for NCI-screened compounds by different rules.

Compd. ID	CMC Rule		Rule like Lead		Rule like MDDR		Lipinski's rule		Rule like WDI	
	R	nV	R	nV	R	nV	R	nV	R	nV
NCI613391	Q	0	V	1	DL	0	S	1	Out of 90% cutoff	3
NCI169676	NQ	1	V	2	DL	0	S	0	Out of 90% cut off	4
NCI281246	Q	0	V	1	MS	1	S	0	In 90% cutoff	0
NCI339580	Q	0	V	1	DL	0	S	1	Out of 90% cutoff	1

R – rule; nV – number of violations; Q – qualified; NQ – not qualified; S – suitable; V – Violated, MS – mid-structure; DL – drug like;



J. Serb. Chem. Soc. 89 (4) 521–537 (2024)
JSCS–5737

Thermoanalytical and spectroscopic studies on medicated jellies with perphenazine

MIHAELA M. BUDIUL^{1,2}, MĂDĂLINA MATEESCU^{1,2*}, GABRIELA VLASE^{1,2},
TITUS VLASE^{1,2}, SIMONA BOCĂNICI¹ and IONELA A. BRADU¹

¹Research Centre for Thermal Analysis in Environmental Problems, West University of Timișoara, Pestalozzi Street 16, 300115 Timișoara, Romania and ²West University of Timișoara – ICAM – Advanced Environmental Research Institute, Timișoara, Romania

(Received 2 April, revised 1 July, accepted 10 October 2023)

Abstract: Medicated jellies are widely used by a large part of patients, especially by people with swallowing difficulties. Preformulation studies play an essential role in the development of new pharmaceutical formulations. The present study aimed to formulate and evaluate medicated jellies containing perphenazine, an antipsychotic drug from the group of phenothiazine compounds used to treat schizophrenia and other mental disorders. Typical gelling agents such as sodium alginate (Alg), gelatine (Gel), and pectin (Pec) were used to develop the medicated jellies. In addition to the biopolymers, components such as benzoic acid (BenzAc), citric acid (CitAc), sodium citrate (NaCit), sorbitol (Sorb) and xylitol (Xyl) were also used. Before preparing the jellies, the moist binary mixture between each component of the jelly and the active substance was analysed to investigate the compatibility of the substances. The active substance, moist binary mixture, and medicated jellies were analysed by FTIR_UATR spectroscopy, UV–Vis spectroscopy and thermogravimetry.

Keywords: antipsychotic drug; pharmaceutical formulations; thermal properties; biocompatible polymers; biopolymers; gelling agents.

INTRODUCTION

Oral medicated jellies (OMJs) are appreciated by a large part of the population, especially by people with swallowing difficulties. These pharmaceutical formulations are used in psychiatry and for patients with Parkinson's, motion sickness and multiple sclerosis.¹ Commercial oral medicated jelly products of donepezil hydrochloride and alendronate are available in some countries.² Dysphasia (difficulty swallowing) has been reported to be common in all age groups, especially in children, geriatric patients, standardized patients, psychiatric patients, and patients with nausea, vomiting and motion sickness. Dysphasia is com-

*Corresponding author. E-mail: madalina.mateescu@e-uvv.ro
<https://doi.org/10.2298/JSC230402077B>

mon in all age groups and is observed in approximately 35 % of the general population, up to 60 % of the elderly institutionalized people and 18–22 % of all patients in long-term care facilities. OMJs with good taste and flavour increase the acceptability of bitter medications in different populations.³ Children prefer jelly when administering medications compared to oral liquids or tablets. Nowadays, jelly candies are popular among children because they like to chew the jelly and can use it as an alternative to solid and liquid dosage forms as a preferred method of drug administration. Medicated jelly can be used for the local treatment of oral cavity ailments and also for the treatment of systemic diseases. Medications with an unpleasant taste, such as erythromycin, paracetamol, aspirin, ibuprofen, antacids, minerals, and vitamin preparations, can be formulated as soft, chewable dosage forms.

According to the USP, medicated jellies are found under the name of chewable gels. Chewing gels are used to deliver drugs or dietary supplement ingredients orally. Chewable gels may consist of any or all of the following: gelling agents, sugars, water, sweeteners and flavourings. The sweeteners and flavouring agents are intended to increase consumer acceptance and mask the taste of the drug or dietary supplement being administered. Chewable gels maintain their shape, are elastic and yield when chewed. They are intended to be chewed before swallowing. Chewable gels are also known as “gummies” in the confectionery and dietary supplement industries, but this term is not used in official article titles.⁴

Chewable dosage forms are more convenient when administering medications for dysphagia patients and offer easier handling compared to liquid and powder formulations. The chewable formulation has a high drug delivery capacity and requires a smaller amount of super-disintegrants. The soft chewable system's esthetic appearance and pleasant taste easily attract children.⁵

Oral medicated jellies, developed as early as the 20th century, remain popular with consumers and continue to be commercially produced.

According to the 17th edition of the Japanese Pharmacopeia, jellies are specific, non-flowable preparations in gelatinous form with a particular size and shape intended for oral administration. Jellies can be defined as transparent or translucent, non-greasy, semi-solid preparations designed for both external and internal use. There are three types of jellies: medicated jelly, lubricating jelly, and other miscellaneous jelly.³

Phenothiazines are a group of drugs used in the treatment of mental illness.⁶ Perphenazine (Per, 4-[3-(2-chlorophenothiazin-10-yl)propyl]-1-piperazineethanol, Fig. 1)⁷ is an antipsychotic drug from the group of phenothiazine compounds used in the treatment of schizophrenia and other mental disorders.⁸

The bioavailability of drugs depends on the physicochemical properties, dosage form, metabolites, various enzymes, restriction by the intestinal barrier and glycoproteins.⁹

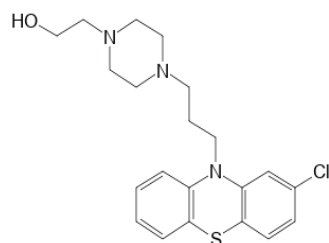


Fig. 1. Chemical structure of Per.

According to the literature, Per's systemic availability appears variable and poor via the oral route.^{10,11} Several studies have investigated different oral dosage forms with Per, such as disintegrating tablets, to overcome this disadvantage of low bioavailability.¹²

OMJs have gained acceptance as a drug delivery system and were included in the 16th edition of the Japanese Pharmacopeia, in 2011, as a type of dosage form.¹³ These pharmaceutical formulations improve the bioavailability of the drug and provide a much earlier onset of action.¹⁴ Other advantages include ease of administration for psychiatric patients and pleasant taste.⁵ In addition, numerous studies have been conducted on OMJs to improve the bioavailability of some active pharmaceutical ingredients.^{15,16}

The polymers used in manufacturing are inexpensive, safe, environmentally friendly, biodegradable, biocompatible, locally available, and well tolerated by patients.¹⁷

Preformulation studies play an essential role in the development of new pharmaceutical formulations. The study of compatibility between the active pharmaceutical ingredient and excipients is a fundamental part of the preformulation data. Chemical and physical interactions between the active ingredient and excipients can influence stability, bioavailability, and therapeutic safety. Thermal analysis such as thermogravimetry, differential thermal analysis, or differential scanning calorimetry is usually used in the physicochemical characterization of pharmaceutical materials. Complementary methods such as FTIR, UV-Vis and others are often used to study pharmaceutical formulations.¹⁸

Our study aims to develop and characterize a new pharmaceutical formulation containing Per. For this purpose, we use common natural polymers such as sodium alginate (Alg), gelatin (Gel) and pectin (Pec), which can be easily administered to patients with dysphagia, people with esophageal problems, children or psychiatric patients. In addition, we use a fast and accurate method to select the optimal excipients and the best jelly base for a stable medicated jelly. Alg is a biomaterial with several properties that make it helpful in formulation aid, especially in polymeric-controlled drug delivery.¹⁹ Gel is traditionally used to prepare jellies and also serves as a gelling ingredient in vitamin capsules or other pharmaceutical preparations.^{20,21} Pec is a natural polymer recognized as a viscosity-

-enhancing agent, approved by the United States Food and Drug Administration, and is officially in the United States Pharmacopeia.²²

In addition to the biopolymers, components such as the preservative benzoic acid (BenzAc), stabilizers such as citric acid (CitAc) and sodium citrate (NaCit), and sweeteners such as sorbitol (Sorb) and xylitol (Xyl) were also used.

The compatibility between the active ingredient and each component used in the jelly bases was investigated on a moist 1:1 binary mixture using FTIR spectroscopy and thermal analysis, TG/DTG/HF.

To investigate the possible interactions, the processes of jelly synthesis were followed. For this purpose, active substances' solubilization and recrystallization were carried out to investigate the changes during the jelly synthesis. Therefore, we will highlight the Per in the moist binary mixture and medicated jellies.

This paper presents the thermal and spectroscopic analysis results of Per, moist binary mixtures and OMJs. The presence of the active ingredient in these pharmaceutical formulations was also confirmed by UV-Vis analysis.

EXPERIMENTAL

The active substance perphenazine Per (SA, see Fig. 1) was received from Stada Hemo-farm Timisoara, Romania; alginic acid sodium salt powder (Alg) from Sigma-Aldrich, Lot# MKCN7477, product of Norway; gelatine (Gel) from Sigma-Aldrich, CAS Number 9000-70-8; pectin (Pec) from Sigma-Aldrich, lot# BCCD1493, product of China; benzoic acid (BenzAc) from Sigma-Aldrich, CAS Number 65-85-0; citric acid (CitAc) from Merck, K93661307 743; xylitol (Xyl), Ref: M-1290, Lot: 75499, Denmark; sorbitol (Sorb) Sigma-Aldrich, CAS Number 50-70-4; sodium citrate (NaCit) from Merck, AM1005848 647.

The binary physical mixtures with Per and the components used in the jelly bases consisted of equal masses of Per and each component. They were prepared by mixing the two substances in an agate mortar with a pestle for a few minutes, moistened by about 5 %, and then dried to 50 °C. The mass ratio of 1:1 was chosen to maximize the probability of observing the interactions between the components studied.

Preparation of medicated jellies

The 40 g/L polymers for Pec and Gel were dissolved in purified water and heated to approximately 50–60 °C. After complete solubilization of the gelling agent, BenzAc, CitAc, and sweeteners was added, the solution was stirred for 30 min, and NaCit was added. The resulting solution was stirred for another 10 min after complete solubilization of all ingredients, resulting in the jelly base. For Alg-based jelly, a prepared alginate solution of 1 % was used (Table S-I of the Supplementary material to this paper). Ingredients were calculated on the basis mass %.

The active substance was dissolved in ethanol and mixed with the jelly base in a 1:4 ratio. The solution was stirred for 10 min and then transferred to a matrix.

Pec-based jelly and Gel-based jelly were stored in air at room temperature for 24 h and then stored in polyethylene bags for analysis. Alg-based jelly was stored in air at room temperature for 48 h and then stored in polyethylene bags for analysis.

Formulations with a relatively high composition of Per were chosen to highlight the thermal behaviour of the active substance and, thus, the possible interactions with the components present in the jelly bases.

The ingredients of the formulated jellies were selected considering their use in the literature and previous studies conducted by our research group in other research as follows: BenzAc is recognized in the literature as a preservative²³ while NaCit and CitAc are recognized as stabilizers and were reported previously in the literature as proper ingredients for medicated jellies with ambroxol,²⁴ cyproheptadine HCl²⁵ preparation being recommended as ingredients for oral drug delivery platforms in pediatrics.³

Methods

FTIR_UATR spectra. FTIR_UATR spectroscopy data were collected using a Perkin Elmer Spectrum 100 instrument and employing the universal attenuated total reflectance (U-ATR) technique. Data were collected after eight consecutive recordings at a resolution of 4 cm^{-1} on the spectral range 4000–650 cm^{-1} .

Thermogravimetric analysis. The thermal behaviour was determined using an aluminium crucible on TG/DTA Diamond thermal analyser produced by Perkin Elmer. Analyses were performed in a dynamic air atmosphere (synthetic air 5.0 Linde Gas with flow 100 $\text{mL}\cdot\text{min}^{-1}$) at a heating rate, $\beta = 10\text{ }^{\circ}\text{C}\cdot\text{min}^{-1}$, in the temperature range of 30–500 $^{\circ}\text{C}$ for Per and temperature range 30–400 $^{\circ}\text{C}$ for moist binary mixtures and medicated jellies. All analysed samples had a mass between 8 and 12 mg.

UV-Vis spectrophotometry. UV-Vis spectra were measured with the T90 + UV-Vis spectrophotometer with a double beam in the photometric range of 190–900 nm. All absorbance measurements were performed in a 10 mm UV-Vis spectroscopy cell at room temperature, using distilled water as a blank. They were executed for the standard active ingredient and medicated jellies. The studies were performed for qualitative purposes. The presence of Per in medicated jellies was detected by UV-Vis spectrophotometric method. The concentration of the standards was 5 mg/mL. The amount used for the jellies was chosen to retain about 0.1 mg/mL of the active ingredient. Since the active substance is soluble in ethyl alcohol and the jelly is not soluble in alcohol, the solutions used for UV-Vis analysis were prepared by the following procedure: The active substance was dissolved in alcohol, and the solution was then diluted with water. The ratio of alcohol: water was 1:2, and for the jellies, the initial solubilization of the jellies were performed in water, and the solution was supplemented with alcohol to achieve the same ratio of alcohol: to water as in the case of Per.

Physical examination

The medicinal jellies were examined for their appearance, texture, consistency, transparency and gumminess, as described in the literature.²⁶

Stickiness and grittiness

Formulated jellies were examined in terms of the stickiness and grittiness by mildly rubbing the jelly between fingers.²⁷

RESULTS AND DISCUSSION

FTIR_UATR study – FTIR_UATR spectra of the active substance

The spectroscopic study of the initial active substance Per (SA) and the recrystallized active substance Per (D) was performed to highlight the active substance's characteristic bands. Therefore, these spectra are used for comparison with the spectra of moist binary mixtures and with the spectra of medicinal jellies based on Alg, Gel and Pec to investigate the compatibility between the com-

pounds. To observe the changes of the active compound in the phase of jelly synthesis, it was moistened with 5 % water and then dried. The spectra of Per (SA) and Per (D) are shown in Fig. S-1 of the Supplementary material.

The spectrum of Per (SA) and Per (D) shows an absorption band at 3440 cm^{-1} corresponding to the stretching vibration of the bond OH. At the same time, other sharp bands at 1455 , 1564 and 1590 cm^{-1} (specific bands for aromatic stretching of C=C bond), bands at 2877 and 2938 cm^{-1} (specific stretching of C–C bond due to CH_2 group), the bands at 2800 cm^{-1} (specific C–H stretching due to a $\text{CH}_2\text{-N}$ group), the vibrations in the range $1200\text{--}1000\text{ cm}^{-1}$ (specific to the C–N stretching of the tertiary amine) and the band at 755 cm^{-1} indicating the C–Cl stretching are highlighted.

From a spectral point of view, it should be noted that solubilization and subsequent drying of the active substance do not lead to changes in the spectrum of Per (D). Thus, all bands are seen equally in both spectra.

FTIR_UATR study of binary mixtures–active substances: Jellies components

The FTIR_UATR study for the moist binary mixtures was performed to observe possible interactions between the active substance and the components of medicated jellies. It was investigated if there are relevant shifts and if there are specific peaks for the active substance. In addition, the presence of –Cl, which attached to the phenothiazine ring enhances the antipsychotic activity,²⁸ is investigated.

In the case of the moist binary mixture Per_Xyl, Fig. 2, most of the peaks characteristic of the active substance are highlighted so that the bond OH is present through the peak at 3422 cm^{-1} . The bands specific for the stretching of the C–C bond of the CH_2 group are observed at 2943 cm^{-1} at higher wavelengths than in the case of the pure active substance. The specific bands for the C–H stretching of the CH_2N group at 2875 cm^{-1} were also highlighted, as in the case of the pure active substance. The specific bands for the stretching of the C=C bond in aromatic compounds are at 1455 and 1565 cm^{-1} . The tertiary amine is argued by the presence of bands from $1200\text{--}1000\text{ cm}^{-1}$. The band specific for the bond with halogen is also at the same wavelength as in the active substance at 745 cm^{-1} , with a small shift. So, we can say that the active substance is present in this mixture.

The FTIR spectrum of the moist binary mixture of Per_Sorb shows several characteristic bands in the range $3400\text{--}2400\text{ cm}^{-1}$, which are hidden or absent. One can observe the specific bands for the stretching of the C–C bond of the CH_2 group at 2985 , 2970 and 2932 cm^{-1} . The specific bands for the C–H stretching of the CH_2N group are also not visible. The specific bands for stretching of the C=C bond in aromatic compounds are found at 1415 and 1564 cm^{-1} . Tertiary amine is argued by the presence of bands in the range $1200\text{--}1000\text{ cm}^{-1}$, and C–Cl specific

band is also not visible. Thus, it can be said that the active ingredient is not completely visible in the FTIR spectrum of the mixture.

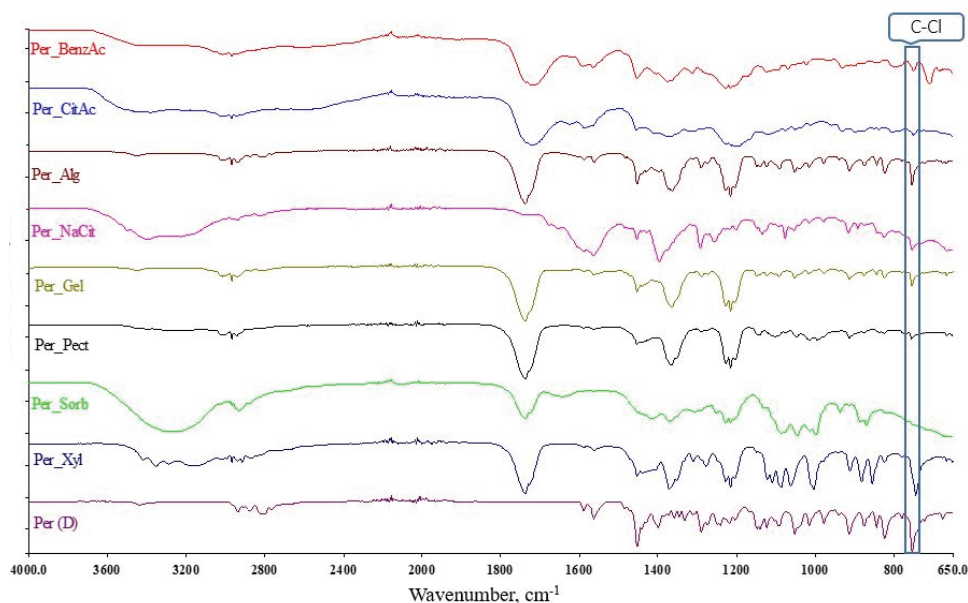


Fig. 2. FTIR spectra for Per (D) compared to binary mixtures of the active substance with the components used in jellies synthesis (1:1) for the spectral region 4000–650 cm^{-1} .

For the moist binary mixture obtained for Per_Pec, the following peaks characteristic of the active substance were highlighted, such as the peak at 3255 cm^{-1} for the bond OH, but much less highlighted. The specific bands of the C–C bond stretching of the CH_2 group appeared at 2944 cm^{-1} . The specific bands for the C–H stretching of the CH_2N group at 2830 cm^{-1} were also highlighted, as in the case of the pure active substance. The specific bands for the stretching of the C=C bond in aromatic compounds are at 1454 and 1565 cm^{-1} . The presence of a tertiary amine is confirmed by the bands in the range 1200 – 1000 cm^{-1} . The C–Cl specific band is also at the same wavelength as in the active substance at 755 cm^{-1} . We can thus say that the active compound is present in this mixture.

The FTIR spectrum of the moist binary mixture Per_Gel also contains most of the important bands of the active substance, so the presence of the bond OH can be observed by the vibration at 3454 cm^{-1} . The C–C bond by vibrations at 2943 and 2970 cm^{-1} , the characteristic bands of C–H stretching of the CH_2N group at 2823 cm^{-1} , and the aromatic C=C bond at 1454 and 1565 cm^{-1} . Tertiary amine is also present at the same wavelengths as in the case of the active substance. C–Cl bond at 755 cm^{-1} as in the case of the pure substance. Thus, this mixture also contains an intact active substance.

FTIR analysis of the moist binary mixture Per_NaCit shows the specific vibration of the bond OH at 3400 cm^{-1} , which corresponds to the stretching vibration of the bond OH. At the same time, other bands specific for the stretching of the C–C bond of the CH₂ group were highlighted at 2941 cm^{-1} , at shorter wavelengths than in the case of the pure active substance. The bands specific for the C–H stretching of the CH₂N group at 2825 cm^{-1} were also highlighted. Tertiary amine is confirmed by the presence of bands at 1295 , 1258 and 1055 cm^{-1} . The specific band for the bond with the halogen is also present at the same wavelength as in the active substance at 755 cm^{-1} . At the same time, other sharp bands were highlighted at 1455 and 1565 cm^{-1} (specific bands for the aromatic stretching of the C=C bond).

Alg, like Gel, does not interact with the active substance in the binary mixture. It shows all the characteristic bands in the FTIR spectrum of the mixture, namely the bond OH (3445 cm^{-1}), C–C bond (2876 , 2822 cm^{-1}), C=C bond (1590 , 1564 and 1454 cm^{-1}), C–H bond (2942 cm^{-1}), tertiary amine (1200 – 1000 cm^{-1}) and C–Cl bond (755 cm^{-1}). Thus, it can be said that Alg can be used as a jelly base to deliver active ingredient.

In the case of the moist binary mixture Per_CitAc, it is observed that some characteristic bands in the range 3400 – 2400 cm^{-1} are hidden or absent in the spectrum of the binary mixture. The vibration of the bond OH is further observed at a lower wavelength, namely at 3400 cm^{-1} . The specific bands for the stretching of the C–C bond of the CH₂ group are at 2970 and 2942 cm^{-1} . The specific bands for the C–H stretching of the CH₂N group at 2876 and 2823 cm^{-1} , which are slightly changed compared to the pure active substance, were also highlighted. The specific bands for the stretching of the C=C bond in aromatic compounds are found at 1454 and 1588 cm^{-1} . The presence of a tertiary amine is proved by the bands in the range of 1200 – 1000 cm^{-1} . The specific C–Cl band is also at the same wavelength as in the active substance at 750 cm^{-1} . Thus, we can say that the active substance is present in this mixture.

The FTIR spectrum of the binary mixture Per_BenzAc shows that some characteristic bands in the range 3400 – 2400 cm^{-1} are hidden or absent, as in the case of the Per_CitAc mixture. The vibration of the bond OH can still be observed at a lower wavelength, 3387 cm^{-1} . The specific bands for the stretching of the C–C bond of the CH₂ group are at 2970 and 2946 cm^{-1} . The specific bands for the stretching of the C=C bond in aromatic compounds are at 1455 and 1566 cm^{-1} . The tertiary amine is present through the bands in the range 1200 – 1000 cm^{-1} . The specific C–Cl band is also present at the same wavelength as in the active substance at 751 cm^{-1} .

FTIR_UATR study of synthesized jellies

Since in the composition of jellies, the amount of active ingredient is much lower, namely the ratio of the solid mass of the jelly base: as in the mass of the

active ingredient it is 1:4, we expect that the active ingredient will not be as visible in the FTIR spectrum of medicated jellies, Fig. 3. It will be looked for the representative bands, namely the group OH, which is undoubtedly covered by the water spectrum, the C–C, C=C and C–H bonds, and the C–Cl bond. The tertiary amine will also be followed in the spectra.

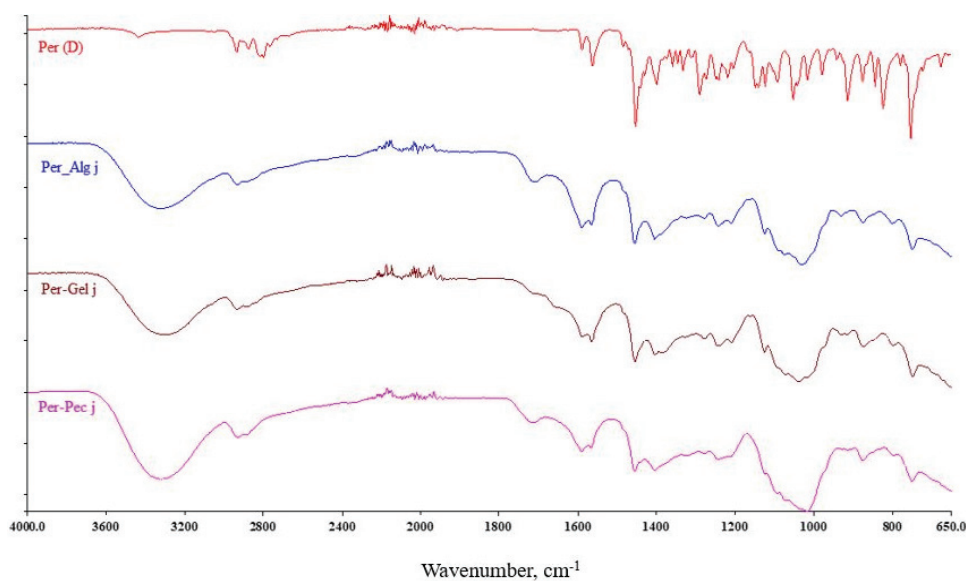


Fig. 3. FTIR spectra for Per (D) and jellies based on Alg, Gel and Pec.

The FTIR spectra of the Alg, Gel and Pec-based jellies are very similar, highlighting the specific bands of the C–C and C–H bonds. Thus, the bands are present at 2930, 1566 and 1455 cm^{-1} . The tertiary amine is also present in the 1200–1000 cm^{-1} range, and the C–Cl bond is visible through the vibrations at 750 cm^{-1} . The same intense bands as in the case of the active substance or the binary mixtures are not visible, but this is justified by the composition of the active substance of the jellies.

Thus, the active ingredient is completely present in the jellies. Although some jelly components have raised question marks, the final jellies suggest that they can be used to administer Per.

Thermal analysis – Thermogravimetric study of the recrystallized active substance

The recrystallized active substance Per (D) and the initial active substance Per (SA) have the same thermal behaviour. The present paper shows the thermo-analytical curves obtained in the case of Per (D), Fig. 4, because this is used as a benchmark. The thermogravimetric study allows us to justify the presence of the

active substance in the jellies and to identify possible interactions with the components of the jellies. To determine the thermal behaviour of the active substance, the analysis was performed in the temperature range of 30–500 °C. To determine the possible interactions in moist binary mixtures and medicated jellies, the thermal behaviour was determined in the temperature range of 30–400 °C. Above this temperature, no significant processes take place, and the last process of the active substance is not completed at the end of the temperature range of the analysis.

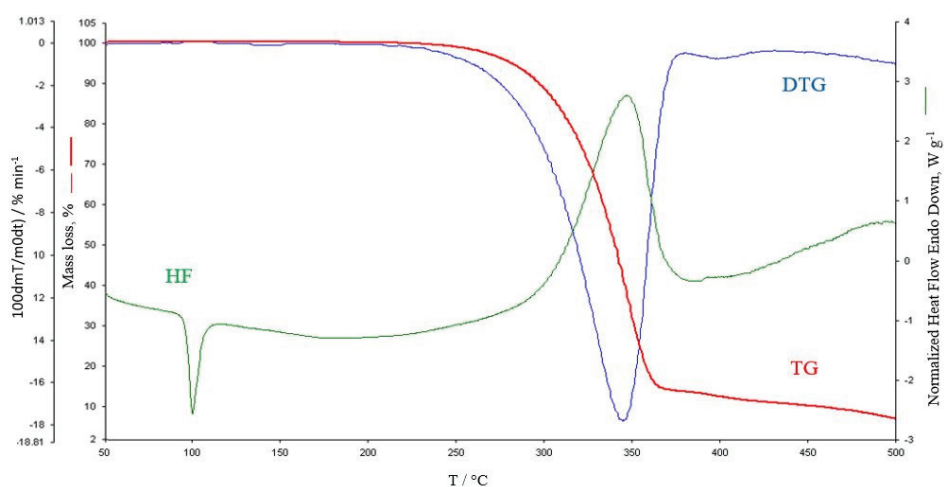


Fig. 4. Thermoanalytical curves obtained for active substance – Per (D), obtained at a heating rate of 10 °C min⁻¹ – 500°C in air atmosphere.

Thermal analysis of the recrystallized active substance was carried out in the range of 50–500 °C with a heating rate of 10 °C/min in the dynamic atmosphere of synthetic air. Analysing the TG and DTG curves, it was found that two decomposition processes occur in the studied temperature range, namely the first process in the range 230–373 °C, where a continuous loss of 85.42 % of the mass of the sample occurs. This process is accompanied by an exothermic process with a maximum of 347 °C and a $\Delta H = -796.33$ J/g. The last process is not yet completed at 500 °C and is accompanied by an exothermic process. On the curve HF, a small endothermic process can be seen at 100.23 °C, which can be attributed to the melting of the active substance.

Thermal analysis of Per binary mixtures with the components used in the synthesis of three types of jellies

Regarding the thermal behaviour of the binary mixture Per_Sorb, the active substance's primary decomposition process partially overlaps with Sorb's primary decomposition process. However, it can still be argued that the first decom-

position of **Per** occurs considering the enthalpy associated with this process in a narrower correlation with that of the active substance, Fig. 5.

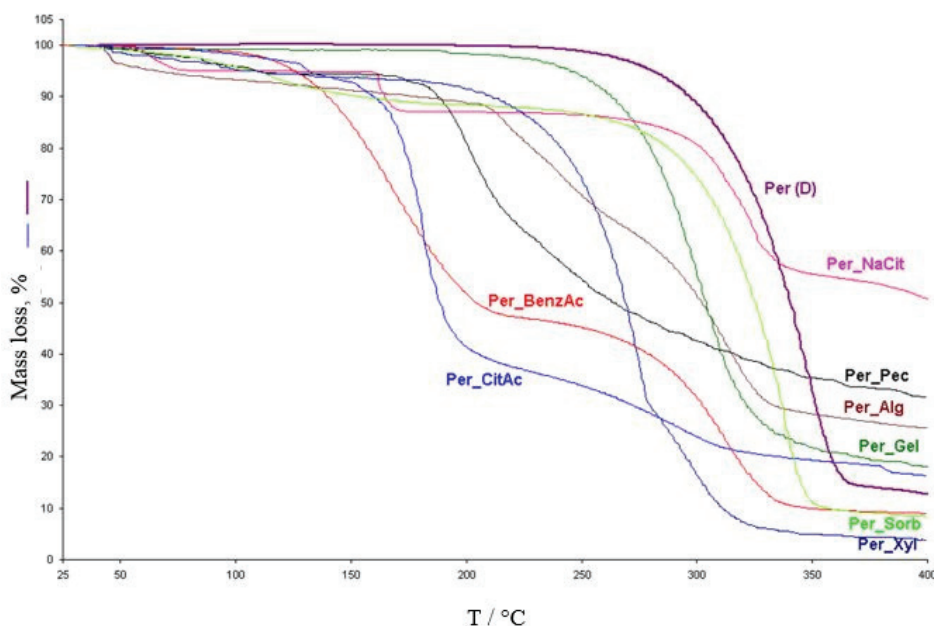


Fig. 5. TG curves obtained for Pec (D) and the moist binary mixture obtained at a heating rate of $10\text{ }^{\circ}\text{C min}^{-1}$ – $400\text{ }^{\circ}\text{C}$.

The thermogravimetric study of the binary mixture Per_BenzAc reveals the main decomposition processes of the two components of the mixture. Thus, it is found that the decomposition process of BenzAc takes place before the degradation of the active ingredient. The degradation of Per takes place in the range of $220\text{--}330\text{ }^{\circ}\text{C}$. It is accompanied by an exothermic process, Fig. 6, with a mass loss of about 40 % of the sample's total mass, closely correlated with the amount of the active substance in the mixture and the mass loss of pure active ingredient.

The binary mixture Per_Pec does not show the thermal behaviour of the active substance within the mixture, which would lead us to the idea of a thermally induced interaction between the two components. We will correlate these data with those from spectroscopic investigations.

In the air atmosphere, the thermal analysis carried out on the binary mixture Per_Gel shows the decomposition of the active substance in the same decomposition interval as that of Gel. The integrity of the active substance is also demonstrated by the melting process's presence with a maximum of $100\text{ }^{\circ}\text{C}$. The total mass loss of the mixture correlates closely with the masses and mass losses

of the components of the binary mixture. Therefore, the fact that Gel can be used in medicated jellies can be supported.

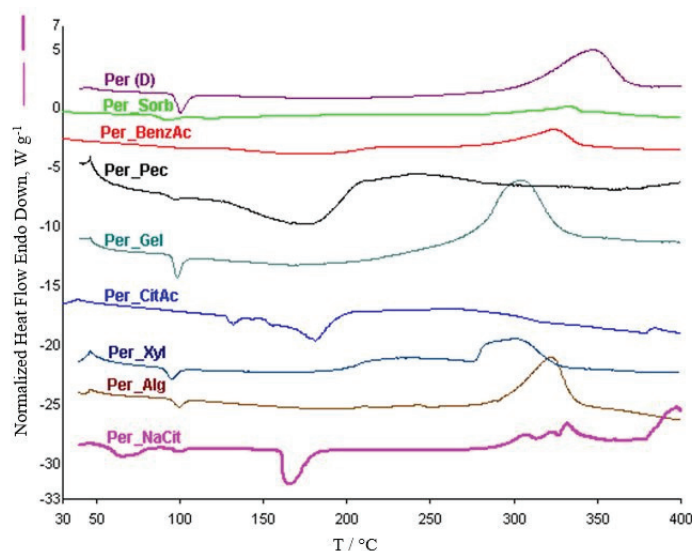


Fig. 6. Heat flow (HF) curves obtained for Per (D) and the moist binary mixture obtained at a heating rate of $10\text{ }^{\circ}\text{C min}^{-1}$ – $400\text{ }^{\circ}\text{C}$ in air atmosphere.

In the case of the binary mixture Per_CitAc, the thermal behaviour of the active substance is hardly visible. A decomposition process is observed in the range of $210\text{--}331\text{ }^{\circ}\text{C}$, similar to the range highlighted in the active substance. Still, it does not closely correlate with the amount of active substance in the mixture. These results do not clearly indicate whether or not the active substance interacted with CitAc, which is known for its properties. The thermogravimetric data must be correlated with the spectroscopic data or the data obtained after dosing the active substance.

The thermal analysis of the binary mixture Per_Xyl shows a destabilization of the active substance in the mixture. It can be observed that the main decomposition process starts faster at a temperature of $50\text{ }^{\circ}\text{C}$ than in the thermal analysis of the pure active substance. The melting point of the active substance is seen on the HF curve at $95\text{ }^{\circ}\text{C}$, which can be explained by the fact that it is present in a mixture.

The case of the moist binary mixture Per_Alg is an example of a thermal analysis that argues the absence of interactions between the two components of the mixture. Thus, the thermal behaviour of the two components can be observed as they exhibit decomposition stages at different temperatures. On the HF curve of the mixture, even the melting point of the active ingredient can be seen at $100\text{ }^{\circ}\text{C}$, indicating that the Alg does not prevent the crystallization of the active sub-

stance. The main decomposition process of Per is observed in the same temperature range, and the mass loss is closely correlated with its concentration in the mixture.

The thermogravimetric study of the binary mixture Per_NaCit showed several clearly separated stages of decomposition in the same temperature range. The first two processes, namely one in the range 39–82 °C with a mass loss of 4.86 % and the next in the range 157.4 and 182 °C with a mass loss of 7.69 %, can be attributed to moisture loss and, respectively, to the decomposition of NaCit. The last two stages are due to the decomposition of the active substance, which occurs in the same interval as in the thermal analysis of the individual component. The active substance accumulates a mass loss of 30 % of the mass of the mixture, which is in close correlation with the data obtained for the active substance.

Thermal analysis of jellies with an active substance

The thermal analysis of the Alg-based jelly with Per showed the thermal behaviour of the active ingredient in the same temperature range and with a weight that correlates closely with the primary degradation process of the active ingredient and the other components within the jelly, Fig. 7. The composition and thermal behaviour highlighted in the studies on the binary mixtures were considered.

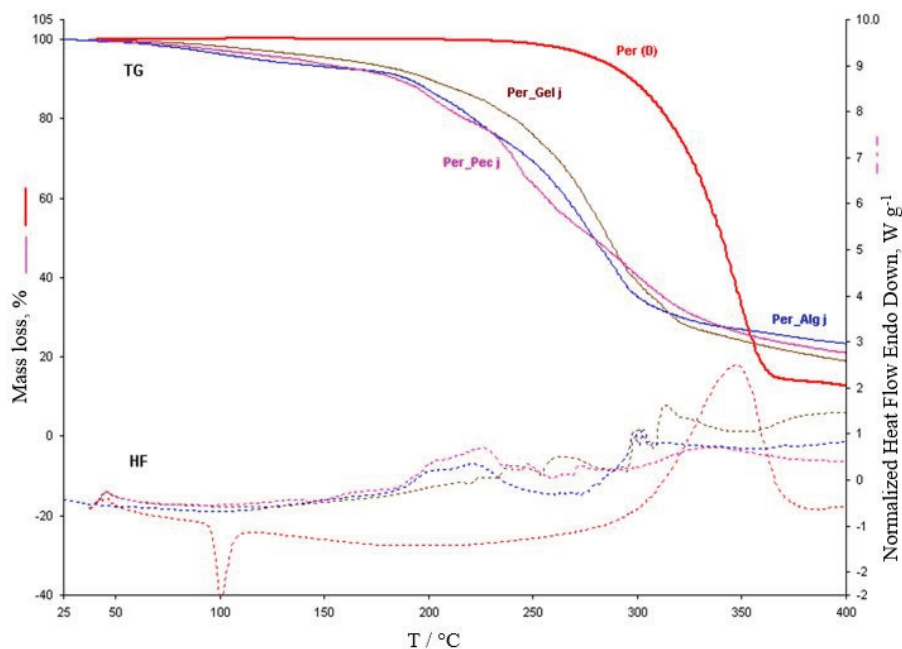


Fig. 7. Comparative of TG and HF for Pec (D) and medicated jellies based on Alg, Gel and Pec obtained at a heating rate of $10\text{ }^{\circ}\text{C min}^{-1}$ – 400 °C.

In the case of Gel-based jelly, good agreement is observed with the thermogravimetric data obtained in the case of the binary mixture Per_Gel. Also, in the case of this jelly, it is observed that the Gel and the active substance have the main degradation process in the same temperature range, but it can be said that the mass loss is in close correlation with the degradation of the constituent components. In this case, more clear results will be obtained in the dissolution studies.

Thermal analysis of jelly based on Pec with active substance shows a variety of decomposition stages that are difficult to separate. The decomposition stage of the active substance is not visible on the thermogravimetric curve of the jelly. In the case of this jelly, confirmation of the presence of the active substance also requires dissolution studies or other UV–Vis spectroscopy studies. The conclusions are correlated with the FTIR spectroscopy studies.

UV–Vis spectrophotometry

All absorbance measurements were performed in a 10 mm UV–Vis spectroscopy cell at room temperature, using water as a blank. The standard active substance and medicated jellies were investigated. The concentration of the standards was $5 \text{ mg}\cdot\text{mL}^{-1}$, and the amount used for the jellies was chosen to retain approximately $0.1 \text{ mg}\cdot\text{mL}^{-1}$. The study conducted at UV–Vis considers a qualitative relevance at about 300 nm. The jellies based on Alg, Gel and Pec were analysed using UV–Vis.

The active substance Per (Fig. 8) is visible in all samples and has a maximum at 300 nm. After UV–Vis spectroscopy analysis, the active substance in the synthesized medicated jellies is found in all cases.

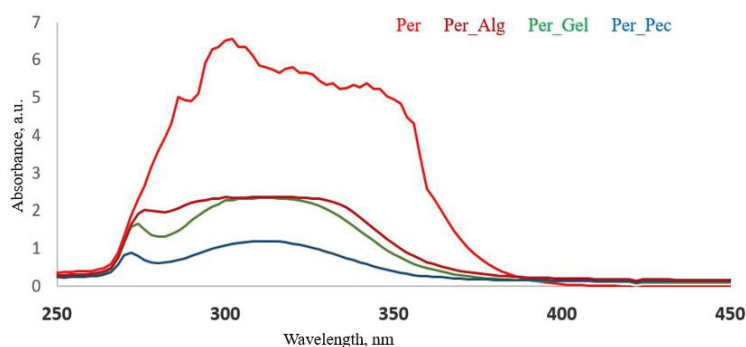


Fig. 8. The UV–Vis spectra for Per, Per-Alg, Per-Gel and Per-Pec, medicated jelly in the range 250–450 nm.

Physical examination

All medicinal jellies prepared presented a smooth texture, a clear appearance. Medicated jellies prepared with Pec and Alg presented a very thick consistency while jelly prepared with Gel presented a moderately thick consistency.

Stickiness and grittiness

The stickiness and grittiness of the jellies prepared with Pec and Alg were non-sticky and non-gritty, while the ones prepared with Gel were slightly sticky and non-gritty.

After thermal analysis, the rest of the prepared jellies were stored in polyethylene bags at room temperature to be re-examined after one and three months. In the physical examination after one month, no change in the jellies' appearance, texture, or stickiness and grittiness was observed. At the final three-month inspection, a slight change in the texture of the jellies prepared with Gel and increased stickiness was observed.

According to the literature, the protocol for stability testing may differ for the same product if it is to be distributed or marketed in other regions, such as in ASEAN regulations which belong to the hot and humid climate zone (zone IV).²⁹

CONCLUSION

In this study, we presented spectroscopy and thermal analysis of Per, an antidepressant drug, moist binary mixtures, and medicated jellies based on the common gelling agents: alginate (Alg), pectin (Pec) and gelatin (Gel). Our work aimed to formulate and investigate new pharmaceutical formulations that can be more easily administered to patients with conditions that make other forms of a drug challenging to administer.

The FTIR spectra of the medicated jellies indicate that all components are compatible for use in the formulations.

The thermogravimetric study of a moist binary mixture shows that components such as BenzAc, Sorb, Xyl, NaCit, Gel and Alg are compatible with the active substance Per and CitAc, which should be used in small amounts. The results obtained for the moist binary mixtures also show that Pec can lead to possible interactions with the active ingredient Per.

Thermal analysis of the medicinal jellies with Per showed that the Alg-based jelly is the only jelly in which the contribution of the active substance is visible. In the other Gel and Pec-based jellies, the thermal analysis contains a variety of decomposition processes that are more difficult to separate, with overlapping decomposition stages, leading to the conclusion that only the thermogravimetric study does not allow definite conclusions.

Thus, by combining the FTIR and UV-Vis spectroscopy results with thermogravimetric analysis, it was possible to obtain motivated confirmations of the presence of the active substance in the studied medicated jellies.

SUPPLEMENTARY MATERIAL

Additional data and information are available electronically at the pages of journal website: <https://www.shd-pub.org.rs/index.php/JSCS/article/view/12343>, or from the corresponding author on request.

ИЗВОД
ТЕРМОАНАЛИТИЧКА И СПЕКТРОСКОПСКА ИСПИТИВАЊА МЕДИЦИНСКИХ
ГЕЛОВА СА ПЕРФЕНАЗИНОМ

MIHAELA M. BUDIUL^{1,2}, MĂDĂLINA MATEESCU^{1,2}, GABRIELA VLASE^{1,2}, TITUS VLASE^{1,2}, SIMONA BOCĂNICI¹
и IONELA A. BRADU¹

¹Research Centre for Thermal Analysis in Environmental Problems, West University of Timișoara, Pestalozzi Street 16, 300115 Timișoara, Romania и ²West University of Timișoara – ICAM – Advanced Environmental Research Institute, Timișoara, Romania

Употреба медицинских гелова је широко распрострањена међу великим бројем пацијената, посебно оних са потешкоћама при гутању. Студије преформулација играју есенцијалну улогу у развоју нових фармацеутских формулација. Циљ овог испитивања је да се формулишу и оцене медицински гелови који садрже перфеназин, антипсихотични лек из групе фенотиазин једињења који се користи при лечењу шизофреније и других менталних поремећаја. Типични агенси за гелирање као што су натријум-алгинат (Alg), желатин (Gel) и пектин (Pec) су коришћени за развој медицинских гелова. Као додаток биополимерима, компоненте попут бензоеве киселине (BenzAc), лимунске киселине (CitAc), натријум-цитрата (NaCit), сорбитола (Sorb) и ксилитола (Xyl). Пре припреме гелова, влажне бинарне смеше сваке компоненте гела и активне супстанце су анализирани да би се испитала комаптибилност супстанци. Активна супстанца, влажна бинарна смеша, и медицински гелови су анализирани FTIR_UATR спектроскопијом, UV-Vis спектроскопијом и термогравиметријом (TGA).

(Примљено 2. априла, ревидирано 1. јула, прихваћено 10. октобра 2023)

REFERENCES

1. S. Sarojini, K. Anusha, C. Maneesha, M. A. Mufaquam, B. Deepika, Y. Krishna Reddy, N. R. Kandukoori, *World J. Pharm. Res.* **7** (2014) 352 (<https://doi.org/10.20959/wjpr20186-11502>)
2. K. H. Kim, M. Jun, M. K. Lee, *Pharmaceutics* **12** (2020) 1 (<https://doi.org/10.3390/pharmaceutics12111073>)
3. A. D. Darade, A. S. Mundada, *World J. Pharm. Res.* **10** (2021) 1628 (<https://doi.org/10.20959/wjpr20216-20658>)
4. L. E. Committee, *USP – Nomenclature Guidelines*, 2006 (<https://doi.org/10.1038/sj.bjp.0706759>)
5. S. Sunil, U. K. Sharma, S. A. Arathy, *J. Pharm. Sci. Res.* **12** (2020) 904
6. A. Lutka, W. Prange, *Acta Pol. Pharm.* **62** (2005) 419
7. Z. Ramezani, M. Shekarriz, A. A. Behfar, S. Kiamarzi, *J. Braz. Chem. Soc.* **28** (2017) 2172 (<https://doi.org/10.21577/0103-5053.20170066>)
8. S. Hong, M. yeong Lee, K. S. Shin, S. J. Kang, *Animal Cells Syst. (Seoul)*. **16** (2012) 20 (<https://doi.org/10.1080/19768354.2011.611256>)
9. S. Beg, S. Swain, M. Rizwan, M. Irfanuddin, D. Shobha Malini, *Curr. Drug Deliv.* **8** (2011) 691 (<https://doi.org/10.2174/156720111797635504>)
10. S. Baboota, G. Mustafa, J. Sahni, J. Ali, *J. Excipients Food Chem.* **4** (2013) 12 (<https://jefc.scholasticahq.com/article/1099-mechanistic-approach-for-the-development-of-ultrafine-oil-water-emulsions-using-monoglyceride-and-blends-of-medium-and-long-chain-triglycerides-enhan>)
11. Z. Saghafi, M. Mohammadi, M. M. Mahboobian, K. Derakhshandeh, *Drug Dev. Ind. Pharm.* **47** (2021) 509 (<https://doi.org/10.1080/03639045.2021.1892745>)

12. L. Wang, F. Zeng, L. Zong, *Pharm. Dev. Technol.* **18** (2013) 1101 (<https://doi.org/10.3109/10837450.2012.700932>)
13. S. H. Almurisi, A. A. Doolaanea, M. E. Akkawi, B. Chatterjee, K. Ahmed Saeed Aljapairai, M. Z. Islam Sarker, *Drug Dev. Ind. Pharm.* **46** (2020) 1373 (<https://doi.org/10.1080/03639045.2020.1791165>)
14. Z. H. Mahdi, *Al Mustansiriyah J. Pharm. Sci.* **20** (2020) (<https://doi.org/10.32947/ajps.v20i3.765>)
15. E. Gomaa, M. M. Ayoub, *Saudi Pharm. J.* **29** (2021) 955 (<https://doi.org/10.1016/j.jsps.2021.07.020>)
16. S. Patel, N. Scott, K. Patel, V. Mohylyuk, W. J. McAuley, F. Liu, *J. Pharm. Sci.* **109** (2020) 2474 (<https://doi.org/10.1016/j.xphs.2020.04.018>)
17. A. Hassen Elshafeey, R. Moataz El-Dahmy, *Saudi Pharm. J.* **30** (2022) 1435 (<https://doi.org/10.1016/j.jsps.2022.07.004>)
18. D. Okolišan, G. Vlase, T. Vlase, C. Avram, *Polymers (Basel)* **14** (2022) (<https://doi.org/10.3390/polym14204275>)
19. N. K. Sachan, P. Seema, A. Jha, A. Bhattacharya, *J. Pharm. Res.* **2** (2009) 1191
20. V. S. Kadam, J. Kendre, G. R. Shendarkar, S. S. Kadam, *Int. J. Pharm. Sci. Res.* **11** (2020) 6251 ([https://doi.org/10.13040/IJPSR.0975-8232.11\(12\).6251-59](https://doi.org/10.13040/IJPSR.0975-8232.11(12).6251-59))
21. M. Chamoli, S. K. Tangri, *Int. J. Sci. Res.* **11** (2022) 1541 (<https://doi.org/10.21275/SR22521115404>)
22. K. Prakash, V. M. Satyanarayana, H. T. Nagiat, A. H. Fathi, A. K. Shanta, A. R. Prameela, *Asian J. Pharm.* **8** (2014) 241 (<https://doi.org/10.4103/0973-8398.143937>)
23. M. Budiul, C. A. Marioane, I. A. Bradu, G. Vlase, T. Vlase, *J. Therm. Anal. Calorim.* **148** (2023) 4589 (<https://doi.org/10.1007/s10973-022-11882-8>)
24. M. Mateescu, G. Vlase, M. M. Budiul, B. D. Cernușcă, T. Vlase, *J. Therm. Anal. Calorim.* **148** (2023) 4601 (<https://doi.org/10.1007/s10973-023-12052-0>)
25. S. H. Kumar, A. Sheikalisha, S. Chandra, R. Suresh, S. Sangeetha, *Int. J. Adv. Pharm. Sci.* **1** (2018) 7
26. R. Taranum, S. Mittapally, *J. Drug Deliv. Ther.* **8** (2018) 65 (<https://doi.org/10.22270/jddt.v8i4.1784>)
27. K. V. S, J. Kendre, G. R. Shendarkar, S. S. Kadam, *Int. J. Pharm. Sci. Res.* **11** (2020) 6251 ([https://doi.org/10.13040/IJPSR.0975-8232.11\(12\).6251-59](https://doi.org/10.13040/IJPSR.0975-8232.11(12).6251-59))
28. A. Jaszczyszyn, K. Gąsiorowski, P. Świątek, W. Malinka, K. Cieślak-Boczula, J. Petrus, B. Czarnik-Matusiewicz, *Pharmacol. Rep.* **64** (2012) 16 ([https://doi.org/10.1016/S1734-1140\(12\)70726-0](https://doi.org/10.1016/S1734-1140(12)70726-0))
29. S. H. Almurisi, K. Al-Japairai, F. Alshammari, F. Alheibshy, R. M. F. Sammour, A. A. Doolaanea, *Gels* **8** (2022) 1 (<https://doi.org/10.3390/gels8030144>).

SUPPLEMENTARY MATERIAL TO
**Thermoanalytical and spectroscopic studies on medicated jellies
with perphenazine**

MIHAELA M. BUDIUL^{1,2}, MĂDĂLINA MATEESCU^{1,2*}, GABRIELA VLASE^{1,2},
TITUS VLASE^{1,2}, SIMONA BOCĂNICI¹ and IONELA A. BRADU¹

¹Research Centre for Thermal Analysis in Environmental Problems, West University of
Timișoara, Pestalozzi Street 16, 300115 Timișoara, Romania and ²West University of
Timișoara – ICAM – Advanced Environmental Research Institute, Timișoara, Romania

J. Serb. Chem. Soc. 89 (4) (2024) 521–537

PREPARATION OF MEDICATED JELLIES

TABLE S-I. Components of the medicated jellies calculated on the basis [%] w/w

Jellies	Biopolymers			BenzAc [%]	CitAc [%]	NaCit [%]	Xyl [%]	Sorb [%]	Water [%]
	Alg [%]	Gel [%]	Pec [%]						
Alg j	50	-	-	0.02	0.5	0.5	10	2	36.98
Gel j	-	50	-	0.02	0.5	0.5	10	2	36.98
Pec j	-	-	50	0.02	0.5	0.5	10	2	36.98

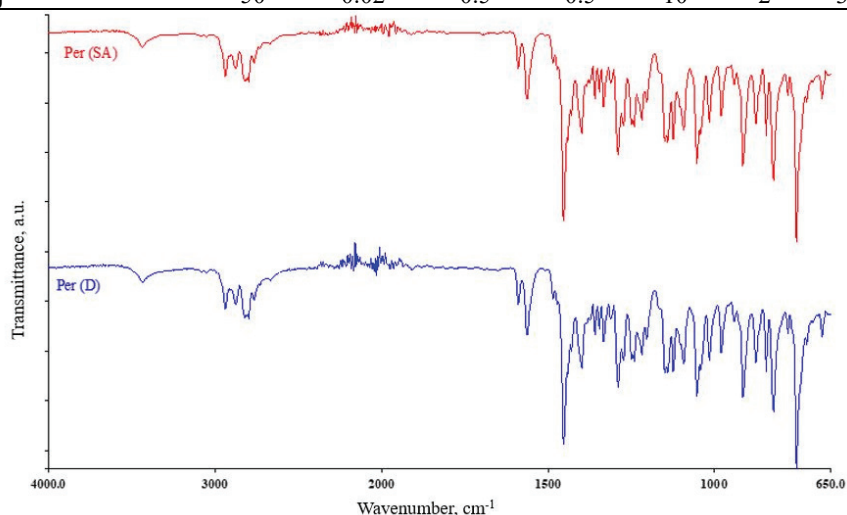
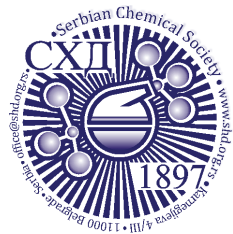


Fig. S-1. FTIR spectra of Per (SA)/Per (D).

* Corresponding author. E-mail: madalina.mateescu@e-uvv.ro



J. Serb. Chem. Soc. 89 (4) 539–549 (2024)
JSCS–5738

Electrochemical analysis of antioxidant status of biological media in different sampling and storage conditions

IRINA V. GORONCHAROVSKAYA*, ANATOLY K. EVSEEV, ASLAN K. SHABANOV
and SERGEY S. PETRIKOV

*N. V. Sklifosovsky Research Institute for Emergency Medicine, B. Sukharevskaya sq., 3,
129090 Moscow, Russia*

(Received 12 October 2023, revised 1 January, accepted 20 February 2024)

Abstract: The use of an electrochemical approach for assessment of the oxidative stress severity is a promising direction for point-of-care testing development, which is especially important for critically ill patients. The aim of this study was to determine the influence of different types of blood collection tubes (with clot activator and separating gel, lithium heparin, sodium citrate and K₂EDTA) and storage conditions (at 25, 4 and –23 °C up to 5 days) on the electrochemical analysis of the antioxidant status of blood plasma, assessed by measuring the open circuit potential of platinum electrode (*OCP*) and antioxidant capacity *via* cyclic voltammetry method (*q*). It was obtained that blood collection tubes with lithium heparin and clot activator are the most suitable for the electrochemical analysis of antioxidant status of blood plasma, since they do not affect the results of measurements. Furthermore, data obtained during storage blood plasma samples in different temperature conditions indicate that it is preferable to perform electrochemical analysis in fresh samples.

Keywords: potentiometry; voltammetry; antioxidants; sample processing.

INTRODUCTION

Determination of antioxidant status of biological media in patients with various pathologies has an important diagnostic value since it allows to assess the severity of oxidative stress, which in turn affects the disease course and outcome.^{1,2} At the present time electrochemical analysis is being actively introduced for the assessment of redox properties of biological media, in particular, methods of potentiometry and cyclic voltammetry (CV), which make it possible to assess both the overall redox balance and the content of low molecular weight antioxidants in analyte.^{3–7}

* Corresponding author. E-mail: GoroncharovskayaIV@sklif.mos.ru
<https://doi.org/10.2298/JSC231012017G>

Important preanalytical phase in these studies include the blood collection procedure, sample preparation and storage prior to analysis. In clinical practice, a large number of vacuum blood collection systems are used with various additives for the biological samples stabilization or isolation a certain blood fraction (Table I).

TABLE I. Blood collection tubes types and their uses⁸

Tube cap color	Specimen type	Additive	Analysis
Yellow	Serum	Clot activator (SiO ₂) + gel	Biochemistry
Red	Serum	No / Clot activator (SiO ₂)	Biochemistry Immunology
Lavender	Whole blood	K2EDTA	Hematology test
	Plasma	K3EDTA	Immunology Molecular diagnostics (PCR etc.)
Green	Plasma	Lithium heparin Sodium heparin	Urgent biochemistry Immunology
Light blue	Whole blood	Sodium citrate 9:1;	Coagulation tests
	Plasma	0.109 M (3.2 %)	Hemostasis
Grey	Plasma	Sodium fluoride + Potassium oxalate	Glucose
		Sodium fluoride + EDTA	

However, while maintaining the stability of some substances, these additives may affect the results of analysis of other substances.⁹

There is a lot of data in the literature on the influence of the type of blood collection tubes used on the results of various routine tests,^{10,11} however, there are significantly fewer studies on the influence of the type of blood collection tubes on the results of analysis of oxidative stress markers. For example, Bastin *et al.*¹² showed that the analysis of the total antioxidant status of blood serum using the ferric reducing antioxidant power (*FRAP*) assay turned out to be sensitive to the components of the test tube – in plastic tubes with a separating gel, the values were significantly lower than in a glass tubes, but were within acceptable limits from a clinical point of view.

A comparison of the redox potential of blood plasma collected in tubes with lithium heparin and sodium citrate (3.2 %) in study,⁵ showed that the values of the redox potential were more negative in heparinized blood plasma.

Studies of total antioxidant capacity of blood plasma containing the anti-coagulants EDTA and lithium heparin showed that lithium heparin had no effect on the antioxidant capacity of blood plasma *in vitro*, while EDTA was an interfering agent.¹³ However, the direction of the effect (overestimation or underestimation of results), probably depends on the method for determination of total antioxidant capacity.

Similar results were obtained when studying the influence of the type of blood collection tubes on the analysis of the content of individual low-molecular weight antioxidants in blood plasma such as ascorbic acid¹⁴ and uric acid,¹⁵ which make a significant contribution to the total antioxidant capacity. It was found that blood plasma ascorbic acid is more stable when stored in tubes with lithium heparin compared with tubes with EDTA. The authors suggest that this phenomenon was associated with the fact that EDTA – chelated iron is redox active and can promote the oxidation of ascorbic acid. Reduced levels of uric acid in blood plasma could also be due to the influence of EDTA on the assay reagents.

It is well known that the duration and temperature of storage of samples before analysis affects the laboratory tests results,¹⁰ especially redox properties of biological media,^{16,17} since antioxidants are easily oxidized upon contact with atmospheric oxygen. Jansen *et al.* showed that the antioxidant status of blood serum of healthy people, determined by the total antioxidant status (*TAS*) assay, decreased during sample storage longer than 24 h. The samples stored at 20 °C exhibited greater decrease in the parameter compared with samples stored at 4 °C.¹⁶

Pawlik-Sobecka *et al.*¹⁷ suggest that *FRAP* assay for determination of antioxidant status of blood serum should be carried out no later than 24 h after blood collection. If deviation of 10 % is acceptable, then the analysis can be carried out within 48 h, provided the samples are stored at 20 °C, and within 120 h (5 days), if the samples are stored at 4 °C.

In our previous study of redox properties of blood plasma stored at –40 °C¹⁸ we observed that during first 14 days of storage there were a fluctuations of open circuit potential (*OCP*) of Pt electrode values, measured in blood plasma, indicating that storage of a biological media at very low temperatures does not exclude the occurrence of redox processes.

It is also important to timely centrifuge the tubes after blood collection to separate the plasma or serum from the blood cells to avoid cell metabolism interfering with the test results.¹⁹

Thus, studies on the influence of the type of blood collection tubes and sample storage conditions on the electrochemical parameters characterizing the antioxidant status of blood plasma or serum are practically not presented in the literature.

The aim of this work is to study the influence of blood collection tubes additives and sample storage conditions on the results of electrochemical assessment of the antioxidant status of blood plasma.

EXPERIMENTAL

Blood plasma and serum sample preparation

In model experiments blood plasma donated by clinically healthy volunteer and collected by automated apheresis was used and was provided by the Department of Transfusion Medi-

cine of the N.V. Sklifosovsky Research Institute for Emergency Medicine in Moscow. Blood plasma was aliquoted into vacuum blood collection tubes with the following additives: clot activator with separating gel (Zhejiang Gongdong Medical Technology Co., China), lithium heparin, sodium citrate (3.2 %, the ratio of citrate to blood is 1:9) and K₂EDTA (Zdravmedtech, Russia). Tubes without additives were used as a control. Blood plasma samples were stored at 4, 25 and -23 °C. Electrochemical measurements were carried out on the day of blood plasma collection and after 1 and 5 days of storage.

Blood serum samples were obtained from 23 critically ill patients (average age 55±19 y) and examined before and after 24 h of storage at 4 °C. Blood was collected in vacuum tubes with clot activator and separating gel; after at least 30 min tubes were centrifuged at 1500 g (Allegra X-15R, Beckman Coulter, USA) at 25 °C for 10 min.

The study was conducted in compliance with the Declaration of Helsinki, International Conference on Harmonization and Good Clinical Practice Guidelines, and was approved by the Ethical Committee of N.V. Sklifosovsky Research Institute for Emergency Medicine, Moscow, Russian Federation.

Electrochemical measurements

In electrochemical measurements in aqueous media two isotonic to blood plasma solutions were used: saline solution (154 mM NaCl, pH 6.3 (JSC LenReactiv, Russia) and phosphate buffered saline solution (137 mM NaCl, 2.7 mM KCl, 10 mM Na₂HPO₄, 1.8 mM KH₂PO₄; pH 7.4 (JSC LenReactiv, Russia). All reagents were of analytical-reagent grade.

Electrochemical analysis of the antioxidant status of biological media consisted of measuring open circuit potential (*OCP*) of platinum electrode and determining its antioxidant capacity by using cyclic voltammetry. In all experiments a saturated silver chloride electrode (sat. Ag/AgCl; all potentials are referred to Ag/AgCl scale) was used as reference electrode and platinized titanium mesh was used as the counter electrode. The *OCP* result values were recorded 15 min after platinum electrode immersion in the sample. Total antioxidant capacity of biological media was assessed from overall quantity of electricity, *q*, spent for the oxidation of low molecular weight antioxidants. The *q* values were determined by integration the area under the polarization curves in a range of potentials from 400 to 1000 mV.³

RESULTS AND DISCUSSION

Electrochemical measurements in aqueous solutions

Initially, measurements in saline solution and phosphate-buffered saline aliquoted into the blood collection tubes were carried out (Table II).

TABLE II. *OCP* of Pt electrode and pH values measured in isotonic solutions in the presence of various additives

Blood collection tube	Saline solution		Phosphate buffered saline	
	<i>OCP</i> / mV	pH	<i>OCP</i> / mV	pH
No additive	180.5	6.3	149.0	7.43
Clot activator + gel	183.6	6.2	146.9	7.48
Lithium heparin	182.8	6.1	147.2	7.46
Sodium citrate (3.2 %, 9:1)	146.5	8.76	132.4	7.51
K ₂ EDTA	208.5	4.7	148.4	6.81

Data presented in Table II show that sodium citrate and K_2EDTA additives significantly affect OCP of Pt electrode values measured in saline solution, which may be associated with changes in the pH values of solutions. Thus, OCP of Pt electrode value decreased by 34 mV in solution with sodium citrate and increased by 28 mV in solution with K_2EDTA compared to solution without additives. In phosphate buffered saline one can see that pH values in all solutions vary slightly and the OCP of Pt electrode values are practically the same except for solution with sodium citrate. In this solution measurements showed a decrease by 16.6 mV of OCP of Pt electrode value as compared to control.

Cyclic voltammetry measurements show that sodium citrate and K_2EDTA additives also affect the polarization curves in saline solution (Fig. 1).

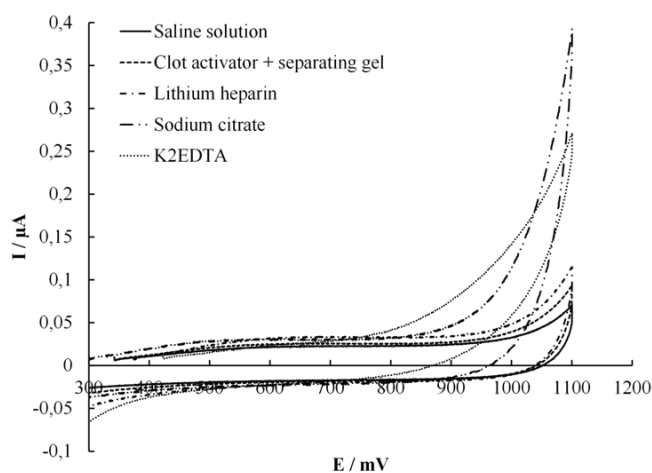


Fig. 1. Cyclic voltammetry in saline solution with various additives.

As can be seen from Fig. 1, the electrochemical oxidation process begins to occur at a potentials more positive than 850 mV in the presence of sodium citrate (dash-double dot line) and more positive than 850 mV in the presence of K_2EDTA (dotted line). According to literature, both sodium citrate^{20,21} and $EDTA$ ^{22,23} are able to adsorb and exhibit electrochemical activity on platinum electrode. Thus, additional electrochemical processes in polarization measurements in biological media will lead to data distortion.

Electrochemical measurements in model blood plasma

After electrochemical measurements in aqueous solutions a model experiments in blood plasma aliquoted into the tubes with various additives and stored at different temperatures were carried out. Fig. 2 shows the results of measurement of OCP of Pt electrode and antioxidant capacity of blood plasma *via* CV method during storage at temperature of 25 °C.

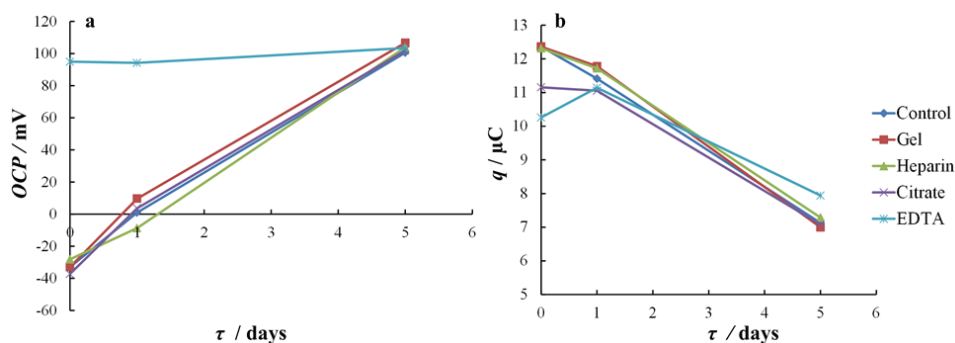


Fig. 2. *OCP* of Pt electrode in blood plasma (a) and antioxidant capacity of blood plasma, measured *via CV* (b) during storage at 25 °C.

From data presented in Fig. 2a it can be seen that the values of *OCP* of Pt electrode measured in blood plasma samples aliquoted into tubes with additives on the day of blood collection practically did not differ from the control sample without additives. On average, the value of *OCP* of Pt electrode was -32.8 ± 4.5 mV. However, this value measured in blood plasma sample with K_2EDTA additive was significantly higher compared with other samples (95 mV, $\Delta = 128$ mV). Throughout the entire storage period, the *OCP* of Pt electrode values measured in all studied blood plasma samples shifted to more positive potentials, which indicates oxidative processes. The shift of *OCP* of Pt electrode value on average was 136.1 ± 3.9 mV, except for the sample with the addition of K_2EDTA , where this value practically did not change during the entire storage period.

As in the case with *OCP* of Pt electrode (Fig. 2b) the presence of such stabilizing additives as lithium heparin and clot activator with separating gel had almost no effect on antioxidant capacity of blood plasma on the day of blood collection. A significant difference in q values was observed in blood plasma samples in tubes with K_2EDTA ($\Delta = 2.1$ μC) and sodium citrate ($\Delta = 1.2$ μC).

After 24 h of storage the values of antioxidant capacity in all blood plasma samples varied slightly, and were on average 11.4 ± 0.3 μC . On the 5th day of storage antioxidant capacity significantly decreased, reaching an average value of 7.3 ± 0.4 μC .

Similar electrochemical measurements in samples stored at 4 °C were carried out (Fig. 3).

During storage at a temperature of 4 °C, the values of *OCP* of Pt electrode measured in all blood plasma samples shifted to more positive potentials (Fig. 3a). By the end of the first day of storage, the average value of the *OCP* of the Pt electrode in the blood plasma, measured in the control sample and in samples in tubes with clot activator with separating gel, lithium heparin and sodium citrate, was -7.5 ± 2.5 mV, and in a blood plasma sample in tube with K_2EDTA additive,

the *OCP* of Pt electrode increased to 105.4 mV ($\Delta = 10$ mV). The value of the *OCP* of the Pt electrode, measured on the 5th day of storage in the control sample and in blood plasma with additives, shifted to an average of 13 ± 2.2 mV, and in the test tube with K_2EDTA to 106 mV.

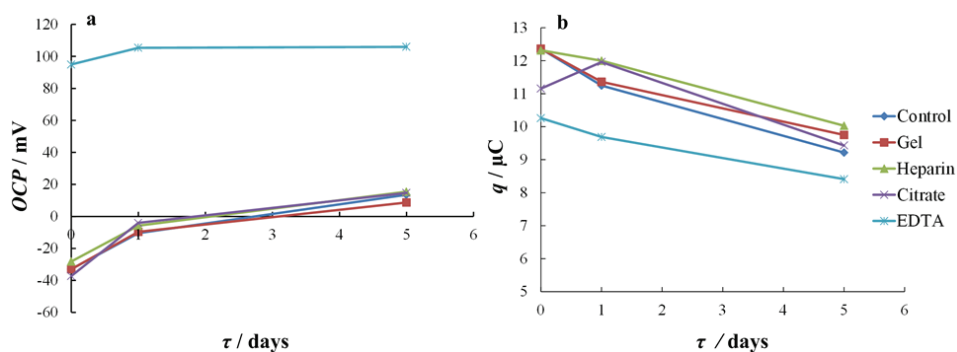


Fig. 3. *OCP* of Pt electrode in blood plasma (a) and antioxidant capacity of blood plasma, measured *via* CV (b) during storage at 4 °C.

The results of measurements of total antioxidant capacity of blood plasma samples demonstrate (Fig. 3b) that the lowest values compared with control were in the samples with K_2EDTA additive, where on the 1st day of monitoring q value was 10.3 μC and by the end of the storage period it was 8.4 μC , while in the other samples, the q value on the 1st day of storage was on average 11.6 ± 0.3 μC , and on the 5th day – 9.6 ± 0.4 μC .

Next electrochemical measurements were carried out in blood plasma samples stored at -23 °C (Fig. 4).

It can be seen (Fig. 4a) that after 5 days of storage at -23 °C in all studied samples, except the sample with K_2EDTA additive, *OCP* of Pt electrode values shifted towards more positive potentials and reached the values on average -15.0 ± 2.2 mV on the 1st day of storage and 18.1 ± 1.3 mV on the 5th day of storage. The value of *OCP* of Pt electrode measured in blood plasma sample with K_2EDTA additive decreased to a value of 87.6 mV after 24 h of storage at -23 °C, in contrast with the measurements in samples stored at 25 and 4 °C, where this value did not change or increased. After 24 h of storage the values of *OCP* of Pt electrode remained unchanged until the end of storage at all temperatures.

Antioxidant capacity of blood plasma stored at -23 °C (Fig. 4b) decreased to 11.8 μC in control sample and increased to 13.3 ± 0.1 μC in samples with lithium heparin, sodium citrate and clot activator with gel additives after 24 h of storage. In the blood plasma sample with K_2EDTA additive the q value increased to 10.8 μC . By the end of storage, the antioxidant capacity of all blood plasma samples decreased, but not as much as when stored in other temperature conditions.

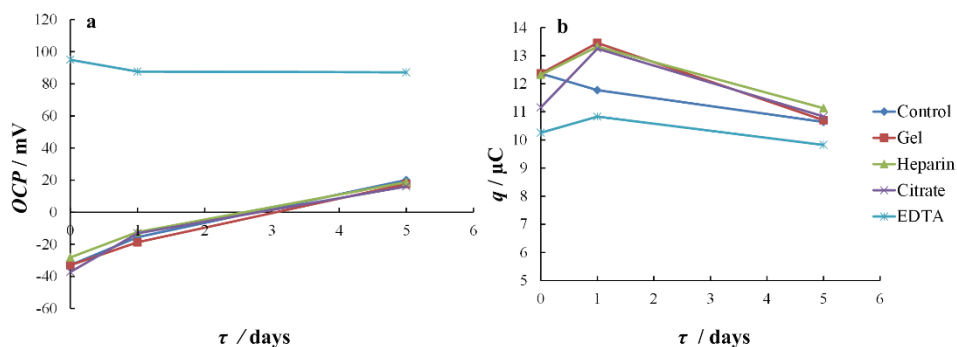


Fig. 4. *OCP* of Pt electrode in blood plasma (a) and antioxidant capacity of blood plasma, measured *via* CV (b) during storage at -23 °C.

Thus we can conclude that parameter of *OCP* of Pt electrode measured in blood plasma turned out to be more sensitive to the storage conditions of biological media. In addition, K_2EDTA and sodium citrate resulted in lower values of total antioxidant capacity of blood plasma measured *via* cyclic voltammetry.

Since both when stored at 4 and -23 °C the *OCP* of Pt electrode values shift towards more positive potentials, and the values of the total antioxidant capacity fluctuate during freezing, it was decided to reduce the measurement time to 24 h and carry out experiments for measuring electrochemical parameters in biological samples from patients under storage temperature of 4 °C in order to avoid additional errors, related to the conditions of the sample thawing.

Electrochemical measurements in critically ill patients' serum

Measurements of *OCP* of Pt electrode and antioxidant capacity in real samples of blood serum collected in tubes with clot activator and separating gel were carried out. In 43 % of cases ($n = 10$) the *OCP* of Pt electrode values measured in blood serum after 24 h of storage shifted to more negative potentials; in 35 % of cases ($n = 8$) the *OCP* of Pt electrode values practically did not change; and in 22 % of cases ($n = 5$) shifted to more positive potentials. Comparison of *OCP* of Pt electrode measurements in model blood plasma of healthy individual and blood serum of several patients in critical condition is presented on Fig. 5.

The data obtained indicate the importance of performing electrochemical measurements in fresh samples, since in real samples the magnitude and direction of the *OCP* of Pt electrode shift during sample storage may be influenced by individual characteristics of the biological media, depending on patients' drug therapy, therapeutic procedures, *etc.*

The value of the antioxidant capacity of blood serum after 24 h of storage at 4 °C significantly ($p = 0.00005$) decreased from 12.1 ± 4.1 μC to 11.4 ± 4.0 μC . It should be noted that this parameter reflects only the content of low molecular weight antioxidants, while the value of *OCP* of Pt electrode measured in blood

serum is an integral parameter and reflects overall balance between pro- and anti-oxidants.

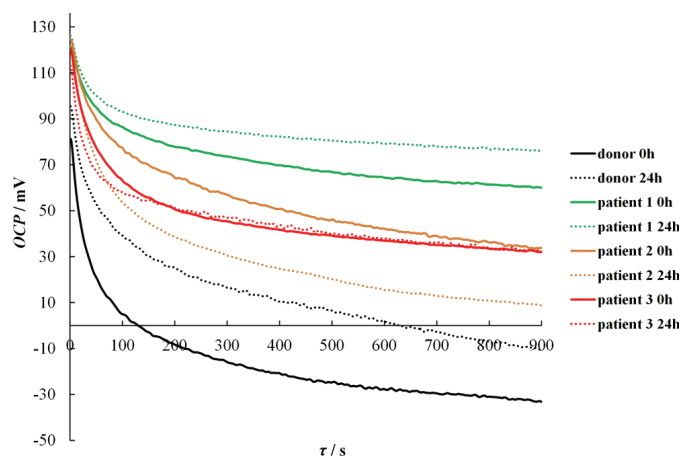


Fig. 5. *OCP* of Pt electrode in blood plasma of healthy individual and blood serum of patients in critical condition before and after 24 h of storage at 4 °C.

CONCLUSION

Electrochemical methods of analysis continue to find their application in laboratory practice for the evaluation of the redox properties of biological media in a group of analyses of oxidative stress markers. The preparation of biological samples is one of the key factors influencing the stability and accuracy of any measurement results, especially the results of assessing redox properties, which is associated with the stability of antioxidants contained in biological media.

In this paper blood plasma and sera samples with various additives stored at three temperatures were studied. It was found that storage conditions have significant effect on the results of electrochemical measurements in blood plasma. This study indicates that blood collection tubes with lithium heparin and clot activator with separating gel are preferable for blood collection and storage due to the least influence on the electrochemical parameters of biological media. Electrochemical analysis in blood plasma should be carried out in fresh samples avoiding storage.

ИЗВОД

ЕЛЕКТРОХЕМИЈСКА АНАЛИЗА АНТИОКСИДАТИВНОГ СТАТУСА БИОЛОШКОГ МЕДИЈУМА У РАЗЛИЧИТИМ УСЛОВИМА УЗОРКОВАЊА И СКЛАДИШТЕЊА

IRINA V. GORONCHAROVSKAYA, ANATOLY K. EVSEEV, ASLAN K. SHABANOV и SERGEY S. PETRIKOV

N. V. Sklifosovsky Research Institute for Emergency Medicine, B. Sukharevskaya sq., 3,
129090 Moscow, Russia

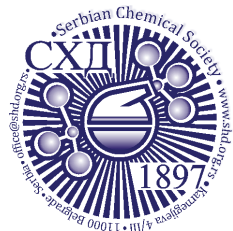
Примена електрохемијског приступа за процену јачине оксидативног стреса је обећавајући правац за развој тестирања на лицу места, што је посебно важно за критично болесне пацијенте. Циљ овог истраживања био је да се утврди утицај различитих типова епрувета за сакупљање крви (са активатором згрушавања и гелом за сепарацију, литијум-хепарином, натријум-цитратом и K₂EDTA) и услова складиштења (на 25, 4 и –23 °C до 5 дана) на електрохемијску анализу антиоксидативног статуса крвне плазме, процењеног мерењем потенцијала отвореног кола платинске електроде (ОСР) и антиоксидативног капацитета методом цикличне волтаметрије (q). Утврђено је да су епрувете за прикупљање крви са литијум-хепарином и активатором угрушака најпогодније за електрохемијску анализу антиоксидативног статуса крвне плазме, јер не утичу на резултате мерења. Штавише, подаци добијени током складиштења узорка крвне плазме у различитим температурним условима указују на то да је пожељно извршити електрохемијску анализу у свежим узорцима.

(Примљено 12. октобра 2023, ревидирано 1. јануара, прихваћено 20. фебруара 2024)

REFERENCES

1. A. F. Rogobete, D. Sandesc, M. Papurica, E. R. Stoicescu, S. E. Popovici, L. M. Bratu, C. Vernic, A. M. Sas, A. T. Stan, O. H. Bedreag, *Burns Trauma* **5** (2017) 8 (<https://doi.org/10.1186/s41038-017-0073-0>)
2. M. Simic, J. Kotur-Stevuljevic, P. Jovanovic, M. Petkovic, M. Jovanovic, G. Tasic, V. Savic, *J. Serb. Chem. Soc.* **88** (2023) 589 (<https://doi.org/10.2298/JSC221221017S>)
3. I. V. Goroncharovskaya, A. K. Evseev, A. K. Shabanov, O. Denisenko, *Electroanalysis* **33** (2021) 550 (<https://doi.org/10.1002/elan.202060356>)
4. A. K. Shabanov, A. K. Evseev, I. V. Goroncharovskaya, S. A. Badygov, R. A. Cherpakov, V. V. Kulabukhov, E. V. Klychnikova, N. V. Borovkova, O. A. Grebenchikov, S. S. Petrikov, *Polytrauma* **4** (2022) 56 (<https://doi.org/10.24412/1819-1495-2022-4-56-65>)
5. D. Polson, N. Villalba, K. Freeman, *Redox Rep.* **23** (2018) 125 (<https://doi.org/10.1080/13510002.2018.1456000>)
6. H.-W. Wang, C. Bringans, A. J. R. Hickey, J. A. Windsor, P. A. Kilmartin, A. R. J. Phillips, *Signals* **2** (2021) 138 (<https://doi.org/10.3390/signals2010012>)
7. M. Selaković, M. M. Aleksić, J. Kotur-Stevuljević, J. Rupar, B. Ivković, *Molecules* **28** (2023) 2113 (<https://doi.org/10.3390/molecules28052113>)
8. G. Lippi, A. von Meyer, J. Cadamuro, A.-M. Simundic, *Diagnosis* **6** (2019) 25 (<https://doi.org/10.1515/dx-2018-0018>)
9. R. A. R. Bowen, A. T. Remaley, *Biochem. Med.* **24** (2014) 31 (<https://doi.org/10.11613/BM.2014.006>)
10. C. Oddoze, E. Lombard, H. Portugal, *Clin. Biochem.* **45** (2012) 464 (<https://doi.org/10.1016/j.clinbiochem.2012.01.012>)

11. N. Ayala-Lopez, S. E. Conklin, B.J. Tenney, M. Ness, M. A. Marzinke, *Clin. Chim. Acta* **520** (2021) 118 (<https://doi.org/10.1016/j.cca.2021.05.019>)
12. A. Bastin, S. Fooladi, A. H. Doustimotlagh, S. Vakili, A. H. Aminizadeh, A. Faramarz, H. Shiri, M. H. Nematollahi, *PLoS One* **17** (2022) e0266567 (<https://doi.org/10.1371/journal.pone.0266567>)
13. C. Ialongo, *Clin. Biochem.* **50** (2017) 356 (<https://doi.org/10.1016/j.clinbiochem.2016.11.037>)
14. J. M. Pullar, S. Bayer, A. C. Carr, *Antioxidants* **7** (2018) 29 (<https://doi.org/10.3390/antiox7020029>)
15. D. Duplancic, L. Kukoc-Modun, D. Modun, N. Radic, *Molecules* **16** (2011) 7058 (<https://doi.org/10.3390/molecules16087058>)
16. E. H. J. M. Jansen, P. K. Beekhof, J. W. J. M. Cremers, D. Viezeliene, V. Muzakova, J. Skalicky, *Biomarkers* **2013** (2013) Article ID 316528 (<https://dx.doi.org/10.1155/2013/316528>)
17. L. Pawlik-Sobecka, K. Sołkiewicz, I. Kokot, A. Kiraga, S. Płaczkowska, A. M. Schlichtinger, E. M. Kratz, *Diagnostics* **10** (2020) 51 (<https://doi.org/10.3390/diagnostics10010051>)
18. I. V. Goroncharovskaya, V. B. Khvatov, A. K. Evseev, A. K. Shabanov, M. M. Goldin, S. S. Petrikov, *Gen. Reanimatol.* **15** (2019) 47 (<https://doi.org/10.15360/1813-9779-2019-1-47-53>)
19. B. L. Boyanton, K. E. Blick, *Clin. Chem.* **48** (2002) 2242 (<https://doi.org/10.1093/clinchem/48.12.2242>)
20. M. Donten, J. Osteryoung, *J. Appl. Electrochem.* **21** (1991) 496 (<https://doi.org/10.1007/BF01018601>)
21. O. I. González-Peña, T. W. Chapman, Y. M. Vong, R. Antaño-López, *Electrochim. Acta* **53** (2008) 5549 (<https://doi.org/10.1016/j.electacta.2008.02.104>)
22. B. Zhao, W. Zhu, T. Mu, Z. Hu, T. Duan, *Int. J. Environ. Res. Public Health* **14** (2017) 819 (<https://doi.org/10.3390/ijerph14070819>)
23. J. W. Johnson, H. W. Jiang, S. B. Hanna, W. J. James, *J. Electrochem. Soc.* **119** (1972) 574 (<https://doi.org/10.1149/1.2404264>).



J. Serb. Chem. Soc. 89 (4) 551–563 (2024)
JSCS–5739

Journal of
the Serbian
Chemical Society

JSCS-info@shd.org.rs • www.shd.org.rs/JSCS

Original scientific paper
Published 15 April 2024

Simultaneous determination of emtricitabine and tenofovir disoproxil fumarate in pharmaceutical preparations using spectrophotometric, chemometric and chromatographic methods

AYSUN DİNÇEL*, ELIF DAMLA GÖK-TOPAK and FEYYAZ ONUR

*Lokman Hekim University, Faculty of Pharmacy, Department of Analytical Chemistry,
06510, Ankara, Türkiye*

(Received 9 September 2023, revised 14 January, accepted 12 March 2024)

Abstract: Simple, accurate and sensitive spectrophotometric, chemometric and chromatographic methods were used for the simultaneous determination of emtricitabine (ETC) and tenofovir disoproxil fumarate (TDF) in tablets. In 1st derivative spectrophotometry, the first derivative spectra of the solution of ETC and TDF in water were recorded as $\Delta\lambda = 4$ nm and the first derivative absorbances were measured at the zero-crossing points at 297.3 and 281.2 nm for ETC and TDF, respectively. In ratio of the 1st derivative spectrophotometry measurements were recorded at 239.0 and 270.2 nm for ETC and TDF, respectively. Then analytical signals were measured at the wavelengths corresponding to either maximum or minimum for both drugs. For these spectrophotometric methods Beer's law is obeyed in the concentration range of 2–15 $\mu\text{g mL}^{-1}$ for both drugs. As chemometric method, the PLS technique was used. In chromatographic method, the separation was achieved on a C18 column with DAD (262 nm) and isocratic elution of methanol, acetonitrile and 0.1 % orthophosphoric acid in the volume ratio of 40:40:20, respectively, containing the mobile phase. The mean recovery and the relative standard deviation of the methods were found as 97.51–100.17 % and 0.55–1.26 % respectively. All these methods were statistically compared, and they were successfully applied to a pharmaceutical preparation.

Keywords: tenofovir disoproxil fumarate; emtricitabine; first derivative; ratio; PLS; HPLC.

INTRODUCTION

ETC (Fig. 1) is a nucleoside reverse transcriptase inhibitor also, chemically named 4-amino-5-fluoro-1-[(2*R*,5*S*)-2-(hydroxymethyl)-1,3-oxathiolan-5yl]-1,2-dihydropyrimidin-2-one. Both it and TDF are active drugs against hepatitis B

* Corresponding author. E-mail: aysun.dincel@lokmanhekim.edu.tr
<https://doi.org/10.2298/JSC230909031D>

virus and used for the treatment of human immunodeficiency virus (HIV) infection in adults and children.^{1,2}

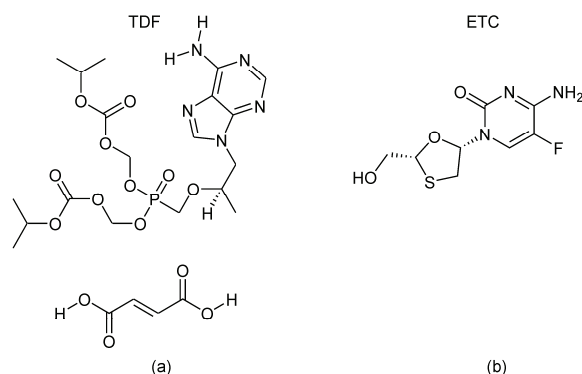


Fig. 1. Chemical structures of: a) tenofovir disoproxil fumarate b) emtricitabine.

TDF (Fig. 1) is an acyclic nucleoside phosphonate di ester analogue of adenosine monophosphate, a nucleoside reverse transcriptase inhibitor. The molecular formula is $C_{23}H_{34}N_5O_{14}P$ and chemically named [[[(2*R*)-1-(6-aminopurin-9-yl)propan-2-yl]oxymethyl-(propan-2-yloxycarbonyl-oxymethoxy)phosphoryl]-oxymethyl propan-2-yl carbonate; (*E*)-but-2-enedioic acid, respectively.^{3,4}

Several analytical methods were studied using the reverse-phase HPLC (RP-HPLC),⁴⁻⁸ ultra-performance liquid chromatography,⁹ UV-Vis spectroscopic methods,¹⁰⁻¹⁵ HPTLC¹⁶ and LC-MS¹⁷⁻²⁰ which have been reported in literature for the assessment of TNF and ETC in their single formulations and in combination together or with other drugs. Limited number of studies²¹ are available in literature about chemometric approach for these two substances and so far there is no study for the determination and the comparison of chemometric approach of spectrophotometric method and chromatographic method.

The derivative spectrophotometry is an analytical technique of a highly useful method for both qualitative and quantitative analysis of the spectra composed of unresolved bands. The zero-crossing approach involves measuring the absolute value of the total derivative spectrum at an abscissa value matching the derivative spectra, of the first derivative in this study (¹D) of each individual component's zero-crossing wavelengths. The wavelength that is chosen because it has the best linear correlation to the analyte concentration in terms of the absolute value of the derivative absorbances at that wavelength.²² In ratio of the 1st derivative spectra method; the ratio spectra of the solutions of ETC or TDF at different concentrations were obtained by dividing each with the stored standard spectrum of the TDF or ETC and then the first derivatives of these spectra are traced (¹DD). The unknown analyte concentrations can be calculated by reading the analytical signals at various points within the selected wavelength range.²³

The chemometric approach is the easiest technique for the determination of active ingredients in mixtures and of pharmaceutical preparation, because using different solutions that contain various concentrations of active ingredients, without separation methods, each ingredient concentration can be calculated in a few seconds. There are many techniques available for this purpose, the principal component regression (PCR) and the partial least-squares (PLS) are the mainly preferred. These techniques have some advantages over other multicomponent analytes.^{24–27} By creating the matrixes that include such variables, as for instance the absorbance value and concentration, the assessment of the exact concentration of the active ingredients of preparation can be reached.

The aim of this study was to develop the appropriate spectrophotometric (derivative and ratio spectra derivative) and chemometric methods for the determination of ETC and TDF simultaneously in their binary mixture and comparing these techniques with a new RP-HPLC method. In addition, it was also aimed to apply all methods developed in order to enable the determination of TDF and ETC in marketed pharmaceutical formulations, such as a tablet, containing these two drugs.

EXPERIMENTAL

Materials

Reference standards of ETC, 99.8 % purity and TDF, 99.7 % purity were obtained as a gift from İLKO Drug Ind. (İstanbul, Türkiye). H_3PO_4 were purchased from Sigma Aldrich. HPLC-grade acetonitrile and methanol were purchased from Merck. Ortho-phosphoric acid, analytical-grade hydrochloric acid and analytical-grade sodium hydroxide from Merck. Quercetin (internal standard) was purchased from Merck. “Hivent” is a commercial pharmaceutical preparation which includes both TNF and ETC, used for the treatment of HIV, were obtained as a gift from İLKO Drug Ind. (İstanbul, Türkiye and Batch no: 2203910002).

Instrumentation and chromatographic conditions

The spectrophotometric analyses were performed using Jasco V-730 (C246261798) UV–Vis spectrophotometer connected to a computer. The standard quartz cuvette (10 mm) was used for the measurement of the absorbance values. In the PLS method, the multi-variate analysis Add-ing for Excel v. 1.3 software (Brereton, 2002) was used.²⁸ The zero-order absorbance spectra were recorded over the wavelength range of 200–320 nm for the 1st derivative with the zero-crossing and for the ratio spectra of the the 1st derivative spectra methods. The suitable settings were response time, 0.015 s; scan speed, 1000 nm min⁻¹; spectral slit width, 1 nm; data interval, 0.2 nm; $\Delta\lambda = 4$ nm.

The chromatographic system consisted of a Shimadzu liquid chromatograph equipped with a pump (LC-10AT VP), a controller (SCL-10A VP) connected to a computer using a software (Class-VP 5.03), an autosampler (SIL-10AD VP), 30 μ L injection loop and diode array detector (DAD, SPD-10A VP). The system was controlled through a system controller (SCL-10A) using a personal computer using a CLASS-VP 5.0 workstation with a data processing system (Shimadzu, Kyoto, Japan) installed on it. The separation was performed on a XTerra, C18 (100 mm \times 4.6 mm i.d., 3.5 μ m) analytical column (Waters, Milford, MA, USA). The column temperature was set to 25 °C. The mobile phase consisted of 0.1 vol. % ortho-

-phosphoric acid, (pH adjusted to 2.5 with NaOH), acetonitrile and methanol in the volume ratio of 40:40:20 in the isocratic mode and DAD detector was set to the wavelength of 262 nm. 10 μL of the sample solutions were injected into the HPLC system at the flow rate 0.5 mL min^{-1} . Quercetin was chosen as the internal standard as its peak was very well resolved from the two drugs peaks and baseline. All solutions were prepared in type 1 water (Simplicity 185 Water System, Millipore Corp., Bedford, MA, USA). The mobile phase was filtered through a membrane filter with a pore diameter of 0.45 μm and kept in an ultrasonic bath for 15 min to remove the soluble gases. At the end of the analysis column was flushed with approximately 20 times of column volume of HPLC grade water and then methanol. Finally, the column was stored in pure methanol. This procedure was applied for every analysis.

Chemicals and solutions

The stock solutions of ETC and TDF (1 mg mL^{-1}) were prepared in 0.05 M HCl and stored at $-20\text{ }^{\circ}\text{C}$ for one week. Quercetin (IS, 1 mg mL^{-1}) was prepared in methanol. The standard solutions were prepared daily by diluting the stock solutions with water to the desired concentrations. All solutions were prepared in type 1 water (Simplicity 185 Water System, Millipore Corp., Bedford, MA, USA).

Sample preparation

Twenty Hivent tablets (each tablet contains 200 mg ETC and 300 mg TDF) weighed accurately and crushed in a mortar. An amount equivalent to one tablet was transferred into a 100-mL volumetric flask. Then, it was dissolved in 0.05 M 50 mL HCl, and the volume was completed to the mark with distilled water. After 30 min of shaking the solution was filtered through the filter paper and it was used for the spectrophotometric and chemometric analysis after the dilution with the distilled water in order to obtain the final concentrations within the specified range of ETC and TDF (Final solution). In RP-HPLC method, this final solution was sonicated for 45 min. and filtered through a membrane filter with a pore diameter of 0.45 μm .

RESULT AND DISCUSSION

Method development

For the validation, studies were performed within the scope of International Conference on Harmonization (ICH) requirements.^{29,30} In this context, the retention time, the capacity factor, the tailing factor and the theoretical number of plates for each active ingredients were calculated according to the data obtained from the HPLC method. For the validation studies, the specificity, the limit of detection (*LOD*), the limit of quantification (*LOQ*), the linearity, the accuracy and the intra-day and the inter-day precision parameters were investigated for spectrophotometric, chemometric and HPLC methods.

For the accuracy, a stock solutions of active ingredients of 1000 $\mu\text{g mL}^{-1}$ were prepared in 0.05 M HCl. The working standard solutions were prepared in the range of 1–15 $\mu\text{g mL}^{-1}$. The linearity was calculated using the regression equation ($y = mx + n$) data including concentration the ranges, the correlation coefficients, and the standard error of intercept.

Using the standard addition method at various concentration the levels were studied and compared by the difference between the found and the actual value

show the accuracy of the method. The precision studies were carried out by analysing three different concentration levels at six replicates. Fig. 2 shows the zero-order absorption spectra of the solution of ETC and TDF in water. In the first derivative by the zero-crossing method the first derivative spectra were traced with the interval of 4 nm (1D). Fig. 3 shows the 1st derivative spectra obtained at the increasing concentrations for ETC and TDF. The derivative absorbances ($\Delta A/\Delta\lambda$ values) read at 281.2 and 297.3 nm (zero-crossing points for ETC and TDF, respectively) in their 1D spectra were used for the analysis of ETC and TDF in pure form and in pharmaceutical tablets.

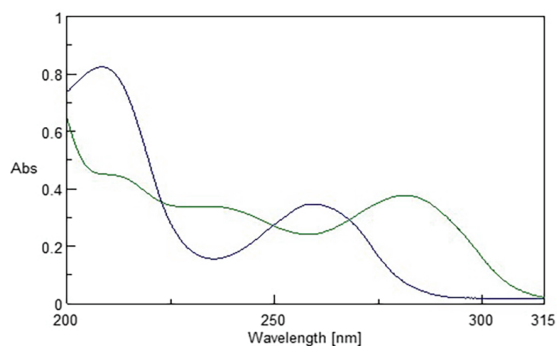


Fig. 2. Zero-order absorption spectra of 15 µg mL⁻¹ solutions of ETC and TDF in water.

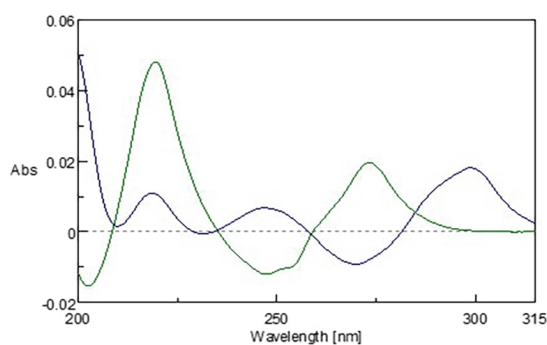


Fig. 3. 1st Derivative absorption spectra of 10 µg mL⁻¹ ETC and 10 µg mL⁻¹ TDF solutions in water.

For the ratio of the 1st derivative spectra studies, the solutions containing both ETC and TDF were prepared in their increasing concentrations. The solutions of the co-existing component were also prepared in a constant concentration (selected as 10 µg mL⁻¹ for both, because the optimum condition were obtained with this concentration) as divisor and their spectra are stored. The ratio spectra of different standards at the increasing concentrations were obtained by dividing each with the stored spectrum of the stored spectra of another drug (divisor).

Then, their first derivative spectra were recorded as $\Delta\lambda = 4$ nm. The analytical signals were read at 239.0 and 270.2 nm, for ETC and TDF respectively, which gave a linear correlation for these substances. The obtained spectra are shown in Fig. 4a and b according to the increasing concentrations of ETC (each solution composed of $10 \mu\text{g mL}^{-1}$ TDF and increasing concentration of 2, 5, 7.5, 10, 15 $\mu\text{g mL}^{-1}$ ETC) and TDF (each solution composed of $10 \mu\text{g mL}^{-1}$ ETC and the increasing concentration of 2, 5, 7.5, 10, 15 $\mu\text{g mL}^{-1}$ TDF). The divisor concentration was kept constant at $10 \mu\text{g mL}^{-1}$ for both TDF and ETC. Table I summarized the wavelengths selected and the calibration results for ETC and TDF. The calibration curves were prepared by plotting the analytical signals read against to the concentrations.

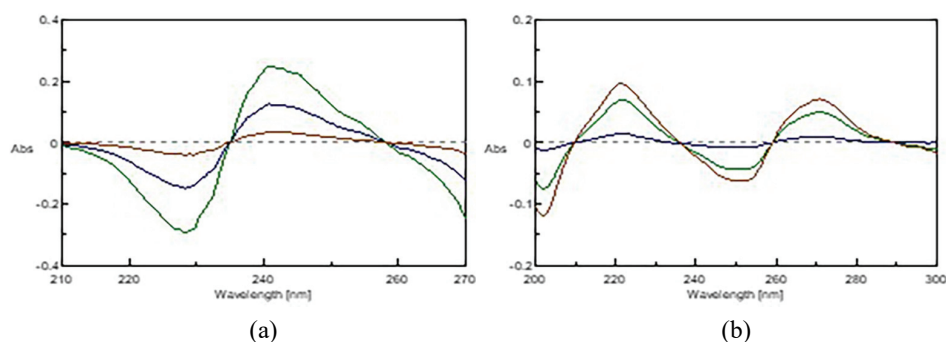


Fig. 4. Ratio 1st derivative spectra samples obtained increasing concentrations (2, 7.5, 15 $\mu\text{g mL}^{-1}$) of both ETC and TDF in water.

TABLE II. Results of regression analysis for TDF and ETC in 1st Derivative and ratio 1st derivative spectra and HPLC method; *SE* – standard error

Parameter	1 st Derivative – zero crossing		Ratio 1 st D. spec.		HPLC	
	ETC	TDF	ETC	TDF	TDF	ETC
λ / nm	297.3	281.2	239.0	270.2	262	262
Linearity range, $\mu\text{g mL}^{-1}$	2–15	2–15	2–15	2–15	1–15	1–15
Slope (<i>m</i>) \pm <i>SE</i> ($y = mx+n$)	$0.001681 \pm 0.001858 \pm$ 0.0001	$0.001858 \pm$ 0.0002	$0.0151 \pm$ 0.003	$-0.0191 \pm$ 0.003	$0.396 \pm$ 0.0004	$0.447 \pm$ 0.0005
Intercept (<i>n</i>) \pm <i>SE</i>	$0.000606 \pm 0.000815 \pm$ 0.0001	$0.000815 \pm$ 0.00015	$-0.0007 \pm$ 0.00016	$-0.0006 \pm$ 0.0001	$-0.064 \pm$ 0.0004	$0.075 \pm$ 0.0001
R^2	0.9988	0.9973	0.9999	0.9998	0.9998	0.9998

To optimize the simultaneous determination of ETC and TDF using the ratio of the 1st derivative spectra method, it is necessary to test the divisor concentration. For this purpose, some different divisor standard concentrations were studied. $10 \mu\text{g mL}^{-1}$ was found optimal as the divisor concentration. The first derivative spectra were recorded as $\Delta\lambda = 4$ nm interval and the analytical signals

were recorded at the selected wavelengths (239.0 and 270.2 nm for ETC and TDF, respectively) were plotted against the concentration. In the regression analysis the correlation coefficients obtained in the linear range values of all the methods studied were very close to 1 (Table I).

For PLS method the absorbance data matrix for the training set in different compositions (in the working range of 2.0–15.0 $\mu\text{g mL}^{-1}$ for ETC and TDF) were obtained by the measurements of the absorbance values between 240 and 320 nm in the 4 nm wavelengths intervals in the zero-order absorption spectra.

The PLS technique was chosen as chemometric technique. In this technique, the calibration or regression was obtained using the absorbance matrix and the concentration matrix for prediction of the unknown concentrations of ETC and TDF in their binary mixtures and the pharmaceutical formulations. The standard error of prediction (*SEP*) in the prediction step can be used to describe the prediction ability of this technique:

$$SEP = \sqrt{\frac{\sum_{i=1}^n (C_i^{\text{added}} - C_i^{\text{found}})^2}{n}} \quad (1)$$

where C_i^{added} is the added concentration of a drug and n is the total number of samples. In this method, the absorbance values (A) and the concentration values (C) are used to create the data matrix using the absorbances read in the UV–Vis spectra. The multivariate calibration technique was applied for the training set prepared using 20 mixtures in the concentration range of 2–15 $\mu\text{g mL}^{-1}$ for ETC and TDF (Table II).

In RP-HPLC method, the retention times for ETC, TDF and IS (quercetin) were found as 5.623, 6.865 and 10.560 min, respectively, in the chromatogram. In this method, the calibration curve was obtained by the peak area under the analyte peak was divided to the peak area of IS peak area and the obtained values were plotted against the concentration values. For the evaluation of system suitability parameters retention time, the capacity factor, the tailing factor and the theoretical number of plates for the each active ingredient for the developed new RP-HPLC method are calculated and given in Table III. No interfering peaks from the tablet excipients were observed (Fig. 5).

The accuracy and precision were studied using three different solutions for ETC and TDF for four methods developed. The Inter-day and the intra-day precision and accuracy values are shown in Table IV. PLS algorithms were performed with four components in the range of 2–15 $\mu\text{g mL}^{-1}$. After obtaining, the data prediction was employed using the training set, and the standard errors of the prediction values were calculated by the PLS software program. The calculated values are 0.325 and 0.318 from experimental results. The limit of detection (*LOD*) and the limit of quantification (*LOQ*) are calculated by the ratio of the

standard deviation (SD) of the response to the slope (m) of the calibration curves ($LOQ = 10(SD/m)$ and $LOD = 3.3(SD/m)$), where m is the slope of the calibration curve. LOD and LOQ values in the 1st derivative with zero-crossing, ratio spectra of the 1st derivative spectra methods and the PLS technique are 0.05 and 0.15 $\mu\text{g mL}^{-1}$ for ETC and TDF, respectively. In HPLC, LOD and LOQ values are 0.1 and 0.4 $\mu\text{g mL}^{-1}$ for ETC and TDF, respectively.

TABLE II. Training set used in PLS technique for ETC and TDF ($C / \mu\text{g mL}^{-1}$)

Mixture No.	ETC	TDF
1	5	2
2	8	2
3	10	2
4	13	2
5	2	2
6	15	2
7	2	5
8	5	5
9	8	5
10	10	5
11	13	5
12	15	5
13	2	8
14	5	8
15	8	8
16	13	8
17	10	10
18	15	10
19	2	15
20	5	15

TABLE III. System suitability parameters

Active ingredients	Retention time ^a min	Capacity factor	Tailing factor	Theoretical number of plates
TDF	6.865±0.002	5.84	1.194±0.002	9841.19
ETZ	5.623±0.001	4.61	1.372±0.001	7480.12
IS	10.56± 0.002	4.23	1.241±0.001	6492.41

^aResults are given by mean ± standard deviation, $n = 6$

Analysis of pharmaceutical preparation

When the results obtained in the pharmaceutical formulation using the 1st derivative spectra, ratio of the 1st derivative spectra, HPLC and PLS technique were summarized in Table V, it was observed that the values obtained were very close to each other when compared for the pharmaceutical formulation selected. There is no significant difference observed among the value of results using the ANOVA at the $p < 0.05$ level for the commercial formulations. It can be said that

all developed methods were found selective and specific for the simultaneous determination of ETC and TDF in commercial preparations, such as tablets. No interfering peaks from the tablet excipients were observed in chromatograms in RP-HPLC method developed (Fig. 5). When compared the spectra of ETC and TDF in standard and tablet formulation solutions showed that excipients placed in the commercial preparations did not interfere the wavelength of maximum absorbance in the zero-order spectra and the quantitation of active ingredients of in these methods.

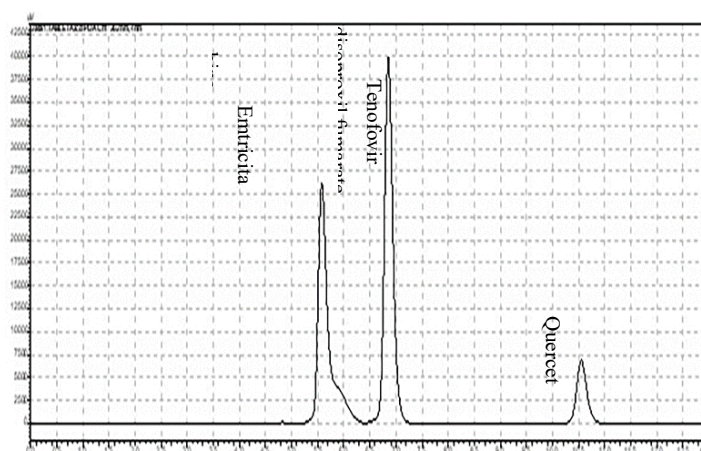


Fig. 5. Representative chromatogram of tablet form containing ETC ($10 \mu\text{g mL}^{-1}$) and TDF ($15 \mu\text{g mL}^{-1}$); IS: $1 \mu\text{g mL}^{-1}$.

TABLE IV. Inter-day and intra-day precision and accuracy results

Added $\mu\text{g mL}^{-1}$	Inter-day			Intra-day		
	Found ^a $\mu\text{g m L}^{-1}$	Precision ^b <i>RSD</i> / %	Accuracy ^c Bias, %	Found ^a $\mu\text{g m L}^{-1}$	Precision ^b <i>RSD</i> / %	Accuracy ^c Bias, %
1 st derivative-zero crossing (TDF)						
2.0	1.96±0.003	0.347	-1.90	1.97±0.05	0.587	-1.73
7.5	7.47±0.015	0.487	-0.67	7.46±0.02	0.67	-0.54
10.0	10.04±1.01	2.45	0.41	10.05±0.96	2.34	0.54
1 st derivative-zero crossing (ETC)						
2.0	1.99±0.01	0.87	-0.71	1.99±0.16	1.92	-0.12
7.5	7.48±0.14	0.47	-0.18	7.51±0.29	0.96	1.33
10.0	10.10±0.62	1.49	1.02	10.12±0.52	1.27	1.15
Ratio 1 st derivative (TDF)						
2.0	1.98±0.003	0.39	-0.67	1.99±0.07	0.80	-0.32
7.5	7.51±0.016	0.54	0.18	7.52±0.022	0.73	0.31
10.0	10.11±0.11	2.54	1.12	10.10±0.11	0.31	1.55

TABLE IV. Continued

Added $\mu\text{g mL}^{-1}$	Inter-day			Intra-day		
	Found ^a $\mu\text{g mL}^{-1}$	Precision ^b <i>RSD</i> / %	Accuracy ^c Bias, %	Found ^a $\mu\text{g mL}^{-1}$	Precision ^b <i>RSD</i> / %	Accuracy ^c Bias, %
Ratio 1 st derivative (ETC)						
2.0	1.98±0.12	1.53	-0.65	1.97±0.014	1.72	-1.44
7.5	7.51±0.19	0.65	0.16	7.51±0.022	0.71	0.07
10.0	9.90±0.79	0.16	-0.98	9.87±0.97	2.39	-1.32
RP-HPLC (TDF)						
1.0	1.04±0.022	5.21	0.001	1.04±0.063	5.11	4.39
7.5	7.57±0.056	1.84	0.15	7.49±0.019	0.64	0.89
15.0	14.96±0.072	1.17	0.25	15.07±0.030	1.17	0.47
RP-HPLC (ETC)						
1.0	1.05±0.010	2.46	4.23	1.04±0.011	2.58	0.0005
7.5	7.53±0.043	1.40	1.11	7.42±0.029	0.96	0.44
15.0	14.93±0.085	1.40	0.86	14.87±0.026	0.60	0.48
PLS (TDF)						
2.0	2.03±0.02	2.37	1.22	2.02±0.02	2.38	1.20
7.5	7.57±0.04	1.22	1.01	7.61±0.02	0.65	1.44
10.0	9.96±0.05	0.98	-0.40	9.99±0.03	0.84	-0.067
PLS (ETC)						
2.0	1.99±0.006	0.76	-1.32	1.99±0.007	0.83	-0.37
7.5	7.52±0.017	0.56	0.20	7.52±0.017	0.56	0.20
10.0	9.95±0.062	1.52	-0.536	9.91±0.74	1.83	-0.87

^aMean value±standard error; ^brelative standard deviation; ^c100(amount found – amount added)/amount found

TABLE V. Results obtained for the commercial preparation “Hivent” (contains 200 mg ETC and 300 mg TDF per tablet)

Parameter	1 st Derivative- -zero crossing		Ratio spectra 1 st derivative		RP-HPLC		PLS	
	ETC	TDF	ETC	TDF	ETC	TDF	ETC	TDF
Found, mg/tablet	197.12	298.18	197.46	300.52	199.46	299.52	195.62	299.18
<i>RSD</i> ^a	0.97	0.55	1.26	0.56	0.87	1.25	0.68	0.84
Bias ^b	-1.46	-0.61	-1.29	0.17	-0.27	-0.16	-2.24	-0.27
Recovery, %	98.56	99.39	98.73	100.17	99.73	99.84	97.81	99.73

^aRelative standard deviation ($n = 6$), ^b100(amount found – amount added)/amount found

CONCLUSIONS

Four new analysis methods, the 1st derivative spectra zero-crossing, the ratio spectra of the 1st derivative spectra methods, the chemometric method (PLS technique), and the new HPLC method for the determination of TDF and ETC were proposed for the simultaneous determination in their mixture. These methods were also applied for the determination of TDF and ETC in pharmaceutical tablets formulation, containing their binary mixture. All developed methods were

evaluated according to the ICH guidelines for validation. The comparison of methods was assessed by the parameters such as linearity, recovery, accuracy, precision and bias values. When the results of commercial preparation according to the 1st derivative and ratio of the 1st derivative spectra and the PLS technique are compared to the HPLC method results, it was found that there was no significant difference statistically between the results using these methods in $p < 0.05$ level. The PLS technique is superior to many analysis methods. It does not require an excessive time for the preparation of samples, neither liquid-liquid extraction process, complex gradient elution program, pretreatment process nor any derivatization process. It requires only a computer program for calculations. In the literature, there are various spectrophotometric methods for the analysis of ETC and TDF, but there is no study for the simultaneous analysis of ETC and TDF in their binary mixture using chemometric techniques and spectrophotometric data. For this reason, our developed chemometric method (PLS) gives a new approach. Also, a few spectrophotometric methods were also available for the analysis of ETC and TDF in their binary mixture, such as the derivative methods in the literature, our derivative and the ratio of the 1st derivative spectra method, which are all different and new methods. After all, in this study four new accurate, precise, and selective methods for the analysis of ETC and TDF in their binary mixture were developed and the results obtained by the spectrophotometric and the chemometric technique (PLS) were compared to our developed and validated RP-HPLC method.

For the analysis of a selected pharmaceutical formulation that is currently on the market, all proposed procedures were effectively used. There was no statistically significant difference in the results. These methods were found suitable as simple, accurate, selective, and precise for the routine analysis of the pharmaceutical preparations, such as the tablets, for the simultaneous analysis of ETC and TDF.

Acknowledgements. The authors wish to send their gratitude to the Richard G. Brereton and İLKO Drug, India.

ИЗВОД

СИМУЛТАНО ОДРЕЂИВАЊЕ ЕМТРИЦИТАБИНА И ТЕНОФОВИР ДИЗОПРОКСИЛ-ФУМАРАТА У ФАРМАЦЕУТСКИМ ПРЕПАРАТИМА ПРИМЕНОМ СПЕКТРОФОТОМЕТРИЈСКИХ, ХЕМОМЕТРИЈСКИХ И ХРОМАТОГРАФСКИХ МЕТОДА

AYSUN DİNÇEL, ELIF DAMLA GÖK-ТОПАК и FEYYAZ ONUR

Lokman Hekim University, Faculty of Pharmacy, Department of Analytical Chemistry, 06510, Ankara, Türkiye

У овом раду су за истовремено одређивање емтрицитабина (ЕТС) и тенофовир дизопроксил-фумарата (ТДФ) у таблетама примењене једноставне, тачне и осетљиве спектрофотометријске, хеометријске и хроматографске методе. Применом деривативне спектрофотометрије, деривативни спектри првог реда раствора ЕТС и

TDF у води су измерени као $\Delta\lambda = 4$ nm, а апсорбанце су мерене на нулној тачки пресека, на 297,3 и 281,2 nm за ETC и TDF, редом. Деривативном спектрофотометријом заснованој на односу спектра урађена су мерења на 239,0 nm за ETC и на 270,2 nm за TDF. Затим су мерени аналитички сигнали на таласним дужинама које одговарају или максимуму или минимуму за оба лека. Беров закон је, за оба лека, примењен у опсегу концентрација 2–15 $\mu\text{g mL}^{-1}$. Као хеометријска метода коришћена је PLS техника. Применом хроматографије, одвајање је постигнуто на C18 колони са DAD детектором (262 nm) и изократским елуирањем мобилном фазом метанол:ацетонитрил:0,1 % ортофосфорна киселина у запреминском односу 40:40:20. Добијени резултат је у опсегу 97,51–100,17 %, а релативна стандардна девијација 0,55–1,26 %. Методе су успешно примењене у анализи фармацевтских узорака, а добијени подаци су анализирани и поређени применом статистичких тестова.

(Примљено 9. септембра 2023, ревидирано 14. јануара, прихваћено 12. марта 2024)

REFERENCES

1. L. M. Bang, L. J. Scott, *Drugs* **63** (2003) 2413 (<http://dx.doi.org/10.2165/00003495-200363220-00003>)
2. C. Orkin, J. M. Llibre, S. Gallien, A. Antinori, G. Behrens, A. Carr, *HIV Medicine* **19** (2018) 18 (<http://dx.doi.org/10.1111/hiv.12534>)
3. C. Wassner, N. Bradley, Y. Lee, *J. Int. Assoc. Providers AIDS Care* **19** (2020) 1 (<http://dx.doi.org/10.1177/2325958220919231>)
4. K. A. Lyseng-Williamson, N. A. Reynolds, G. L. Plosker, *Drugs* **65** (2005) 413 (<http://dx.doi.org/10.2165/00003495-200565030-00006>)
5. C. Runja, P. R. Kumar, S. R. Avanapu, *J. Chromatogr. Sci.* **54** (2016) 759 (<http://dx.doi.org/10.1093/chromsci/bmw004>)
6. B. Lavanya, P. Hariprasad, A. Venkatapaveen, D.P. Lakshmi, M. Ramireddy, *Pharm. Lett.* **4** (2012) 99 (<https://www.scholarsresearchlibrary.com/abstract/simultaneous-estimation-of-emtricitabine-and-tenofovir-disproxil-fumerate-by-rnhplc-method-5960.html>)
7. R. R. Jampala, V. K. Kumar, A. R. Nemala, *Pharm. Methods* **5** (2014) 7 (<http://dx.doi.org/10.5530/phm.2014.1.2>)
8. K. Anandakumara, G. Abirama, S. Murugana, B. Ashokb, *J. Anal. Chem.* **68** (2013) 815 (<http://dx.doi.org/10.1134/S1061934813090025>)
9. M. Yadav, T. Mishra, P. Singhal, S. Goswami, P. S. Shrivastav, *J. Chromatogr. Sci.* **47**(2009) 140 (<http://dx.doi.org/10.1093/chromsci/47.2.140>)
10. P. Tiwari, R. Yadav, K. Avinash, V. Vaidya, P.A. Sathe, D. Gangrade *Anal. Chem. Ind. J.* **9** (2010) 247 (<https://www.tsijournals.com/articles/development-and-validation-of-uplc-method-for-emtricitabine-tenofovir-and-efavirenz-in-pharmaceutical-preparation.pdf>)
11. M. H. AbdelHay, A. A. Gazy, R. A. Shaalan, H. K. Ashour, *J. Spectrosc.* **2013** (2013) 937409 (<https://doi.org/10.1155/2013/937409>)
12. J. Saminathan, T. Vetrichelvan, *Bangladesh Pharm. J.* **19** (2016) 114 (<https://doi.org/10.3329/bpj.v19i1.29247>)
13. B. Lavanya, P. Hariprasad, A. Venkatapaveen, D. Prasannalakshmi, *Int. J. Res. Pharm. Life Sci.* **3** (2012) 104 (https://irjponline.com/admin/php/uploads/1542_pdf.pdf)

14. S. Venkatesan, N. Kannappan, *Int. Scholarly Res. Notices* **2014** (2014) 541727 (<https://doi.org/10.1155/2014/541727>)
15. H. K. Ashour, T. S. Belal, *Arab. J. Chem.* **10** (2017) S1741 (<https://doi.org/10.4103/0250-474X.51951>)
16. M. Joshi, A.P. Nikalje, M. Shahed, M. Dehghan, *Ind. J. Pharm. Sci.* **71** (2009) 95 (<https://doi.org/10.4103/0250-474X.51951>)
17. M.K. Matta, N.R. Pilli, S. Rao J.V.L.NA, *Acta Chromatogr.* **1** (2015) 27 (<https://doi.org/10.1556/achrom.27.2015.1.3>)
18. M. Takahashi, Y. Kudaka, N. Okumura, A. Hirano, K. Banno, T. Kaneda, *Biol. Pharm. Bull.* **30** (2007) 1784 https://www.jstage.jst.go.jp/article/bpb/30/9/30_9_1784/_pdf
19. C. Bennetto-Hood, M.C. Long, E.P. Acosta, *Rapid Commun. Mass Spectrom.* **21** (2007) 2087 (<https://doi.org/10.1002/rcm.3056>)
20. S. Thomas, P. Shanmugasundram, *Ind. Drugs* **55** (2018) 44 (<https://doi.org/10.53879/id.55.01.10819>)
21. V. D. Singh, V. K. Singh, S. J. Daharwal, *J. AOAC Int.* (2023) qsad067 (<https://doi.org/10.1093/jaoacint/qsad067>)
22. B. Morelli, *J. Pharm. Biomed. Anal.* **13** (1995) 219 ([https://doi.org/10.1016/0731-7085\(95\)01250-O](https://doi.org/10.1016/0731-7085(95)01250-O))
23. V.P. Choudhari, S. Ingale, S.R. Gite, D.D. Tajane, V.G. Modak, A. Ambekar, *Pharm. Methods* **2** (2011) 47 (<https://doi.org/10.4103/2229-4708.81096>)
24. M. G. Caglayan, I. M. Palabiyik, M. Bor, F. Onur, *Chem. Papers* **65** (2011) 754 (<https://doi.org/10.2478/s11696-011-0078-2>)
25. E. Dinc, I. M. Palabiyik, O. Üstundag, F. Yurtsever, F. Onur, *J. Pharm. Biomed. Anal.* **28** (2002) 591 ([https://doi.org/10.1016/S0731-7085\(01\)00694-X](https://doi.org/10.1016/S0731-7085(01)00694-X))
26. I. M. Palabiyik, F. Onur, C. Yardimci, N. Özaltın, *Quim. Nova* **31** (2008) 1121 (<https://www.scielo.br/j/qn/a/CkbnNDw4jqQx8TNzNppFJVy/>)
27. S. Wold, M. Sjöström, L. Eriksson, *Chemomet. Intell. Labor. Systems* **58** (2001) 109 ([https://doi.org/10.1016/S0169-7439\(01\)00155-1](https://doi.org/10.1016/S0169-7439(01)00155-1))
28. R. G. Brereton, *Chemometrics, Data Analysis for the Laboratory and Chemical Plant*, John Wiley & Sons, New York, 2002 (computer program)
29. ICH, *Harmonized tripartite guideline validation of analytical procedures: text and methodology Q2(R1)* (assessed August 31, 2023) (<https://database.ich.org/sites/default/files/Q2%28R1%29%20Guideline.pdf>)
30. ICH, *Harmonized Tripartite Guideline, on validation of analytical procedures Q2(R2)*, ICH Steering Committee, 2022 (assessed August 31, 2023) (https://database.ich.org/sites/default/files/ICH_Q2-R2_Document_Step2_Guideline_2022_0324.pdf)



J. Serb. Chem. Soc. 89 (4) 565–580 (2024)
JSCS–5740

Defluoridation using pinecone-based activated carbon: Adsorption isotherm, kinetics, regeneration and co-ions effect investigation

PARIMAL CHANDRA BHOMICK^{1,2*}, AOLA SUPONG^{2,3}, AKITO I. SEMA⁴
and DIPAK SINHA²

¹Department of Chemistry, St Joseph University, Chumoukedima, Nagaland, 79115, India,

²Department of Chemistry, Nagaland University, Lumami, Nagaland, 798627, India,

³Department of Chemistry Sao Chang College, Tuensang, Nagaland, 798612, India and

⁴Department of Chemistry, National Institute of Technology, Nagaland, 797103, India

(Received 28 April, revised 18 June 2023, accepted 19 February 2024)

Abstract: In this work, cheap and locally available pinecones of *Pinus kiseya* were used as a precursor to prepare activated carbon using single-step KOH activation for the removal of fluoride from water. The prepared activated carbon's BET surface area, and total pore volume, were determined as 972.13 m² g⁻¹ and 0.469 cm³ g⁻¹, respectively. Batch adsorption studies were evaluated at different contact times, solution pH, adsorbent dose and concentration to obtain the optimum conditions for maximum adsorption. The adsorption data were fitted with the isotherm models (Langmuir, Freundlich and Temkin isotherm model) and the adsorption kinetic models. The experimental data were found to best fit using the Langmuir isotherm which confirmed the formation of a monolayer coverage with a maximum adsorption capacity of 2.845 m² g⁻¹. The adsorption kinetics was well described by the pseudo-second-order model. A study on the effects of co-existing ions showed that fluoride adsorption capacity was observed to decrease in the order: CO₃²⁻ > SO₄²⁻ > NO₃⁻ > Cl⁻. The regeneration studies were investigated to determine the reusability of the spent adsorbent. In summary, these findings demonstrated substantial evidence that the activated carbon can be prepared from *P. kiseya* cones as an eco-friendly adsorbent for the removal of ions such as fluoride from water.

Keywords: pinecone; activated carbon; fluoride; biomass; regeneration; water treatment.

INTRODUCTION

There is no doubt that fluorine is an essential element for the development of bones and teeth yet it is regarded as an element of “boon and bane”. It is known

* Corresponding author. E-mail: paribhomick15589@gmail.com
<https://doi.org/10.2298/JSC230428015B>

to have healing characteristics, but exceeding its permissible limit of 1.5 mg L^{-1} (WHO guidelines) could ultimately result in serious health problems in the long run. The World Health Organization also recognizes the fluorides as the drinking water contaminants, alongside arsenic and nitrate, that contribute to significant health issues on a large scale.¹ Some of the problems associated with fluorides are dental and skeletal fluorosis, brittle bones, Alzheimer's syndrome and thyroid disorder, neurological damage, low haemoglobin levels, gastrointestinal problems and infertility.^{2,3} The global prevalence of fluorosis is estimated to affect approximately 70 million individuals.⁴ Fluorides enters water from various sources, including naturally the occurring geological sources such as fluorine-containing rocks and minerals (*e.g.*, granite, basalt, syenite, fluorite, biotites and topaz) as well as the industrial activities such as metallurgical, electrodeposition, phosphate production, electronics, brick and iron-works, and ceramics.^{5,6} The elevated concentrations of fluorides are prevalent in many water sources, particularly in regions such as China, Sri Lanka, Rift Valley countries in Africa and India. In India, chronic fluorides levels of $12\text{--}18 \text{ mg L}^{-1}$ have been reported with 17 states showing the excessive fluorides levels.^{2,7}

Since the fluorides levels in drinking water is an issue of global health concern, it needs to be reduced below acceptable level to provide safe drinking water. To date, numerous technologies and methods have been applied for the removal of fluoride such as nanofiltration (NF), reverse osmosis (RO), ion-exchange method, electrodialysis and adsorption.^{6,8–11} But, most of these techniques fail when it comes to the rural population because of their cost except the adsorption method. Adsorption is an ancient and widely used method because of its high efficacy, operational and budget-friendliness for the removal of fluoride and other pollutants as well from water.^{2,12}

In this regard, adsorbent such as activated carbon from biomass origin has been widely used to investigate studies related to fluoride removal. Biomass-based carbon over the years has gained a significant place as an alternate adsorbent due to its high surface area and reactivity, low-cost, eco-friendly characteristics, and renewability.^{3,13,14} For instance, Gebrewold *et al.* 2019 synthesised activated carbon from biomass of rice husk and corn cob for the removal of fluorides from groundwater with an adsorption capacity of 7.9 and 5.8 mg g^{-1} ;¹⁵ Fito *et al.* 2019 also used *Catha edulis* as a potential precursor for the synthesis of activated carbon for the removal of fluorides from water;¹⁶ Jayashree *et al.* 2021 studied the removal of fluorides from water using the activated carbon prepared from pods of *Bauhinia variegata* by both physical and chemical methods with BET surface area of 71.59 and $124.82 \text{ m}^2 \text{ g}^{-1}$. They found that the chemically prepared activated carbon was having a higher fluorides adsorption capacity (15.74 mg g^{-1}) over physically prepared carbon by a difference of 5 mg g^{-1} .¹⁷

Therefore, the biomass materials such as pinecones that are often discarded as waste can be potentially utilised to obtain a value-added product like the activated carbon to remove fluoride from water. Our group have been working on the preparation of the activated carbon from locally available biomass – *Manihot esculenta*, *Schima wallichii* and *Mucina sp.*—for the removal of fluorides from water.^{4,18,19}

Thus, in this piece of work, we explored the pinecone of *Pinus kesiya* as the precursor for the synthesis of activated carbon because of its easy availability, abundance and low cost for the removal of fluorides from water. The characterization of the adsorbent was analysed with various techniques to study the physicochemical properties, surface morphology and functionalities to access the capability of the adsorbent for the fluorides removal. Further, motivated by the presence and effects of existing co-ions on the adsorption efficiency, the prepared adsorbent was applied for defluoridation studies in the presence of various co-ions, using a batch method to understand the efficacy of the adsorbent in a real-time situation. The regeneration of the adsorbent was also explored in order to understand its recyclability.

EXPERIMENTAL

Materials

Pinecones were collected locally, washed, and grounded using a mixer grinder to fine particles. All other chemicals used in this work were of analytical grade.

Synthesis of pinecone activated carbon

For the synthesis of activated carbon, a single-step method published in our earlier work was followed.⁴ In a typical method, the dried particles of pinecone biomass were grounded into finer particles in a ball mill. The dried biomass powder was then activated by carbonizing it in a muffle furnace at 600 °C for 2 h at a heating rate of 20 °C min⁻¹ by mixing it with KOH at a 1:2 ratio. The black carbonized sample was then cooled and washed with hot water and finally with cold distilled pH of the wash solution becomes neutral. The sample was then dried in an oven overnight at 110 °C and stored in an airtight sealed container, labelled as Pc-AC (pinecone activated carbon) for further characterization and use.

The yield percentage of Pc-AC was calculated as:

$$\text{Yield} = 100 \frac{\text{Mass of final carbon after activation process}}{\text{Initial mass of the dry impregnated sample}} \quad (1)$$

Adsorbent's characterization

The prepared carbon was characterized through different analytical techniques. The carbon, hydrogen and nitrogen percentage in the prepared carbon were determined using an elemental analyzer (model: PE 2400 Series II, Perkin Elmer). The batch equilibrium method was employed to determine the zero point charge.²⁰ To measure the pH_{pzc}, a 50 mL solution of 0.1 M KNO₃ was prepared in a conical flask, to which the prepared Pc-AC was added. The adsorbent suspended was kept in this 0.01 M KNO₃ solution until the pH reached a stable state. The initial pH values were adjusted in the range of 2 to 12 by adding HCl or NaOH. The mixture was continuously stirred for 2 days on a magnetic stirrer. Afterward, the final pH

values were measured, and the difference between the initial and final pH values ($\Delta\text{pH} = \text{pH}_{\text{initial}} - \text{pH}_{\text{final}}$) was plotted against the initial pH values (shown in Fig. S-1 of the Supplementary material to this paper). Surface functionalities of the prepared carbon was determined using the FT-IR spectrometer (model: Spectrum Two, Perkin Elmer) in the range 4000–400 cm^{-1} . Surface morphology was determined using the scanning electron microscopy (JSM-6360, JEOL). The BET surface area and pore volume were measured by using a BET surface area analyzer (Smart instrument, SS93/02).

Preparation of standard fluoride stock solution

The standard fluoride solution was prepared by dissolving 2.178 g of NaF (Merck) in 1000 ml of double-distilled water in a 1000 ml volumetric flask. The solution was then further diluted to 100 mg L^{-1} of the fluoride solution. All test solutions of the desired concentrations were prepared by the successive dilutions of 100 mg L^{-1} fluoride solution to get the required initial experimental concentration (2, 5 and 8 mg L^{-1}). The pH of all the solutions was adjusted by adding 0.1 M HCl or 0.1 M NaOH before the addition of the adsorbent and was measured by pH meter (Eutech).

Fluoride adsorption by batch mode experiments

For any adsorption study, a batch adsorption experiment is vital as it provides information about the different parameters that control the adsorption process. This method helps to find out the optimum condition for the reaction to be carried out effectively. Thus, the adsorption parameters such as contact time, adsorbent dosage, pH, and the fluorides concentration are investigated by this method. An optimized condition is established from the different experimental data and enables us to fix the experimentally obtained optimal conditions to perform further experiments in the future.

In the current study, the batch mode experiments were accomplished by taking 50 mL of fluoride known solution in an Erlenmeyer flask, which was stirred with a known weight of pinecone activated carbon at 150 rpm in a rotary shaker. The solution was filtered after the adsorption equilibrium was achieved, and the unadsorbed fluorides concentration was measured with the help of a fluoride meter (model: Hanna Hi 98402 ISE Fluoride Meter). The effect of the adsorption parameters like pH (pH 2 to 12), activated carbon quantity (0.05 to 0.30 g), contact time (0 to 180 min), and the fluoride concentration of 2, 5, and 8 mg L^{-1} were conducted. The removal percentage efficiency and the defluoridation capacity (mg g^{-1}) for Pc-AC was determined as:

$$\text{Removal efficiency} = 100(C_0 - C_e) / C_0 \quad (2)$$

$$\text{Defluoridation capacity } (q_e) = V(C_0 - C_e) / M \quad (3)$$

where c_0 = initial fluoride concentration in mg L^{-1} ; c_e = equilibrium fluoride concentration in mg L^{-1} ; q_e = amount of adsorbate adsorbed at equilibrium in mg g^{-1} ; M = mass of pinecone activated carbon in g; V = volume of fluoride solution in L.

RESULTS AND DISCUSSION

Pinecone-activated carbon characterization

The results indicated that the yield and ash content values of Pc-AC were 16.88 and 3.07 %, respectively; the carbon, hydrogen, nitrogen and oxygen content as determined by ultimate analysis was 87.69, 2.01, 0.72 and 6.51 %, respectively (Table I). The BET surface area and the total pore volume of Pc-AC

were $972.13 \text{ m}^2 \text{ g}^{-1}$ and $0.469 \text{ cm}^3 \text{ g}^{-1}$ as compared to the sample activated without any KOH which had a surface area of $108.54 \text{ m}^2 \text{ g}^{-1}$ and the pore volume of $0.057 \text{ cm}^3 \text{ g}^{-1}$. The higher BET surface area and the pore volume upon KOH activation could be attributed to the elimination and release of volatile matter from the carbon skeleton to form voids, leading to an increase in the availability of active sites for adsorption.

TABLE I. Properties of Pc-AC with and without KOH impregnation

Condition	Yield, %	BET Surface area, $\text{m}^2 \text{ g}^{-1}$	Pore volume, $\text{cm}^3 \text{ g}^{-1}$
Without KOH	35.13	108.54	0.057
With KOH	16.88	972.13	0.469

The pH of the zero point charge (pH_{zpc}) of Pc-AC was found to be 6.93 reflecting the fact that the surface of the adsorbent was positive below this pH and negatively charged when $\text{pH} > \text{pH}_{\text{zpc}}$.²¹ Fig. 1a shows the SEM image of the pinecone-activated carbon. The SEM analysis of the adsorbent indicates that the surface of the adsorbent was irregular and rough, with different pore sizes and shapes. The presence of such pore sizes is expected to influence the adsorption process and thus makes it appropriate for the adsorption of fluoride.

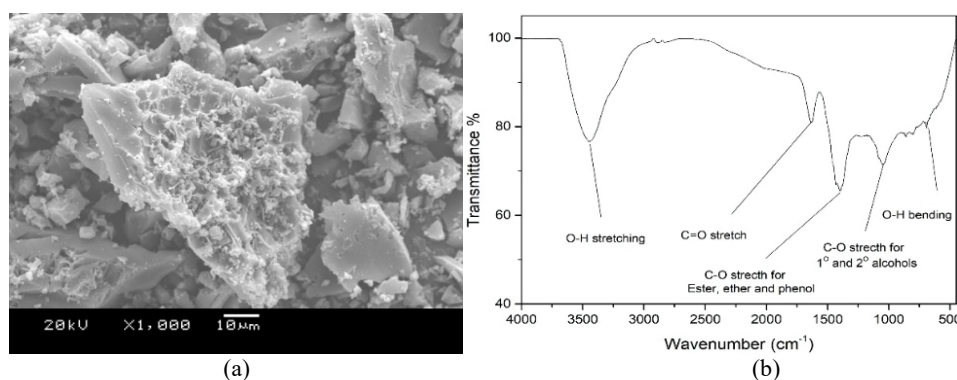


Fig. 1. a) SEM micrograph of Pc-AC; b) FTIR spectrum of Pc-AC.

FT-IR study was used to determine the major surface functionality on the Pc-AC surface. The FTIR is shown in Fig. 1b. A very prominent peak around 3450 cm^{-1} was observed for Pc-AC which is due to the O–H stretching mode of hydroxyl groups, –NH group. It is also due to the adsorption and presence of moisture on the PC-AC surface. The functional groups include alcohols, phenols, carboxylic acids and amine. The peaks around 1637 cm^{-1} account for the presence of C=O groups such as in carboxylic acids.²² While the band appearing at 1435 cm^{-1} has been assigned to the aromatic structure of Pc-AC, that are coupled to the highly conjugated carbonyl groups or attributed to the stretching vibrations

of C=O moieties of conjugated systems.²³ Bands near 1395 cm^{-1} is assigned to C–O stretching vibration from ester, ether and phenolic functional groups.²⁴ While the bands around 1048 cm^{-1} account for C–O vibrational stretching for primary and secondary alcohols. Finally, bands at $700\text{--}900\text{ cm}^{-1}$ corresponds to =C–H bending of the substituted aromatic rings, while broad peaks at $\sim 640\text{ cm}^{-1}$ account for O–H bending.²⁵ The FT-IR studies show that the various surface functionalities makes them an ideal adsorbent for adsorption study.

Batch adsorption studies

Effect of contact time and initial concentration. The effect of the contact time on the adsorption of fluoride at three different initial concentration were investigated and reflected in Fig. 2a. The adsorption in all cases is found to increase rapidly with time and becomes saturated as time continues, and an equilibrium is achieved. The rapid adsorption in the initial period is caused by the availability of active adsorption sites, but as time proceeds, these sites get accumulated with the adsorbate, which does not allow any further adsorption. The equilibrium time for maximum fluoride adsorption was found to be 120 min for Pc-AC.

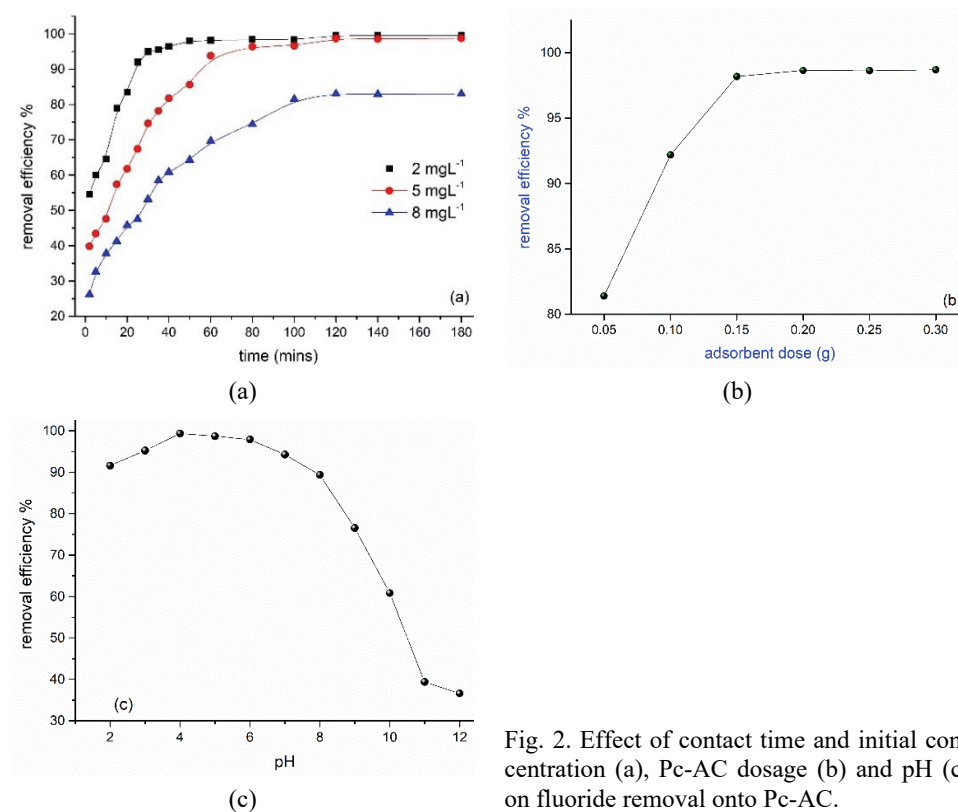


Fig. 2. Effect of contact time and initial concentration (a), Pc-AC dosage (b) and pH (c) on fluoride removal onto Pc-AC.

Moreover, it is well-known that adsorption depends on the relationship between the unoccupied adsorption sites and the concentration of fluoride. Accordingly, Figs. 2a and S-2a of the Supplementary material shows that, with the increasing initial concentration of fluorides, the removal percentage decreases (increase in the adsorption capacity). This was due to the saturation of the available adsorption sites on the adsorbent. It was observed that at 2 mg L⁻¹ fluoride concentration, there seemed to be easy availability of the unoccupied sites, which led to the complete adsorption of fluoride from the solution. However, as fluoride concentrations increased, a decrease in the number of active sites was noticed due to the increased adsorption of fluoride on the surface of the active sites, which led to a reduction in the available active sites. It was found that the removal percentage of fluoride by Pc-AC, at concentrations of 2, 5 and 8 mg L⁻¹ were 99.9, 98.7 and 83 %, respectively. Based on these observations, the fluoride concentration of 5 mg L⁻¹ concentration was taken for all other experiments as the optimal concentration.

Effect of adsorbent dose. To confirm the proper dosage of the adsorbent, the adsorption process was conducted at different PC-AC dosages. Figs. 2b and S-2b show the effect of the adsorbent dosage (0.05–0.30 g) on the removal of fluorides by PC-AC. It was found that with an increase in the adsorbent dosage, the fluorides removal efficiency increased, but it reached the equilibrium at an adsorbent dosage of 0.15 g with no further increase in the removal percentage after that. The high removal percentage at this dosage was due to the availability of the active binding sites on the adsorbent as a result of its surface area.²⁶ The porous nature of the adsorbent also facilitates the fluorides adsorption, which is consistent with the observations obtained from the scanning electron microscopy (SEM) analysis. However, with a further increase in the adsorbent dose, there was no further increase in the removal rate (as there was a decrease in the adsorption capacity). This was due to the accumulation or the partial overlapping, which lead to a decrease in the total adsorption sites for fluorides.²⁷ Thus, for the subsequent studies, an adsorbent dose of 0.15 g was used.

Effect of solution pH. The pH of the solution is one of the basic parameters that affect the adsorption of fluorides. A study on the effect of pH on the adsorption of fluoride was done at different pH from 2 to 12 keeping the other parameters like adsorbent dose and the fluoride concentration constant (Fig. 2c). It can be seen that; the adsorption of fluoride was more significant at lower pH (acidic medium) when compared to the alkaline condition. This could be because at lower pH (pH < p_{Hpzc}) most of the surface becomes positively charged which further facilitates the adsorption of fluoride. The maximum fluoride adsorption was found to take place at pH 4. But below pH 4, the fluorides removal was found to decrease due to the formation of weak hydrofluoric acid.²⁸ On the other hand, when the solution pH was alkaline, there was a reduction in the adsorption

of fluorides because of the competition between the negatively charged surface hydroxyl ions and the fluoride ions on the active sites.²⁹

Thus, for further studies, the optimum fluorides concentration was taken at 5 mg L⁻¹ with the adsorbent dose of 0.15 g at 120 min. As the maximum fluorides removal takes place at pH 4, all further adsorption experiments were done at that pH value.

Isotherm studies

The study of the adsorption isotherms is important as it elucidates the most significant isotherm model that determines the interlaying relationship between the adsorbate and adsorbent, useful for the designing purposes. The experimental equilibrium data were modelled using three classical adsorption models: the Langmuir, Freundlich and Temkin isotherms. These models were employed to describe fluoride adsorption on Pc-AC. The equations and the calculated equilibrium isotherm parameters are given in Table II.

TABLE II. Different parameters of adsorption isotherm models for fluoride removal using Pc-AC; q_e = adsorption caPc-ACity at equilibrium (mg g⁻¹); C_e = residual concentration at the equilibrium state of the system (mg L⁻¹); Q_{\max} = maximum adsorption caPc-ACity (mg g⁻¹) K_L = Langmuir constant; K_F = Freundlich constant (L mg⁻¹); R_L = separation factor (provides insight into the favourability of the adsorption process); $1/n_F$ = intensity of the adsorption, respectively; B_T = Temkin constant related to the heat of sorption (J mol⁻¹); A_T = equilibrium binding constant that corresponds to the maximum binding energy (L g⁻¹)

Isotherm model	Equation	Parameters	Value
Langmuir	$C_e / q_e = 1 / (Q_{\max} K_L) + 1 / (Q_{\max} C_e)$	Q_{\max}	2.845
		K_L	18.375
		R_L	0.011
		R^2	0.999
		χ^2	0.0001
Freundlich	$\log q_e = (1 / n_F) \log C_e + \log K_F$	K_F	2.459
		$1/n_F$	0.221
		R^2	0.906
		χ^2	0.0060
Temkin	$q_e = RT / b_T (\ln A_T + \ln C_e)$	A_T	542.19
		B_T	0.358
		R^2	0.980
		χ^2	0.0174

The fitting of data with Langmuir isotherm for the adsorption of fluoride onto Pc-AC as shown in Fig. S-3a of the Supplementary material, gave the Q_{\max} (maximum adsorption capacity) value of 2.845 mg g⁻¹. The correlation coefficient R^2 for Langmuir isotherm for the fluoride adsorption by Pc-AC was found to be 0.999 (Table II). Further, the separation (R_L), was found to be 0.011, thereby indicating the favourable adsorption of fluoride onto Pc-AC. The Freund-

lich isotherm, the plot of the model is shown in Fig. S-3b and the parameters calculated from the slope and intercept are given in Table II. It can be seen that, $1/n_F$, for the adsorption of fluoride by Pc-AC was found to be 0.22, thereby suggesting the favourability of the fluoride adsorption onto Pc-AC. It also indicates that the adsorption follows a normal Langmuir isotherm.³⁰ The correlation coefficient R^2 value for fluoride adsorption by Pc-AC for Freundlich isotherm was found to be 0.906, which, when compared to Langmuir isotherm is way much lower. While the fitting of the experimental data onto the Temkin isotherm model for fluoride adsorption by Pc-AC is shown in Fig. S-2c. The calculated parameters for the Temkin model are given in Table II. The heat of adsorption (B_T) was found to be 0.358 kJ mol⁻¹. The correlation value for Temkin isotherm for fluoride adsorbed onto PC-AC was 0.980.

For the determination of the appropriateness of the fit, the best adsorption isotherm model for the adsorption of fluoride by Pc-AC, chi-square analysis was performed on all the isotherm models, and the results are shown in Table II. For the adsorption of fluoride by Pc-AC, the chi-square value for the Langmuir isotherm model was found to be the least and therefore, the most suitable to describe the adsorption of fluoride. Since the Langmuir equation assumes that the surface is homogeneous, it indicates a homogeneous distribution of the adsorption sites on the adsorbent and the adsorption of fluoride by Pc-AC took place as a monolayer coverage on the carbon surface containing a finite number of adsorption sites of uniform energy. The isotherm study also suggests that there is no transmigration of adsorbate in the plane of the adsorbed site.

The fitness of the isotherm for fluoride adsorption by Pc-AC follows the order: Langmuir >> Temkin > Freundlich

Adsorption kinetics

The adsorption kinetics for the removal of fluoride by Pc-AC was investigated with pseudo first order, pseudo second order kinetic models and the intraparticle diffusion model using the equation provided in Table III. The graph of $\log (q_e - q_t)$ versus t was plotted for the pseudo-first-order while for the pseudo-second-order kinetics models the graph of t/q_t versus t was plotted and for the intraparticle diffusion model, q_t is plotted against $t^{1/2}$. Fig. S-4 of the Supplementary material shows the plot of the pseudo-first-order kinetics, the pseudo-second-order kinetics and the intraparticle diffusion model for the fluorides adsorption by Pc-AC. The results of the kinetic studies are listed in Table III.

Table III shows that the measured q_e value of the pseudo-first-order kinetic model do not tally with the experimental q_e values for the adsorption of fluorides and even the appropriateness of the fit was not satisfactory. In the case of the pseudo-second-order kinetics model, the measured equilibrium adsorption capacity, $q_{e,meas}$ of Pc-AC was found to be in good agreement with the experimental

data. A good correlation coefficient (R^2) value of 0.999, 0.997 and 0.991 was found for the pseudo-second-order kinetic model at 2, 5 and 8 mL⁻¹ of fluoride concentration which in the case of pseudo-first-order model was 0.927, 0.930 and 0.918, respectively. Thus, the suitability of the pseudo-second-order kinetics model can describe the adsorption of fluoride onto Pc-AC, which suggests that the overall rate of adsorption is predominantly chemisorption.

TABLE III. Kinetic parameters for the adsorption of fluoride onto the pinecone-activated carbon; q_e = the amounts of adsorbate (mgg⁻¹) adsorbed at equilibrium; q_t = amounts of adsorbate (mgg⁻¹) adsorbed at a given time t (min); k_1 = the rate constant of adsorption (min⁻¹); k_2 = pseudo-second-order adsorption rate constant (g/mg.min); k_{ipd} = intraparticle diffusion constant; C =intraparticle diffusion constant

C_0 mg L ⁻¹	$q_{e, exp}$ mg g ⁻¹	Pseudo-first-order kinetics ³¹			Pseudo-second-order kinetics ^{32,33}			Intraparticle diffusion ³⁴		
		$\log(q_e - q_t) =$			$t/q_t = 1/(k_2 q_e) + t/q_e$			$q_t = k_{ipd} t^{0.5} + C$		
		$\log q_e - k_1 / 2.303t$								
		$q_{e, meas}$ mg g ⁻¹	k_1 min ⁻¹	R^2	$q_{e, meas}$ (mg g ⁻¹)	k_2 g/(mg min)	R^2	k_{ipd}	C	R^2
2	0.796	0.044	0.106	0.927	0.813	0.404	0.999	0.028	0.516	0.620
5	1.975	6.921	0.127	0.930	2.114	0.045	0.997	0.112	0.772	0.864
8	2.656	14.089	0.101	0.918	2.920	0.021	0.991	0.169	0.748	0.942

It was established through SEM analysis that the prepared adsorbent is porous; thus, it is essential to consider how fluoride diffuses into the pores of Pc-AC. The experimental data were therefore, examined using the intra-particle diffusion model to gain insights into the diffusion of fluoride adsorption onto Pc-AC. Fig. S-4c of the Supplementary material illustrates three distinct sections in the plot. The first straight portion corresponds to the rapid transport of the fluoride from the bulk liquid to the boundary layer, surrounding the adsorbent due to the readily available adsorbing sites on the adsorbent surface. It represents the fast adsorption of the fluorides on the external surface of pinecone activated carbon *via* macropore diffusion. The second linear portion accounts for the transport of the fluorides from the adsorbent surface into interior sites. The final step accounts for the slow diffusion of fluoride into micropores which are the less accessible sites of adsorption. It can also be seen that the proportion of C increases with the increase in the fluorides ion concentrations indicating an increase in boundary layer effects.

When compared to the pseudo-second-order kinetic model, the R^2 value for the intra-particle diffusion was lower, as evident from Fig. S-4c. Additionally, the intercept of the line does not pass through the origin, indicating that the adsorption mechanism of fluoride onto Pc-AC does not agree with this model. This observation adequately suggests that the chemisorption predominantly controls the

overall adsorption rate, following the pseudo-second-order kinetics. Similar results were also reported in the literature.^{35–39}

Effect of co-ions on fluoride adsorption

The presence of co-ions like nitrate, sulphate, carbonate, chloride and bromide normally occurs in the fluorides-contaminated water. During the adsorption, these ions compete with fluorides for the adsorption sites, which results in a decrease in the adsorption capacity of the adsorbent.^{40–42} Thus, it is important to study the effect of co-ions to understand the efficacy of the prepared adsorbent. Therefore, the adsorption of the fluorides in the presence of the competing anions such as bromides, chlorides, nitrates, carbonates and sulphates was investigated. For this study, 20 mg L⁻¹ concentration of anions was stirred with an initial fluoride concentration of 5 mg L⁻¹; pH 7; contact time for 120 min for PC-AC, at temperature 303 K and an adsorbent dose of 0.15 g.

As an effect of the presence of co-ions, the adsorption capacity was observed to decrease for carbonate, followed by sulphate, nitrate and chloride, as depicted in Fig. 3. We found that the defluoridation efficiency reduces significantly in the presence of sulphate and carbonates, *i.e.*, for the sulphate adsorption of fluorides reduces from ~99 % (without any co-ions) to 84.17 %; for carbonate, the adsorption of fluorides reduces from ~99 to 72.13 %. The reduction in the removal efficiency could be because of a change in the pH of the fluoride solution because of the addition of the competing ions (the pH values of fluoride solution, pH 7, mixed with Cl⁻, NO₃⁻, SO₄²⁻ and CO₃²⁻ increased for both the carbons as shown in Fig. 3). So as the pH increases, the pH of the solution shifts towards the alkaline end, thereby reducing the fluorides adsorption efficiency.

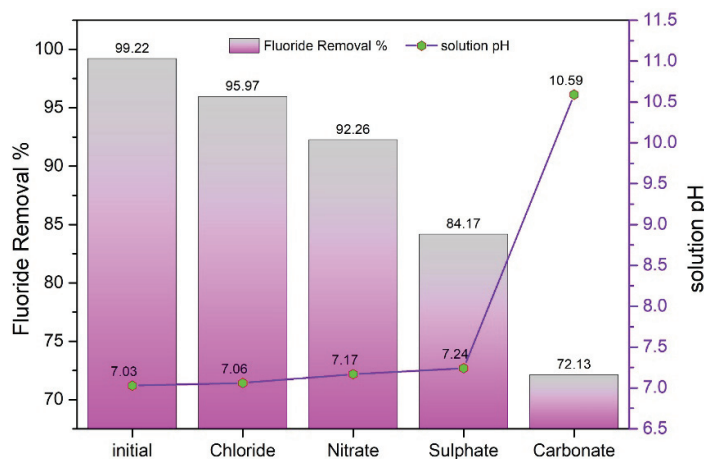


Fig. 3. Effect of co-ions on fluoride removal by PC-AC.

The reduced adsorption of fluorides in the presence of sulphate could be due to the formation of both outer-sphere and inner-sphere surface complexes.⁴³ On the other hand, the reduction due to the presence of carbonates could be because of the reduction of the positive charges on the active sites of the adsorbent by the carbonates and thus reduces the active sites for the adsorption of fluoride thereby lowering the removal efficiency.^{44,45} But, the presence of chloride and nitrate showed a weaker effect on fluoride adsorption as compared to sulphate and carbonate. This might be due to the outer-sphere surface complex formation (for chloride and nitrate).

Regeneration study

In an adsorption process, the regeneration of the adsorbent is one of the crucial aspects as it reduces the cost and determines the cost-effectiveness of wastewater treatment. A regeneration study also allows a researcher to understand the economic viability of the adsorbent. In this study, the regeneration of the adsorbent saturated with fluoride was stirred in a 20 % NaOH solution for 1 h. It was then washed with distilled water until the pH of the desorbed carbon became neutral and oven-dried at 110 °C. For the estimation of the removal efficiency of the regenerated carbon, the adsorption experiments were repeated under the same conditions, *i.e.*, 0.1 g of the regenerated samples with 50 ml of 5 mg L⁻¹ of standard fluoride solution was agitated for 120 min at a pH of 7. It was found that the removal efficiency of the regenerated carbon was 93.23 % in the first cycle, 90.14 in the second cycle, 86.45 in the third, and subsequently decreased to 79.83 % in the fourth cycle, as shown in Fig. 4. However, further studies are required in the future to increase the efficiency of the regenerated adsorbent in the subsequent cycles and also to explore the use of milder chemicals for the regeneration of the adsorbent.

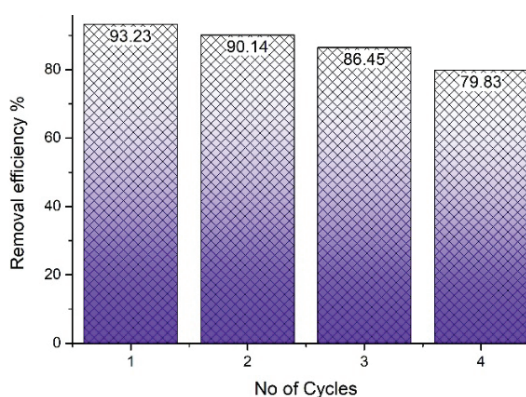


Fig. 4. Regeneration cycle of Pc-AC.

Comparison of Pc-AC with other adsorbents

The fluoride adsorption efficiency for the prepared activated carbon was compared with the other adsorbents reported in the literature and is listed in Table S-I of the Supplementary material.

CONCLUSION

The use of activated carbons derived from the locally abundant pinecone biomass was investigated for the fluorides removal from water in this study. The activated carbon exhibited an irregular surface and varied pores, as determined by the SEM micrographs. The FTIR analysis revealed the presence of different oxygen functionalities, including hydroxyl, ether, ester, carbonyls, *etc.* The batch adsorption experiments demonstrated that the fluorides adsorption was favourable at a pH of 4 and followed a monolayer adsorption type, with a chemisorptive mechanism and a maximum adsorption capacity of 2.845 mg g⁻¹. The presence of co-ions, specifically sulphates and carbonates, influenced the fluorides' adsorption process. The regenerated activated carbon using 20 % NaOH demonstrated promising results and could be used for the fluorides removal for a certain cycle. In summary, the results indicate that the pinecone-derived activated carbon exhibits to be a sustainable and efficacious adsorbent for the defluoridation purposes, particularly in the context of delivering the potable water to individual residences, small communities, and rural regions.

SUPPLEMENTARY MATERIAL

Additional data and information are available electronically at the pages of journal website: <https://www.shd-pub.org.rs/index.php/JSCS/article/view/12451>, or from the corresponding author on request.

Acknowledgements. P. C. B. and A. S. are grateful to the Department of Science and Technology-INSPIRE Fellowship.

ИЗВОД

ДЕФЛУОРИДАЦИЈА КОРИШЋЕЊЕМ АКТИВНОГ УГЉА НА БАЗИ ШИШАРКИ: ИЗОТЕРМА АДСОРПЦИЈЕ, КИНЕТИКА, РЕГЕНЕРАЦИЈА И ИСПИТИВАЊЕ ЕФЕКТА КО-ЈОНА

PARIMAL CHANDRA BHOJICK^{1,2}, AOLA SUPONG^{2,3}, AKITO I. SEMA⁴ и DIPAK SINHA²

¹Department of Chemistry, St Joseph University, Chumoukedima, Nagaland, 79115, India, ²Department of Chemistry, Nagaland University, Lumami, Nagaland, 798627, India, ³Department of Chemistry Sao Chang College, Tuensang, Nagaland, 798612, India и ⁴Department of Chemistry, National Institute of Technology, Nagaland, 797103, India

У овом раду, јефтине и локално доступне шишарке *Pinus kiseya* коришћене су као прекурсор за припрему активног угља коришћењем једноступене КОН активације за уклањање флуорида из воде. ВЕТ површина припремљеног активног угља и укупна запремина пора су одређени као 972,13 m² g⁻¹, односно 0,469 cm³ g⁻¹. Адсорпција је процењена за различита времена контакта, рН вредности раствора, дозу адсорбента и концентрацију, да би се утврдили оптимални услови за максималну адсорпцију. Подаци

о адсорпцији фитовани су са различитим моделима изотерми (Langmuir, Freundlich и Temkin модел) и кинетичким моделима адсорпције. Утврђено је да се експериментални подаци најбоље уклапају са Langmuir изотермом која је потврдила формирање једно-слојног покривања са максималним капацитетом адсорпције од $2,845 \text{ m}^2 \text{ g}^{-1}$. Кинетика адсорпције је добро описана моделом псеудо-другог реда. Студија о ефектима коегзистирајућих јона је показала да је примећено да се капацитет адсорпције флуорида смањује по редоследу: $\text{CO}_3^{2-} > \text{SO}_4^{2-} > \text{NO}_3^- > \text{Cl}^-$. Испитиване су студије регенерације да би се утврдила могућност поновне употребе истрошеног адсорбента. Резултати су показали да се активни угаљ може припремити из шишарки *Pinus kiseya*, као еколошки прихватљив адсорбент за уклањање јона из воде, као што је нпр. флуорид.

(Примљено 28. априла, ревидирано 18. јуна 2023, прихваћено 19. фебруара 2024)

REFERENCES

1. WHO, *Guidelines for drinking-water quality*, Fourth ed., World Health Organization, Geneva, 2017
2. S. Jagtap, M. K. Yenkie, N. Labhsetwar, S. Rayalu, *Chem. Rev.* **112** (2012) 2454 (<https://doi.org/10.1021/cr2002855>)
3. R. L. Moirana, J. Mkunda, R. Machunda, M. Paradelo, K. Mtei, *Environ. Adv.* **11** (2023) 100329 (<https://doi.org/10.1016/J.ENVADV.2022.100329>)
4. P. C. Bhomick, A. Supong, R. Karmaker, M. Baruah, C. Pongener, D. Sinha, *Korean J. Chem. Eng.* **36** (2019) 551 (<https://doi.org/10.1007/s11814-019-0234-x>)
5. A. Bhatnagar, E. Kumar, M. Sillanpää, *Chem. Eng. J.* **171** (2011) 811 (<https://doi.org/10.1016/j.cej.2011.05.028>)
6. P. I. Ndiaye, P. Moulin, L. Dominguez, J. C. Millet, F. Charbit, *Desalination* **173** (2005) 25 (<https://doi.org/10.1016/j.desal.2004.07.042>)
7. S. Singh, A. Khare, S. Chaudhari, *J. Environ. Chem. Eng.* **8** (2020) 103704 (<https://doi.org/10.1016/j.jece.2020.103704>)
8. A. Amalraj, A. Pius, *Appl. Water Sci.* **7** (2017) 2653 (<https://doi.org/10.1007/s13201-016-0479-z>)
9. S. Bason, A. Ben-David, Y. Oren, V. Freger, *Desalination* **199** (2006) 31 (<https://doi.org/10.1016/j.desal.2006.03.137>)
10. Z. Amor, B. Bariou, N. Mameri, M. Taky, S. Nicolas, A. Elmidaoui, *Desalination* **133** (2001) 215 ([https://doi.org/10.1016/S0011-9164\(01\)00102-3](https://doi.org/10.1016/S0011-9164(01)00102-3))
11. M. Grzegorzec, K. Majewska-Nowak, A. E. Ahmed, *Sci. Total Environ.* **722** (2020) 137681 (<https://doi.org/10.1016/j.scitotenv.2020.137681>)
12. R. C. Bansal, M. Goyal, *Activated carbon adsorption*, CRC Press, Boca Raton, FL, 2005
13. K. P. Gopinath, D. V. N. Vo, D. Gnana Prakash, A. Adithya Joseph, S. Viswanathan, J. Arun, *Environ. Chem. Lett.* **19** (2021) 557 (<https://doi.org/10.1007/s10311-020-01084-9>)
14. D. S. G. D. Senewirathna, S. Thuraisingam, S. Prabagar, J. Prabagar, *Curr. Res. Green Sustain. Chem.* **5** (2022) 100304 (<https://doi.org/10.1016/J.CRGSC.2022.100304>)
15. B. D. Gebrewold, P. Kijjanapanich, E. R. Rene, P. N. L. Lens, A. P. Annachhatre, *Environ. Technol. (U.K.)* **40** (2019) 2913 (<https://doi.org/10.1080/09593330.2018.1459871>)
16. J. Fito, H. Said, S. Feleke, A. Worku, *Environ. Syst. Res.* **8** (2019) 1 (<https://doi.org/10.1186/s40068-019-0153-1>)
17. D. E. Jayashree, P. S. Kumar, P. T. Ngueagni, D. V. N. Vo, K. W. Chew, *Environ. Pollut.* **272** (2021) 115969 (<https://doi.org/10.1016/j.envpol.2020.115969>)

18. C. Pongener, D. Kibami, K. S. Rao, R. L. Goswamee, D. Sinha, *J. Water Chem. Technol.* **39** (2017) 108 (<https://doi.org/10.3103/S1063455X17020096>)
19. C. Pongener, P. C. Bhomick, A. Supong, M. Baruah, U. B. Sinha, D. Sinha, *J. Environ. Chem. Eng.* **6** (2018) 2382 (<https://doi.org/10.1016/j.jece.2018.02.045>)
20. B. M. Babic, S. K. Milonjic, M. J. Polovina, B. V. Kaludierovic, *Carbon N. Y.* **37** (1999) 477 ([https://doi.org/10.1016/S0008-6223\(98\)00216-4](https://doi.org/10.1016/S0008-6223(98)00216-4))
21. R. Araga, S. Soni, C. S. Sharma, *J. Environ. Chem. Eng.* **5** (2017) 5608 (<https://doi.org/10.1016/j.jece.2017.10.023>)
22. George Socrates, *Infrared and Raman Characteristic Group Frequencies Contents*, Third ed., Wiley, New York, 2001
23. L. M. Harwood, T. D. W. Claridge, *Introduction to Organic Spectroscopy*, Oxford University Press, 1997
24. B. Smith, *Fundamentals of Fourier transform infrared spectroscopy*, Second Ed., CRC Press, New York, 2011
25. A.-N. A. El-Hendawy, *Appl. Surf. Sci.* **255** (2009) 3723 (<https://doi.org/10.1016/j.apsusc.2008.10.034>)
26. O. Aksakal, H. Uzun, *J. Hazard. Mater.* **181** (2010) 666 (<https://doi.org/10.1016/j.jhazmat.2010.05.064>)
27. R. K. Gautam, P. K. Gautam, M. C. Chattopadhyaya, J. D. Pandey, *Proc. Natl. Acad. Sci. India, A* **84** (2014) 495 (<https://doi.org/10.1007/s40010-014-0154-4>)
28. S. Swarupa, J. Bersillon, K. Gopal, *Separ. Purific. Technol.* **50** (2006) 310 (<https://doi.org/10.1016/j.seppur.2005.11.036>)
29. M. H. Dehghani, M. Farhang, M. Alimohammadi, M. Afsharnia, G. McKay, *Chem. Eng. Commun.* **205** (2018) 955 (<https://doi.org/10.1080/00986445.2018.1423969>)
30. R. Mallampati, S. Valiyaveetil, *RSC Adv.* **2** (2012) 9914 (<https://doi.org/10.1039/c2ra21108d>)
31. K. S. Lagergren, *Sven. Vetenskapsakad. Handlingar* **24** (1898) 1
32. G. Blanchard, M. Maunay, G. Martin, *Water Res.* **18** (1984) 1501 ([https://doi.org/10.1016/0043-1354\(84\)90124-6](https://doi.org/10.1016/0043-1354(84)90124-6))
33. Y. S. Ho, G. McKay, *Process Biochem.* **34** (1999) 451 ([https://doi.org/10.1016/S0032-9592\(98\)00112-5](https://doi.org/10.1016/S0032-9592(98)00112-5))
34. W. J. Weber, J. C. Morris, *J. Sanit. Eng. Div.* **89** (1963) 31 (<https://doi.org/10.1080/002689796173345>)
35. D. Haddad, A. Mellah, D. Nibou, S. Khemaissia, *J. Environ. Eng. (U.S.A.)* **144** (2018) ([https://doi.org/10.1061/\(ASCE\)EE.1943-7870.0001349](https://doi.org/10.1061/(ASCE)EE.1943-7870.0001349))
36. R. Zaidi, S. U. Khan, I. H. Farooqi, A. Azam, *RSC Adv.* **11** (2021) 28744 (<https://doi.org/10.1039/d1ra00598g>)
37. S. K. Theydan, M. J. Ahmed, *J. Anal. Appl. Pyrolysis* **97** (2012) 116 (<https://doi.org/10.1016/j.jaap.2012.05.008>)
38. Z. Li, D. Xiao, Y. Ge, S. Koehler, *ACS Appl. Mater. Interfaces* **7** (2015) 15000 (<https://doi.org/10.1021/acsami.5b03994>)
39. S. P. Kumar, S. Ramalingam, C. Senthamarai, M. Niranjanaa, P. Vijayalakshmi, S. Sivanesan, *Desalination* **261** (2010) 52 (<https://doi.org/10.1016/j.desal.2010.05.032>)
40. J. Zhang, N. Chen, Z. Tang, Y. Yu, Q. Hu, C. Feng, *Phys. Chem. Chem. Phys.* **17** (2015) 12041 (<https://doi.org/10.1039/C5CP00817D>)
41. L. Xu, X. Gao, Z. Li, C. Gao, *Desalination* **369** (2015) 97 (<https://doi.org/10.1016/j.desal.2015.04.033>)

42. J. Saikia, S. Sarmah, T. H. Ahmed, P. J. Kalita, R. L. Goswamee, *J. Environ. Chem. Eng.* **5** (2017) 2488 (<https://doi.org/10.1016/j.jece.2017.04.046>)
43. M. S. Onyango, Y. Kojima, O. Aoyi, E. C. Bernardo, H. Matsuda, *J. Colloid Interface Sci.* **279** (2004) 341 (<https://doi.org/10.1016/j.jcis.2004.06.038>)
44. S. P. Kamble, S. Jagtap, N. K. Labhsetwar, D. Thakare, S. Godfrey, S. Devotta, S. S. Rayalu, *Chem. Eng. J.* **129** (2007) 173 (<https://doi.org/10.1016/j.cej.2006.10.032>)
45. Y. Chen, Q. Zhang, L. Chen, H. Bai, L. Li, *J. Mater. Chem. A* **1** (2013) 13101 (<https://doi.org/10.1039/c3ta13285d>).



SUPPLEMENTARY MATERIAL TO
**Defluoridation using pinecone-based activated carbon:
Adsorption isotherm, kinetics, regeneration and co-ions
effect investigation**

PARIMAL CHANDRA BHOMICK^{1,2*}, AOLA SUPONG^{2,3}, AKITO I. SEMA⁴
and DIPAK SINHA²

¹Department of Chemistry, St Joseph University, Chumoukedima, Nagaland, 79115, India,

²Department of Chemistry, Nagaland University, Lumami, Nagaland, 798627, India,

³Department of Chemistry Sao Chang College, Tuensang, Nagaland, 798612, India and

⁴Department of Chemistry, National Institute of Technology, Nagaland, 797103, India

J. Serb. Chem. Soc. 89 (4) (2024) 565–580

Zero-Point Charge of PAC

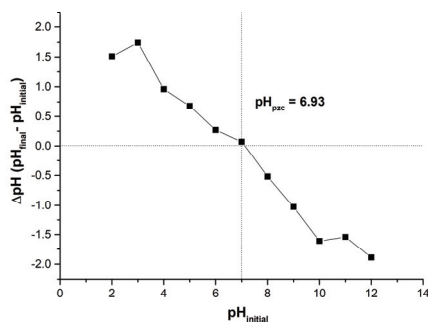


Figure S-1. Zero-point charge of Pc-AC

* Corresponding author. E-mail: paribhomick15589@gmail.com

Adsorption results

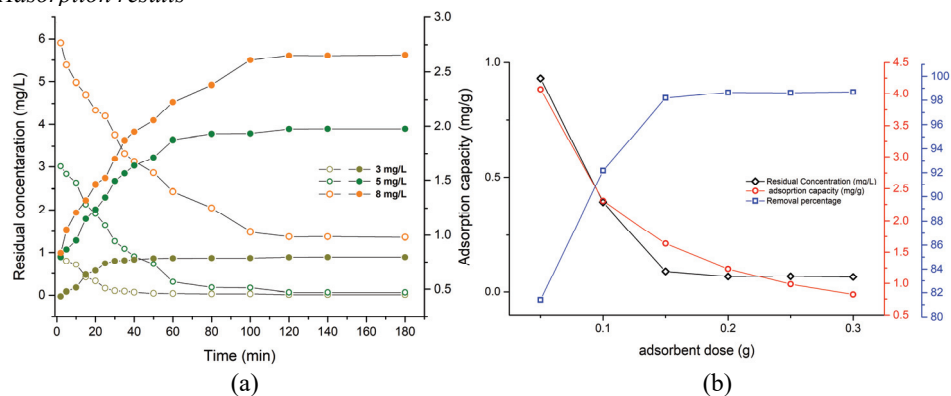


Fig S-2. (a) Contact time on adsorption capacity and residual concentration (b) adsorbent dose on adsorption capacity and residual concentration

Adsorption Isotherm

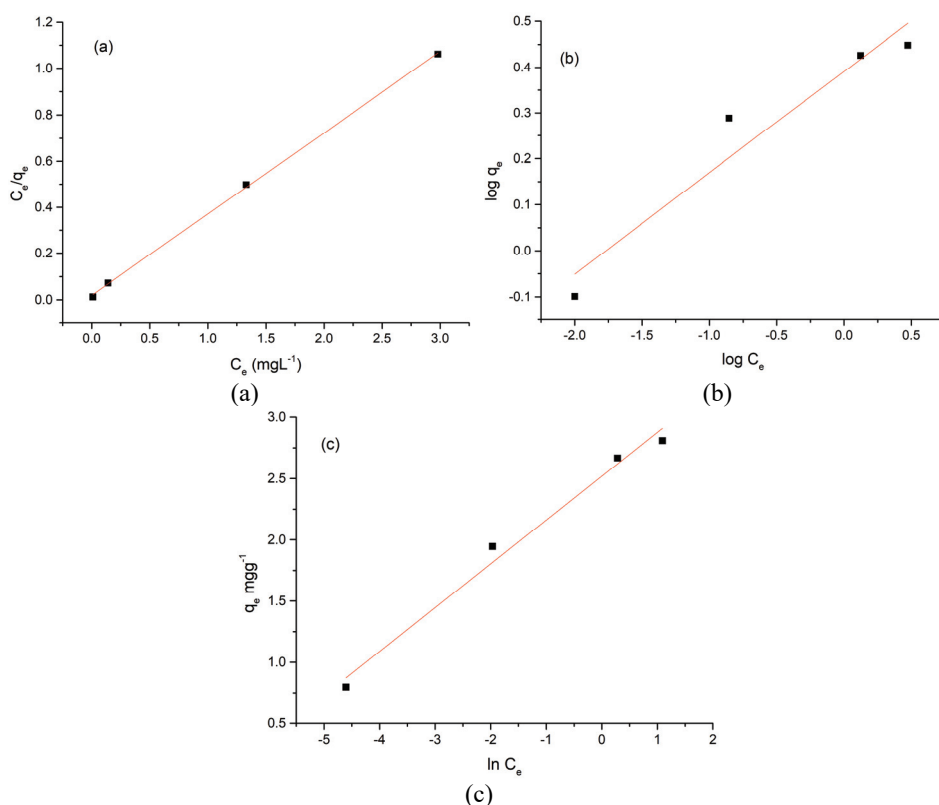


Figure S-3. (a) Langmuir (b) Freundlich (c) Temkin adsorption isotherm model for adsorption of fluoride onto Pc-AC

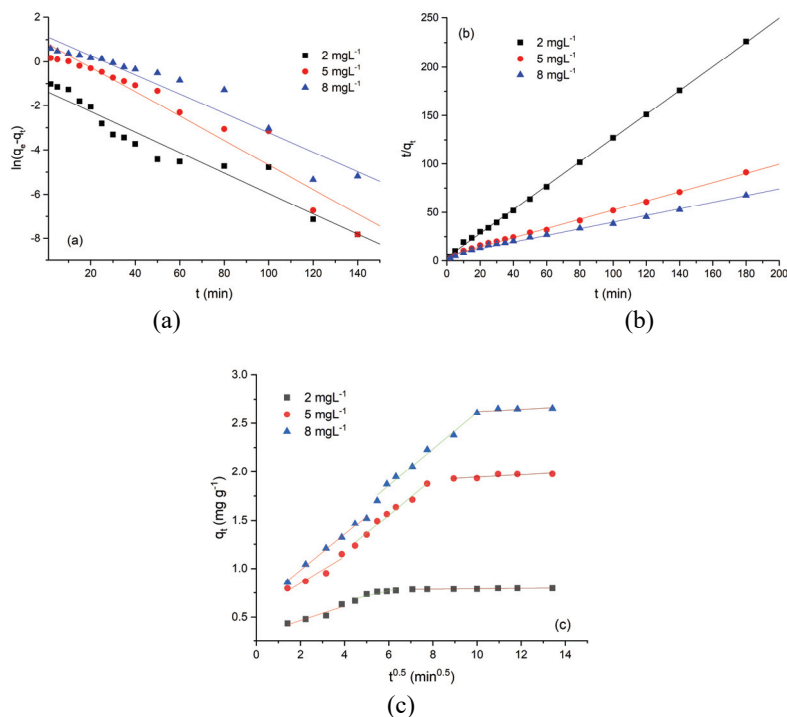
Adsorption Kinetics

Fig. S-4. Fits of (a) pseudo-first order kinetics for Pc-AC (b) pseudo-second order kinetics (c) intraparticle diffusion model for adsorption of fluoride on Pc-AC

Comparison of Pc-AC with other adsorbents

The fluoride adsorption efficiency for the prepared activated carbon was compared with other adsorbents reported in the literature and is listed in Table S-I.

To determine the efficiency of Pc-AC, the maximum adsorption capacity (Q_{\max}) was considered as the appropriate parameter for the comparison of different adsorbents with the present study. It is evident the defluoridation capacity of Pc-AC was comparable with other adsorbents and thus may be considered a suitable adsorbent for fluoride adsorption from water. Work is ongoing to study how the doping of metal ions into Pc-AC will affect the adsorption efficiency of fluoride and what would be the cost related to the incorporation of metal ions into the adsorbent.

Table S-I. Comparison of pinecone activated carbons with some other adsorbents for fluoride removal

Adsorbent	Dose (g)	pH	CT (min)	Conc. (mg L^{-1})	Isotherm	Q_{max} (mg g^{-1})	References
<i>Catha edulis</i> Activated carbon	1.5	2	60	30	Freundlich	18	1
CaCl ₂ -modified <i>Crocus sativus</i> leaves activated carbon	15	4.5	70	6.5	Langmuir	2.01	2
Bael (<i>Aegle Marmelos</i>) Shell Activated Carbon	2	6	60	8	--	2.4	3
<i>Morinda tinctorial</i> activated carbon coated with aluminium hydroxide	0.1	7	60	10	Langmuir	26.03	4
<i>Schima wallichii</i> activated carbon	1.15	4	100	5	Langmuir	2.524	5
Activated cotton nutshells carbon	1.75	7	180	3	Freundlich	2.472	6
Jamun seed activated carbon	0.4	2.5	120	10	Dubinin-Radushkevich	3.65	7
Pinecone activated carbon	1.5	4	120	5	Langmuir	2.845	Present Study

REFERENCES

1. J. Fito, H. Said, S. Feleke, A. Worku, *Environ. Syst. Res.* **8** (2019) 1–10 (<https://doi.org/10.1186/s40068-019-0153-1>)
2. M. H. Dehghani, M. Farhang, M. Alimohammadi, M. Afsharnia, G. McKay, *Chem. Eng. Commun.* **205** (2018) 955–965 (<https://doi.org/10.1080/00986445.2018.1423969>)
3. K. Singh, D. H. Lataye, K. L. Wasewar, *J. Fluor. Chem.* **194** (2017) 23–32 (<https://doi.org/10.1016/j.jfluchem.2016.12.009>)
4. A. Amalraj, A. Pius, *Appl. Water Sci.* **7** (2017) 2653–2665 (<https://doi.org/10.1007/s13201-016-0479-z>)
5. P. C. Bhomick, A. Supong, R. Karmaker, M. Baruah, C. Pongener, D. Sinha, *Korean J. Chem. Eng.* **36** (2019) 551–562 (<https://doi.org/10.1007/s11814-019-0234-x>)
6. R. Mariappan, R. Vairamuthu, A. Ganapathy, *Chinese J. Chem. Eng.* **23** (2015) 710–721 (<https://doi.org/10.1016/j.cjche.2014.05.019>)
7. R. Araga, S. Soni, C. S. Sharma, *J. Environ. Chem. Eng.* **5** (2017) 5608–5616 (<https://doi.org/10.1016/j.jece.2017.10.023>).



J. Serb. Chem. Soc. 89 (4) 581–595 (2024)
JSCS–5741

Cost-effective method of simultaneous removal of copper and phosphate on environmentally friendly nanomaterial

JOVANA JOKIĆ GOVEDARICA¹, DRAGANA TOMAŠEVIĆ PILIPOVIĆ^{1#*},
VESNA GVOIĆ^{2#}, ĐURĐA KERKEZ^{1#}, ANITA LEOVAC MAČERAK¹,
NATAŠA SLIJEPČEVIĆ^{1#} and MILENA BEČELIĆ-TOMIN^{1#}

¹University of Novi Sad, Faculty of Sciences, Department of Chemistry, Biochemistry and Environmental Protection, Trg Dositeja Obradovića 3, 21000, Novi Sad, Serbia and

²University of Novi Sad, Faculty of Technical Sciences, Department of Graphic Engineering and Design, Trg Dositeja Obradovića 6, 21000, Novi Sad, Serbia

(Received 14 September, revised 20 October 2023, accepted 6 March 2024)

Abstract: Environmentally friendly and economically viable methods are essential in the selection of materials and techniques for the synthesis of nano-zero-valent iron. Plants, with their high polyphenol content and antioxidant capacity, have found application in eco-friendly synthesis processes. The definitive screening design (DSD) monitored four key process parameters for the concurrent removal of copper and phosphate: copper concentration (ranging from 1 to 9 mg L⁻¹), phosphate concentration (ranging from 1 to 9 mg L⁻¹), initial pH values (ranging from 2 to 10), and the dosage of nano-zero-valent iron (ranging from 2 to 16 mL). The analysis results provide valuable insights into the significant individual factors influencing the process, along with the potential for their interactions. The model also proposes process optimization to attain maximum removal efficiency, and subsequent verification confirmed its superiority among the alternatives. Mechanisms such as sorption, reduction, complexation, electrostatic attraction, and ligand exchange play pivotal roles in the effective removal of copper and phosphate using nano-zero-valent iron. In summary, this research yields several benefits: the utilization of environmentally sustainable materials, a substantial reduction in experimental complexity, coupled with the ease of the entire procedure, simultaneous and highly efficient copper and phosphate removal, favorable pH levels and, notably, no requirement for additional treatment.

Keywords: eco-friendly green synthesized nano zero-valent iron; metal ions; definitive screening design.

* Corresponding author. E-mail: dragana.tomasevic@dh.uns.ac.rs

Serbian Chemical Society member.

<https://doi.org/10.2298/JSC230914025G>

INTRODUCTION

A decade behind us, nanoscale iron particles (nZVI) are being tested for water treatment, primarily potentially toxic metals, but also other pollutants of interest, because the most important thing is to choose remediation technology that will ensure the desired water quality at acceptable process costs. Compared to materials in macro dimensions, nanomaterials are characterized by multiplied specific surface area as a function of mass, and the advantage is manifested by achieving the same goals, which theoretically leads to savings in the amount of material used, reduced energy consumption, and thus reduced remediation costs.^{1,2}

One of the aspects of the nano revolution is the use of synthesized nanomaterials with “green” solvents in the process of remediation of contaminated water. The synthesis of nanomaterials performed in this way is considered cheaper, environmentally friendly because it uses extracts of natural products such as plants that are less toxic and biodegradable.¹ Another important fact when using plants, primarily leaves, that the content of polyphenols and antioxidant capacity are very significant factors for the production of nZVI. The nZVI particle is composed of a Fe⁰ nucleus and a shell layer, *i.e.*, different forms of Fe oxide. The core has the potential for reduction, while the surface has reaction site properties and affinity for chemisorption and electrostatic interactions, and based on that it is concluded that mechanisms of removal of potentially toxic metals can be reduction, absorption, precipitation, and mineralization.³

Copper ion, when present in trace amounts, is considered an essential micro-nutrient due to its direct involvement in hemoglobin formation, collagen constitution, and hair keratin. However, elevated concentrations of this metal resulting from anthropogenic sources can lead to increased levels of copper, thereby causing undesired effects.⁴ Cu²⁺ is widely used in the household, as well as in industries, technological aids, agriculture and many other spheres of life. Good conductive properties, lower prices compared to silver and gold, and possible recycling and reuse are some of the advantages of using copper.⁵ The reason for choosing copper as a metal of interest for the purposes of this study is the detection of increased concentrations of copper in watercourses and seas, as a consequence of its prevalence and wide application.

Phosphorus is considered a autotrophic element in water resources, which leads to the deterioration of water quality and reduction of biodiversity. Excessive non-selective use of fertilizers, industrial waste, municipal waste in landfills are just some of the ways to get phosphorus into the environment. In order to resist this problem, it is necessary to apply some of the available methods for phosphorus removal, which include biological methods, adsorption and precipitation.^{6,7} Since nZVI has already been mentioned as a suitable adsorbent for the removal of various pollutants, adsorption is imposed as suitable for the removal of phosphates and is considered a very efficient, easy to perform and cheap

method. Nanoparticles of zero-valent iron (nZVI) were applied using sodium borohydride in the treatment of wastewater with an elevated content of copper ions, and the removal efficiency was 96 %.⁸ The removal of phosphates using zero-valent iron nanoparticles (nZVI) has been investigated in several studies. Most of them have focused on the adsorption of phosphates on the surface of nZVI.⁹

Given that optimizing a process involves conducting a considerable number of experiments, the utilization of definitive screening design (DSD) was deemed beneficial for design of experiments (DoE), developing mathematical models, and statistically interpreting the obtained results. The DSD statistical method operates on the principle of employing a numerical algorithm to maximize the matrix determinant of the main effect model. This analysis helps identify significant factors, predict their two-factor interactions and estimate the coefficients of the equation model describing the total experiments conducted. In contrast to traditional statistical methodologies like Response surface methods with Box-Behnken or central composite design, this approach enables a substantially reduced number of experiments while maintaining maximum precision.¹⁰ Therefore, DSD might be used as powerful experimental design technique applied in the adsorption process to efficiently investigate and optimize various factors influencing adsorption efficiency. In this context, DSD allows researchers to systematically vary multiple factors, such as adsorbent dosage, contact time, pH, temperature or initial concentration of adsorbate, in a structured and resource-efficient manner. By conducting a series of experiments based on the DSD, researchers can identify key factors and their interactions that significantly impact the adsorption process. This approach aids in the development of robust and cost-effective adsorption systems by minimizing the number of experimental runs required while maximizing the amount of information obtained.¹¹

The focus of this paper is to examine the influence of various factors on the removal of copper in the presence of phosphate, i.e. phosphate in the presence of copper from the synthetic wastewater matrix. Parameters of interest for this study were: copper concentration, phosphate concentration, dose nZVI and pH value. Their individual influences were monitored, as well as two-factor interactions. The process has been optimized, and a possible mechanism for removing pollutants of interest has been proposed.

EXPERIMENTAL

Preparation of "green" zero-valent iron nanoparticles

Oak leaves were used for the preparation of the extract for further synthesis of nanomaterials due to their antioxidant capacity as an important factor in the production of nZVI. Also, the advantage of using oak leaves is its distribution in Vojvodina. Drying at 50 °C for 48 h as well as grinding the material to a size of <2 mm are indispensable steps in preparing the leaves for extraction. The guide for the preparation of the extract was the study¹² according to which 3.7 g of prepared leaves were weighed in 100 ml of water. During 20 min, it is neces-

sary to heat the extract with 80 °C with continuous stirring, after which it is cooled and filtered. A 3:1 ratio was chosen for the ratio in which the leaf extract and 0.1 M Fe(III) are mixed.

Definitive screening design (DSD)

Definitive screening design (DSD) is still a young statistical method for constructing experiments based on a numerical algorithm.¹³ For the purposes of this study, four operational parameters were monitored: copper concentration from 1 to 9 mg L⁻¹, concentration phosphate from 1 to 9 mg L⁻¹, nanomaterial dose from 2 to 16 mL, and pH value from 2 to 10. The concept of the analysis is based on determining significant process parameters and predicting their two-factor interactions. The advantage of using this concept is the reduced number of experiments because based on operational factors we get 13 experiments performed in duplicate and plus two central points, we come to the number of 28 experiments (Supplementary material to this paper, Table S-I).

Experimental procedure

Based on known parameter values, the experiment followed the following procedure. First, a base solution with a concentration of 100 mg L⁻¹ was prepared by dissolving the appropriate amounts of CuSO₄·5H₂O and KH₂PO₄. In order to meet the initial copper and phosphate concentrations, required by the model (1, 5 and 9 mg L⁻¹), the base solution was subjected to dilution with deionized water to achieve the desired concentration. The efficiency of removing selected pollutants was monitored by adding nZVI in doses of 2, 9 and 16 mL. The final volume of the reaction mixture was 0.1 L. pH adjustments were made by adding 0.1 M HNO₃ or NaOH (2, 6, 10). After adjusting the pH values, the samples were placed on a horizontal shaker (IKA-Werke KS501 digital) at 180 rpm for 60 min, at a constant temperature of 23±1 °C. After mixing, it was necessary to centrifuge the samples at 4000 rpm for 12 min. To determine the residual concentrations of metal ions or anions, samples had to undergo the proper preparation procedure for future analysis. The samples were filtered through a 0.22 µm filter, after which the residual concentrations of metal ions were analyzed using inductively coupled plasma-mass spectrometry (ICP-MS). Residual phosphate content was determined using the SRPS EN ISO 6878: 2008 methods.

Characterization

Application of a TEM model apparatus (TEM-EDX; JEOL-JEM 2100, Jeol, Italy) produced a more concrete picture of the morphological features of the examined nanomaterial. Sample, received as suspension were diluted 1:100 in Milli-Q water. Three µL of each suspension were manually drop on 200 mesh Cu-formvar carbon coated grids (Ted Pella, Inc.). Grids were left to dry in desiccator overnight and analysed in TEM mode to assess morphology and primary size distribution.

RESULTS AND DISCUSSION

Characterization oak-nZVI

Fig. 1 shows TEM analysis to understand the shape and dispersity of the synthesized nZVI particles. The particles take a spherical shape together with irregular shapes and tend to form chain-like aggregates. The surface of the layer is covered with a transparent layer, which serves as a sealing and stabilizing agent and plays a key role in improving its dispersion and stability as the basic

ingredient of green nZVI. The structural information obtained by TEM analysis is in accordance with the observations of other authors.³

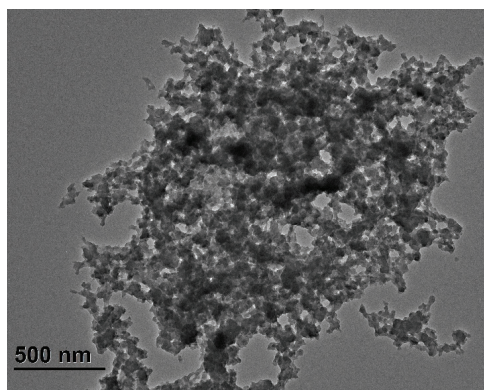


Fig. 1. Characteristics of oak-nZVI, TEM image.

Statistical analysis for the removal of copper and phosphate

DSD model evaluation – copper/phosphate. In order to remove copper in the presence of phosphate, the removal efficiency was monitored at different process parameters: nanomaterial dose, copper concentration, phosphate concentration and pH value, using statistical analysis of DSD. The efficiency results are shown in Table S-II of the Supplementary material, and the established efficiency range is from 2.25 to 98.98 %, while the percentage of phosphate removal in the presence of copper ranges from 54.70 to 91.50 %.

Descriptive factors for the selected statistical models that best approximate the experimental data are shown in Table I. A lower value of the correlation factor (0.859 and 0.750) was found, but the results in Table S-III of the Supplementary material confirm the validity of the selected model based on the results of the ANOVA test ($F < 0.0001$) and the “lack of fit” test ($F > 0.05$). Approximate values of *AIC* and *BIC* parameters imply a good approximation of experimental data.

TABLE I. Standard selection criteria for the regression models (copper and phosphate)

Descriptive factor	Copper	Phosphate
R^2	0.859	0.750
R^2 adj	0.809	0.703
<i>AIC</i>	234.407	220.997
<i>BIC</i>	236.396	223.374
<i>RMSE</i>	11.417	6.121

Based on the approximated parameter values and standard error, the factors with statistical significance shown in Table II (bold values) were singled out,

which in turn contributed to the efficiency of copper removal in the presence of phosphate and phosphate removal efficiency in the presence of copper.

TABLE II. Estimated regression coefficients sorted by statistical significance

Parameter	Estimate	Std Error	<i>t</i> ratio	Prob > <i>t</i>
Copper				
nZVI (mL) * copper (mg L ⁻¹)	17.924	2.948	6.080	<0.0001*
Copper (mg L ⁻¹)	16.879	2.553	6.610	<0.0001*
Phosphate (mg L ⁻¹)	-11.447	2.553	-4.480	0.0002*
nZVI (mL)	-10.401	2.553	-4.0700	0.0006*
Copper (mg L ⁻¹) * pH	7.322	2.948	2.48	0.0220*
pH	-0.523	2.553	-0.200	0.8398
Phosphate				
Copper (mg L ⁻¹) * Phosphate (mg L ⁻¹)	-6.032	1.829	-3.300	0.0038*
Phosphate (mg L ⁻¹) * pH	4.124	1.716	2.400	0.0266*
pH	-2.918	1.369	-2.130	0.0463*
nZVI (mL) * Phosphate (mg L ⁻¹)	3.293	1.716	1.920	0.0701
nZVI (mL) * pH	-3.498	1.829	-1.910	0.0710
Copper(mg L ⁻¹)	2.485	1.369	1.820	0.0852
nZVI (mL)	0.924	1.369	0.680	0.5077
Phosphate (mg L ⁻¹)	0.162	1.369	0.120	0.9073

Copper and phosphate concentration, as well as nZVI dose exhibit statistical significance for copper removal, which also reflects in the magnitude of their estimates. A positive sign before the linear term of copper concentration (16.879) suggests that the increase of this parameter contributes to the copper removal efficiency up to a certain point, after which further increase has an adverse effect on the removal process.¹⁴ This is corroborated by the optimization plot (Figure 3) which shows that, within the adopted regression model, the optimal removal efficiency lies between the center and high level, equaling approximately 7.4 mg L⁻¹ of copper concentration. In contrast, the negative regression estimation coefficient is interpreted in such a way that the two variables tested have opposite associations. Referring to the case study, the negative estimated phosphate (-11.447) and nZVI (-10.401) coefficient affects the copper removal efficiency in a negative direction. Interpretation can be that if the phosphate concentration and nZVI dose are increased, it will affect the copper removal efficiency to decrease and *vice versa*. The value of significance 0.0002 and 0.0006 for phosphate concentration and nZVI dose, respectively indicates that the *p*-value <0.05, so it can be concluded that the both parameters have a significant effect on copper removal efficiency with a negative sign.

Copper concentration and dose of nZVI have an individual influence and mutual interaction, while the other is a two-factor interaction between copper concentration and pH value. In the following text, two-factor interactions will be

presented using 3D diagrams and more will be said about them. Phosphate concentration has only a single effect.

On the efficiency of phosphate removal, pH has a single effect and a two-factor interaction with the phosphate concentration. In addition to pH, the phosphate concentration builds another significant interaction, and that is the copper concentration.

By increasing the concentration of copper, at a constantly high dose of nano-materials, the efficiency of copper removal increases, because by increasing the dose of adsorbent, new active centers appear on the surface of the adsorbent (Fig. 2a).

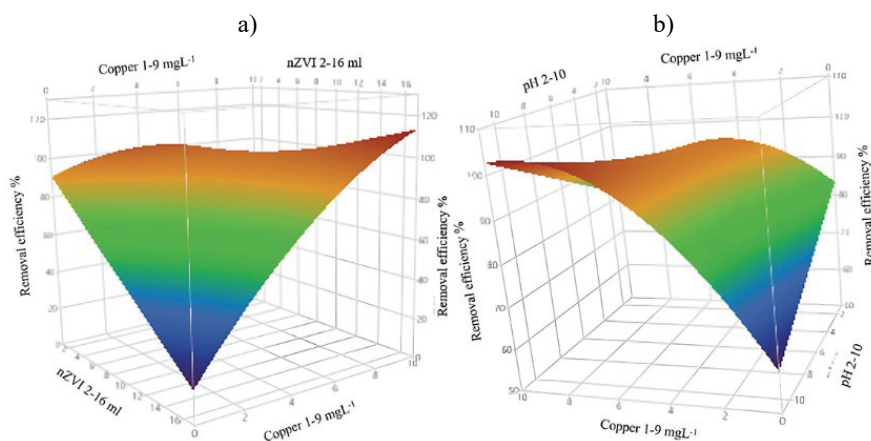


Fig. 2. Statistically significant two-factor interactions in the copper removal process: a) nZVI and copper; b) copper and pH.

The interaction of copper concentration and pH value (Fig. 2b) can be explained in 2 different ways, *i.e.*, two mechanisms of copper removal differ. To explain the mechanisms, it is first necessary to know the forms in which copper can be found in water depending on the pH conditions. $\text{pH} < 6$, Cu^{2+} , between 6 and 8.5 $\text{Cu}_2\text{Cl}(\text{OH})_3$, 8.5 and 12 $\text{Cu}_2\text{CO}_3(\text{OH})_2$, 12 and 13 HCuO_2^- and >13 CuO_2^{2-} .¹⁵ By fixing the pH value at a low level of ≈ 2 , the copper form is Cu^{2+} and the removal takes place via a redox mechanism up to Cu^0 , and the remaining Cu^{2+} is adsorbed on the nZVI surface and complexed with available FeOOH . The second mechanism is related to the pH value of ≈ 8 . Above pH 6, the present forms of copper are poorly soluble hydroxides, which leads to the conclusion that the main mechanism of copper removal under such conditions is precipitation.

The interaction of copper concentration and phosphate concentration is shown in Fig. 3a. By keeping the copper concentration at a low level, and by increasing the phosphate concentration, the efficiency of phosphate removal increases. The same observation is in the opposite case. The reason for this is that

copper on the surface of the nanomaterial can solidify as zero valence copper, which accelerates the corrosion of iron and releases Fe(III) into solution and as a result, improves phosphate removal.⁸

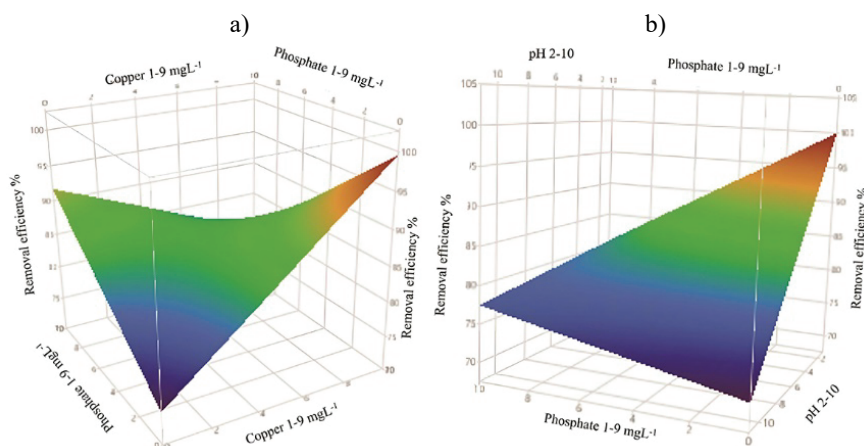
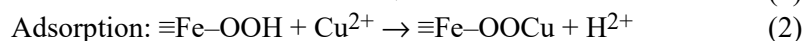
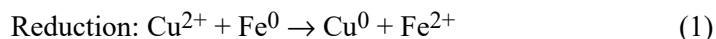


Fig. 3. Statistically significant two-factor interactions in the phosphate removal process: a) copper and phosphates; b) phosphates and pH.

The second diagram (Fig. 3b) shows a large dependence of phosphate removal efficiency on pH values. Acidic conditions are more suitable for phosphate removal because in that case the surface of the nanomaterial is positively charged and electrostatic attraction occurs with the phosphate ion. By changing the pH of the medium from acidic to basic, there is a decrease in the removal efficiency for two reasons. The first is because there is competition between OH^- and phosphates for adsorption sites on the adsorbent surface, and the second is that the adsorbent surface is more negatively charged and as such has a lower affinity for attracting phosphate species.

Process optimization of copper and phosphate adsorption. In order to achieve the most efficient results, the optimization of the entire process is carried out. To achieve the maximum efficiency of 97.71 %, it is necessary to apply the following conditions: dose of 5.64 mL, copper concentration 7.4 mg L^{-1} , phosphate concentration 3.16 mg L^{-1} and pH value of 6 (Fig. 4). Based on knowledge of the pH of the medium and form of copper, ($\text{pH} \geq 6$, Cu^{2+}), it is clear that the mechanisms of copper removal are reduction to Cu^0 and adsorption of residual Cu^{2+} ,¹ and this can be shown as:



The second model (Fig. 5) represents the optimization of the phosphate removal process in the presence of copper which proposes a phosphate removal effi-

ciency of 95.38 %: dose nZVI 16 mL, copper concentration 9 mg L⁻¹, phosphate concentration 1 mg L⁻¹ and pH value of 2. At the proposed pH value, phosphate is found in the forms H₃PO₄ and H₂PO₄⁻, so the removal mechanism may include the possibility of removal by physical sorption on the surface of the nano-material, while the other is chemical sorption, *i.e.*, the construction of the inner spherical complex with (hydro) iron oxides.

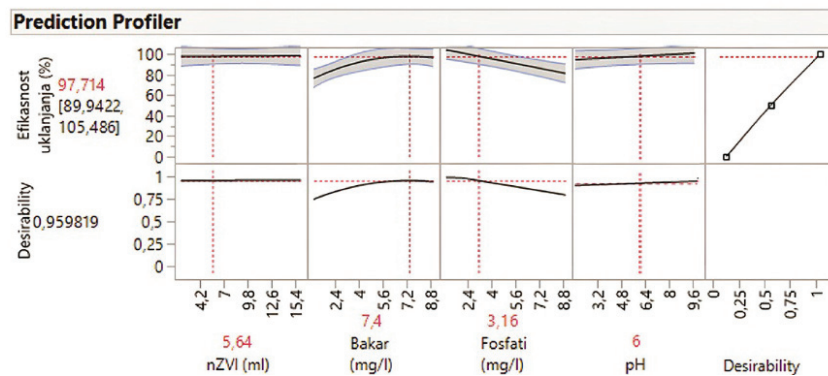


Fig. 4. Diagram of optimization of copper removal in the presence of phosphate.

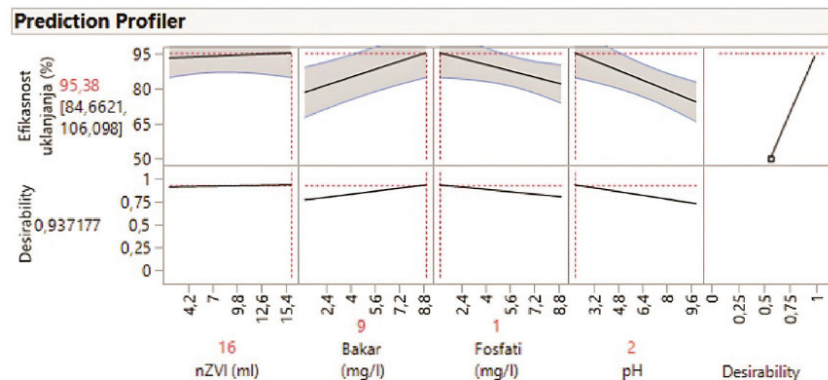


Fig. 5. Diagram of optimization of phosphate removal optimization diagram in the presence of copper.

In order to propose a phosphate removal mechanism, it is necessary to consider other factors of this medium. Under the given pH conditions, H₃PO₄ dissociated, which further led to the protonation of nZVI-FeOH as described by the following reactions:



The positively charged surface facilitates the electrostatic attraction of anionic phosphate due to the formation of new active sites and surface complexation, which explains the dominant role of acidic environmental conditions in the highly efficient phosphate adsorption process:



Experimental verification

Verification of optimized processes was performed to realize a set of eight-point experiments. Based on this, the confidence interval was calculated with 95 % confidence (Table III). The proposed efficiencies in the process of removing copper, *i.e.*, phosphate using nZVI, fit into the confidence interval proposed by the process optimization, which confirmed that the models have passed the validation test for this phase of research.

TABLE III. Experimental verification of optimized processes

Run	Copper	Phosphate
1	97.55	96.70
2	96.78	95.90
3	98.00	95.50
4	97.45	94.80
5	98.12	95.40
6	97.69	95.20
7	98.35	95.80
8	99.09	96.00
95 % Confidence interval	97.31–98.45	95.18–96.14

Possible removal mechanism

Observing the model for removing copper in the presence of phosphate at pH 6 and removing phosphate in the presence of copper at pH 2 based on knowledge of the chemistry of monitored pollutants, it can be pointed out that pollutants of interest for both operating conditions are in the same forms. This would further mean that in both cases we have copper in the form of Cu^{2+} which is reduced to Cu^0 and the residual Cu^{2+} sorbs on the surface of the nanomaterial. Phosphate is up to $\text{pH} \geq 7.2$ in the form of H_3PO_4 and H_2PO_4^- and as such is complexed on the surface of nanomaterials. Fig. 6 shows the mechanism of removal of copper and phosphate on nZVI.

Consideration for environmental applicability

The merged wastewater represents the bulk of industrial and domestic wastewater, so the urgent need for simultaneous removal of coexisting different kinds of heavy metals (in our case, Cu) and anions (*e.g.*, PO_4^{3-}) is indispensable. Many scientific results, gathered by authors,¹⁶ indicate that the nZVI is one of the most

important materials for water purification and environmental remediation. nZVI particles have a core-shell structure, which enables them to behave as an electron source (core) and a site for surface complexation (shell). Precipitation and adsorption on the surface is the most common sequestration mechanism of metal ion removal by nZVI.¹⁷

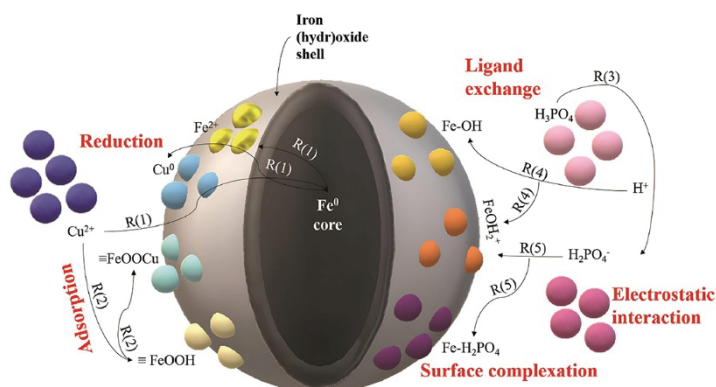


Fig. 6. Schematic diagram of possible mechanisms removal for copper and phosphate.

The green synthesis of nZVI makes this research favorable from both economic and environmental points of view. Cheap and green starting materials and the use of water as a green reaction medium is a promising option for large-scale synthesis.

Obtained high removal efficiencies of investigated pollutants (>99 % for Cu, and >92 % for PO₄³⁻) makes this material a promising candidate for implementation of a new generation of adsorbent used in a full-scale system.

Nanotechnology in environmental applications is experiencing significant growth, reflecting the real need for progress in both practice and research. However, since its initial use, nZVI has primarily been employed for remediating contaminated groundwater and soil, with its application in real wastewater, has yet to be extensively documented. Treating industrial effluents poses unique challenges due to their often high concentrations of pollutants in the presence of complex mixtures of different chemicals and impurities.

Key questions regarding nZVI technology relate to recirculation and reuse in treatment processes, enhancing material efficiency, reducing nZVI dosage and overall treatment cost. Green synthesis emerges as a cost-effective method for large-scale nZVI production, utilizing waste and further reducing treatment costs. The construction of this process requires minimal investment, with short reaction times. Additionally, nanoparticle regeneration, becomes crucial for economic reasons. Investigation into regeneration and the potential reuse of nZVI after Cu²⁺ adsorption shows promise for cost reduction and increased sustainability.¹⁸

Researchers have focused on regenerating waste from a solution used in fixing radiological and photographic films. The achieved results highlight success in extracting silver and directly synthesizing nanoparticles from this waste, contributing to a circular economy and reducing overall waste. The end product carries a high concentration of precious metals, which can contribute to offsetting treatment costs.¹⁹

Addressing limitations in nZVI application, issues such as agglomeration and sludge production stand out. However, these challenges can be directed towards the production of biochar and reuse in wastewater treatment.²⁰ Another avenue is the application of solidification and stabilization after wastewater treatment, producing construction materials. Applications include road construction, embankments, and other infrastructure projects, where these materials can serve as alternatives to traditional ones.

This integrated approach to nanotechnology in remediation demonstrates significant potential for achieving sustainability and meeting the growing demand for clean water.

CONCLUSION

In this study, there were two removal efficiencies (copper and phosphates), and based on the obtained efficiency values, DSD proposed two models. The first model monitored the efficiency of copper removal in the presence of phosphate, while the second model monitored the efficiency of phosphate removal in the presence of copper. Since the entire study was promoted as “green”, in terms of the application of nanomaterial synthesized from oak leaves, as well as in terms of the application of the DSD model itself which, in addition to accuracy and precision, reduced the number of experiments, we can make our experiment even more economical. According to the Decree on emission limit values for pollutants in water and deadlines for their achievement (Official Gazette of RS, No. 67/2011, 48/2012 and 1/2016), the emission limit values for phosphate wastewater are 2 mg L⁻¹. While the verified model for phosphates suggested a higher efficiency of ≈95 %, considering other parameters, the most important being the pH value (proposed value 2), the process is unfavorable in terms of the need for additional neutralization treatment which requires additional operating costs and chemicals. During the verification of the model for removing copper in the presence of phosphate, in addition to the analyzed copper residue, it also monitored the phosphate residue. Based on the analysis, a removal efficiency of ≈74 % was obtained, *i.e.*, the phosphate concentration was ≈0.85 mg L⁻¹, which satisfies the legal regulations. Since we have already mentioned that at pH 2 and 6 the pollutants of interest are in the same form, it can be concluded that at pH 6, phosphate would have the same removal mechanism as at pH 2. Copper on the nZVI surface changes from Cu²⁺ to Cu⁰ covers the surface of the nZVI, which acceler-

ates the removal of phosphate because the copper in this case is attributed to the properties of the catalyst. From this study, several conclusions can be drawn, first nano adsorbents such as nZVI significantly affect the improvement of pollutant removal, which is responsible for their large specific surface area, associated with sorption sites and surface chemistry. And the other main conclusion is that in the examined process there was a simultaneous removal of copper and phosphate on the so-called green adsorbent. The “green” adsorbent was used, we removed two pollutants in one process, no additional tertiary treatment is needed to remove phosphate and it is not necessary to neutralize the effluent, because according to the previously mentioned regulation, the pH value should be 6–9 before discharge into the recipient. There are many publications on the application of nZVI, their modification, removal of various pollutants from all environmental media, but it must be taken into account that everything is still at the level of laboratory research. To achieve practical application, it is necessary to focus on the following challenges:

- 1) The use of large-scale with a guarantee of efficiency, safety and economy.
- 2) Monitoring terrain data due to the presence of numerous environmental influences.
- 3) Long-term effects on biological cycles and their fate in the environment.

SUPPLEMENTARY MATERIAL

Additional data and information are available electronically at the pages of journal website: <https://www.shd-pub.org.rs/index.php/JSCS/article/view/12592>, or from the corresponding author on request.

Acknowledgements. The authors gratefully acknowledge the financial support of the Ministry of Science, Technological Development and Innovation of the Republic of Serbia (Grants No. 451-03-66/2024-03/ 200125, 451-03-65/2024-03/200125). This research has been supported by the Ministry of Science, Technological Development and Innovation (Contract No. 451-03-65/2024-03/200156), the Faculty of Technical Sciences, University of Novi Sad through project “Scientific and Artistic Research Work of Researchers in Teaching and Associate Positions at the Faculty of Technical Sciences, University of Novi Sad” (No. 01-3394/1) and within Project no. 2019-2.1.11-TÉT-2020-00152 implemented with the support provided by the Ministry of Innovation and Technology of Hungary.

ИЗВОД
ЕКОНОМИЧНА МЕТОДА ИСТОВРЕМЕНОГ УКЛАЊАЊА БАКРА И ФОСФАТА НА
ЕКОЛОШКИ ПРИХВАТЉИВОМ НАНОМАТЕРИЈАЛУ

ЈОВАНА ЈОКИЋ ГОВЕДАРИЦА¹, ДРАГАНА ТОМАШЕВИЋ ПИЛИПОВИЋ¹, ВЕСНА ГВОИЋ², БУРЂА КЕРКЕЗ¹,
АНИТА ЛЕОВАЦ МАЂЕРАК¹, НАТАША СЛИЈЕПЧЕВИЋ¹ и МИЛЕНА БЕЧЕЛИЋ-ТОМИН¹

¹Универзитет у Новом Сагу, Природно–математички факултет, Дејарман за хемију, биохемију и
заштитну животно средине, Трi Досићеја Обрадовића 3, 21000 Нови Саг и ²Универзитет у Новом
Сагу, Факултет техничких наука, Катедра за графичко инжењерство и дизајн, Трi Досићеја
Обрадовића 6, 21000 Нови Саг

Еколошки одрживе и економски оправдане методе су неопходне при одабиру материјала и техника за синтезу нано-нултовалентног гвожђа. Биљке, са својим високим садржајем полифенола и антиоксидативним капацитетом, пронашле су примену у еколошки прихватљивим процесима синтезе. Definitive screening design (DSD) надгледао је четири кључна процесна параметра за истовремено уклањање бакра и фосфата: концентрацију бакра (у распону од 1 до 9 mg L⁻¹), концентрацију фосфата (у распону од 1 до 9 mg L⁻¹), почетне рН вредности (у распону од 2 до 10) и дозу нано-нултовалентног гвожђа (у распону од 2 до 16 mL). Резултати анализе пружају драгоцене увиде у значајне појединачне факторе који утичу на процес, као и потенцијал за њихове међусобне интеракције. Модел такође предлаже оптимизацију процеса ради постизања максималне ефикасности уклањања, а накнадна верификација потврдила је његову супериорност у односу на алтернативне методе. Механички процеси као што су сорпција, редукција, комплексација, електростатичка привлачност и размена лиганда играју кључну улогу у ефикасном уклањању бакра и фосфата применом нано-нултовалентног гвожђа. Укратко, ово истраживање доноси низ користи: употребу еколошки одрживих материјала, значајно смањење експерименталне сложености, уз истовремено високу ефикасност уклањања бакра и фосфата, повољне рН вредности и, посебно, непотребност додатних третмана.

(Примљено 14. септембра, ревидирано 20. октобра 2023, прихваћено 6. марта 2024)

REFERENCES

1. M. M. Tarekegn, A. M. Hiruy, A. H. Dekebo, *RSC Adv.* **11** (2021) 18539 (<https://doi.org/10.1039/d1ra01427g>)
2. S. Poguberović, *PhD Thesis*, University in Novi Sad, 2017 (<https://nardus.mpn.gov.rs/handle/123456789/6294>) (in Serbian)
3. A. M. Abdelfatah, M. Fawzy, A. S. Eltaweil, M. E. El-Khouly, *ACS Omega* **16** (2021) 25397 (<https://doi.org/10.1021/acsomega.1c03355>)
4. B. Sutcliffe, A. A. Chariton, A. J. Harford, G.C. Hose, P. Greenfield, D. J. Midgley, I. T. Paulsen, *Ecology* **34** (2018) 28 (<https://doi.org/10.1016/j.funeco.2018.03.003>)
5. J. Yang, Y. Xie, K. Jeppe, S. Long, V. Pettigrove, X. Zhang, *Environ. Toxicol. Chem.* **37** (2017) 599 (<https://doi.org/doi:10.1002/etc.3980>)
6. Y. H. Zhang, F. Q. Liu, C. Q. Zhu, X. P. Zhang, M. M. Wei, F. H. Wang, C. Ling, A. M. Li, *J. Hazard. Mater.* **329** (2017) 290 (<https://doi.org/10.1016/j.jhazmat.2017.01.054>)
7. O. Eljamal, I. P. Thompson, I. Maamoun, T. Shubair, E. Kareman, K. Lueangwattanapong, Y. Sugihara, *J. Mol. Liq.* **299** (2020) 112144 (<https://doi.org/10.1016/j.molliq.2019.112144>)
8. S. Li, W. Wang, F. Liang, W. X. Zhang, *J. Hazard. Mater.* **16** (2017) 163 (<https://doi.org/10.1016/j.jhazmat.2016.01.032>)

9. J. Suazo-Hernández, P. Sepúlveda, L. Cáceres-Jensen, J. Castro-Rojas, P. Poblete-Grant, N. Bolan, M. L. Mora, *Nanomaterials* **13** (2023) 399 (<https://doi.org/10.3390/nano13030399>)
10. V. Gvoić, M. Prica, M. Turk Sekulić, S. Pap, O. Paunović, A. Kulić Mandić, M. Bečelić-Tomin, Dj. Vukelić, Dj. Kerkez, *Environ. Technol.* (2022) (<https://doi.org/10.1080/09593330.2022.2154082>)
11. H. Boulika, M. El Hajam, M. H. Nabih, I. Riffi Karim, N. Idrissi Kandri, A. Zerouale, *Mater. Today: Proc.* **72** (2023) 336 (<https://doi.org/10.1016/j.matpr.2022.07.358>)
12. J. Jokić Govedarica, D. Tomašević Pilipović, V. Gvoić, Đ. Kerkez, A. Leovac Maćerak, N. Slijepčević, M. Bečelić-Tomin, *Water Sanit. Technol.* **2** (2022) 13 (502.51:504.5:546.48 546.72:502.174)
13. B. Jones, C. J. Nachtsheim, *J. Qual. Technol.* **45** (2017) 121 (<https://doi.org/10.1080/00224065.2013.11917921>)
14. D. Movrin, O. Luzanin, V. Guduric, *Rapid Prototyping J.* **25** (2018) 653 (<https://doi.org/10.1108/RPJ-07-2018-0177>)
15. A. Šučurović, *PhD Thesis*, University in Novi Sad, 2017 (<https://nardus.mpn.gov.rs/handle/123456789/8836>) (in Serbian)
16. T. Tosco, P. M. Papini, C. V. Cruz, R. Sethi, *J. Clean. Prod.* **77** (2014) 10 (<https://doi.org/10.1016/j.jclepro.2013.12.026>)
17. T. Pasinszki, M. Krebsz, *Nanomaterials* **10** (2020) 917 (<https://doi.org/10.3390/nano10050917>)
18. A. O. Dada, F. A. Adekola, E. O. Odebunmi, A. S. Ogunlaja, O. S. Bello, *Sci. Rep.* **11** (2021) 16454 (<https://doi.org/10.1038/s41598-021-95090-8>)
19. S. Azordeg Molkabadi, M. Asadi, *Pollution* **9** (2023) 1074 (<https://doi.org/10.22059/poll.2023.349294.1640>)
20. A. Leovac Maćerak, A. Kulić Mandić, V. Pešić, D. Tomašević Pilipović, M. Bečelić-Tomin, Đ. Kerkez, *Molecules* **28** (2023) 1425 (<https://doi.org/10.3390/molecules28031425>).



SUPPLEMENTARY MATERIAL TO

Cost-effective method of simultaneous removal of copper and phosphate on environmentally friendly nanomaterial

JOVANA JOKIĆ GOVEDARICA¹, DRAGANA TOMAŠEVIĆ PILIPOVIĆ^{1*}, VESNA GVOIĆ², ĐURĐA KERKEZ¹, ANITA LEOVAC MAČERAK¹, NATAŠA SLIJEPČEVIĆ¹ and MILENA BEČELIĆ-TOMIN¹

¹University of Novi Sad, Faculty of Sciences, Department of Chemistry, Biochemistry and Environmental Protection, Trg Dositeja Obradovića 3, 21000, Novi Sad, Serbia and

²University of Novi Sad, Faculty of Technical Sciences, Department of Graphic Engineering and Design, Trg Dositeja Obradovića 6, 21000, Novi Sad, Serbia

J. Serb. Chem. Soc. 89 (4) (2024) 581–595

Table S-I. DSD experimental design layout

Run	Metal concentration	Ion concentration	pH	nZVI concentration
1	9	9	10	9
2	1	1	2	9
3	1	5	10	16
4	9	5	2	2
5	5	1	2	16
6	5	9	10	2
7	1	9	6	16
8	9	1	6	2
9	9	9	2	16
10	1	1	10	2
11	9	1	10	16
12	1	9	2	2
13	5	5	6	9
14	9	9	10	9
15	1	1	2	9
16	1	5	10	16
17	9	5	2	2
18	5	1	2	16
19	5	9	10	2
20	1	9	6	16
21	9	1	6	2
22	9	9	2	16
23	1	1	10	2
24	9	1	10	16

* Corresponding author. E-mail: dragana.tomasevic@dh.uns.ac.rs

25	1	9	2	2
26	5	5	6	9
27	5	5	6	9
28	5	5	6	9

Table S-II. Process efficiency (%) in copper and phosphate removal

Proba	Copper	Phosphate
1	86,87	76,10
2	76,16	74,60
3	97,05	62,70
4	62,23	78,77
5	36,11	84,40
6	91,43	83,18
7	98,64	92,80
8	93,25	69,56
9	86,73	77,16
10	75,99	73,60
11	2,25	88,61
12	98,57	85,90
13	86,30	80,26
14	89,68	73,73
15	80,87	81,10
16	96,79	54,70
17	68,24	77,44
18	39,33	83,60
19	91,15	84,18
20	98,77	88,80
21	93,74	68,86
22	89,04	78,29
23	86,87	68,60
24	7,72	89,01
25	98,98	91,50
26	87,94	79,76
27	89,34	80,44
28	88,67	80,26

Table S-III. ANOVA and "Lack of fit" test (copper and phosphate)

Source	^a DF	^b SS	^c MS	F - parametar	Verovatnoća > F
<i>Copper</i>					
Model	7	15844,545	2263,510	17,364	<0,0001*
Error	20	2607,083	130,350		
C. Total	27	18451,628			
<i>Phosphate</i>					
Model	8	1322,7549	165,344	4,414	0,0038*
Error	19	711,7533	37,461		
C. Total	27	2034,5083			

^aDegrees of freedom; ^bThe sum of square; ^cVariance (mean of square)



J. Serb. Chem. Soc. 89 (4) 597 (2024)

Journal of
the Serbian
Chemical Society

JSCS-info@shd.org.rs • www.shd.org.rs/JSCS

Errata (printed version only)

Issue No. 2 (2024), Vol. 89, paper No. *JSCS-5714*:

– page 177, footnote should read:

* Corresponding author. E-mail: abida.ejaz@iub.edu.pk; abidaejaz2010@gmail.com
<https://doi.org/10.2298/JSC230307050E>

Issue No. 3 (2024), Vol. 89, paper No. *JSCS-5723*:

– page 321, footnote should read:

* Corresponding author. E-mail: kemalg@dicle.edu.tr
<https://doi.org/10.2298/JSC230707053E>